The dynamics of epigenetic regulation in the neuronal nucleus in health and disease

A thesis presented for the degree of

Doctor of Philosophy,
University College London

Eva Wan-Ying So

Department of Cell and Developmental Biology,
University College London

2013

I, Eva Wan-Ying So declare that the work presented in this thesis is my own. Where information has been derived from other sources, I confirm that this has been fully acknowledged.

Abstract

The neuronal nucleus is highly specialized with a unique and characteristic organization of the genome, transcription and epigenetic regulation. Little is known about its chromatin organization as most studies have focused on rapidly growing and dividing cells. This study has determined the ultrastructural and molecular organization of the mouse striatal neuronal nucleus and to correlate this with the distribution of a range of epigenetic modifications. The relationship of the structural organization to a functional assay of *in vivo* transcription detecting nascent RNA together with the localization of RNA pol I, II and III have been explored. These provide strikingly different results to the literature, foremost is the highest level of transcription mediated by RNA pol III within the perinucleolar heterochromatin. A novel mechanistic theory of the neuronal nucleolar complex is postulated which may underlie the establishment and maintenance of the post-mitotic, non-regenerating and growth restricted status of neurons. Surprisingly, this unique neuronal nucleolar complex appears to be a focus for disorganization upon HDAC inhibition and in various neurodegenerative disease models. The cellular process observed for the extrusion of TDP-43 aggregates out of the neurons in the novel TDP-43^{M337V} transgenic mouse models of ALS/FTLD further implicates a novel mechanism for the extracellular spread of transmissible proteinopathies. In agreement with recent literature, it is speculated that prion-like propagation involving RNA-binding proteins with putative prion domains might underlie the cell-to-cell emanation of neurodegenerative pathology throughout the nervous system.

Acknowledgements

There are many people who have made my PhD an enjoyable and unforgettable journey over the past three years. I am extremely grateful to all of them for their help and support. In particular I would like to express my deep gratitude to my supervisor, Prof. Stephen W. Davies, for his continued support and guidance throughout the years. His inspiration and passion for research have stimulated many exciting discussions of the scientific discoveries made in the lab. I would also like to thank current and former members of the lab for their invaluable advice and friendship. Dr. Elizabeth Slavik-Smith and Dr. Aysha Raza have always been supportive and willing to share their knowledge and experiences in many aspects. A very special thank to Mark Turmaine for his help and expertise in electron microscopy.

I would like to extend my appreciation to Tim Robson and Daniel Ciantar for their assistance in confocal microscopy. I would also like to send my gratitude to Prof. Steve Hunt for his support and encouragement during my research. Special thanks also go to Dr. Michel Goedert and his group at the MRC/LMB Cambridge for the supply of TDP-43^{M337V} and Tau^{P301S} transgenic mice. I am very grateful to the BBSRC for providing funding throughout my research.

My sincere appreciation also goes to my closest friends Yvonne Kam and Amanda Wong for their precious friendship. Their constant support and encouragement have lifted me up during times of frustration. I would like to extend my deepest gratitude to my beloved parents Stewart So and Cindy So,

my brother James So, and Ben Sin, who have offered me endless love, patience and care. It is a blessing from God to have them all beside me to share my sadness and joy, and to provide me the courage allowing me to become a determined scientist to pursue my dreams.

Contents

Figures and Tables

Introduction

Materials & Methods

Results

List of Abbreviations

Aβ	amyloid beta
AcH3	acetylated histone H3
AcH4	acetylated histone H4
Act D	Actinomycin D
AD	Alzheimer's disease
ALS	amyotrophic lateral sclerosis
ATRX	alpha-thalassemia mental retardation X-linked
BDNF	brain-derived neurotrophic factor
CB	Cajal body
CHMP2B	charged multivesicular body protein 2B
CNS	central nervous system
CpG	cytosines preceding guanine
CTFs	C-terminal fragments
CTs	chromosome territories
DAPI	4', 6-diamidino-2-phenylindole
DFC	dense fibrillar component
DM	myotonic dystrophy
DNMTs	DNA methyltransferases
EDMD	Emery-Dreifuss muscular dystrophy
EM	electron microscopy
EWSR1	Ewing sarcoma break point region 1
FC	fibrillar centre
FISH	fluorescence in situ hybridization
FITC	fluorescein isothiocyanate
FTDP-17	frontotemporal dementia with Parkinsonism-17
FTLD	frontotemporal lobar degeneration
FUS/TLS	fused in sarcoma/translocated in liposarcoma
GC	granular component
GEMs	Gemini of coiled bodies
HD	Huntington's disease
HDAC	histone deacetylases
HDACi	histone deacetylase inhibitors
H3K9M3	trimethylation of histone H3 on Lys9
hnRNP	heterogeneous nuclear ribonucleoprotein
HP1	heterochromatin protein 1

htt	huntingtin
ICC	immunocytochemistry
kDa	kiloDaltons
lncRNA	long non-coding RNA
MAPT	microtubule-associated protein tau
MBD	methyl-CpG binding domain
MBNL-1	muscleblind-like 1
MeCP2	methyl-CpG binding protein 2
ncRNA	non-coding RNA
NFT	neurofibrillary tangles
NIIs	neuronal intranuclear inclusion
NLS	nuclear localization signal
NORs	nucleolar organizing regions
PD	Parkinson's disease
PNH	perinucleolar heterochromatin
PS	paraspeckles
PSPC1	paraspeckle protein 1
PTMs	Post-translational modifications
PYY	Pyronin Y
RBP	RNA binding protein
RNAP	RNA polymerase
RNP	ribonucleoprotein particle
RRM	RNA-recognition motif
rRNA	ribosomal RNA
RTT	Rett syndrome
SAHA	suberoylanilide hydroxamic acid
SCA	spinocerebellar ataxia
SFS	splicing factor speckles
SINEs	short interspersed nuclear elements
SMA	spinal muscular atrophy
SMN	survival of motor neuron protein
snoRNP	small nucleolar ribonucleoprotein particle
snRNA	small nuclear RNA
snRNP	small nuclear ribonucleoprotein particle
SR proteins	arginine/serine rich domain proteins
TAF15	TATA-binding protein-associate factor 15
TDP-43	transactive response DNA-binding protein
TEM	transmission electron microscopy

TSA	trichostatin A
TSEs	transmissible spongiform encephalopathies
VCP	valosin-containing protein
VPA	sodium valproate
WT	wild type
Xi	inactive X chromosome

Introduction

CHAPTER 1

Introduction

"The nervous system is constituted by numerous nervous units (neurons)" The term "neurons" was defined by Heinrich Wilhelm Gottfried von Waldeyer back in 1892, decades after the first description of nerve cells by Christian Gottfried Ehrenberg and Jan Evangelista Purkinje in 1836 and 1837 (Lopez-Munoz et al., 2006, Waldeyer, 1891). The nature of neurons was recognized in the 1880s through the groundbreaking work by Santiago Ramón y Cajal on the structure of the nervous system, in which the basic cellular features of neurons including dendrites, soma (cell body), axons and small contact zones (synapses) were revealed (Lopez-Munoz et al., 2006). His study of the nuclear subcompartments together with the remarkable discovery of the "accessory body" (Cajal body) had provided great insight into the organization of the mammalian neuronal nucleus (Lafarga et al., 2009). Following Cajal's meritorious description of the morphology of individual neuron, the principal biophysical properties of neurons such as their excitability through ion channel conductance and signal transmission at synapse were elucidated during the first half of the 20th century (Albright et al., 2000) (Fig1.1). At present, the selective loss of neurons and progressive failure of neuronal functions in neurodegenerative diseases of late onset has become the major focus in the field and represent one of the greatest challenges to our aging society in the 21st century.

Neurons are arguably the most varied cell type in terms of morphology and

function. Their fate during differentiation and development, as well as the activity of mature neurons is fundamentally determined by chromatin (Takizawa and Meshorer, 2008). Most neurons in the adult brain are fully differentiated post-mitotic cells which neither divide nor grow substantially. These unique features may allow the establishment of a stable and specialized nuclear organization providing a framework for efficient RNA transcription and processing (Akhmanova et al., 2000). Up to now, there are very few studies of the organization of nuclear structure and function in post-mitotic neurons. In this project, I shall focus on the unique nuclear organization of the interphase post-mitotic neurons in the adult mouse brain.

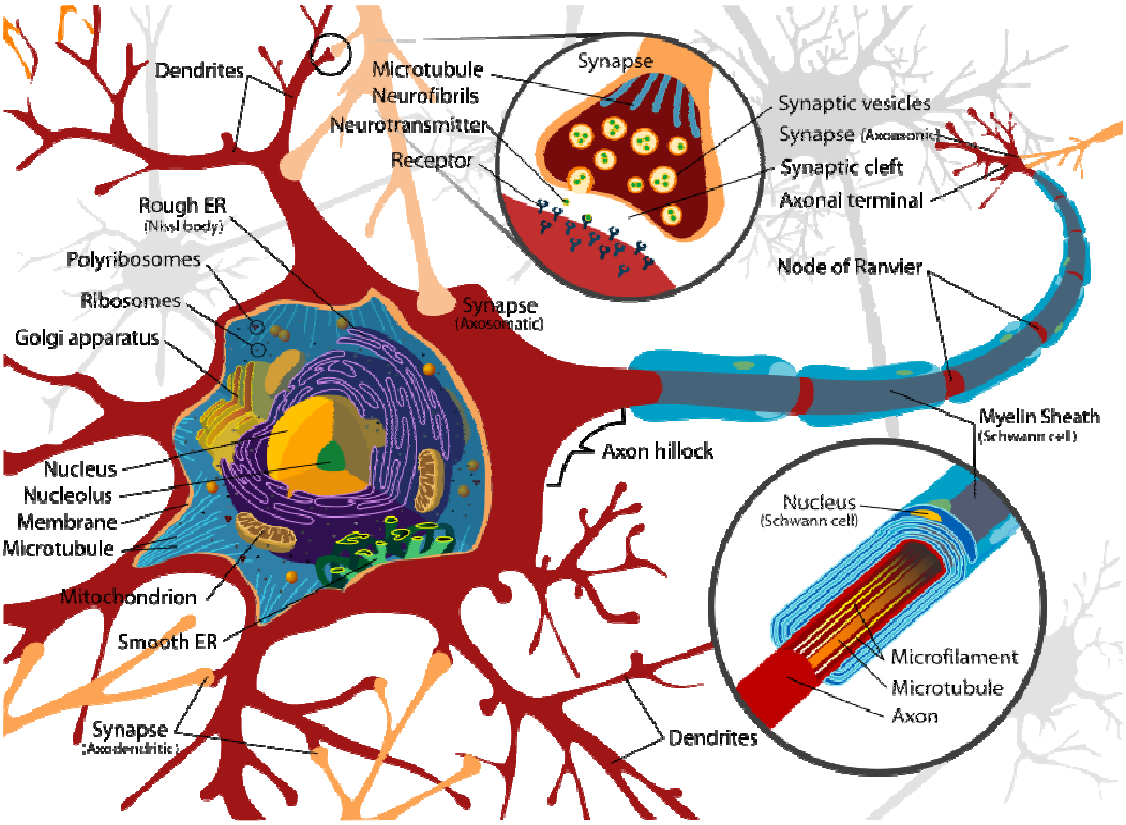

Figure 1.1

Diagram of a typical myelinated vertebrate motoneuron, an electrically excitable cell that processes and transmits information in the nervous system.

(Taken from http://en.wikipedia.org/wiki/File:Complete_neuron_cell_diagram_en.svg)

1.1 Architectural Organization of the Nucleus

The mammalian nucleus is a dynamic organelle which is highly compartmentalized into distinct nuclear compartments. Such compartmentalization, nuclear architecture, both reflects and controls the arrangement of chromosomes and the genes within them, the distribution of numerous nuclear bodies as well as the interplay between all these factors (Takizawa and Meshorer, 2008) (Fig1.2). Within the nucleus, genetic material is packaged in the form of chromatin consisting of DNA, histones and associating architectural proteins. Distinct chromatin domains, euchromatin and heterochromatin, are formed with specific patterns of histone modifications (Grewal and Elgin, 2007). These regions may be held in position by the nuclear matrix providing a scaffold of three-dimensional organization in space. According to their gene density, individual chromosomes are non-randomly arranged in a radial manner in the interphase nucleus. This territorial organization of chromosomes, chromosome territories, is the major feature of nuclear architecture which enables efficient regulation of transcription (Cremer and Cremer, 2010).

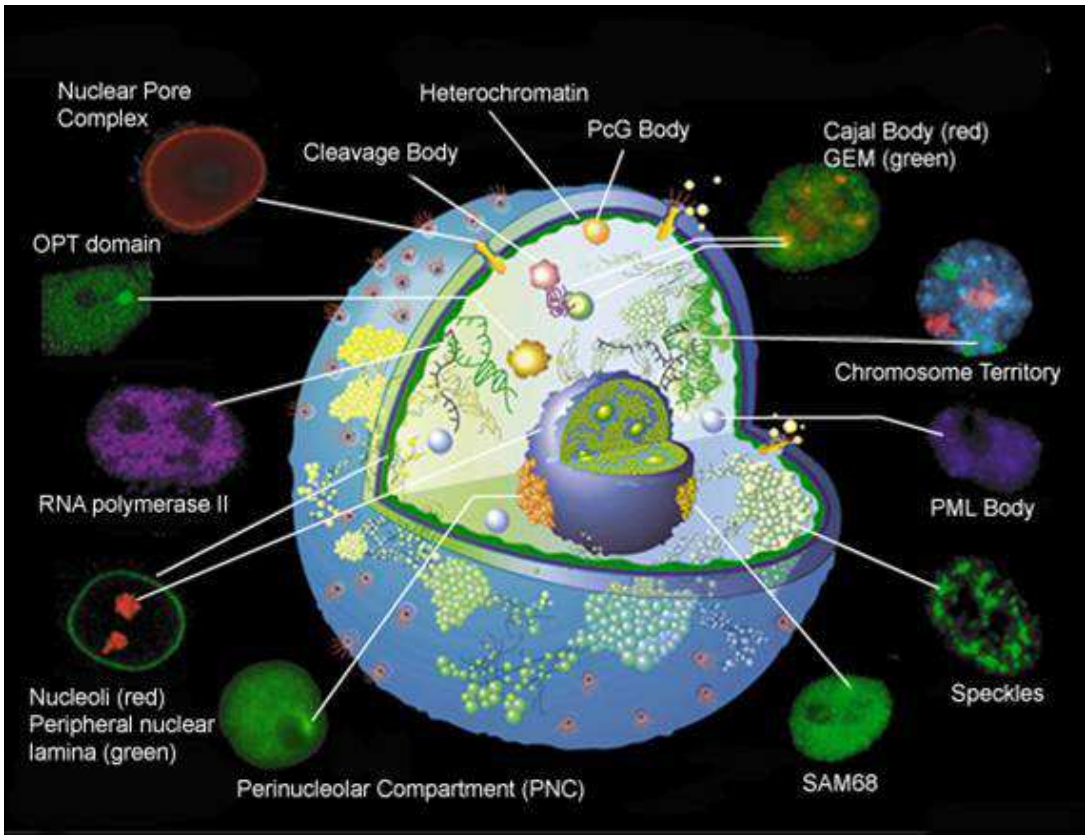

Figure 1.2

The mammalian cell nucleus with various distinct nuclear domains (Adapted from Spector, 2003).

1.1.1 Chromosome Territories

The territorial organization of chromosomes in the animal interphase nuclei was first suggested by Carl Rabl in the late 19th century (Rabl, 1885) and later termed chromosome territory (CT) by Theodor Boveri (Boveri, 1909), in which both studies demonstrated that chromatin was not randomly organized but each chromosome retained its individuality and remained confined to a distinct part of the nuclear space (Cremer and Cremer, 2010). More recently, a growing number of studies have focused on the organization and positioning of human chromosomes using probes specific for individual chromosomes with fluorescence *in situ* hybridization (FISH) (Spector, 2003). In an extensive

study, Bickmore and coworkers found that in human lymphocytes and fibroblasts CTs are organized in a radial manner correlating with their gene density (Croft et al., 1999, Boyle et al., 2001). Most gene-rich chromosomes occupy more interior positions of the nucleus, whereas more gene-poor chromosomes are found towards the nuclear periphery (Fig1.3). It is suggested that such arrangements of chromosomes have been conserved in vertebrates and are established early in the cell cycle and maintained throughout interphase (Fedorova and Zink, 2008).

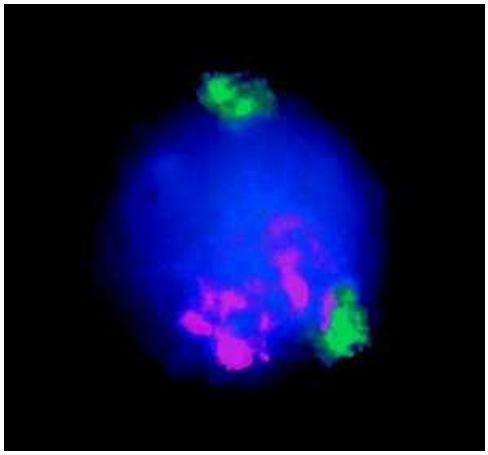

Figure 1.3

Visualization of individual chromosomes in a human primary peripheral blood lymphocyte after FISH. Gene-poor chromosomes 18 (green) are localized at the nuclear periphery and gene-rich chromosomes 19 (red) at more internal regions (Adapted from Croft, Bridger et al., 1999).

Similar gene density-correlated radial chromosome arrangements have also been observed in a parallel study by Cremer and colleagues (Cremer et al., 2001) who compared the chromosome arrangements in human cell types with different shaped nuclei, including flat-ellipsoid nuclei of amniotic fluid cells and fibroblasts as well as spherical B and T lymphocytes. However, their study further depicted the different radial arrangements of large and small CTs in ellipsoid and spherical nuclei of human cells.

1.1.2 Chromatin Dynamics

Although the patterns of chromosome arrangement appears to be conserved during evolution, these territories are nevertheless dynamic (Babu et al., 2008). In a quantitative study of chromosome organization in resting and activated human lymphocytes using cryo-FISH, it was found that different transcriptional profiles correlate with specific changes in CT organization (Branco et al., 2008). These include differences in chromosome intermingling, CT volume and radial position between the two cellular states, indicating an adaptation to the new transcriptional program. Other studies similarly revealed changes in the architecture of CTs during cellular differentiation. For instance, change in chromosome positioning during human adipocyte differentiation (Kuroda et al., 2004), and reorganization of centromeres, chromosomes and gene loci during mouse T-cell differentiation (Kim et al., 2004). These demonstrate the potential impact of higher-order chromatin organization on the regulation of gene expression and silencing during differentiation.

1.1.3 Higher-order Chromatin Organization

The completion of the Human Genome Project has revealed an estimate of 30,000 – 75,000 genes distributed among 3.2 billion base pairs of DNA which is hierarchically packaged into a higher-order chromatin structure (Spector, 2003). Although it has been found that only 1.5% -2% of the DNA in the human genome encodes for proteins, recent studies demonstrate that the rest of the genome is not “junk DNA” as previously suggested but contains elements

linked to important regulatory functions (Ecker et al., 2012). The fundamental repeating subunit of chromatin, nucleosome, consists of 146 base pairs of DNA wrapped in 1.7 superhelical turns around a histone protein octamer of four core histone proteins (H2A, H2B, H3 and H4). The nucleosomal array, “beads-on-a-string” fiber, constitutes the first level of chromatin organization (Li and Reinberg, 2011). The 30-nm chromatin fiber which comprises nucleosomal arrays in a more condensed form is generally regarded as the second structural level of DNA organization. The folding of chromatin fiber continues with increasing DNA-packing density such that the genes are arranged in the cell nucleus among the 46 chromosome territories with accessibility to transcriptional regulators which allow their expression or repression (Dorigo et al., 2004, Li and Reinberg, 2011) (Fig1.4). It is important to realize that the plasticity and dynamics of such higher-order chromatin compaction are crucial in the regulation of transcription as well as other biological processes inherent to DNA (Li and Reinberg, 2011).

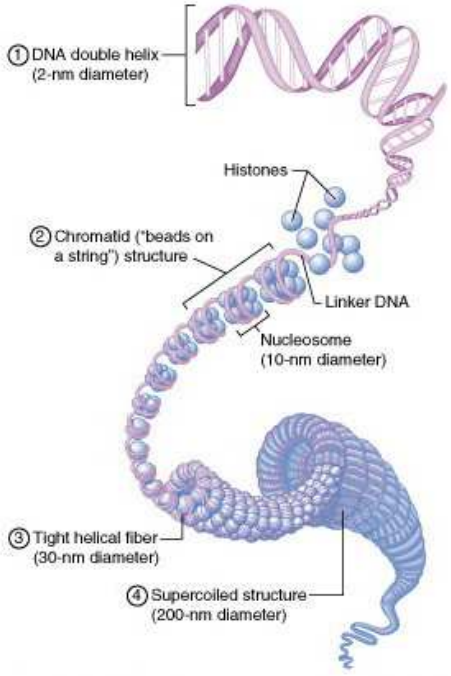

Figure 1.4

The hierarchical packaging of genomic DNA into higher-order chromatin structure with several levels of organization (Adapted from Cummings, 2001).

1.1.4 Chromatin Compaction—Heterochromatin and Euchromatin

Heterochromatin was originally described by the German botanist Emil Heitz as the nuclear regions which stained strongly with basic dyes (Heitz, 1928). Together with euchromatin, they give a qualitative indication of the state of chromatin compaction (Woodcock and Ghosh, 2010) (Fig1.5). Euchromatin refers to the regions of chromatin which are decondensed and tend to be transcriptionally active, with the characteristic nucleosomes enriched in histone H3 trimethylated at lysine 4 (H3K4me3) and H3 acetylated at lysine 9 (H3K9ac) (Takizawa and Meshorer, 2008). Heterochromatin is condensed and normally consists of transcriptionally silent regions. Constitutive heterochromatin tends to be enriched in repetitive DNA sequences such as the highly repetitive pericentric satellite DNA and typically marked by histone H3 trimethylated at lysine 9 (H3K9me3), whereas trimethylation of H3K27 (H3K27me3) is commonly found at facultative heterochromatin, which can reversibly undergo transitions from condensed, transcriptionally inactive to become more open and allow transcriptional activation (Fedorova and Zink, 2008). In general, both constitutive and facultative heterochromatin are found at the nuclear periphery, although the areas surrounding the nucleolus are also preferred sites of heterochromatin assembly. An important feature of heterochromatin is its ability to “spread” or propagate along the chromosome to adjacent regions (Hines et al., 2009). The crowded environment typically found in heterochromatin may associate with more efficient trapping of chromatin binding proteins, which is suggested to facilitate heterochromatin maintenance (Woodcock and Ghosh, 2010).

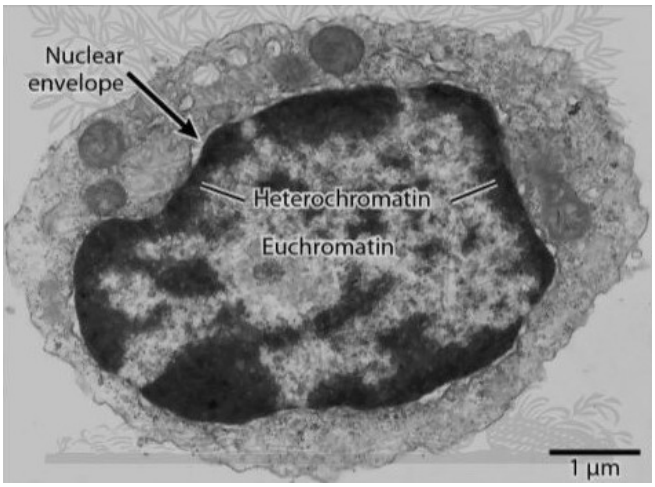

Figure 1.5
Electron micrograph of a lymphocyte. The darkly stained heterochromatin around the periphery and the lightly stained euchromatin in the center are shown. Adapted from (Ovalle and Nahirney, 2007)

1.2 Epigenetic Regulation

The term “epigenetics” was derived from Conrad Waddington in 1942 with the definition as “the branch of biology which studies the causal interactions between genes and their products, which bring the phenotype into being” (Waddington, 1942). With the completion of the human genome sequence, the existence of a more complex non-coding genome becomes apparent in which the organization and regulation may reveal a more thorough understanding of our phenotype (MacDonald and Roskams, 2009). Epigenetics is now more broadly referred as a variety of processes resulting in mitotically and/or meiotically heritable changes in gene function without changing the DNA sequence. However in neurons, the absence of cell division indicates that epigenetics refers to the long lasting and stable regulation of gene expression. Together with regulatory proteins and non-coding RNAs, epigenetic modifications interplay with each other to bring about chromatin remodeling and compartmentalization of the nucleus such as the formation of euchromatin and heterochromatin (Delcuve et al., 2009). Although epigenetic mechanisms are established early during cellular differentiation and development,

alterations in cell signaling in response to intrinsic and environmental stimuli may lead to remodeling of epigenetic marks. These may be further altered in age-related neurodegeneration and other neurological disorders (Meaney and Ferguson-Smith, 2010).

The complex hierarchical organization of the genetic material allows the expression of the encoded genes to be regulated at various levels (Fig 1.6). The first is at the level of DNA sequence including regulatory elements and DNA methylation. The second level includes post-translational modification of histones and nucleosome remodeling at the level of chromatin. The third level includes chromosomal positioning and spatial organization of specific loci within the nucleus (Babu et al., 2008).

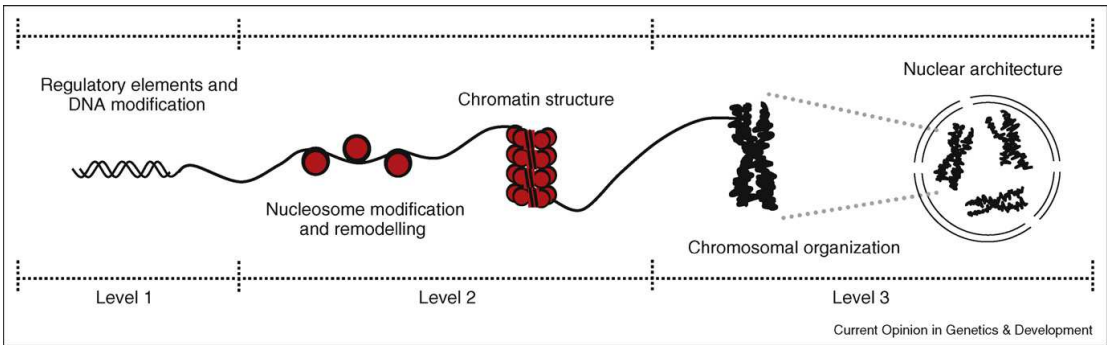

Figure 1.6

Hierarchical organization of the genetic material and the several layers of regulation of gene expression within the nucleus (Adapted from Babu et al., 2008).

1.2.1 DNA Methylation

DNA methylation is one of the best characterized epigenetic modifications which contributes to gene silencing and is crucial to the stability of gene

expression states (MacDonald and Roskams, 2009). In the DNA sequence, a methyl (CH3-) group can be added to the pyrimidine ring of cytosine residues at position 5 (Fig 1.7B). The majority of cytosines preceding guanine (CpG) sites in the human genome are found in non-coding regions which are methylated in order to prevent translocation as well as to maintain chromosomal stability (Urdinguio et al., 2009). Other CpG sites are found in clusters called CpG islands surrounding promoters which comprise 1-2% of the genome. These short CpG-rich regions may escape methylation and thus allow gene expression (Clouaire and Stancheva, 2008, Delcuve et al., 2009). DNA methylation is catalyzed by specific DNA methyltransferases (DNMTs) dividing into two functionally different classes: maintenance methyltransferases and de novo methyltransferases (MacDonald and Roskams, 2009). DNMT1, the primary maintenance methyltransferase, is the most abundant DNMT in somatic cells which associates with the replication fork and acts at hemi-methylated CpGs during DNA replication. Its primary role is therefore to preserve methylation patterns from the parental to the daughter cells. DNMT3a and DNMT3b are de novo methyltransferases which are highly expressed in embryonic and non-differentiated cells. They target unmethylated DNA and establish novel methylation patterns (Espada and Esteller, 2007, MacDonald and Roskams, 2009).

DNA methylation is essential for proper mammalian development and contributes to a variety of cellular functions as well as pathologies. Apart from gene repression, it is also involved in different processes such as genomic imprinting, inactivation of X chromosome in females, suppression of repetitive genomic elements, carcinogenesis and aging (Bird, 2002, Jaenisch and Bird,

2003). Different mechanisms by which methylated cytosines may cause transcriptional repression are posited. A direct mode of repression may be due to its intervention with protein binding to a specific target DNA sequence and in this case transcription factors would be released from the chromatin fiber (Espada and Esteller, 2007). In the second (indirect) model, it is proposed that specific binding of regulatory proteins, methyl-CpG-binding domain (MBD) proteins, to the methylated cytosines may recruit histone deacetylase (HDAC) containing repressor complexes and therefore lead to chromatin condensation (MacDonald and Roskams, 2009, Bird, 2002) (Fig 1.7C).

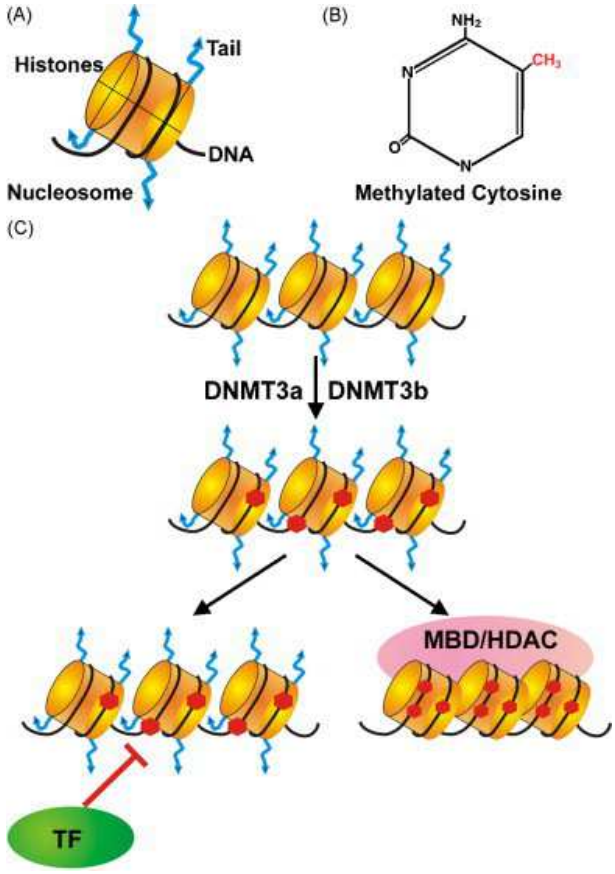

Figure 1.7

Mechanisms of DNA methylation-mediated gene silencing. (A) The basic repeating subunit of chromatin, nucleosome. (B) Methylated cytosine with a methyl group (CH_3 in red) at the 5' position. (C) De novo methyltransferases DNMT3a and DNMT3b catalyze the methylation of cytosine residues. Methylated cytosines (red hexagons) can repress transcription via two distinct mechanisms, either by inhibiting the binding of transcription factors (TF) to the promoter of a gene, or being bound by methyl binding domain proteins (MBD) which recruit repressor complexes with histone deacetylase (HDAC) and result in chromatin condensation. (Adapted from MacDonald and Roskams, 2009)

1.2.1.1 Methyl-CpG Binding Domain Proteins (MBDs)

Methyl-CpG binding domain (MBD) proteins recognize and occupy sites of DNA methylation and act as methylation-dependent transcriptional repressors, linking DNA methylation with chromatin modification (Clouaire and Stancheva, 2008). MBDs establish a repressive chromatin environment by recruiting enzymatic machinery as well as various chromatin modifiers (Bogdanovic and

Veenstra, 2009). Histone deacetylases (HDAC) and histone methylases have been identified as the co-repressor complexes associated with MBDs to mediate chromatin modification and prevention of transcription initiation (Clouaire and Stancheva, 2008).

In mammals, there are currently five MBD family proteins known as MeCP2, MBD1, MBD2, MBD3 and MBD4 (Urdinguio et al., 2009) (Fig1.8). A major action of MBD proteins is to repress transcription via interacting with HDAC-associated complexes, with the exception of MBD4, which appears to be involved in DNA repair. Out of the five classic MBD protein family members, MBD1 is the only one also with the ability to repress transcription from unmethylated promoters through one of its three zinc-coordinating CXXC domains (MacDonald and Roskams, 2009).

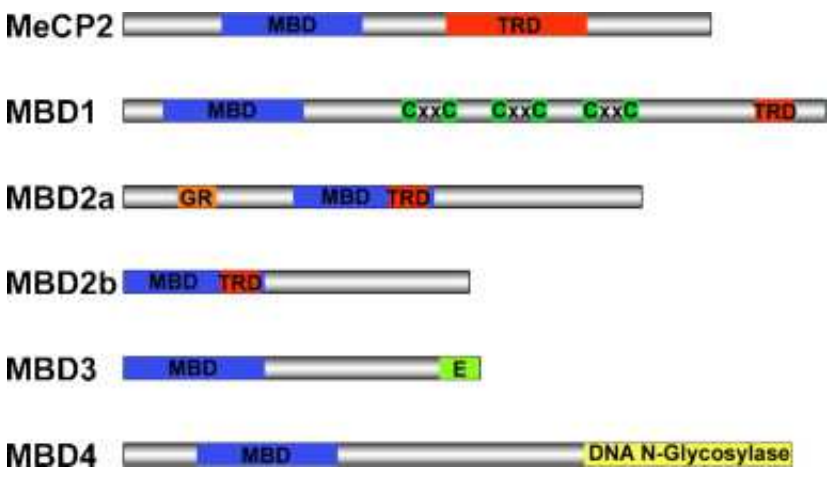

Figure 1.8

The five classic MBD protein family members identified by a conserved MBD (blue). Other main domains of the proteins are indicated such as the common transcriptional repression domain (TRD) and the zinc binding domains (CxxC) of MBD1, through which it interacts with unmethylated DNA and represses transcription. (Adapted from MacDonald and Roskams, 2009)

1.2.1.2 MeCP2 and Rett Syndrome

MeCP2 was first identified by Adrian Bird and co-workers in 1992 as a 53-kDa protein which functions as a transcriptional repressor by recruiting HDAC and Sin3a through its TRD resulting in chromatin silencing (Lewis et al., 1992, Nan et al., 1998, Cohen and Greenberg, 2010). A few years later, Huda Zoghbi and colleagues discovered that MeCP2 mutations cause a progressive neurodevelopmental disorder, Rett syndrome (RTT), a severe X-linked autism spectrum disorder striking mostly girls with a prevalence of ~1/10,000 female live births and represents one of the most common causes of mental retardation in females (Chahrour et al., 2008, Delcuve et al., 2009). Patients with classic RTT have a normal period of post-natal development until 6-18 months of age, at which point development regresses with loss of speech and purposeful hand movements, mental retardation, autistic features, ataxia and apraxia, as well as motor and respiratory abnormalities (MacDonald and Roskams, 2009). A number of different mutations, deletions and rearrangements have been identified in the MECP2 gene and such genetic variability, together with the pattern of X chromosome inactivation resulting in mosaic expression of the mutant gene, give rise to a high level of RTT phenotypic variability. It was found that both loss of function and gain in MECP2 dosage lead to RTT-like clinical symptoms (Chahrour and Zoghbi, 2007). In addition, studies reveal that high levels of MeCP2 are crucial to postnatal neuronal maturation in which case MeCP2 deficiency selectively causes neuronal symptoms and abnormalities in dendritic branching and synapse formation in the brains of RTT patients. The link between MeCP2 dysfunction and defective postnatal neuronal maturation has been further

confirmed by studies with a number of mouse models for RTT (LaSalle, 2004, Delcuve et al., 2009).

Since the discovery of MeCP2 as the gene causing RTT, the understanding of MeCP2 behavior and function has evolved. Despite the long held view that MeCP2 is a transcriptional repressor involved in chromatin remodeling, surprising results from studies with different approaches have re-examined the original hypothesized role of MeCP2 (Lasalle and Yasui, 2009, Cohen and Greenberg, 2010). Recently, mounting evidence has argued against the predominant “enzymatic” model of MeCP2 function and instead an unexpected twist in the understanding of MeCP2 role has emerged from studies which reflect a multifunctional nature of MeCP2. Studies in gene expression profiles of the hypothalamus in MeCP2 mouse models indicated that MeCP2 regulates the expression of many different genes and unexpectedly up to 85% of genes appeared to be activated by MeCP2 (Chahrour et al., 2008). Moreover, it was shown that MeCP2 associates with the major transcriptional activator CREB1 (cAMP responsive element binding protein1) at the promoter of an upregulated gene and therefore suggesting a potential activation mechanism (Chahrour et al., 2008). The view that MeCP2 function extends beyond transcriptional repression was further supported by integrated epigenomic analyses of neuronal MeCP2 which revealed that 63% of MeCP2-bound promoters were actively expressed, however only 6% were highly methylated (Yasui et al., 2007). These together suggested a more predominant role of MeCP2 in the modulation of active genes. Apart from the above, there are indeed other models of MeCP2 functions in the chromatin implicated by various studies which were summarized in Figure 1.9 (Lasalle

and Yasui, 2009).

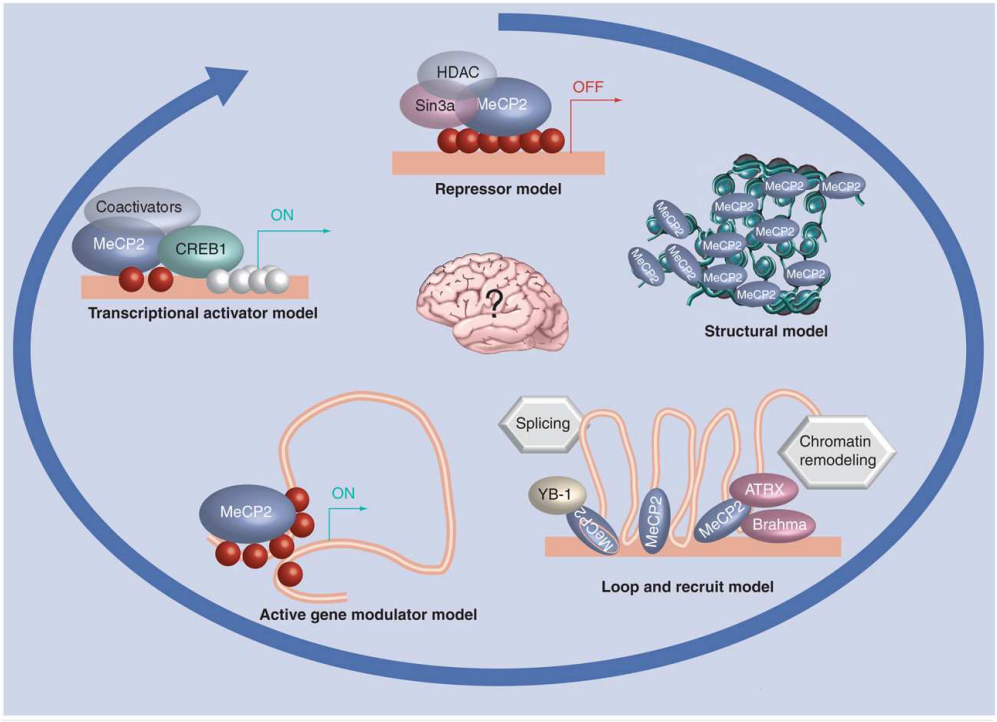

Figure 1.9

The evolving models of MeCP2. The functional role of MeCP2 has been evolving since the "transcriptional repressor" model in the 1990s. A structural model was proposed as MeCP2 was found to make tight bridges and connections between DNA molecules (Georgel et al., 2003). The "loop and recruit" model was then suggested which implicated the involvement of MeCP2 in chromatin loop structure and recruitment of chromatin remodeling and RNA splicing factors (Horike et al., 2005). The "active gene modulator" model was postulated by Yasui and colleagues in 2007 as MeCP2 was shown to bind to actively expressed promoters. A year later, Chahrour and co-workers proposed the "transcriptional activator" model as they discovered the interaction between MeCP2 and the activating factor CREB1 in the mouse hypothalamus. (Adapted from LaSalle & Yasui, 2009)

The main goal among researchers studying RTT has focused on both the identification of MeCP2 target genes and the phosphorylation status of MeCP2. Neuronal activity-dependent phosphorylation of MeCP2 was discovered as a mechanism involved in MeCP2 modulation of gene expression (Chao and Zoghbi, 2009, Tao et al., 2009). In resting neurons, MeCP2 is predominately phosphorylated at serine 80 but dephosphorylated at serine 421, such that

S80 phosphorylation induces binding of MeCP2 to promoters leading to repressed expression of target genes. In contrast, MeCP2 in active neurons is dephosphorylated at S80 but phosphorylated at S421 and this activity-dependent phosphorylation results in its dissociation from the promoters and therefore induces transcription. This dynamic balance between different phosphorylation sites mediates the ability of MeCP2 to regulate specific gene transcription (Zhou et al., 2006, Tao et al., 2009, Chao and Zoghbi, 2009). One of the identified MeCP2 target gene, BDNF (brain-derived neurotrophic factor), has attracted much attention due to its role in neuronal survival and synaptic changes which are fundamental to learning and memory. It was found that phosphorylation of MeCP2 allows it to regulate dendritic patterning, spine morphogenesis as well as activity-dependent induction of BDNF transcription. It appears that the role of MeCP2 in regulating the expression of genes such as BDNF is essential in modulating synaptic function and plasticity (Zhou et al., 2006).

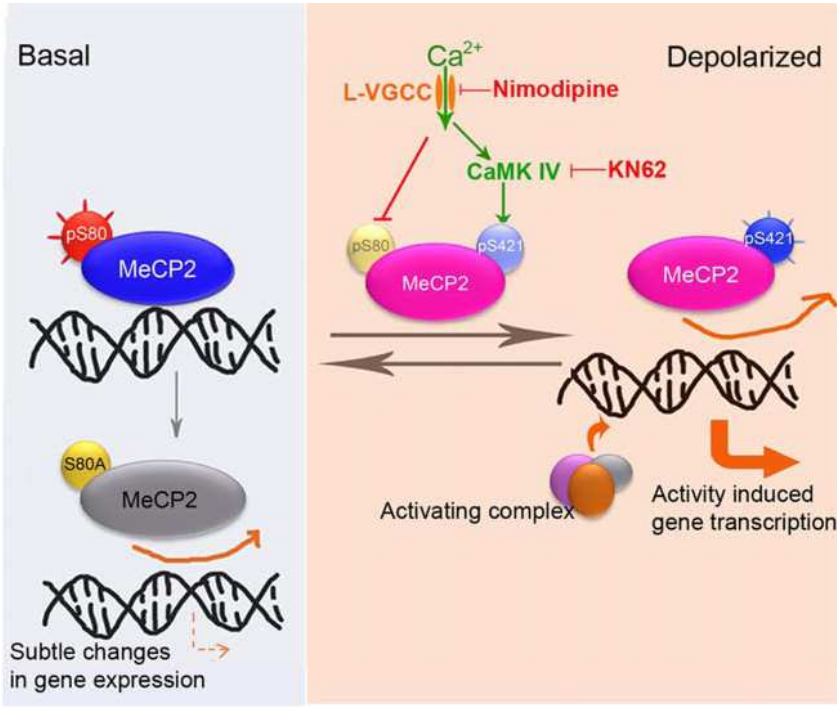

Figure 1.10

Neuronal activity-dependent phosphorylation of MeCP2 and the resultant shift in gene transcription program. In resting neurons, S80 phosphorylation of MeCP2 facilitates binding to promoters and represses transcription. In depolarized neurons, S421 phosphorylation causes MeCP2 to dissociate from promoters and induces gene transcription. S80A phosphorylation-deficient mutation reduces MeCP2 binding to promoters leading to increased gene expression in resting neurons. (Adapted from Tao et al., 2009)

1.2.2 Post-translational Modifications of Histones

The N- and C- terminal tails of the core histones H2A, H2B, H3 and H4 protrude out from the nucleosome and are subjected to a variety of post-translational modifications (PTMs), including acetylation, methylation, phosphorylation, ubiquitination and ADP-ribosylation (Takizawa and Meshorer, 2008, Kiefer, 2007). Histone PTMs are crucial in the epigenetic regulation of genes. Although there is still a lot to explore about their role, they are believed to function in a combinatorial manner to alter or disrupt chromatin structure, and to provide a “code” for recruiting specific non-histone chromosomal proteins or factors to chromatin (Delcuve et al., 2009). Histone PTMs are often

reversible and they are fundamental for the formation of distinct chromatin domains.

1.2.2.1 Chromatin Domain Formation

Acetylation and methylation of histone are the most well-studied epigenetic marks (Fig1.11) H3K4, H3K36 or H3K79 trimethylation results in an open and relaxed chromatin structure, and therefore accessibility of DNA to binding proteins which is the characteristic of euchromatin (Bartova et al., 2008). Acetylation of histones is generally a marker of euchromatin which is associated with chromatin decondensation and transcriptional activation. Histone acetylation is carried out by histone acetyltransferases (HATs) and this action can be reverted by the more recently discovered histone deacetylases (HDACs) (Urdinguio et al., 2009, Bartova et al., 2005). Trimethylation of H3K9, H3K27 and H4K20 contribute to chromatin condensation and transcriptional repression. Methylated H3K9 is recognized and bound by heterochromatin protein 1 (HP1) whereas Polycomb protein binds to methylated H3K27 and these result in silencing of genes (Delcuve et al., 2009, Kiefer, 2007). Histone methyltransferases are responsible for the methylation of histones and such modification can be reversed by histone demethylases. H3K9me3 is a typical marker of constitutive heterochromatin, whereas H3K27me3 specifically marks facultative heterochromatin which can be activated when needed, an example is the inactive X chromosome (Xi) in females (Urdinguio et al., 2009, Takizawa and Meshorer, 2008).

In addition to the dynamics of histone PTMs, core histone can also be

exchanged for a specific histone variant within its own class, which serves as another important mechanism of chromatin remodeling. Examples include the H2A variant macroH2A involved in X chromosome inactivation, and the H3 variant CENP-A localized at the centromeres (Kiefer, 2007). Due to the structural differences between the variants, nucleosome structure and the subsequent binding of transcription factors are affected resulting in chromatin remodulation (Shelby et al., 1997).

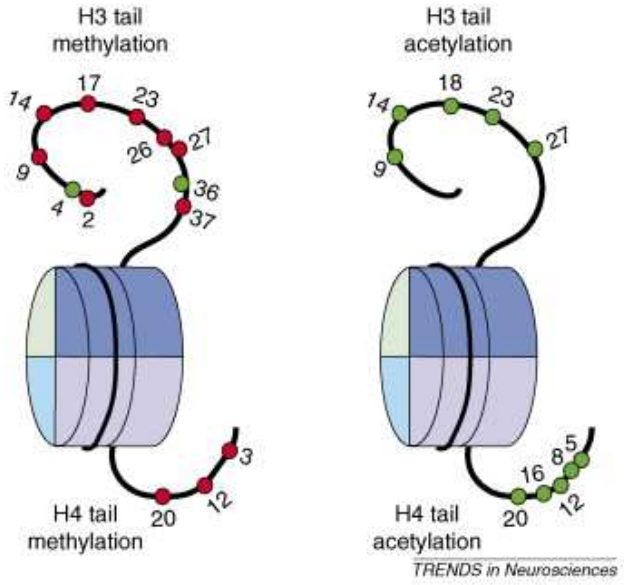

Figure 1.11

Tail methylations and acetylations of histones H3 and H4. Numbers indicate the lysine positions along the histone tails. Histone marks associated with transcriptional activity are denoted by green dots, while red dots denote histone modifications which are correlated with transcriptional silencing. (Adapted from Takizawa and Meshorer, 2008)

1.2.2.2 Histone Deacetylases (HDACs)

HDACs are enzymes that remove the acetyl modifications from core histones and shift them from a negative to a positive charge, which enhance their interaction with the negatively charged DNA. This reaction is reversible

and in general, histone hyperacetylation is associated with increased transcription whereas hypoacetylation (or deacetylation) contributes to repression of gene expression (MacDonald and Roskams, 2009). The classical HDAC family is divided into three phylogenetic classes; class I, II and IV in which members display different patterns of expression (Yang and Seto, 2008). Class I is comprised of small proteins (377-488 amino acids) which includes HDAC1, 2, 3 and 8. These proteins are found almost exclusively within the nucleus (Bjerling et al., 2002, Yang and Seto, 2008). Class II includes HDAC4, 5, 6, 7, 9 and 10 which are larger proteins (669-1215 amino acids) and capable of shuttling in and out of the nucleus in response to cellular signals (Yang and Seto, 2008). Although HDAC11 displays sequence similarity to both class I and II HDACs, it is phylogenetically classified as a separate class which makes it the only member of class IV (MacDonald and Roskams, 2009).

1.2.2.3 Histone Deacetylase Inhibitors (HDACi)

Recent years have witnessed an explosion in the identification and development of HDAC inhibitors (HDACi). A range of naturally occurring and synthetic HDACi were identified, many of which have been investigated for their potential effectiveness as anti-cancer, neuropsychiatric agents, and candidate drugs for neurodegenerative disorders (MacDonald and Roskams, 2009). Studies suggested two important neuroprotective mechanisms of HDACi involved in the pathomechanisms of a number of neurodegenerative diseases. These include transcriptional activation of disease-modifying genes and restoration of proper histone acetylation homeostasis. Both *in vitro* and *in*

vivo analyses have shown promising results and clinical trials have been initiated to further evaluate these epigenetic therapy strategies (Hahnen et al., 2008).

There are four different classes of HDACi which differ in potency and HDAC isoenzyme selectivity. These include the short chain fatty acids, hydroxamic acids, benzamides and cyclic tetrapeptides. The fatty acid class comprises the compounds butyrate, phenylbutyrate and valproic acid (VPA) (MacDonald and Roskams, 2009). VPA has been commonly employed as an anticonvulsant and mood stabilizer which achieved FDA approval in 1987. Its HDAC inhibitory function was discovered in 2001 and various studies have postulated VPA as a class I-selective HDACi with a pronounced activity against HDAC2 at submillimolar doses (Hahnen et al., 2008). A well-studied mode of VPA action is on sodium channels, where it acts at the voltage-dependent Na+ channel and inhibits neurons firing at high frequency. It has also been shown that VPA can reduce sodium conductance and delay recovery from inactivation (Johannessen, 2000). Members of the hydroxamic group include trichostatin A (TSA) and vorinostat (also known as suberoylanilide hydroxamic acid, SAHA). Both TSA and SAHA are potent pan-HDAC inhibitors of class I/II HDACs, and crystallographic modeling has revealed that these HDACi bind directly to the zinc ion in the conserved HDAC catalytic site and thus eliminate the deacetylase activity (MacDonald and Roskams, 2009). Moreover, other studies demonstrated that they have a specific action on gene expression and prominently induce growth arrest, differentiation, apoptotic cell death of transformed cells *in vitro* and *in vivo* (Hockly et al., 2003). SAHA has been approved by the FDA in 2006 for

treating cutaneous T-cell lymphoma. Although it is active at submicromolar concentrations, neither SAHA nor TSA show profound HDAC isoenzyme selectivities. These illustrate that different classes of HDACi differ in their potency and HDAC isoenzyme selectivity (Fig1.12). Regarding the potential treatment of neurodegenerative diseases, the main focus is on the well-established experimental drug TSA as well as the clinically used HDACi including butyrate, phenylbutyrate, VPA and SAHA, which are all known to cross the blood-brain barrier (Hahnen et al., 2008).

Inhibitor	Class I IC_{50}				Class IIa IC_{50}				Class IIb IC_{50}	
	HDAC1	HDAC2	HDAC3	HDAC8	HDAC4	HDAC5	HDAC7	HDAC9	HDAC6	HDAC10
TSA	0.002 µM	0.003 µM	0.004 µM	0.456 µM	0.006 µM	*	0.005 µM	0.006 µM	0.003 µM	*
Vorinostat (SAHA)	0.068 µM	0.164 µM	0.048 µM	1.524 µM	0.101 µM	*	0.104 µM	0.107 µM	0.090 µM	*
Romidepsin (FK-228)	0.036 µM	0.047 µM	*	*	0.510 µM	*	*	*	§	*
redFK-228‡	0.002 µM	0.004 µM	*	*	0.025 µM	*	*	*	0.790 µM	*
Apicidin	§	0.120 µM	0.043 µM	0.575 µM	§	*	§	§	§	*
SNDX-275 (MS-275)	0.181 µM	1.155 µM	2.311 µM	§	§	*	§	0.505 µM	§	*
VPA	1.6 mM	3.1 mM	3.1 mM	7.4 mM	*	*	§	§	§	*

*Not determined.

‡On entering the cell, romidepsin (FK-228) is reduced to its active form, redFK-228.

§No complete inhibition found at doses of 10 µM (romidepsin, apicidin, SNDX-275) or 100 mM (VPA).

HDAC: Histone deacetylases; IC_{50}: Half maximal inhibitory concentration; TSA: Trichostatin A; VPA: Valproic acid.

Figure 1.12

HDAC inhibitors differ in potency and HDAC isoenzyme selectivity. (Adapted from Hahnen et al., 2008)

1.3 Functional Organization of Transcription

Transcription is the crucial step in gene expression, yet it remains challenging to decipher the complex organization of transcription at a cellular level. With the completion of the human and mouse genome sequences and the accumulated data on the mammalian transcriptome, it has become clear that the nucleus is highly organized with particular conformations of the

genome adapted for transcriptional programs and gene expression which are tissue-specific (Chakalova and Fraser, 2010). The way specific genes are arranged in the nucleus is believed to be affected by transcriptional activity and there are observations of genes moving into and out of a chromosome territory which may allow specific loci or sets of genes to engage the transcription machinery. If such machinery is preassembled at high local concentrations, the efficiency of transcription of these coregulated genes relying on the same transcription factors would be much increased (Rajapakse and Groudine, 2011). Indeed, studies on nascent transcripts revealed their localization as discrete sites or foci throughout the nucleoplasm which led to the concept of the transcription factory mode (Jackson et al., 1993, Wansink et al., 1993).

1.3.1 Transcription Factories

Transcription factories were first visualized as discrete nuclear foci of nascent transcripts by *in vivo* pulse-labeling with bromo-uridine (Jackson et al., 1993, Wansink et al., 1993). These studies revealed that transcription did not occur in a uniform manner throughout the nucleoplasm, but in a limited number of discrete sites which were sensitive to transcriptional inhibitors. Moreover, it was shown that RNA polymerase II (RNAPII) accumulated in these transcription factories at much higher concentrations than elsewhere in the nucleoplasm (Iborra et al., 1996a) (Fig1.13). The work by Jackson and co-workers illustrated that the total number of transcription sites were much less than the number of active transcription units, suggesting that multiple genes were present at each site (Jackson et al., 1993). The transcription factory model was therefore coined to reflect the potential assembly of several

transcription units to each factory (Iborra et al., 1996a).

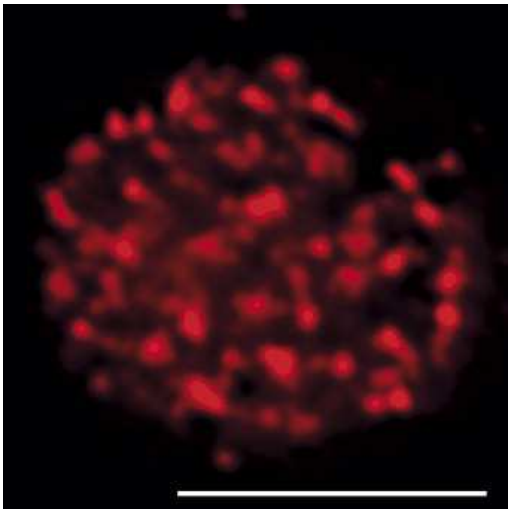

Figure 1.13

Transcription factories visualized as concentrated RNA polymerase foci. Immunofluorescence of hyper-phosphorylated RNA polymerase II in a single optical section of a mouse E12.5 fetal liver nucleus after deconvolution. Scale bar = 5μm. Image courtesy of L. Chakalova. (Adapted from Sexton et al., 2007)

In agreement with this transcription factory model, more recent observations appeared to provide additional support. The classical model of eukaryotic transcription, in which promoter bound factors recruit an RNA polymerase enzyme that slides along the DNA and RNA transcript, has been turned on its head by various studies. These studies demonstrated that it is the DNA template that slides past a polymerase immobilized in a factory (Fig1.14), a concept rather controversial for many as it contradicts the traditional view that the gene is the central scaffold to which other complexes are recruited (Iborra et al., 1996b, Papantonis and Cook, 2011).

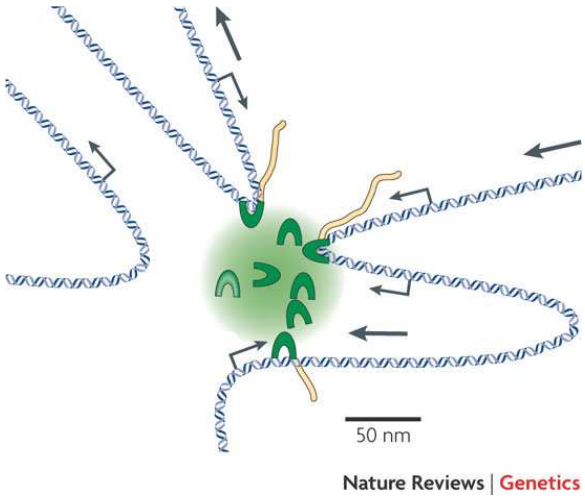

Figure 1.14

Immobilized RNA polymerases within a transcription factory. Eight RNA polymerase II enzymes (green crescents) in a transcription factory with a diameter of ~70nm. Genes are reeled through the polymerases in the direction of large arrows and nascent RNA (yellow) is released as they are transcribed. Small arrows represent direction of transcription at the start site. (Adapted from Sutherland and Bickmore, 2009)

1.3.2 Specialization of Transcription Factories by RNAPI, II and III

Apart from the realization that the active form of RNAPII is compartmentalized into a limited number of discrete factories in the nucleus, other studies further demonstrated the specialization of transcription factories depending on the type of polymerases, promoters, transcription factors and the chromosomal regions present. Indeed, there appears to be clear spatial separation of transcription by RNA polymerases I, II and III in the nucleus. The paradigm for such a spatial organization is the nucleolus, in which nucleolar factories containing RNAPI are dedicated to ribosome synthesis. During interphase, nascent rRNA is localized in the “dense fibrillar component” on the surface of the “fibrillar centre” which contains RNAPI. Newly completed transcripts are processed in the “granular component” and the mature ribosomal subunits then enter the nucleoplasm. This illustrates that a dedicated factory containing the machinery for ribosome synthesis is comprised of a number of active transcription units clustered together (Carter

et al., 2008). Active forms of RNAPII and III are also concentrated in dedicated factories that are localized in mutually exclusive nucleoplasmic regions. In each HeLa cell nucleus containing approximately 90000 nascent transcripts, around 15000, 65000 and 10000 are transcribed by RNAPI, II and III respectively (Pombo et al., 1999).

Only a limited set of genes are transcribed by RNAPI and III. RNAPI transcribes the large rRNA (45S rRNA), whereas RNAPIII synthesizes mainly the small tRNA and 5S rRNA. Other RNAPIII products include the 7SL RNA, U6 snRNA and a number of small stable RNAs, in which many are involved in RNA processing. In contrast, RNAPII transcribes a huge variety of genes (mRNA) that encode proteins and therefore gains most attention. Nevertheless, the activities of RNAPI and III together are responsible for the bulk of RNA synthesis especially in growing cells (Paule and White, 2000).

Evidence from various studies illustrated that the three nuclear polymerases I, II and III active on different genes cluster into their own dedicated factories, such that high local concentrations and efficient interaction can be achieved within these clusters. It is therefore postulated that different regions of the nucleus are specialized in transcribing different types of genes (Cook, 1999, Pombo et al., 1999).

1.3.3 Post-Transcriptional Processing

Following transcription, the main contributor to RNA biogenesis, a series of post-transcriptional processing events such as 5’ capping, splicing and 3’-end

polyadenylation take place which regulate and determine the fate of the RNA transcripts. Studies over the last decade have made it clear that these processes are integrated and coordinated which occur co-transcriptionally in the nucleus (Bentley, 2002, Moore and Proudfoot, 2009). The large number of protein factors required for these nuclear processing steps are recruited to the C-terminal domain (CTD) of RNAPII, the essential domain that has equally important functions in transcription and mRNA processing (Fong and Bentley, 2001). By adding a layer of regulatory information, these post-transcriptional events determine the export, localization and stability of the transcripts, as well as providing an extra level of complexity to our understanding of gene regulation (Hocine et al., 2010).

1.3.3.1 Capping of the 5'-end

The first stage of mRNA processing is capping of the 5’-end of the emerging nascent transcript which involves three enzymatic activities. Occurring early in transcription when the nascent transcript is about 30 nucleotides long, the RNA triphosphatase first removes the 5’ terminal phosphate, the guanylyltransferase then transfers a guanosine 5’-monophosphate to form a 5’-5’-triphosphate linkage which is protected from ribonucleases. 7-methyltransferase subsequently methylates the N-7 position of the new guanine ring such that additional mRNA protection can be achieved (Shuman, 2001). Capping of the 5’-end confers stability. Apart from protecting the transcript from 5’ to 3’ exonucleases, it is crucial in recruiting mRNA to ribosomes. The cap is recognized by protein complexes which assemble on the cap structure, co-ordinate and facilitate downstream processes including

splicing, nuclear mRNA export and translation, thereby enhancing protein synthesis (Shatkin and Manley, 2000).

1.3.3.2 RNA Splicing

Splicing is responsible for the precise removal of non-coding introns from pre-mRNA which is required for proper protein expression. Within exons and adjacent introns, regulatory sequences (*cis* elements) are present and are essential for exon recognition. These elements are recognized by a number of *trans*-acting factors which assemble into a large macromolecular ribonucleoprotein (RNP) complex called the spliceosome (Matlin and Moore, 2007). The spliceosome is a dynamic and multi-component machine that catalyzes splicing through two transesterification reactions and consists of U1, U2, U4, U5 and U6 small nuclear RNPs (snRNPs) together with many other additional proteins (Stark and Luhrmann, 2006). Splicing factors which are non-snRNP proteins are also recruited to the spliceosome for efficient removal of introns (Matlin and Moore, 2007).

In some instances, the same gene can be processed differently by the splicing machinery such that two different protein isoforms are produced as a result of the exclusion of particular exon from the transcript. This process is called alternative splicing and is considered one of the most important generators of functional complexity as well as human proteome diversity given our surprisingly small number of genes (Lee and Irizarry, 2003) (Fig1.15). Up to 92-94% of the genes in the human genome are subjected to alternative splicing and thus also represents serious implications in health and disease. Genome-wide analysis of alternative splicing revealed that the largest set of

tissue-specific alternatively spliced isoforms was found in the brain. Indeed in the nervous system, alternative splicing is crucial for genes involved in information processing and for those encoded proteins with specialized brain functions acting in the synapse (Lee and Irizarry, 2003, Ule et al., 2005). Similar to capping, RNA splicing occurs co-transcriptionally in which the CTD of RNAPII also plays an important role. Several studies demonstrated that phosphorylation of the CTD enabled efficient and accurate splicing by recruiting splicing factors to the nascent transcripts (Hocine et al., 2010).

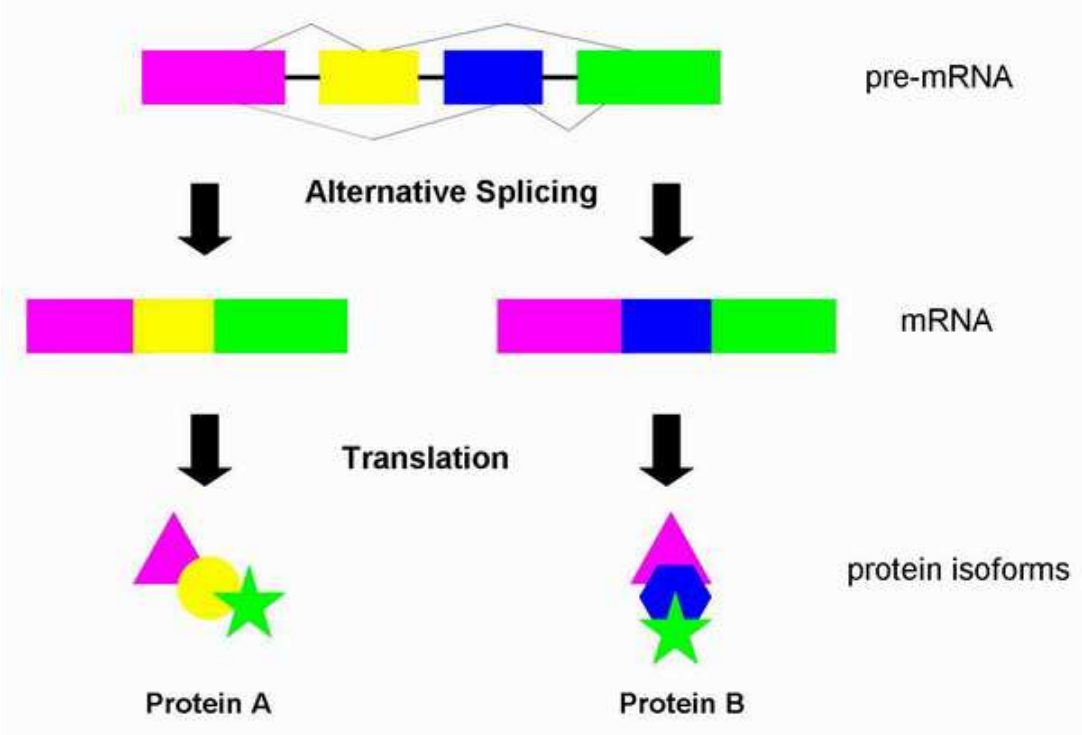

Figure 1.15

A schematic illustration of alternative splicing in which two different protein isoforms are generated from the same pre-mRNA.

1.3.3.3 Polyadenylation of the 3'-end

In order to protect the mRNA against ribonucleases and to increase translational efficiency, the 3’-end is also subjected to post-transcriptional modification which involves endonucleolytic cleavage and addition of a poly(A) tail. Polyadenylation begins with endonucleolytic cleavage occurring 10-30 nucleotides downstream of a signal sequence, a conserved AAUAAA sequence in mammals, and followed by the addition of up to 250 adenine residues to the 3’-end by poly(A) polymerase (Proudfoot, 2004, Shatkin and Manley, 2000). The enzymatic complexes and factors participate in mRNA 3’-end cleavage and polyadenylation are much more complicated as the recognition of polyadenylation signals and poly(A) tail synthesis require a protein machinery with multisubunit factors and numerous polypeptides (Shatkin and Manley, 2000). Moreover, alternative polyadenylation can also alter the stability, localization and transport of RNA transcripts. It has been estimated that such processing occurs in more than half of the genes in human which can be tissue specific and thus have implications in health and disease. Nevertheless, the mechanism and machinery involved in alternative polyadenylation are yet to be explored (Hocine et al., 2010).

As with 5’-capping and splicing, many factors associated with polyadenylation are found to have interaction with the CTD of RNAPII, which therefore suggest that such processing also begins co-transcriptionally and continues after transcription (Shatkin and Manley, 2000). Studies further demonstrated that specific CTD phosphorylation mediates coupling between transcription and 3’-end processing, some of which illustrated that functional

poly(A) signals can facilitate efficient transcription termination (Proudfoot, 2004, Hocine et al., 2010).

1.3.3.4 RNA Editing

Apart from these extensive post-transcriptional processing events, RNA editing of transcripts further increases the transcriptome and proteome diversity. It is considered a crucial mechanism in which environmental signals overwrite information encoded by the genes leading to changes in gene expression and function (Mattick and Mehler, 2008). RNA editing involves alteration of individual bases of the transcripts including nucleotide modifications, deletions and insertions which can alter the sequence and secondary structure with consequences for splicing, interaction with RNA-binding proteins and degradation (Agranat et al., 2008). The most common type of RNA editing mechanism in mammals is the transition from adenosine to inosine (A-to-I) in double stranded RNA by adenosine deaminases acting on RNAs (ADARs) and predominantly these editing sites are found in intronic and intergenic sequences. These non-coding RNAs, for instance microRNAs, are highly important in RNA-mediated regulation of gene expression (Zinshteyn and Nishikura, 2009).

RNA editing is a particularly active process and important in the CNS for modifying RNAs that encode proteins such as neuronal ion channels and pre-synaptic proteins (Jepson and Reenan, 2008). In addition to neural transmission and plasticity, studies have also implicated a role for RNA editing in brain development as well as altered brain functions such as learning and memory (Mattick and Mehler, 2008).

1.4 Nuclear Bodies

The physical and functional organization of the genome into higher order complex structures reveals that the mammalian cell nucleus is a highly organized and dynamic organelle. One prominent feature of the nucleus is its ability to harbor a myriad of distinct subnuclear organelles, nuclear bodies, which provide a multitude of specific functionally compartmentalized environments within the nucleoplasm (Dundr and Misteli, 2001, Mao et al., 2011) (Fig1.16). This compartmentalization paradigm allows the concentration of reactants and substrates required for specific biological processes, such that nuclear bodies can serve as reaction sites to facilitate these reactions efficiently as well as to function as sites for storing or modifying RNAs and proteins (Mao et al., 2011).

Studies have shown that these nuclear bodies are morphologically and molecularly distinct as they carry out specialized nuclear functions. Thus, many of them can be identified by light and electron microscopy as discrete nuclear foci with characteristic patterns of distribution, and with specific protein markers detected by fluorescence microscopy (Dundr and Misteli, 2010, Carmo-Fonseca and Rino, 2011). Nevertheless, nuclear bodies lack a lipid membrane to separate them from the surrounding nucleoplasm. It rather appears that the interactions between proteins and proteins/RNA bring about their structural integrity. Nuclear bodies are dynamically regulated which respond to both normal physiological processes as well as alterations in cellular and metabolic conditions. Understanding their functional connections to the 3D organization of the genome is crucial to decipher the regulation of

gene expression and their relevance in human pathology (Dundr and Misteli, 2010, Mao et al., 2011).

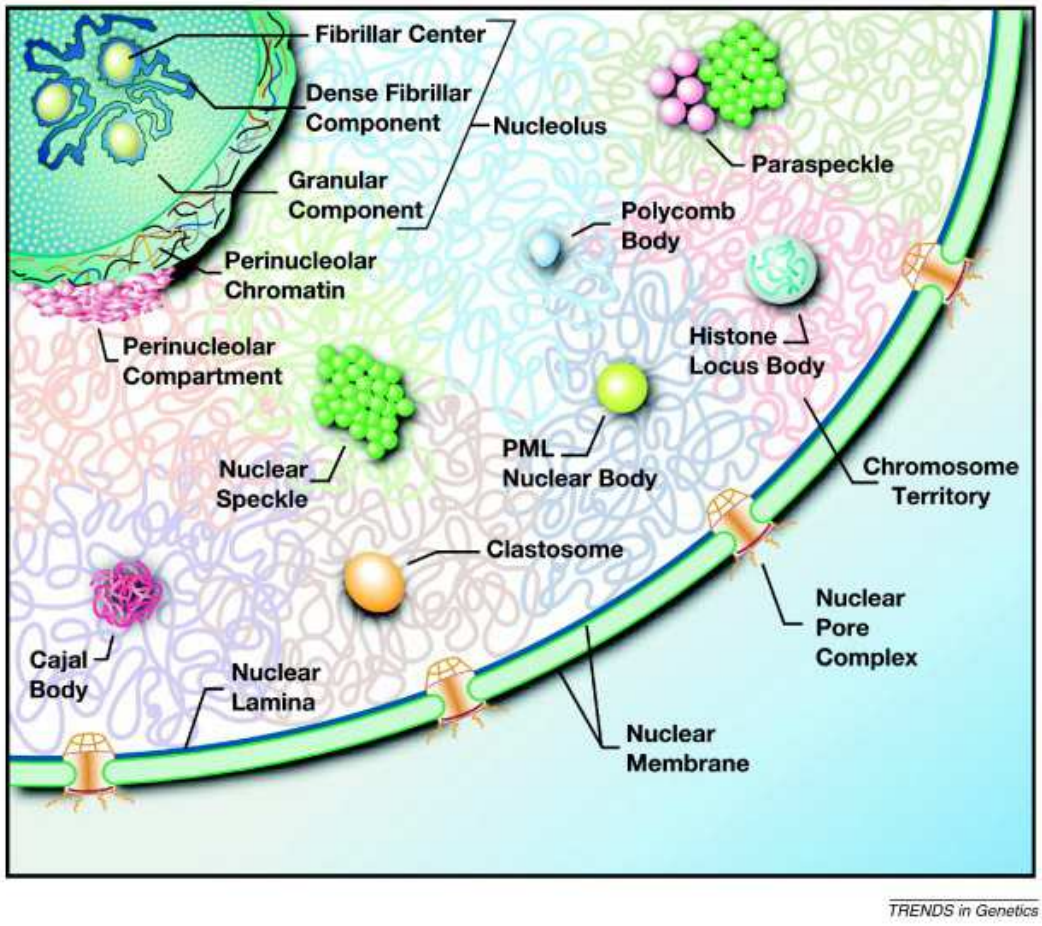

Figure 1.16

A schematic illustration representing the nuclear landscape and the diversity of nuclear bodies in the mammalian cell nucleus during interphase. (Adapted from Mao et al., 2011)

1.4.1 The Nucleolus

The most prominent structure within nucleus is the nucleolus which is the most extensively studied nuclear body and the best-known example of functional nuclear compartmentalization (Sirri et al., 2008). It is organized around clusters of rDNA known as the nucleolar organizer regions (NORs) and is the site for ribosomal RNAs (rRNAs) synthesis, processing and assembly

with ribosomal proteins (Pederson, 2011). Nucleoli in mammals typically exhibit a tripartite organization with three morphologically distinct subregions: fibrillar centers (FCs), dense fibrillar component (DFC) and granular component (GC) (Raska, 2003) (Fig.1.16 and 1.17). Nucleolar organization is intimately linked to ribosome biogenesis in which its function can be reflected by the tripartite architecture; rDNA transcription by RNA polymerase I occurs in the FCs or at the border between the FC and the DFC region; pre-rRNAs are processed by small nucleolar ribonucleoproteins (snoRNPs) within the DFC; pre-rRNP are then matured and assembled with ribosomal proteins in the GC region (Boisvert et al., 2007). The level of rDNA transcription is intricately linked to ribosome biogenesis and hence the requirement of protein synthesis of the cell (Mao et al., 2011).

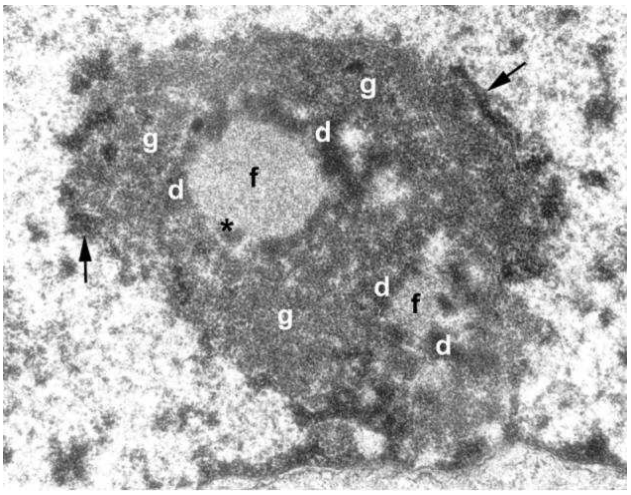

Figure 1.17
The tripartite architecture of the nucleolus. Electron micrograph of a mouse fibroblast nucleolus showing the (f) fibrillar center, (d) dense fibrillar component and (g) granular component. Asterisk denotes dense fibrillar components clump in fibrillar centers. Arrows indicate perinucleolar heterochromatin. (Adapted from Raska, 2003)

Other functions of the nucleolus have been described apart from rRNA synthesis. The nucleolus is implicated in the processing and nuclear export of certain RNAs, as well as the assembly and maturation of multiple RNP complexes including telomerase RNA, signal recognition particle RNA and

microRNAs. Post-translational modifications of a number of nuclear proteins, regulation and coordination of multiple aspects during the cell cycle have also been associated with the nucleolus (Pederson, 2011). Furthermore, the nucleolus senses stress and plays an essential role in coordinating the stress response. One important example is the stress-induced regulation of the tumor suppressor protein p53 which has been intensively studied (Boulon et al., 2010). Specific changes in the morphology and composition of the nucleolus in response in many forms of stress have also been reviewed.

The nucleolus is characteristically surrounded by a shell of highly condensed chromatin known as the perinucleolar heterochromatin (Fig1.16) which contains clusters of rDNA as well as satellite DNA surrounding the NORs (Zhao et al., 2009). The perinucleolar region also contains a number of other nuclear bodies including the perinucleolar compartments (PNC) and the Sam68 nuclear body (SNB) whose functions are yet to be determined. A range of RNA-binding proteins have been found in both PNC and SNB and additionally the PNC also harbors nascent pol III transcripts (Mao et al., 2011). More details regarding the perinucleolar region will be discussed in the following section. In summary, the nucleolus is now increasingly recognized as a plurifunctional organelle. Apart from rRNA synthesis, it is the site for assembling and modifying different RNAs/RNPs, and is further involved in the regulation of proteins which are crucial in multiple aspects of cell cycle progression and many forms of stress (Pederson, 2011).

1.4.2 Perinucleolar Heterochromatin

Perinucleolar heterochromatin (PNH) is the highly compact region of chromatin surrounding the nucleolus that contains satellite DNA and clusters of silent rDNA (Fig1.16). Such perinucleolar localization appears to provide a unique compartment for establishing and preserving the silent state of genes. Condensation of the highly repeated rDNAs into PNH prevents recombination therefore maintaining rDNA stability (Zhao et al., 2009).

In fact, studies have illustrated that the perinucleolar region is associated with the silencing of non-ribosomal genomic regions. For instance, in X-chromosome inactivation, 80%-90% of the inactive X chromosome (Xi) is targeted to this perinucleolar region during S phase which is dependent on the long non-coding RNA (lncRNA) Xist. It is also postulated that the Xi has to continuously visit this distinct region in order to maintain its silencing epigenetic state (Zhang et al., 2007). Another lncRNA has also been implicated in transcriptional silencing of chromosomal domains by targeting them to the perinucleolar compartment enriched in heterochromatic machinery. The lncRNA Kcnq1ot1 targets the imprinted chromatin domain to the perinucleolar region during mid S phase resulting in long-range bidirectional silencing (Mohammad et al., 2008). Interestingly, studies in the yeast *Saccharomyces cerevisiae* demonstrate that tRNA gene-mediated silencing is also dependent on perinucleolar localization, in which RNA pol II transcription is antagonized by nearby RNA pol III transcribed tRNA genes (Wang et al., 2005). Taken together, the perinucleolar localization acts as a fundamental mechanism in the establishment and maintenance of the repressive epigenetic

states of various chromosomal regions including the Xi, imprinted chromatin domains as well as other heterochromatic domains (Mao et al., 2011).

The perinucleolar region additionally harbors the perinucleolar compartment (PNC) with an unknown function (Fig1.16). Despite the physical association with the nucleolus, there are little to no known nucleolar factors or ribosomes synthesized within the structure. A number of studies illustrate that the PNC is enriched with nascent small RNA pol III transcripts and RNA binding proteins primarily involved in pre-mRNA processing which suggest a role in RNA metabolism (Pollock and Huang, 2009). It has been shown that continuous RNA pol III transcription is crucial for the structural integrity of the PNC and remarkably its prevalence is closely correlated with the malignant state of various types of cancer cells. Recent studies suggest that increased expression of RNA pol III transcripts such as tRNAs and 5S rRNA plays a direct role in driving cell proliferation and oncogenic transformation and thus may serve as a potential marker for cancer diagnosis and anti-cancer drug selection (Pollock and Huang, 2009, Marshall et al., 2008).

1.4.3 The Cajal Body

The Cajal body (CB) was originally described by Ramon y Cajal back in 1903 as a small spherical structure within the nucleus of various neurons which he named the nucleolar “accessory body” (Cajal, 1910). Using the silver nitrate method he developed, Cajal noticed that this nuclear structure appears as a separate entity which can be clearly distinguished from other intranuclear components by its size and silver staining properties (Fig1.18). The accessory

body however attracted little attention following Cajal's characterization until the 1950s when Barr and colleagues started to investigate the organization of the accessory body and performed quantitative analysis of its incidence and provided the first evidence of its dynamic behavior following changes in gene expression (Nayyar and Barr, 1968). With the introduction of electron microscopy, ultrastructural studies of the nucleus including the accessory body became possible. Monneron and Bernhard performed such studies of the interphase nucleus in mammalian cells in which they reported a nuclear component comprised of coiled threads of dense material and called it the "coiled body" (Monneron and Bernhard, 1969). It was later on confirmed that the accessory body Cajal discovered was indeed the coiled body observed under electron microscopy (Lafarga et al., 2009). It was not until 1999 that the nomenclature "Cajal body" was adopted by Gall, almost 100 years after its first description by Cajal (Gall, 2000).

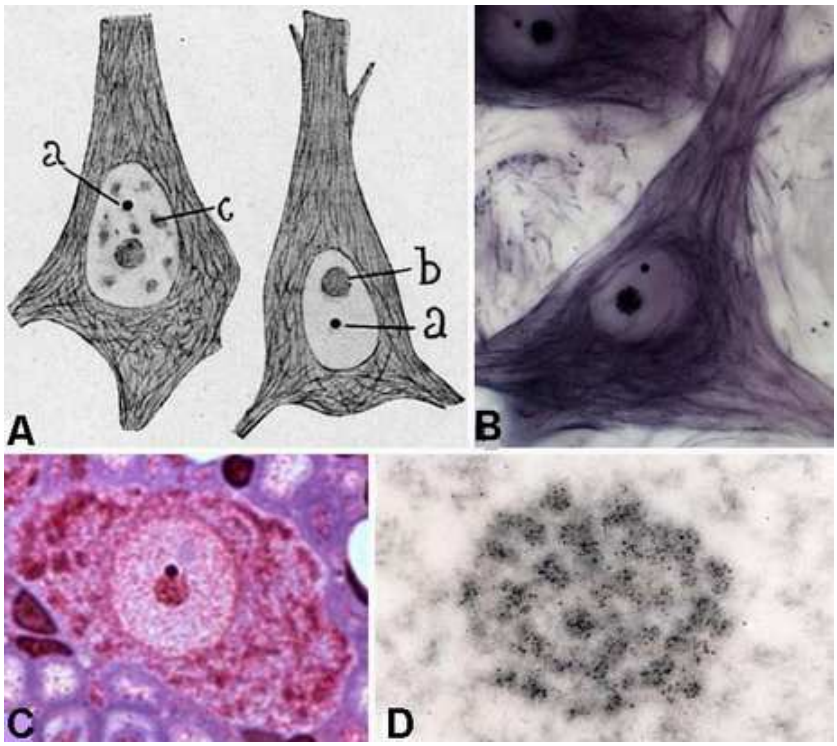

Figure 1.18

The Cajal body. A) Cajal's original drawing of the pyramidal neurons in the human cerebral cortex illustrating (a) the accessory body, (b) nucleolus, (c) nuclear speckles and neurofilaments in the cytoplasm. B) Neuron stained with the reduced silver nitrate method developed by Cajal revealing the nucleolus, Cajal body and neurofilaments. C) Sensory ganglion neuron stained using the reduced silver nitrate method and counterstained with cresyl violet demonstrating the different silver affinity of the nucleolus and the Cajal body. D) The Cajal body (coiled body) of a silver stained Purkinje neuron under electron microscopy in which the coiled threads are clearly decorated with silver precipitates. (Adapted from Lafarga et al., 2009)

The identification of p80 coilin as the principal marker protein using human auto-antibodies marked the modern era of CB research, which has since been used almost exclusively in studies to label the CB in mammalian cells (Andrade et al., 1991). The coiled threads of coilin were found to be essential for the integrity and function of CB. Through interacting with and concentrating the components of other proteins in the CB, coilin enhances the efficiency of a number of nuclear processes (Morris, 2008). The most prominent example is

the modification and assembly of small nuclear RNP (snRNPs), in which some of the newly assembled snRNPs eventually form the RNA splicing machinery and spliceosome (Mao et al., 2011). During the last decade, studies on the CB function have been greatly influenced by the discovery of the survival motor neuron protein (SMN) as an important component of the CB. SMN is essential for proper functioning of motor neurons in mammals, particularly those in the spinal cord and deficiency of this protein leads to the inherited neurodegenerative disease spinal muscular atrophy (SMA). It has also been shown that SMN plays a critical role in the assembly of spliceosomal snRNPs in the cytoplasm and their transport to the CB in the nucleus (Morris, 2008, Nizami et al., 2010).

Apart from p80 coilin and SMN, a number of molecular components involved in transcription, processing and splicing of RNAs are also localized in the CB. For instance, the five major splicing snRNPs U1, U2, U4, U5, U6 and their associated proteins as well as the nucleolar components fibrillarin and Nopp140 (Cioce and Lamond, 2005, Lafarga et al., 2009). The CB has been implicated in several important cellular processes and one of the best-understood functions is the assembly and modification of snRNPs and snoRNPs (Lafarga et al., 2009). It is also suggested to take part in the final steps of snRNP maturation and to facilitate the formation of high-order complexes from individual snRNPs (Morris, 2008, Nizami et al., 2010). Furthermore, studies in cultured cells reported that a group of CB-specific RNAs (scaRNAs) are present in the CB which are important for post-transcriptional modifications e.g. methylation and pseudouridylation of snRNAs (Darzacq et al., 2002). These modifications however may occur

even in the absence of CBs, suggesting the role of CB in promoting the efficiency and specificity of snRNP assembly and modification by locally enriching the reactants, while this might not be essential under normal physiological condition but becomes crucial in particular stress or pathological conditions (Nizami et al., 2010).

Despite the idea that CBs are storage sites for many components involved in various important cellular processes due to their specific CB localization, evidence has shown that the CBs are also dynamic structures in many ways. Studies reported that CB abundance is influenced by snRNP levels, changes in transcription and RNA processing rates in the nucleus. Interestingly, the nuclei of certain cell types in adult tissues for instance, smooth and cardiac muscle cells and skin cells may completely lack CBs (Morris, 2008). In cultured cells, CBs are identified as highly mobile structures which can move freely throughout the nucleoplasm (Platani et al., 2000). Fluorescence recovery after Photobleaching (FRAP) studies also implicate a continuous traffic, interaction and exchange of proteins such as SMN and coilin between CBs and the nucleoplasm (Sleeman et al., 2003). Furthermore, CBs disassemble during mitosis and do not reform until G1 phase after reinitiation of transcription (Carmo-Fonseca et al., 1993). Therefore taken together, it is postulated that the CBs are kinetic nuclear structures in which their assembly and formation may be regulated in interphase and mitosis (Morris, 2008).

1.4.4 Nuclear Speckles

Nuclear speckles are among the most widely studied nuclear domains which are also known as interchromatin granule clusters as they are found in the interchromatin regions of the nucleus (Spector and Lamond, 2011). They were first described based on their distinct morphology. Under immunofluorescence microscopy, they generally appear as 20-50 irregularly shaped domains of varying sizes and such punctate nuclear localization pattern is termed a “speckled pattern” (Fig1.19). Speckles are regarded as the compartment for storing and modifying the splicing machinery and are enriched in pre-mRNA splicing factors including snRNPs, spliceosome subunits and other non-snRNP splicing factors such as the serine/arginine-rich (SR) proteins (Mao et al., 2011).

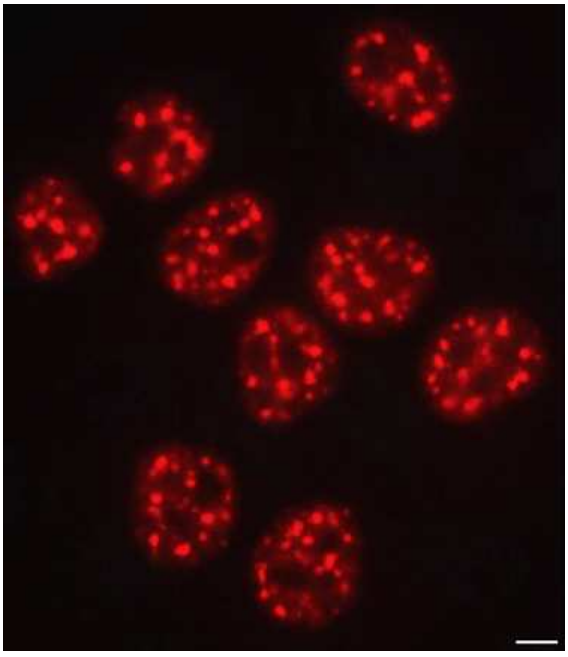

Figure 1.19

Nuclear speckles in the interchromatin space in HeLa cells, demonstrating a punctate nuclear localization of splicing factors in a speckled pattern throughout the nucleoplasm. Scale bar = 5 μm. (Adapted from Spector and Lamond, 2011)

Speckles are dynamic organelles with varying size, shape and number between different cell types and within a cell type, depending on the level of gene expression and the availability of active splicing and transcription factors (Spector and Lamond, 2011). Studies have provided evidence for the dynamic organization of splicing factors during viral infection when transcription levels are high, which is correlated to the status of viral gene expression (Bridge et al., 1995). In the infected cells, splicing factors redistribute to nucleoplasmic transcription sites and their accumulation in the speckles is reduced. Therefore, some of the speckle components can exchange continuously with the nucleoplasm as well as active gene loci (Spector and Lamond, 2011).

A number of poly(A)$^+$ RNAs have been found to be localized in speckles, and a recent study revealed that one such nuclear-retained long non-coding RNA (lncRNA) Malat1, metastasis-associated lung adenocarcinoma transcript 1, is enriched in speckles (Bernard et al., 2010). Knock-down studies suggested that Malat1 is crucial for splicing factor dynamics which has been shown to recruit SR family splicing factors to the transcription site of a gene expression array (Hutchinson et al., 2007). Other studies have also implicated Malat1 in pre-mRNA splicing and processing (Bernard et al., 2010, Mao et al., 2011).

It has been observed previously that speckles are very close to many active genes and indeed some particular genes are identified surrounding a nuclear speckle. It is therefore postulated that nuclear speckles can serve as hubs for enhanced mRNA metabolic activity and gene activation (Shopland et al., 2003). Nevertheless, it remains to be explored and confirmed whether the

active genes move together while recruiting numerous splicing factors and thus appear as a speckle, or if there is an actual movement of genes to an existing speckle (Mao et al., 2011). In summary, nuclear speckles are regarded as the sites for storing and modifying splicing factors which are recruited to active genes located at other nuclear sites or the periphery of speckles. Such proximity between speckles and splicing factors may enhance the splicing efficiency of some particular genes (Shopland et al., 2003, Mao et al., 2011).

1.4.5 Paraspeckles

Paraspeckles are one of the most recent classes of subnuclear bodies identified in the mammalian cells in 2002. These newly identified structures were found diffusely distributed within the nucleoplasm and enriched in about 5-20 subnuclear foci (Fox et al., 2002). These foci were detected in the interchromatin space as discrete bodies adjacent to nuclear speckles and thus were named “paraspeckles” and the novel protein found within this nuclear domain was then named “Paraspeckle Protein 1” (PSPC1) (Fox and Lamond, 2010) (Fig1.20).

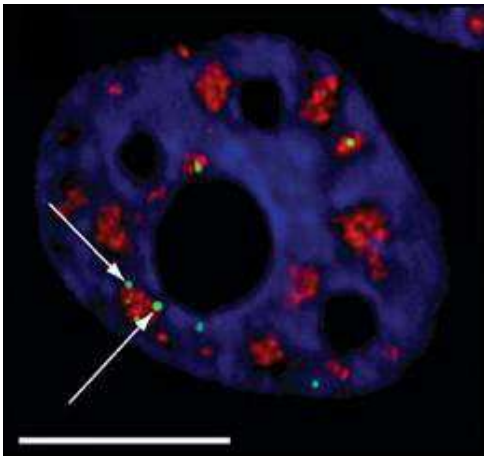

Figure 1.20

Fluorescence micrograph of a HeLa cell stained with anti-SC35 (red), anti-PSPC1 (green) and DAPI (blue) illustrating the localization of nuclear speckles (red) and paraspeckles (green) in the interchromatin space. Scale bar = 10 μm. (Adapted from Fox and Lamond, 2010)

Paraspeckles are punctate RNA-protein structures associated with the nuclear retention of hyperedited mRNAs (Souquere et al., 2010). The core paraspeckle proteins are the members of the DBHS (*Drosophila* Behavior Human Splicing) family: P54NRB/NONO, PSPC1 and PSF/SFPQ. These proteins are found to interact with an lncRNA, *NEAT1/Menε/β*, which acts as an important structural scaffold for the *de novo* assembly of paraspeckles (Fox and Lamond, 2010). This is the first description of an lncRNA with a function in the formation of nuclear body and studies illustrate that *NEAT1* is the limiting factor in the formation of paraspeckles as their prevalence is correlated to *NEAT1* expression levels (Souquere et al., 2010). Paraspeckles may contribute to the control of gene expression through a mechanism in which RNA transcripts with double-stranded RNA regions are subject to adenosine-to-inosine editing and retained in the nucleus within paraspeckles. This mechanism associated with the formation of paraspeckles has been reported in a number of endogenous genes and exogenously expressed genes, which provides an important paradigm for the role of nuclear-retained RNA transcripts in the regulation of gene expression during several cellular processes such as differentiation, viral infection and stress responses (Prasanth et al., 2005, Fox and Lamond, 2010).

Despite the fact that there are no examples of diseases found to be associated with the absence or presence of paraspeckles, there are however a number of RNA dominant disorders linked with the production of toxic nuclear RNAs (Osborne and Thornton, 2006). The most prominent example is the neuromuscular disorder myotonic dystrophy, in which expanded RNA transcripts from the mutated genes are retained in the nucleus as small

aggregates. These aggregates form hairpin structures and sequester the splicing regulator muscleblind-like proteins resulting in the misregulation of alternative splicing of several transcripts (Klein et al., 2011, Osborne and Thornton, 2006). This presents intriguing parallels to paraspeckles which involve specific RNA-protein interactions, nuclear retention of RNA and regulatory splicing activities of the proteins. Such parallels implicate the common themes in nuclear RNA retention both under normal cell conditions and in diseases (Fox and Lamond, 2010).

1.5 The Neuronal Nucleus and Neurodegenerative Diseases

There is now a growing consensus that the neuronal nucleus is implicated in many neurological diseases and studies have shown that dysregulation within the neuronal nucleus including alterations in a number of nuclear bodies are associated with these diseases. Loss of the survival motor neuron (SMN) gene is observed in patients with spinal muscular atrophy (SMA), a progressive and fatal neurodegenerative disease resulting in muscle wasting and paralysis (Zimber et al., 2004). Mutation in the methyl-CpG binding protein 2 (MeCP2) gene causes the neurodevelopmental disorder Rett syndrome (RTT) characterized by a range of neuropsychiatric abnormalities including motor and cognitive impairment affecting girls almost exclusively (Chahrour et al., 2008). Abnormal pathological inclusions in the neuronal nucleus are also present in many of the CAG repeat expansion diseases such as Huntington's disease (Davies et al., 1997) and spinocerebellar ataxia (Paulson et al., 1997).

Here, I shall focus on the neurodegenerative diseases Huntington's disease (HD), amyotrophic lateral sclerosis/frontotemporal lobar degeneration (ALS/FTLD) and frontotemporal dementia with parkinsonism-17 (FTDP-17) in which studies are carried out in this project with mouse models of these diseases.

1.5.1 Huntington's Disease

Nuclear subdomains such as the nucleolus, CB and nuclear speckles have been implicated in polyglutamine (polyQ) diseases caused by expansion of CAG trinucleotide repeats in which the nucleus is the major site for polyQ toxicity. There are a variety of polyQ diseases including many spinocerebellar ataxias (SCAs): SCA1, SCA2, SCA3, SCA6, SCA7, SCA12 and SCA17, as well as spinal and bulbar muscular atrophy (SBMA) and Huntington's disease (HD). HD is the most common among the group with well-documented alterations within the nucleus (DiFiglia et al., 1997, Davies et al., 1997). HD is a dominantly inherited neurodegenerative disease caused by an expansion of a CAG repeat in exon 1 of the HD gene, leading to a long polyQ tract in the encoded protein huntingtin (htt) (HDCR, 1993). It affects approximately 1 in 10,000 people and is clinically characterized by a progressive chorea and a mental decline which ultimately leads to dementia and death. Studies have illustrated neuronal dysfunction and neurodegeneration in HD associated with a prevalent loss of medium spiny neurons which constitute the majority of striatal neurons (Reiner et al., 1988), though recently more widespread degeneration has been found occurring in the brain including the cortical regions. Several mechanisms accounting for the neuronal death caused by the mutant htt protein have been proposed. However, the exact mechanisms

on how this mutant protein results in the specific neuronal degeneration and pathological changes despite its ubiquitous expression in the brain and body remain unclear.

There is a preponderance of evidence suggesting an alteration of gene expression and hence transcriptional dysregulation as the central mechanism underlying neuronal dysfunction in HD. The pivotal role of transcriptional dysregulation has been implicated by the subcellular localization of the mutant htt protein in HD. Immunocytochemical studies showed that the proteolytic N-terminal fragments of mutant htt are found in both the cytoplasm and the nucleus as insoluble inclusions in the brains of R6/2 transgenic mice, the disease models of HD, whereas wild type htt is found mostly in the cytoplasm associating with cytoplasmic granules and microtubules (Davies et al., 1997). Immunoreactivity of htt in the transgenic mice demonstrated the appearance of “densely stained circular inclusion” within the neuronal nuclei, and such neuronal intranuclear inclusion (NII) could also be labeled with anti-ubiquitin antibodies (Davies et al., 1997). This distinctive labeling of NIIs was observed in various parts of the CNS such as the cerebral cortex, striatum, cerebellum and the spinal cord in transgenic mice exhibiting the neurological phenotype. At the ultrastructural level, EM studies revealed that these inclusions were accumulated within a specific nuclear region which is quite distinct from the nucleolus, CB and the surrounding heterochromatin (Davies et al., 1997) (Fig1.21). Other morphological changes in the nucleus apart from the NII were detected including prominent indentations of the nuclear membrane, increased clustering of nuclear pores and condensation of chromatin (Davies et al., 1997, Davies et al., 1999) (Fig1.21). The appearance of these NIIs as

well as nuclear abnormalities were found to be similar to those observed in HD post-mortem tissues (DiFiglia et al., 1997). A role for transcriptional dysregulation in HD has been postulated by the specific localization of the mutant htt in the nucleus and in fact, these NIIs also represent a pathologic hallmark for other polyQ diseases (Zoghbi and Orr, 2000).

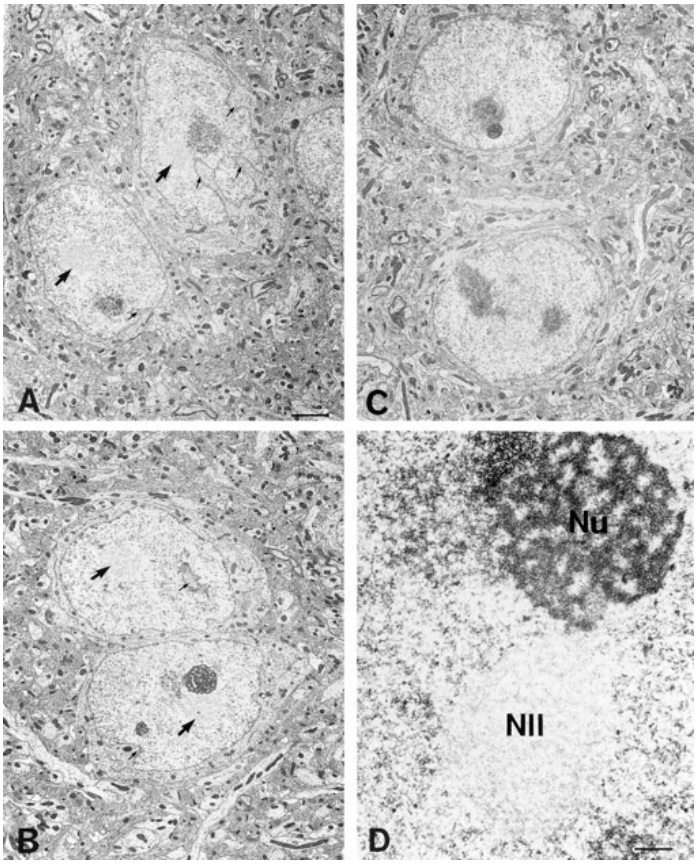

Figure 1.21

Neuronal intranuclear inclusions (NIIs). A and B) Under conventional EM, NIIs (large arrows) together with frequent indentations of the nuclear membrane (small arrows) were found in the striatal neuronal nuclei. C) A typical striatal neuron with a smooth nuclear profile without any inclusion. D) The NII as a pale staining structure distinctive from the darkly stained nucleolus (Nu) and the surrounding heterochromatin. Scale bars in A-C =2 μm and in D = 200nm. (Adapted from Davies et al., 1997)

Tremendous progress with respect to gene expression studies has been made using transgenic mouse and cellular models of HD and further in human HD which provide more direct evidence for transcriptional abnormalities in HD

(Cha, 2007). In line with earlier findings demonstrating a decrease in specific mRNA species in the striatal neurons of post-mortem human HD brain, studies in gene expression in the R6/2 mice confirmed the altered mRNA levels of D1 and D2 dopamine receptors preceding the development of clinical symptoms (Cha et al., 1999). These are further supported by other studies showing transcriptional dysregulation in a number of animal models and human samples (Cha, 2007, Buckley et al., 2010).

Apart from the mutant protein htt, a toxic role for the mutant expanded CAG repeat transcripts has also been suggested by recent studies. In human HD fibroblasts, It was demonstrated that these transcripts are retained in the nucleus and adopt a double stranded RNA (dsRNA) hairpin-like structure which interact abnormally with dsRNA-binding proteins, such as the splicing factor muscleblind-like 1 (MBNL1), and thus result in the loss of a normal function in RNA regulation. In addition, a greater silencing efficiency and cleavage by a CAG repeat-targeting siRNA was found in mutant transcripts compared with normal transcripts (de Mezer et al., 2011). Misregulation of alternative splicing caused by the sequestration of MBNL1 with nuclear inclusions containing the mutant transcripts has been demonstrated by another study implicating its potential contribution to the pathology of polyQ diseases (Mykowska et al., 2011).

There is now an increasing awareness that ncRNAs are crucial for the regulation of gene expression. Indeed, a parallel dysregulation of ncRNAs such as microRNAs is suggested to play a role in neurodegenerative disorders including HD (Buckley et al., 2010). In both murine models of HD and human

HD brain tissues, studies demonstrated that the expression of multiple neuronal-specific microRNAs is decreased, which might be associated with an increased repression by RE1 Silencing Transcription Factor (REST) (Johnson et al., 2008b). Another important study illustrated a direct role of mutant htt in gene silencing activity by microRNAs, in which both exogenous and endogenous microRNA silencing are greatly impaired (Savas et al., 2008). These indicate that the molecular pathology of HD may include dysregulation of both transcriptional and post-transcriptional mechanisms (Buckley et al., 2010).

More recently, the idea of epigenetic dysregulation in HD has gained much more attention and there are strong indicators of epigenetic changes preceding the appearance of symptoms in animal models of HD. Aberrant levels of histone acetylation and methylation in R6/2 mice and HD brain were reported in various studies, which showed a decreased levels of histones H3 and H4 acetylation but an increase in H3K9 methylation (Ferrante et al., 2003, Ryu et al., 2006). In fact, targeting histone deacetylase (HDAC) activity by using HDAC inhibitors has become a major platform for HD therapeutic development (Buckley et al., 2010). Various studies have demonstrated the use of HDACi such as sodium butyrate, phenylbutyrate and SAHA in the attenuation of neuronal loss, motor dysfunction and increased survival in R6/2 mice (Hockly et al., 2003, Ferrante et al., 2003). These suggest that the altered epigenetic signatures in HD may be corrected and this ameliorates some aspects of gene dysregulation resulting in the behavioral recovery observed.

1.5.2 Amyotrophic Lateral Sclerosis/Frontotemporal Lobar Degeneration

It is now established that the transactive response DNA-binding protein with a Mr of 43kDa (TDP-43) is the critical disease protein associated with the pathogenesis of amyotrophic lateral sclerosis (ALS) and frontotemporal lobar degeneration with ubiquitin-positive inclusions (FTLD-U), now known as FTLD-TDP (Geser et al., 2010). Recent advances in the understanding of TDP-43 and its role in neurodegeneration have verified that ALS and FTLD-TDP are multi-system diseases and a novel disease concept of TDP-43 proteinopathy is established. TDP-43 proteinopathies encompass a spectrum of disease that align along a broad disease continuum with shared disease mechanisms linked to pathological TDP-43, in which ALS and FTLD-TDP represent two ends of the spectrum (Chen-Plotkin et al., 2010).

TDP-43 is a predominantly nuclear protein encoded by the *TARDBP* gene on chromosome1 which can shuttle between the nucleus and cytoplasm. Although its physiological function is yet to be fully characterized, studies have demonstrated that it can bind to both DNA and RNA and has several roles in regulating transcription and RNA processing (Ayala et al., 2008b, Ito and Suzuki, 2011) (Fig.1.22).

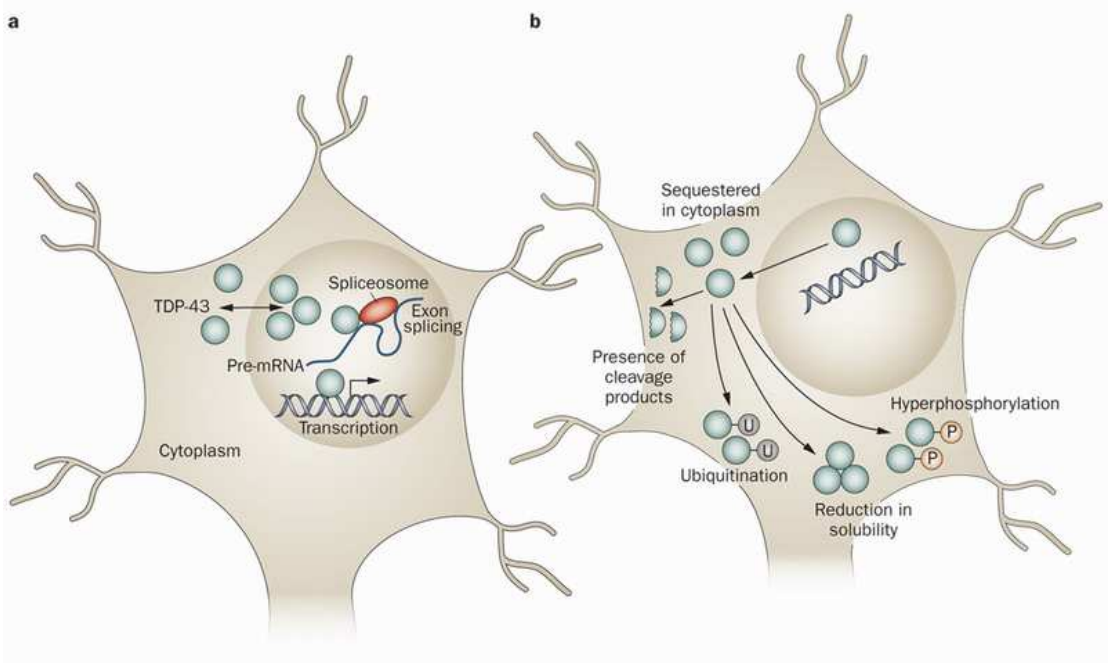

Figure 1.22

TDP-43 under physiological and pathophysiological conditions. a) Under normal physiological conditions, the majority of TDP-43 resides in the nucleus with functions in regulating gene expression, splicing and mRNA stability. b) Under pathophysiological conditions, TDP-43 is lost from the nucleus and accumulates in the cytoplasm. Hyperphosphorylated, ubiquitinated and C-terminal truncated fragments of TDP-43 are found in the disease state. Pathological TDP-43 has a reduced solubility and thus more prone to aggregation. The resulting loss-of-function or toxic-gain-of-function mechanisms due to the changes in TDP-43 may underlie the pathogenesis of TDP-43 proteinopathies. (Adapted from Chen-Plotkin et al., 2010)

TDP-43 is a ubiquitously expressed protein in rodents and humans predominantly localized in the nucleus with low levels in the cytoplasm. It has been identified as a multi-functional protein with structural resemblance to heterogeneous ribonucleoproteins (hnRNPs) and contains five known functional domains: two RNA recognition motifs (RRM1 and RRM2), a glycine-rich carboxy-terminal region, nuclear localization signal (NLS) and nuclear export signal (NES) (Warraich et al., 2010, Geser et al., 2010). Various studies have reported the diverse physiological functions of TDP-43 through its binding to DNA, RNA and proteins. For instance, by binding to DNA,

it can act as a transcriptional repressor for several mammalian genes. Its ability to interact with RNA such as mRNA and pre-mRNA also allows it to regulate exon splicing of genes including those involved in motor neuron diseases (Wang et al., 2004, Abhyankar et al., 2007, Chen-Plotkin et al., 2010). Apart from transcriptional and splicing regulation, studies illustrated that TDP-43 plays important post-transcriptional roles including the promotion of mRNA stability (Strong et al., 2007) and microRNA biogenesis and processing through its association with Drosha (Lagier-Tourenne et al., 2010). In addition, independent studies in mouse models and human cells have further implicated it as a developmentally regulated protein crucial for normal prenatal development and cell survival by maintaining genomic stability (Kraemer et al., 2010, Ayala et al., 2008a).

TDP-43 pathology has been found in a number of neurodegenerative diseases and is the most prominent cytopathological feature in ALS and FTLD-TDP. TDP-43 inclusions are detected in the neuronal cytoplasm, nucleus, dystrophic neuritis and glial cells in FTLD-TDP. In ALS, round inclusions of TDP-43 are found in the cytoplasm of motor neurons and there is a lack of intact TDP-43 protein in the neuronal nuclei (Neumann et al., 2007). It has therefore been suggested that the inclusions may pull out intact TDP-43 from the nucleus and contribute to subsequent degeneration of motor neurons (Ito and Suzuki, 2011). ALS is a fatal adult-onset neurodegenerative disease characterized by selective death of both upper and lower motor neurons resulting in progressive weakness, muscular wasting, leading to paralysis and death (Banks et al., 2008). FTLD is the second most common form of dementia in the presenile age group (<65 years) after Alzheimer's disease (AD)

with prominent atrophy of the frontal and temporal lobe, characterized by progressive deterioration in behavior, personality and language (Rademakers et al., 2012). It is often associated with manifestation of movement disorders such as Parkinsonism or motor neuron disease (MND) and studies demonstrated that 60% of the phenotypes associated with FTLD are manifested in FTLD-TDP (Kwong et al., 2008).

In 2006, TDP-43 was identified by two groups as the major disease protein and component of the ubiquitin-positive cytoplasmic inclusions in ALS and FTLD-TDP (Neumann et al., 2006, Arai et al., 2006). Rapid advances have since been made in the understanding of the physiological function of TDP-43 and its role in neurodegenerative diseases. These advances link ALS and FTLD-TDP to a disease spectrum with shared mechanism involving TDP-43 (Arai et al., 2006, Neumann et al., 2006). This relationship has been verified by different groups in 2008 reporting pathogenic missense mutations in TDP-43 gene in ALS, which therefore indicate the causative link between TDP-43 mutations and neurodegeneration (Sreedharan et al., 2008, Kabashi et al., 2008). In addition, mutations in TDP-43 were also found in patients with FTLD suggesting that abnormal TDP-43 pathology is involved in neurodegeneration associated with both ALS and FTLD-TDP (Benajiba et al., 2009). The accumulating data led to the idea of a spectrum of TDP-43 proteinopathies (Ito and Suzuki, 2011, Chen-Plotkin et al., 2010). Apart from the shared accumulation of TDP-43-positive inclusions and overlapping clinical and pathological features, the transition forms between ALS, ALS with dementia (ALS-D), FTLD-MND and FTLD-TDP have been reported which indicate that these TDP-43 proteinopathies may represent different points along one

continuous and broad clinico-pathological spectrum (Geser et al., 2010, Chen-Plotkin et al., 2010) (Fig1.23).

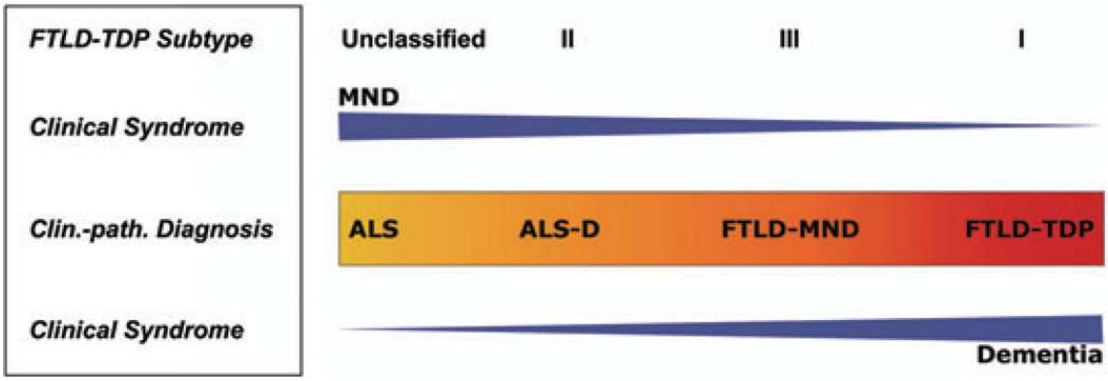

Figure 1.23

Clinico-pathological spectrum of the major TDP-43 proteinopathies extending from FTLD-TDP at one end to FTLD-MND, ALS-D and ALS at the other end. Blue arrows indicate decreasing clinical syndrome with MND and increasing with dementia from left to right. The central yellow-to-red central box represents the spread and severity of TDP-43 pathology in which yellow denotes predominant involvement of the spinal cord and red denotes involvement of cortical regions of the brain. FTLD-TDP subtype is the classification of the pattern of inclusions according to (Chen-Plotkin et al., 2010) and the unclassified type represents absence of TDP-43 pathology or insufficient degree of pathology for subtyping. (Adapted from Geser et al., 2010)

Since the identification that mutations in TDP-43 cause ALS and FTLD-TDP, enormous effort has been focused on how this protein leads to the development of neurodegeneration and neuronal death. Studies revealed that C-terminal fragments (CTF) with length between 25-35kDa found in the brains of patients with ALS/FTLD-TDP are highly phosphorylated, implicating the role of TDP-43 fragmentation and phosphorylation in the disease pathogenesis (Ito and Suzuki, 2011). Indeed, there are a number of studies together suggesting that the abnormally modified TDP-43 may promote mislocalization and aggregation of TDP-43. In cultured cells, it is demonstrated that impaired autophagic degradation caused by downregulating the expression of ESCRT

(endosomal sorting complex required for transport) subunits, which are crucial in the multivesicular body pathway, may result in depletion of nuclear TDP-43 and accumulation of ubiquitin-positive TDP-43 in the cytoplasm (Filimonenko et al., 2007). It is also postulated that aberrant proteolytic cleavage of TDP-43 may lead to its cytoplasmic deposition as the CTFs no longer contain a NLS and therefore unable to gain access back to the nucleus. In addition, the recovered CTFs which are sarkosyl-insoluble may initiate the seeded aggregation of TDP-43 into cytoplasmic inclusions, in which subsequent sequestration of full-length TDP-43 by the cytoplasmic aggregates could result in further depletion of TDP-43 in the nucleus (Neumann et al., 2006). Furthermore, phosphorylation of TDP-43 has been demonstrated as another disease-specific phenomenon which may promote TDP-43 oligomerization and have potential impact on various functions of TDP-43 (Gendron et al., 2010).

Taken together, it appears that TDP-43-mediated neurotoxicity may be caused by both toxic gain of function from the cytoplasmic inclusions as well as loss of TDP-43 function. There is mounting evidence from studies in yeast and human cells that cytoplasmic TDP-43 aggregates are cytotoxic. The aggregation of CTFs, the caspase cleavage products of TDP-43, was shown to be associated with increased cytotoxicity, inducing cell death through a toxic gain-of-function (Zhang et al., 2009). It is important to note that the presence of toxic cytoplasmic inclusions is accompanied by a loss of nuclear TDP-43 and hence normal TDP-43 function, including its involvement in transcription, pre-mRNA splicing and further the biogenesis of microRNAs (Gendron et al., 2010). In addition to its nuclear activities, loss of important functions within the

cytoplasm, such as RNA stabilization, translation and degradation, may also underlie TDP-43-mediated toxicity (Wang et al., 2008, Geser et al., 2010, Gendron et al., 2010).

Apart from TDP-43, other pathological proteins have also been identified as the cause of ALS/FTLD-TDP via different disease mechanisms. For instance, mutations in charged multivesicular body protein-2B (CHMP2B), a subunit of ESCRT-III, as well as valosin-containing protein (VCP) have been associated with FTLD and ALS, which are both involved in autophagic dysregulation (Chen et al., 2012). Recent findings have further strengthened the concept of the overlapping molecular pathogenesis of the ALS/FTLD-TDP spectrum. In 2009, mutations in the RNA-binding protein fused in sarcoma/translated in liposarcoma (FUS/TLS), the functional homolog of TDP-43, were identified as the cause of autosomal dominant ALS (Kwiatkowski et al., 2009, Vance et al., 2009). Subsequently, FUS-immunoreactive cytoplasmic inclusions were detected in the brains of FTLD patients without either tau or TDP-43 pathology, a condition named FTLD-FUS (Neumann et al., 2009). Inclusions containing both TDP-43 and FUS have also been reported in sporadic ALS, suggesting a possibility of crosstalk and involvement of the two RNA-binding proteins in the disease cascade of the ALS/FTLD-TDP (Ito and Suzuki, 2011). More recently, Ewing's sarcoma (EWS) and TATA-binding protein-associated factor 15 (TAF15), which comprise the FET family of DNA/RNA-binding proteins together with FUS, were found as the pathological proteins in FTLD-FUS (Neumann et al., 2011). After years of intense effort made by researchers worldwide, the ALS/FTLD gene on chromosome 9p was identified by two independent groups

in 2011, in which they found an abnormal expansion of a noncoding GGGGCC hexanucleotide repeat in the chromosome 9 open reading frame 72 (*C9orf72*) gene in both familial and sporadic ALS and FTLD (DeJesus-Hernandez et al., 2011, Renton et al., 2011), This discovery has brought huge excitement in the field of ALS/FTLD as findings indicate that the *C9orf72* mutation is currently the most common genetic cause of both ALS and FTLD. At the moment, a number of cellular and animal models involving the manipulation of *C9orf72* gene expression are being generated in order to decipher the disease mechanisms leading to degeneration and TDP-43 aggregation in neurons (Rademakers et al., 2012).

1.5.3 Frontotemporal Dementia with Parkinsonism-17

One class of neurodegenerative diseases exhibiting a classic form of cytoplasmic pathology are the tauopathies, in which a prominent and complex network of filamentous tau (microtubule-associated protein tau, *MAPT*) protein is deposited. The accumulation of insoluble and hyperphosphorylated tau filaments constitute a defining characteristic of tauopathies including Alzheimer's disease (AD), Pick's disease, frontotemporal dementia with Parkinsonism linked to chromosome 17 (FTDP-17), progressive supranuclear palsy and corticobasal degeneration (Lee et al., 2001). The tau protein aggregates adopt the form of neurofibrillary tangles (NFT) with a fibrous appearance forming straight filaments, twisted filaments and paired helical filaments (PHF) (Gendron and Petrucelli, 2009). The discovery of FTDP-17 caused by mutations in *Tau* established that misregulation and dysfunction of the tau protein result in neurodegeneration and dementia (Poorkaj et al., 1998,

Hutton et al., 1998, Spillantini et al., 1998). It is therefore crucial to decipher the mechanisms underlying filamentous tau aggregation which are central to the neurodegenerative process in tauopathies (Goedert et al., 2012).

Tau was identified as a microtubule-assembly factor in the mid-1970s (Weingarten et al., 1975), which was subsequently found to be the most commonly misfolded protein in a number of neurodegenerative diseases. It is believed to promote microtubule assembly and stabilization and is predominantly expressed in neurons. It is usually found in axons as a cytosolic protein important for axonal transport and maintenance (Morris et al., 2011), however a redistribution to the cell body and dendrites are observed in the tauopathies. In adult human brain, alternative mRNA splicing from a single gene around the N-terminal region and microtubule-binding domain (MBD) produces six main tau isoforms (Goedert et al., 1989). These isoforms are named by the number of microtubule binding repeat sequences expressed (R) in the carboxy-terminal half and by which N-terminal exons (N) are included (Fig1.23 and 1.25A). In the normal adult human cerebral cortex, similar levels of three- and four-repeat isoforms are expressed (Morris et al., 2011, Goedert and Spillantini, 2011). An intrinsically disordered structure is found in tau which is subject to a variety of post-translational modifications (Fig1.24). Under both physiological and pathological conditions, the serine and threonine residues can be phosphorylated by different kinases. It has been demonstrated that phosphorylation of tau may change its MBD conformation leading to the detachment of tau from microtubules. The accumulating tau may then form insoluble filaments and eventually NFTs in the cell bodies and neurites (Morris et al., 2011).

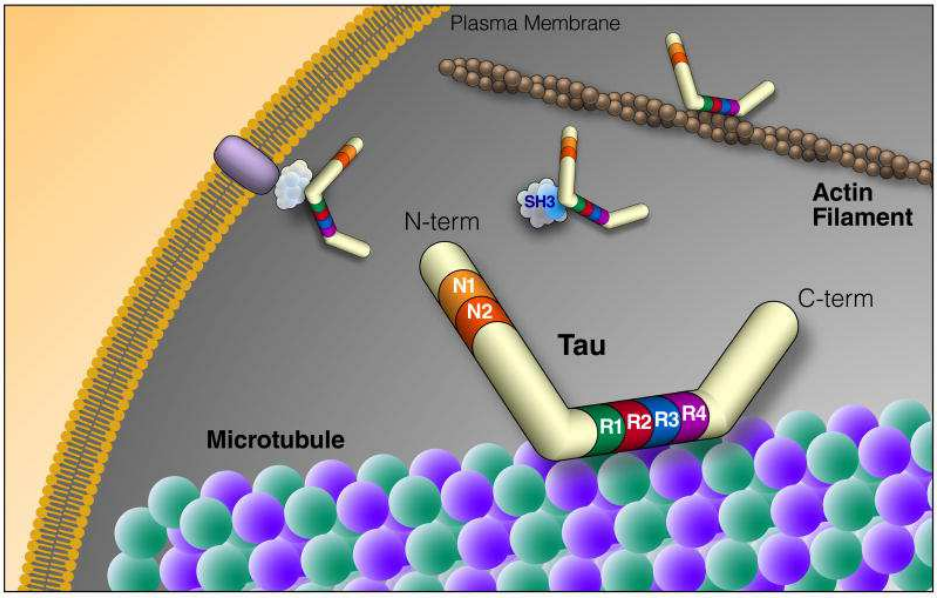

Figure 1.24

The structure and function of tau. Tau is an intrinsically disordered protein in which alternative mRNA splicing can take place at N terminal exons (N1,2) and the microtubule repeat domains (R). The variety of tau binding partners implicates its role in signaling pathways and the organization of cytoskeleton. (Adapted from Morris et al., 2011)

Due to the lack of genetic evidence linking tau dysfunction to the neurodegenerative process, tau inclusions were generally regarded as epiphenomena of little or no consequence. In 1994, a dominantly inherited form of frontotemporal dementia with parkinsonism was linked to a region containing the *MAPT* gene, chromosome 17q21-22 (Wilhelmsen et al., 1994). Following this work, additional forms of FTD were identified to be linked to this region which led to the classification of this FTD subtype as “frontotemporal dementia and parkinsonism linked to chromosome 17” (FTDP-17). The first mutations in *MAPT* were described in FTDP-17 patients in June 1998 (Hutton et al., 1998, Poorkaj et al., 1998, Spillantini et al., 1998). The identification of filamentous and hyperphosphorylated tau pathology in these cases established that tau dysfunction is sufficient to cause neurodegeneration and

dementia. By 2012, 46 pathogenic mutations in *MAPT* have been reported including 39 coding region mutations and 7 intronic mutations (Fig1.25B). The significance of these findings is that it provides crucial evidence linking *MAPT* mutations to the formation of NFTs and neurodegeneration in the absence of Aβ amyloid deposits (Goedert et al., 2012). Although it has been reported that mutations in the progranulin gene may cause tau-negative FTDP-17 (Baker et al., 2006), *MAPT* mutations are present in the majority cases of FTDP-17.

FTDP-17 is characterized by early behavioral changes followed by progressive cognitive, language and motor dysfunction. Patients usually display a unique pattern of frontotemporal atrophy which is closely linked to the distribution of filamentous and hyperphosphorylated tau (Poorkaj et al., 1998). Mutations of the tau gene affect all six isoforms of tau which are incorporated into the filaments. However the filamentous tau deposits may vary in terms of their morphologies, isoform compositions and distribution patterns depending on the type of *MAPT* mutation (Brandt et al., 2005).

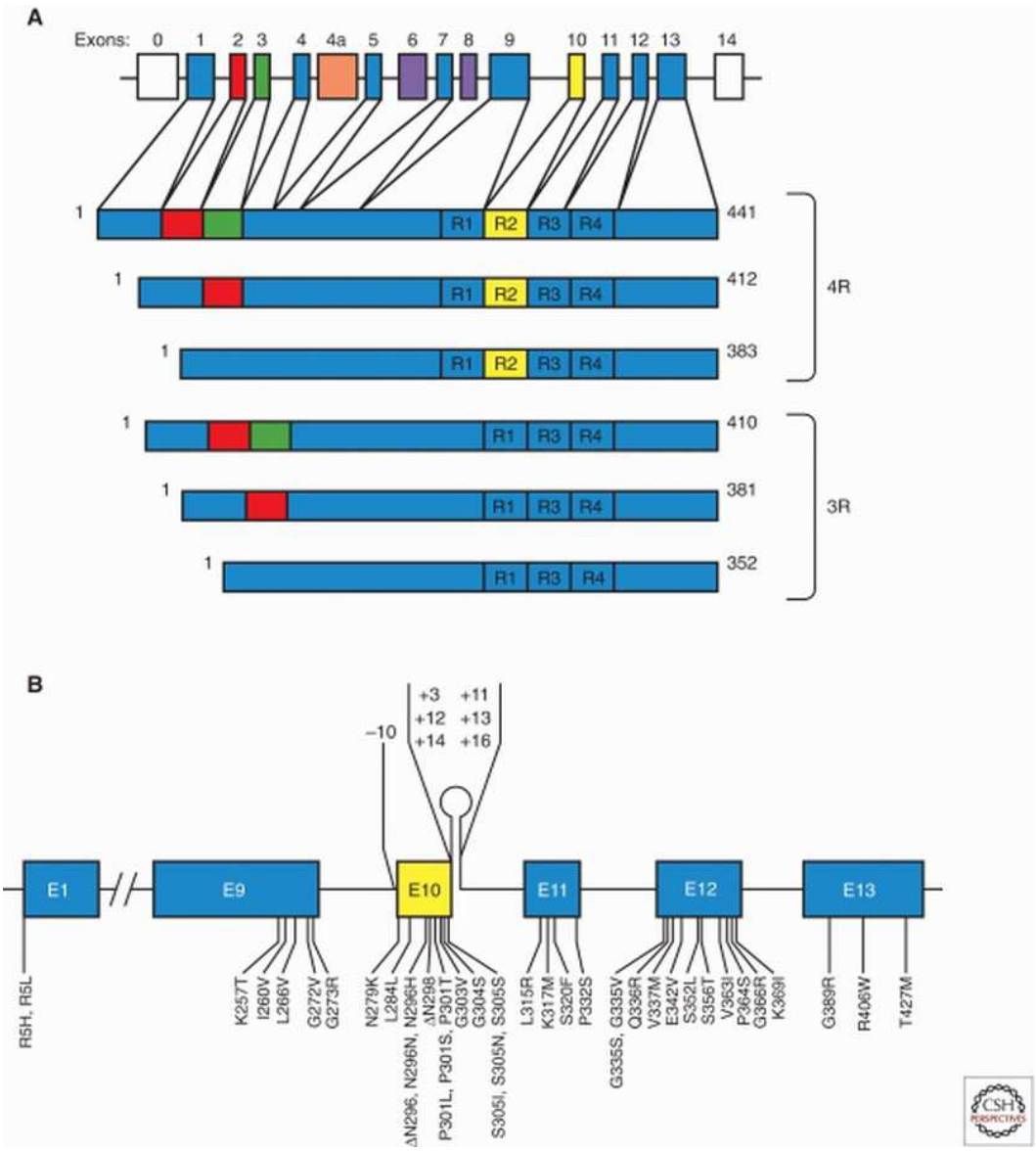

Figure 1.25

The *MAPT* gene and the six isoforms of tau and mutations in FTDP-17. A) 16 exons (E) are present in *MAPT* and the six tau isoforms (352-441 amino acids) are generated by alternative splicing of E2 (red), E3 (green) and E10 (yellow). Exons in blue are constitutively spliced. E0 and E14 (white) are noncoding. E6 and E8 (violet) are not transcribed in the adult human brain. E4a (orange) is not expressed in the CNS. The microtubule binding repeats (R1-R4) are illustrated. There are three isoforms with four repeats each (4R) and three isoforms with three repeats each (3R). Each repeat consists of 31 or 32 amino acids. B) Shown are 46 pathogenic mutations in *MAPT* in which 39 are coding region mutations in E1, E9, E10, E11, E12, E13, and 7 are intronic mutations flanking E10. (Adapted from Goedert et al., 2012)

Mutations in tau are either missense, deletion or silent mutations and most of them are located in exons 9-12 and the adjacent introns (Fig1.25B). Functionally, they can be classified into two largely non-overlapping groups: mutations that have a primary effect at the protein level, and those that affect the alternative splicing of tau pre-mRNA and therefore acting at the RNA level (Gendron and Petrucelli, 2009, Goedert and Spillantini, 2011). About half of the known mutations fall into the first category, including missense and deletion changes in tau which give rise to tau proteins with a reduced binding affinity for microtubules. Studies have shown that this partial loss of tau protein function may increase its propensity to form abnormal aggregation and become hyperphosphorylated which overtime will assemble into filaments (Goedert et al., 1999, Morris et al., 2001). For instance, mutant tau protein with P301S mutation in exon 10 has been found to lose its ability to promote proper microtubule assembly, but instead stimulates tau assembly into filaments (Allen et al., 2002, Bugiani et al., 1999). These suggest that both microtubule dysregulation and the formation of NFTs caused by these mutations may lead to tau-mediated toxicity and subsequent impairment in axonal transport and synaptic damage (Gendron and Petrucelli, 2009). The second group of mutations influence tau alternative mRNA splicing mainly on exon 10 of *MAPT* which perturb the normal ratio of three- to four- repeat isoforms, resulting in an excess of four-repeat tau isoform. The overproduced four-repeat tau may then form filamentous inclusions and the imbalanced ratio of isoform expression may contribute to tau dysfunction (Spillantini et al., 1998, Goedert, 2004, Gendron and Petrucelli, 2009).

Studies of FTDP-17 have verified the causative role of tau dysfunction in

neurodegeneration and dementia, which may also be of central importance for the pathogenesis of other neurodegenerative diseases with a filamentous tau pathology. Recently, tau is further implicated in regulating neuronal excitability and is involved in neuronal deficits and cognitive decline (Morris et al., 2011). Clearly, tau is increasingly being recognized as a multifunctional protein rather than purely a microtubule stabilizer. Accumulating evidence has demonstrated new functions of tau involved in signaling, synaptic functions and cytoskeletal organization. In order to truly decipher the detrimental consequences of tau dysfunction and the mechanisms involved in tau-mediated neurodegeneration, it is crucial to characterize and understand the functions of tau beyond its well-established microtubule-binding capacity (Gendron and Petrucelli, 2009, Morris et al., 2011)..

Several studies have reported nuclear localization of tau in both neuronal (Wang et al., 1993) and non-neuronal cells (Cross et al., 2000). Remarkably, further work has suggested a nuclear role for tau protein found in the nucleus. Tau was identified as a key component of perinucleolar heterochromatin and is involved in nuclear stress response (Sultan et al., 2011). Importantly, it has also been illustrated that tau is capable of binding to pericentromeric satellite DNA sequences, which form neuronal caps of perinucleolar heterochromatin, in both human and mouse (Sjoberg et al., 2006). This implicates a functional role for nuclear tau in nucleolar organization and heterochromatinization of specific RNA genes. Currently, very little is known about tau protein distribution in the nucleus. Although the ultrastructural and molecular organization of the neuronal nucleus in human tauopathies has not been well characterized, tau might be involved in a nuclear pathology. Studies

demonstrated that tau appears to participate in the protection of neuronal genomic DNA in stress conditions, in which it interacts with DNA and facilitates repair in central neurons during heat shock (Sultan et al., 2011). It is postulated that pathological alterations of tau, such as hyperphosphorylation, might affect its affinity for DNA and impair DNA protection. Interestingly, another study has reported that aggregation of tau impairs its ability to interact with DNA (Hua and He, 2002). The disruption of tau-DNA interactions could lead to neuronal dysfunction which might represent an important etiopathological mechanism of tauopathies (Sjoberg et al., 2006, Sultan et al., 2011). There is no doubt that the elucidation of novel functional role of neuronal nuclear tau would provide great insight for a better understanding of the pathogenesis of tauopathies.

1.5.4 Emerging Mechanisms of Pathogenesis

Misfolding of proteins and progressive accumulation of aggregates define most neurodegenerative diseases such as Alzheimer's disease, Huntington's disease, frontotemporal dementia and amyotrophic lateral sclerosis. The molecular mechanisms underlying the generation of protein aggregates and the resultant neurodegeneration have been extensively studied. It has been postulated that alterations in the balance of protein synthesis, aggregation and clearance may have significant roles in the pathogenesis of these diseases (Lee et al., 2010) (Fig1.26). Emerging evidence also suggests that propagation and spreading of protein aggregates may occur in these diseases.

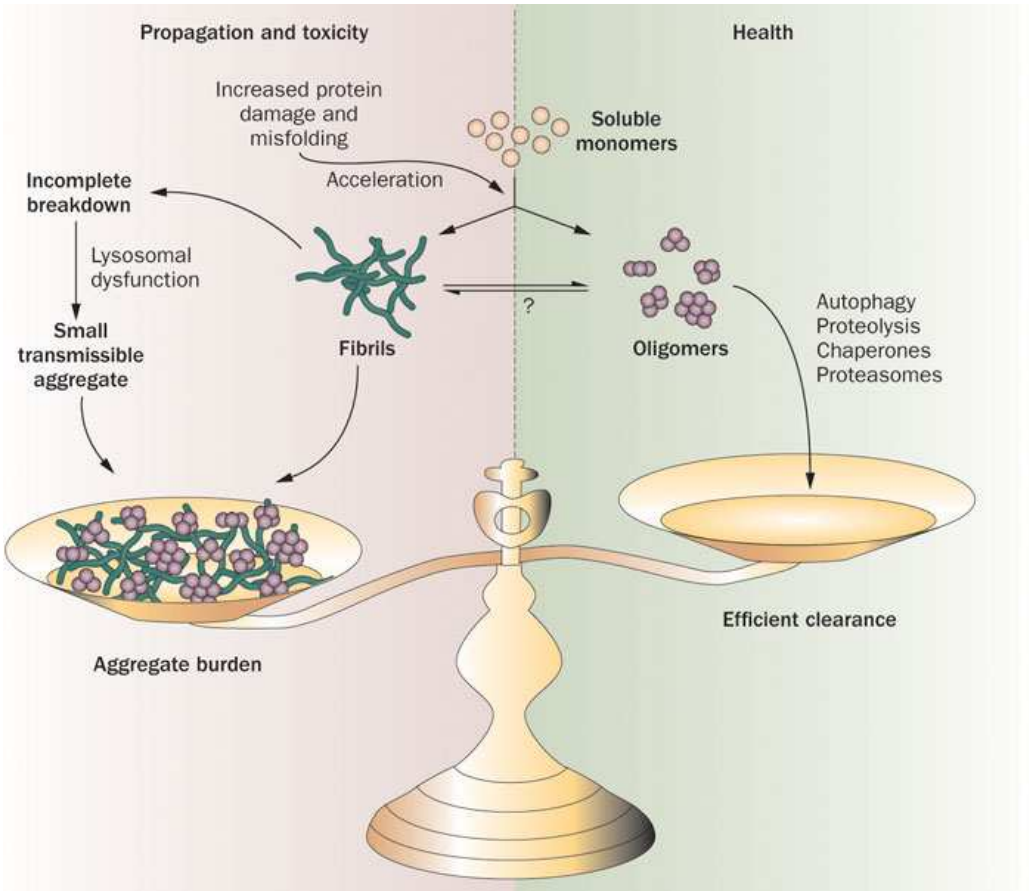

Figure 1.26

Imbalance between protein synthesis, aggregation and clearance. Protein misfolding or aggregation can normally be cleared by cellular degradation processes such as autophagy and ubiquitin-proteasome system. Under disease conditions, protein aggregation is increased due to both an accelerated production and reduced or dysregulated function of protein degradative systems. This leads to the production of smaller fragments seeding for further aggregation and propagation in neurodegenerative diseases. (Adapted from Lee et al., 2010)

1.5.4.1 Dysregulation of Autophagy

Autophagy was first described in 1963 by Christian De Duve as an intracellular process involved in the degradation of cytoplasmic constitutes, delivered via a double-membrane autophagosome, by the lysosomal machinery (De Duve, 1963). It has been increasingly recognized that there is an abundant presence of these autophagosomes in a growing number of neurodegenerative diseases. Recently an emerging consensus appears to

suggest that inadequate or impaired autophagy may be the underlying reason for the buildup of autophagosomes and contributes to neuronal cell death (Wong and Cuervo, 2010). This view is further supported by accumulating evidence demonstrating that dysregulation of this degradative system may play an important role in the pathogenesis of neurodegenerative diseases.

Autophagy has a crucial physiological and homeostatic role in cells in order to balance between the synthesis, degradation and recycling of cytoplasmic components including protein aggregates and damaged cellular organelles (Mizushima, 2007). During autophagy, these are sequestered into double-membrane autophagosomes which then undergo maturation by fusing with multivesicular bodies or endosomes to form amphisome. This is followed by fusion with lysosomes in which the contents are degraded by lysosomal hydrolases (Banerjee et al., 2010). The autophagy-lysosome pathway and the ubiquitin-proteasome system together represent the major routes for the clearance of toxic accumulations in the cells. However, ubiquitin-proteasome system is majorly involved in the degradation of short-lived proteins with low to medium molecular weight. Protein aggregates and oligomers with high molecular weight, such as those commonly found in neurodegenerative diseases, undergo bulk degradation which require the more efficient autophagy-lysosome pathways (Banerjee et al., 2010). A variety of studies using postmortem human tissue, genetic animal and cellular models of neurodegenerative diseases demonstrate that a lot of the etiological factors involved in these diseases, such as mutant proteins, may impair the autophagy process (Pickford et al., 2008, Ravikumar et al., 2004, Li et al., 2008). Elucidation of the pathophysiological roles of autophagy may also give

rise to potential therapeutic targets which can be modulated by pharmacological treatments.

1.5.4.2 Prion-like Transmission of Protein Aggregates

Although protein misfolding and the accumulation of fibrillar aggregates occur in most neurodegenerative diseases, the concept of disease propagation by “infectious” protein aggregates in the CNS has always been confined to prion diseases including Creutzfeldt-Jakob disease (CJD) and bovine spongiform encephalopathy (BSE) (Lee et al., 2010). Recently, the hypothesis of prion-like mechanism has emerged from new evidence suggesting the possibility of protein spreading involving aggregates such as tau, amyloid-β, huntingtin and α-synuclein in Alzheimer’s disease, Huntington’s disease, Parkinson’s disease and frontotemporal dementia. These disease-associated aggregates are also found to share distinct biophysical and biochemical characteristics with prions (Frost and Diamond, 2010).

For two decades, the idea of propagation of protein misfolding in the CNS has been constrained to prion diseases, which are also known as transmissible spongiform encephalopathies (TSEs) (Soto, 2012). It is well established that the accumulation of protein aggregates in these diseases plays a major pathogenic role. TSEs are infectious and studies have implicated the misfolded prion protein as the active and crucial component of the infectious agent (Soto, 2011). Seeded by the misfolded prion protein, autocatalytic conversion of the natively folded prion protein is self-replicated,

which therefore spread throughout the body and occasionally between individuals (Soto, 2012). Accumulating evidence has now expanded this notion of pathological spreading, a characteristic of prion strains, to include other non-prion protein aggregates associated with a variety of neurodegenerative diseases (Aguzzi and Rajendran, 2009, Soto, 2011, Lee et al., 2010). *In vitro* and *in vivo* studies have reported this mechanism of prion-like self-propagation in proteins such as Aβ, α-synuclein, tau and huntingtin (Petkova et al., 2005, Yonetani et al., 2009, Frost et al., 2009, Frost and Diamond, 2010, Ren et al., 2009). In order for these intracellular aggregates to gain access to the extracellular space as well as the neighboring cell's cytosol, there must be mechanisms allowing the transference of disease proteins. Studies suggest that these may include secretory mechanism such as vesicle-mediated exocytosis, or by damage of the host cell leading to leakage through membrane disruption (Guo and Lee, 2011, Lee et al., 2010). The released aggregates may then be internalized into neighboring cells via endocytosis and subsequently bind the natively folded proteins and seed their aggregation (Frost et al., 2009, Guo and Lee, 2011). Alternative mechanisms of direct cellular contact may also take place through tunneling nanotubes or by packaging into exosomes (Aguzzi and Rajendran, 2009, Lee et al., 2010).

Studies in Parkinson's and Alzheimer's disease patients appear to indicate that normally intracellular proteins such as α-synuclein and tau may indeed be released via secretory mechanisms (El-Agnaf et al., 2006, Vandermeeren et al., 1993). The concept of prion-like spreading of NFTs and Aβ amyloid plaques in the brain has been supported by a number of reports (Braak and

Braak, 1991, de Calignon et al., 2012). Other *in vitro* and *in vivo* studies also demonstrated the misfolding and aggregation of tau which is transmissible in a prion-like manner in cultured cells as well as transgenic mice (Clavaguera et al., 2009, Frost et al., 2009, Guo and Lee, 2011). Accumulating evidence from experiments in cultured cells further support the notion that a variety of protein aggregates including Aβ, α-synuclein, tau and polyglutamine may be transferred directly from cell to cell (Frost and Diamond, 2010). There is no doubt that understanding the mechanisms of disease spreading and progression has profound therapeutic implications. Many of the current therapies for neurodegenerative diseases focus on the prevention of cell death and promotion of neuronal survival by targeting nonspecific mechanisms (Frost and Diamond, 2010). The identification of prion-like spreading of disease-associated aggregates may give rise to the development of novel diagnostic techniques and therapeutic strategies aiming to prevent the initial formation of seeds and the subsequent propagation of protein aggregates (Lee et al., 2010, Soto, 2012, Prusiner, 2012).

1.6 Aims and Objectives

The neuronal nucleus is a highly specialized organelle with unique and characteristic organization of the genome, transcription and epigenetic regulation. Little is known about the chromatin organization in the neuronal nucleus as most studies focus on rapidly growing and dividing cells. The aim of this work is to investigate the ultrastructural and molecular organization of the mouse striatal neuronal nucleus and to correlate this with the distribution of a variety of epigenetic modifications. The relationship of the neuronal nuclear

organization to a functional assay of *in vivo* transcription detecting nascent RNA together with the localization of three RNA polymerases I, II and III will be explored. Two clinically used histone deacetylase inhibitors, sodium valporate (VPA) and suberoylanilide hydroxamic acid (SAHA) will be used to study their effects on the neuronal nuclear organization. Furthermore, the architectural and functional organization of the neuronal nucleus in a number of transgenic mouse models of human neurodegeneration, including Huntington's disease, amyotrophic lateral sclerosis and frontotemporal dementia, will be investigated and compared with that in the wild type to see if there are any distinctive changes in the unique neuronal nuclear organization.

Materials & Methods

CHAPTER 2

Materials and Methods

2.1 Transgenic Mice and Controls

2.1.1 Huntington's Disease (htt exon-1 ^{CAG144})

C57BL6/J mice expressing exon 1 of the human HD gene which contains a highly expanded CAG repeat sequence (141-147) were used in the studies. These mice called the R6/2 line are the prototypical transgenic model for early-onset HD and have been extensively studied (Mangiarini et al., 1996, Davies et al., 1997).

2.1.2 ALS/FTLD (TDP-43^{M337V})

The ALS/FTLD mice used in the studies were produced by Veronique Schaeffer and Michel Goedert recently at the MRC/LMB Cambridge and are unpublished. The M337V mutation was introduced by site-directed mutagenesis into the cDNA encoding the human TDP-43 protein. The mutated cDNA was subcloned into a murine *thy1.2* genomic expression vector (gift from Dr. H. van der Putten, Novartis, Basel, Switzerland) and this TDP-43 expression construct was produced by subcloning M337V *TARDBP* cDNA into a unique XhoI site of the expression vector. A Kozak consensus sequence was introduced upstream of the initiation codon and vector sequences were removed before microinjection. By pronuclear injection of (C57BL/6J-CBA) F_1 embryos transgenic mice were produced. With the use of the primer pair

5’-CACAGACACACACCCAGGACATAG-3' and 5’-AGATTTCCCCAGCCAGC ATC-3’, founders were identified by PCR analysis of lysates from tail biopsies. Founder animals were then intercrossed with C57BL/6J mice to establish the lines. The human TDP-43 protein was expressed throughout the nervous system including the spinal cord, brain stem, cerebral cortex and hippocampus. The amounts of total (mouse and human) TDP-43 protein were higher in the brain (×2.2, $p<0.01$) and the spinal cord (×1.7, $p<0.01$) of TDP-43^{M337V} transgenic mice compare to non-transgenic controls. Total TDP-43 was expressed primarily in the nucleus in non-transgenic controls whereas in transgenic mice it was detected in both the nucleus and the cytoplasm.

2.1.3 FTDP-17 (Tau^{P301S})

The neuron-specific mouse thy1 promoter was used to produce transgenic mice expressing the shortest human four-repeat tau isoform with the P301S mutation. Six founders were obtained and five of them transmitted the transgene in a Mendelian manner. Three out of five lines expressed high levels of human tau protein in both the brain and spinal cord which were used to establish homozygous lines. The present study focuses on line 2541. Homozygous mice from this line developed a neurological phenotype characterized by general muscle weakness, tremor and a severe paraparesis at 5-6 months of age, and were unable to extend their hindlimbs when lifted by the tail. A similar phenotype was observed in heterozygous mice at 12-14 months of age. These mice were produced by Bridget Allen and Michel Goedert (MRC/LMB Cambridge) and have been extensively characterized (Allen et al., 2002).

2.1.4 Littermate Controls (C57BL6/J)

Control mice were bred on a C57BL6/J background and in all cases these were the sex matched and age matched littermates of the transgenic mice used in the studies.

2.2 Tissue Preparation

2.2.1 Tissue Preparation for Confocal Light Microscopy

Transgenic mice and their littermate controls received a lethal intraperitoneal injection of sodium pentobarbitone (Sagatal) and then perfused through the left cardiac ventricle with aldehyde containing fixatives. Animals were perfused with 2% sodium periodate-lysine-paraformaldehyde (PLP), or 4% paraformaldehyde (PFA) in 0.1M sodium phosphate buffer (pH 7.4) (Davies et al., 1997). The brains were removed after decapitation and placed in the same fixative at 4˚C for 4-6 hours before being transferred to cryoprotectant solution of 30% sucrose in 0.1M sodium phosphate buffer (pH 7.4) for 48 hours at 4˚C.

Brains were cut into half and placed onto the Leica SM2000R sledge microtome with OCT compound (Miles Laboratories) and frozen with powdered solid CO_2. 40µm thick sections were cut in the coronal plane and collected using a paintbrush and put serially in a “dimple tray” filled with 0.1M sodium phosphate buffer.

C57BL6/J mice were also used in HDACi studies. Sodium valproate (VPA)

was given at 120mg/kg for 120 minutes before perfusion. Vorinostat (suberoylanilide hydroxamic acid, SAHA) was given at 50mg/kg for 120 minutes. Both HDACi were given as intraperitoneal injections and littermate controls received an injection of an equal volume of vehicle (saline).

2.2.2 Tissue Preparation for Electron Microscopy

Brains from transgenic and control mice were removed and for standard transmission electron microscopy (TEM), brains were placed in a fresh solution of 4% PFA with 0.1% glutaraldehyde overnight at 4˚C. Brains for immuno-electron microscopy were placed in either 2% PLP fixative in phosphate buffer (pH 7.4) or 4% PFA with or without 0.1% glutaraldehyde overnight at 4˚C. After post-fixation, coronal sections were cut of either 50 or 200µm on a Vibratome (Agar Scientific Series 1000) and collected in serial order in 0.1M phosphate buffer before being placed in 2% glutaraldehyde in the same buffer for 30 minutes.

2.2.3 *In vivo* Transcription Run-on Assay

The novel *in vivo* transcription run on assay adopted from Casafont and coworkers (Casafont et al., 2006) was developed for these studies. Freely behaving mice were caged in groups of 3-4 in an environmentally enhanced environment and received an intraperitoneal injection of 5'-fluorouridine in sterile saline (5µl per gram of a 0.4 M solution, 524mg/kg) for varying time periods (5, 10, 15, 30, 45, 60 minutes and 24 hours) prior to terminal anaesthesia. Tissue preparation for confocal light microscopy and electron

microscopy were performed using standard protocols.

Control experiments for *in vivo* transcription run-on assay

Three lines of evidence give us confidence that a peripheral injection of 5'-fluorouridine effectively and specifically labels nascent RNA within individual neurons of the mouse brain.

1. Identical patterns of labeling of both nucleoplasmic transcription factories were obtained with both monoclonal and polyclonal antibodies to BrdU (Sigma and AbCam respectively) whereas antibodies directed to IdU/BrdU (Caltag) failed to reveal anti labeling. Identical patterns of labeling were obtained when using confocal laser microscopy and FITC-labeled secondary antibodies for frozen sections or transmission electron-microscopy and nano-gold labeled secondary antibodies on resin embedded (post-embedding) sections.

2. Treatment of frozen sections with RNase A (200 μg/ml at 37 °C for 60 mins) abolished all immuno-labeling whilst pre-treatment of the sections with DNase I (100μg/ml at 37 °C for one 60 mins) was without any effect.

3. A time dependent and progressive change in immuno-labeling was evident for all studies. At early time points discrete punctate foci of labeling were observed throughout the nucleoplasm, over the perinucleolar heterochromatin and the nucleolus, at later time points labeling was observed around the nuclear membrane and through the nuclear pores. After much later time points labeling can be found throughout the neuronal cytoplasm extending into the dendrites and into axons and axon terminals (Stephen Hunt

and Kerri Tokichi, personal communication). These observations are consistent with the temporal gradient in RNA movement throughout the cell.

*Actinomycin D is a potent and specific inhibitor of RNA polymerases, however it appears to have a highly variable ability to penetrate the CNS. Several published reports suggest that only ~10% of peripherally administered drug crosses the blood brain barrier. Although we did find that use of this compound reduced the labeling of RNA following 5'-fluorouridine administration (150 μg/kg for 180 minutes), the results have not been included due to uncertainty of the exact mechanism of action.

2.3 Tissue Processing

2.3.1 Immunocytochemistry for Confocal Light Microscopy

Primary antibody solutions were made up in 1ml of primary antibody buffer (0.1M Tris-HCL, 0.3% Triton, 0.02% sodium azide) as shown in Table 2.2. Sections were incubated free-floating in primary antibody solutions at 4°C for 72 hours, then washed in 0.1M sodium phosphate buffer for 10 minutes (repeated 3 times). Fluorescein isothiocyanate (FITC)-conjugated secondary antibodies (Jackson ImmunoResearch Laboratories Inc.) at a concentration of 1:100 in 1ml of 0.1M sodium phosphate buffer were added to the sections which were incubated in the dark for 90-120 minutes. Sections were washed again in 0.1M sodium phosphate buffer for 10 minutes (repeated 3 times) and then stained with a diluted pyronin Y (PYY, Sigma Aldrich UK) solution made up in 0.1M sodium phosphate buffer (1:3000) for 4 minutes in the dark. For

triple labeling, instead of staining with PYY, sections were first stained with DAPI (4,6-diamidino-2-phenylindol) made up in 0.1M sodium phosphate buffer (1:15000) for 4 minutes in the dark, then sodium phosphate buffer washes were repeated 3 times, followed by PYY staining. Sections were then mounted onto gelatinized glass slides using a paintbrush, coverslipped with the mounting medium Mowiol-DABCO (1,4-diazabicyclo[2.2.2]octane) and sealed with a small rim of clear nail varnish. All slides were stored at 4°C in the dark until they were analyzed with the Leica confocal microscope.

2.3.2 Tissue Processing for Electron Microscopy

After being osmicated (90 min in 1% osmium tetraoxide in 0.1M sodium phosphate buffer or in 1% osmium tetraoxide and 1.5% potassium ferrocyanide in 0.1M sodium phosphate buffer at 4ºC), the sections were washed in 0.1M sodium phosphate .buffer for 10 minutes and dehydrated through a graded ethanol series (25%, 50%, 70%, 90%, 100% × 4). The sections were then cleared in propylene oxide (100% × 4) and incubated in a solution of 33% araldite resin in propylene oxide for 20 minutes, and replaced by a 66% resin mixture for 20 minutes, followed by 100% resin for 3-4 hours. After that, it was replaced with 100% resin and catalyst (0.2ml benzyl dimethylamine) and then left to harden for a few days. Ultrathin sections (approximately 70nm) were cut with a diamond knife on a Reichert Ultracut ultramicrotome. The sections were collected on copper-mesh grids coated with a thin formavar film, counter-stained with lead citrate for approximately 4 minutes and viewed in a Jeol 1010 transmission electron microscope. Digital images were captured on a Gatan Orius CCD camera.

2.3.3 Post-embedding Immuno-gold Labeling

70-90 nm sections were cut on a diamond knife from lowicryl embedded blocks and collected on Formavar coated Nickel-200 grids. Grids were then washed on a 50ul drop of sodium phosphate buffer for 3 x 15 minutes, before incubation in primary antibody dissolved in the same buffer (1:50-1:500) on a similar 50ul drop for 6 hours. Sections were washed in sodium phosphate buffer for 3 x 15 minutes and incubated in secondary antibody (1:200) for 2 hours (10 nm gold labeled anti-rabbit IgG or 10nm gold labeled anti-mouse IgG). Sections were finally washed in sodium phosphate buffer for 3 x 15 minutes and distilled water for 3 x 5 minutes before air drying.

Grids were counterstained with a 2% aqueous Uranyl acetate solution for 4 minutes followed by a further 4 minutes in distilled water. Sections were air dried before analysis in a Jeol 1010 transmission electron microscope. Digital images were captured on a Gatan Orius CCD camera.

2.3.4 Three-Dimensional Fluorescence In Situ Hybridization

3D FISH was carried out for the detection of mouse centromeres and telomeres with PNA (Dako) probes. PNA is a synthetic DNA/RNA analogue capable of binding to DNA/RNA in a sequence-specific manner obeying the Watson-Crick base pairing rules. In PNA the sugar phosphate backbone has been replaced by a neutral peptide/polyamide backbone keeping the distances between the bases exactly the same as in DNA. The neutral peptide

backbone gives PNA excellent properties for hybridizing to DNA/RNA, and in addition, PNAs are highly resistant to degradation by DNases, RNases, proteinases and peptidases.

Pre-treatment

With a diamond pen an area of approximately 20 x 20 mm was marked on Superfrost Plus (Thermo Scientific) glass slides around 2 x 20µm frozen sections of mouse striatum. Slides were immersed in TBS for approximately 2 minutes, then in 3.7% formaldehyde in TBS for 2 minutes. Slides were washed in TBS and then in TBS for 2 x 5 minutes. Slides were then immersed in Pre-Treatment Solution (Vial 1 of Dako kit diluted 1:2000 in TBS) for 10 minutes, and washed in TBS and then again in TBS for 2 x 5 minutes. After that, slides were immersed in cold (4°C) ethanol series (70%, 85% and 95%) for 2 x 2 minutes and left in a vertical position until they were dry, or use a cold air stream to dry (~ 5 minutes).

Denaturation and hybridization

10 µl of PNA Probe (Cy3 or FITC labeled) (Dako Vial 2) was added to the marked area on the slides. Marked area was covered with an 18 x 18 mm coverslip. Slides were placed on a pre-heated PCR hotplate adjusted to 80 °C for 5 minutes. Then they were placed in the dark at room temperature for 90-120 minutes.

Rinse and washing

Slides were immersed in working solution of the Rinse Solution (Vial 3 diluted 1:50) to remove coverslips briefly for approximately 1 minute. Slides

were then immersed in the pre-heated working solution of the Wash Solution (vial 4 diluted 1:50) for 5 minutes at 65 °C. After that, they were immersed in the same cold ethanol series as previously (70%, 85% and 96%) for 3 x 2 minutes. Slides were air dried vertically or dried using a cold air stream for approximately 5 minutes.

Counterstaining and mounting

20 µl of mounting solution was applied onto each slide (Vectashield hard set containing 4´,6-diamidino-2-phenylindole, DAPI at 0.1ug/ml, Vector Laboratories UK) and was covered with a 24 x 50 mm coverslip.

Procedural notes

1. The optimal pre-treatment may vary depending on the metaphase spread preparation. An alternative pre-treatment procedure was incubation with 1 mg/mL pepsin (Code S3002) in 0.01 mol/L HCl for 10 minutes at 37 °C.

2. For convenience, the ethanol series for dehydration could be stored in the freezer at -18 °C, or in a refrigerator at 4-8 °C. Covered with lids, the series could be stored for several weeks and be used for a maximum of 20 times.

3. Denaturation should be performed at minimum 80 °C and maximum 90 °C. Denaturing temperatures below 75 °C may impair results seriously.

4. The hybridization times in the protocol should be regarded as minimum times required. The slides could be left longer up to 2-4 hours.

5. The recommended wash was in a water bath with shaking. Washing temperature should not deviate more than + 3 °C from the target temperature (65 °C).

6. If there was high background staining, an optional wash procedure was washing for 2 x 15 minutes in 70% formamide/ 10 mmol/L PBS (1 ml 1 mol/L PBS + 29 ml pure water + 70 ml formamide) at room temperature followed by 2 x 15 minute wash in PBS.

The 3D FISH protocol was carried out in collaboration with Dr. Aysha S. Raza

Pan Centromeres	Starfish, Cambridge Biosciences Cambridge, UK	Cy3, FITC
Pan Centromeres	Poseidon, Kreatech, Amsterdam, NL	FITC
Mouse X chromosome	Stafish, Cambridge Biosciences	Biotin
Pan Telomeres, PNA	Dako, Ely, UK	Cy3

Table 2.1

A table showing the FISH probes used for detecting the mouse centromeres and telomeres (Dilution as supplied).

2.3.5 Primary Antibodies Table

Primary Antibody	Code	Source	Species	Dilution
Histone H1	AE-4 (05-457)	Upstate	Mouse IgG	1:1000
MacroH2A	Sc-67322	Santa Cruz Biotechnology	Rabbit	1:1000
H3K9M3	07-523	Upstate	Rabbit	1:1000
H3K9Ac	06-942	Millipore	Rabbit IgG	1:1000
H3K27M3	07-449	Upstate	Rabbit	1:1000
H3Ac	06-599	Millipore	Rabbit IgG	1:1000
H4Ac	06-598	Millipore	Rabbit	1:1000

H4K20M3	07-463	Millipore	Rabbit	1:1000
HP1α	07-346	Upstate	Rabbit	1:1000
ATRX	Sc-10078	Santa Cruz Biotechnology	Goat	1:1000
MeCP2	07-013	Upstate	Rabbit	1:1000
Phospho-MeCP2-pS80	AP3595a	Abgent	Rabbit	1:1000
Phospho-MeCP2-pS421	—	ME Greenberg	Rabbit	1:1000
p80 coilin	204/10	Dundee Cell Products	Rabbit	1:1000
p80 coilin	5P10	Dundee Cell Products	Mouse IgG	1:1000
Nopp140	RF12	UT Meier	Rabbit	1:1000
Anti centromere (Kinetochore) protein	15-235	Antibodies Incorporated Davis California USA	Human	1:500-1:1000
CENP-A	RCA	T. Fukagawa	Rat	1:500-1:1000
CENP-A	C51A7	Cell Signalling Technology	Rabbit	1:500-1:1000
CENP-A	07-574	Upstate	Rabbit IgG	1:500-1:1000
RNA Pol I (RPA194)	Sc-28714	Santa Cruz Biotechnology	Rabbit	1:500-1:1000
RNA Pol II 8WG16	MMS-126R	Covance	Mouse IgG	1:500-1:1000
RNA Pol II H5	MMS-129R	Covance	Mouse IgM	1:500-1:1000
RNA Pol II 4H8	Ab5408	ABCAM	Mouse IgG	1:500-1:1000
RNA Pol II H224	Sc-90001	Santa Cruz Biotechnology	Rabbit	1:500-1:1000
RNA Pol II H14	MMS-134R	Covance	Mouse IgM	1:500-1:1000
RNA Pol II C21	Sc-900	Santa Cruz Biotechnology	Rabbit	1:500-1:1000
RNA Pol II A10	Sc-17798	Santa Cruz Biotechnology	Rabbit	1:500-1:1000
RNA Pol III RPC32	Sc-48365	Santa Cruz Biotechnology	Mouse IgG	1:500-1:1000
RNA Pol III RPC32	Sc-28712	Santa Cruz Biotechnology	Rabbit	1:500-1:1000
RNA Pol III RPC39	Sc-21753	Santa Cruz Biotechnology	Mouse IgG	1:500-1:1000
RNA Pol III	HPA 005891	Sigma (Prestige)	Mouse IgG	1:500-1:1000
Fibrillarin	Ab5821	ABCAM	Rabbit	1:1000
UBF-1 (EP2741Y)	Ab75781	ABCAM	Rabbit	1:500-1:1000
UBF-1 (H-300)	Sc-9131	Santa Cruz Biotechnology	Rabbit	1:500-1:1000
DICER	Ab13503	ABCAM	Rabbit	1:500-1:1000
ADAR2 (Red1)	ab64830	ABCAM	Rabbit	1:500-1:1000
Drosha	Ab-07-717	Millipore	Rabbit IgG	1:500-1:1000
DGCR8 (Pasha)	Ab36865	ABCAM	Rabbit	1:500-1:1000
SF2/ASF/SRp30	Sc-28724	Santa Cruz Biotechnology	Rabbit	1:500

9G8/SRp20	Sc-28722	Santa Cruz Biotechnology	Rabbit	1:500
SAFB	NB100-2593	Novus Biologicals	Rabbit	1:500
TARDBP	10782-2-AP	Proteintech Group Europe	Rabbit	1:500-1:1000
FUS/TLS	Sc-47711	Santa Cruz Biotechnology	Mouse	1:500-1:1000
PSPC1	AB1013	Dundee Cell Products	Rabbit	1:1000
SFPQ (PSF)	15585-1-AP	Proteintech Group Europe	Rabbit	1:1000
p54nrb (NONO)	Sc-67016	Santa Cruz Biotechnology	Rabbit	1:1000
MBNL1/2/3	Sc-98455	Santa Cruz Biotechnology	Rabbit	1:500-1:1000
EWSR1	Ab93837	ABCAM	Rabbit	1:500-1:1000
TAF15	Ab69581	ABCAM	Rabbit	1:500-1:1000
IdU/BrdU	IU4	Caltag Laboratories	Mouse IgG	1:500-1:1000
BrdU	BU-33	Sigma	Mouse IgG	1:500-1:2000
BrdU	Ab38890	Abcam	Rabbit	1:500-1:2000

Table 2.2

A table showing the different primary antibodies used in the studies throughout this thesis.

2.4 Image Analysis

Slides were viewed under the Leica TCS SPE confocal laser scanning microscope with a 63×oil immersion objective. Z series stacks were taken and serial sections were acquired. ImageJ 1.43s (2010) was used for quantitative image analyses. Deconvolution and isosurface rendering were performed using the Huygens Professional (SVI) and Imaris software with assistance from Daniel Ciantar. Electron micrographs were obtained by a Gatan Orius digital camera (SC600 CCD) with the Gatan software. In all studies, multiple replicates were performed with several animals. All statistical tests were by Student's unpaired t-test unless otherwise stated in the text. Significance value of $p \leq 0.05$ was used for multiple comparisons.

Results

CHAPTER 3

Results

Studies in this thesis focus on the striatum, in which over 95% of the cells are medium spiny neurons. These GABAergic projection neurons are spherical cells with a diameter of approximately 10μm. The striatal neurons have been well characterized and extensively studied in this laboratory. The structural, functional and molecular organization of the striatal neurons is well understood, and the pathological changes within the striatum in HD, ALS/FTLD and FTDP-17 have also been documented (DiFiglia et al., 1997, Halabi et al., 2012).

3.1 Epigenetic Characterization of the Striatal Neuronal Nucleus

An immunocytochemical study was carried out to localize various epigenetic markers involved in histone modifications, DNA methylation, chromosomal domains and perinucleolar bodies in the striatal neuronal nucleus. All primary antibodies used are well-characterized which produce a distinct staining pattern. Analysis by confocal microscopy of immunofluorescently stained sections revealed the distribution of these proteins and their subnuclear localization in a Z-series stack. The localization in relation to the nucleolus was shown in conjunction with pyronin Y (RNA) staining which clearly demarcated both the nucleolus and the cytoplasm.

3.1.1 Histone Modifications

Immunofluorescence of H3K9M3 (marker of constitutive heterochromatin) and H1 (linker histone 1) revealed a similar distribution as perinucleolar foci around the nucleoli (Fig 3.1A and C). This is very surprising as a linker histone is expected to label all DNA. However, this interesting result has also been reported in a number of studies (Akhmanova et al., 2000). Immunofluorescence of H3K27M3 (a marker of facultative heterochromatin) however illustrated both perinucleolar and nucleoplasmic foci (Fig 3.1B). In contrast to the heterochromatin associated proteins, antibodies against acetylated histones H3K9Ac (marker of euchromatin), AcH3 (acetylation of lysine residues 9 and 14 on H3 tail) and AcH4 (acetylation of lysine residues 5,8,12 and 16 on H4 tail) demonstrated homogeneous nucleoplasmic staining. Nevertheless, nucleoplasmic staining with AcH4 was relatively heterogeneous (Fig 3.1D-F).

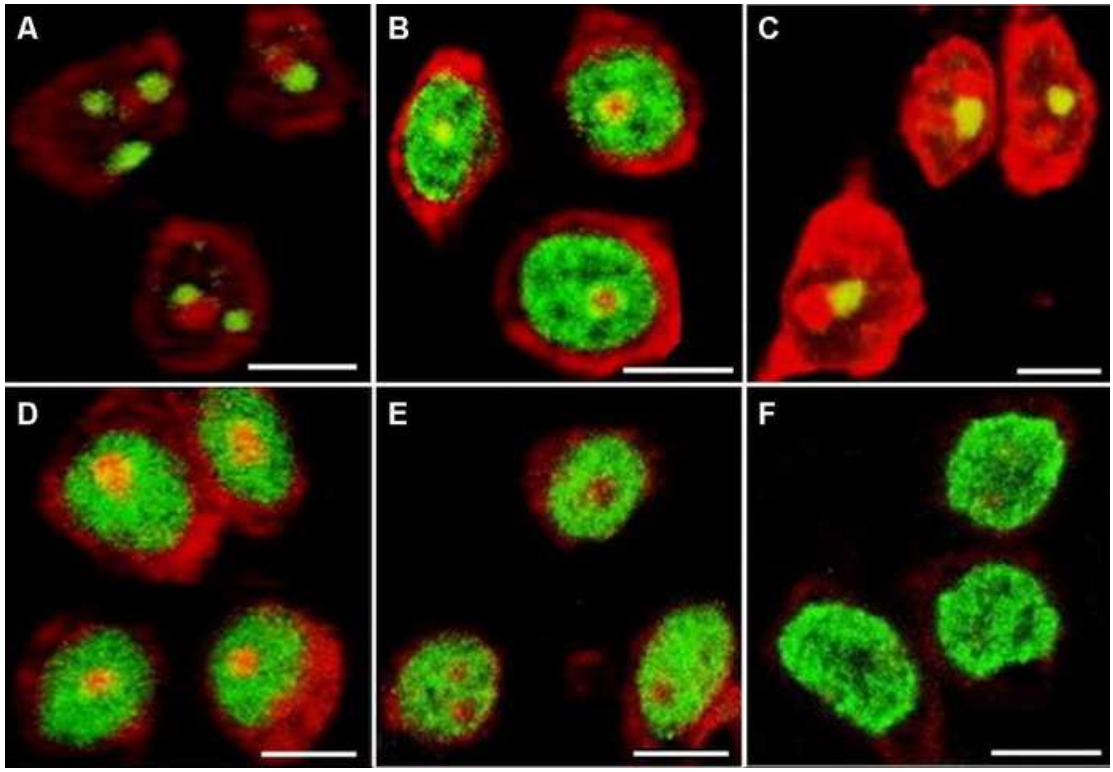

Figure 3.1

Fluorescence immunocytochemistry of striatal neuronal nuclei stained for various histone modifications and RNA

Nucleolus and cytoplasm were counterstained red for RNA with pyronin Y. FITC immunofluorescence (green) staining identified H3K9M3 (A) and Histone H1 (C) as foci around the nucleoli (red structures). Immunofluorescence (green) of H3K27M3 in conjunction with pyronin Y (red) revealed its localization as perinucleolar and nucleoplasmic foci (B). H3K9Ac (D) and AcH3 (E) both revealed homogeneous nucleoplasmic staining (green) whereas AcH4 (F) demonstrated a heterogeneous distribution inside the nucleus. Scale bars = 10µm

3.1.2 MBDs and Other Heterochromatin Associated Proteins

Antibodies to the heterochromatin associated protein MeCP2, methyl-CpG binding protein 2, identified as perinucleolar foci adjacent to the nucleoli (Fig 3.2A). Immunofluorescence analysis of phosphorylation of MeCP2 at serine 80 and 421 with phosphorylation specific antibodies revealed a broadly similar staining pattern (Fig 3.2B-C), although nuclear foci in addition to perinucleolar foci were found in phospho-MeCP2-pS80 stained nuclei (Fig 3.2B). Similar to other heterochromatin associated proteins, immunolocalization revealed perinucleolar foci around the nucleoli with antibodies against ATRX (alpha-thalassemia mental retardation X-linked), a chromatin remodeling protein that recognizes and binds to MeCP2 (Fig 3.2D). Unexpectedly, antibody against HP1α (heterochromatin protein 1), which binds to H3K9M3 leading to DNA methylation and binding of MeCP2, demonstrated a homogeneous nucleoplasmic staining (Fig 3.2E).

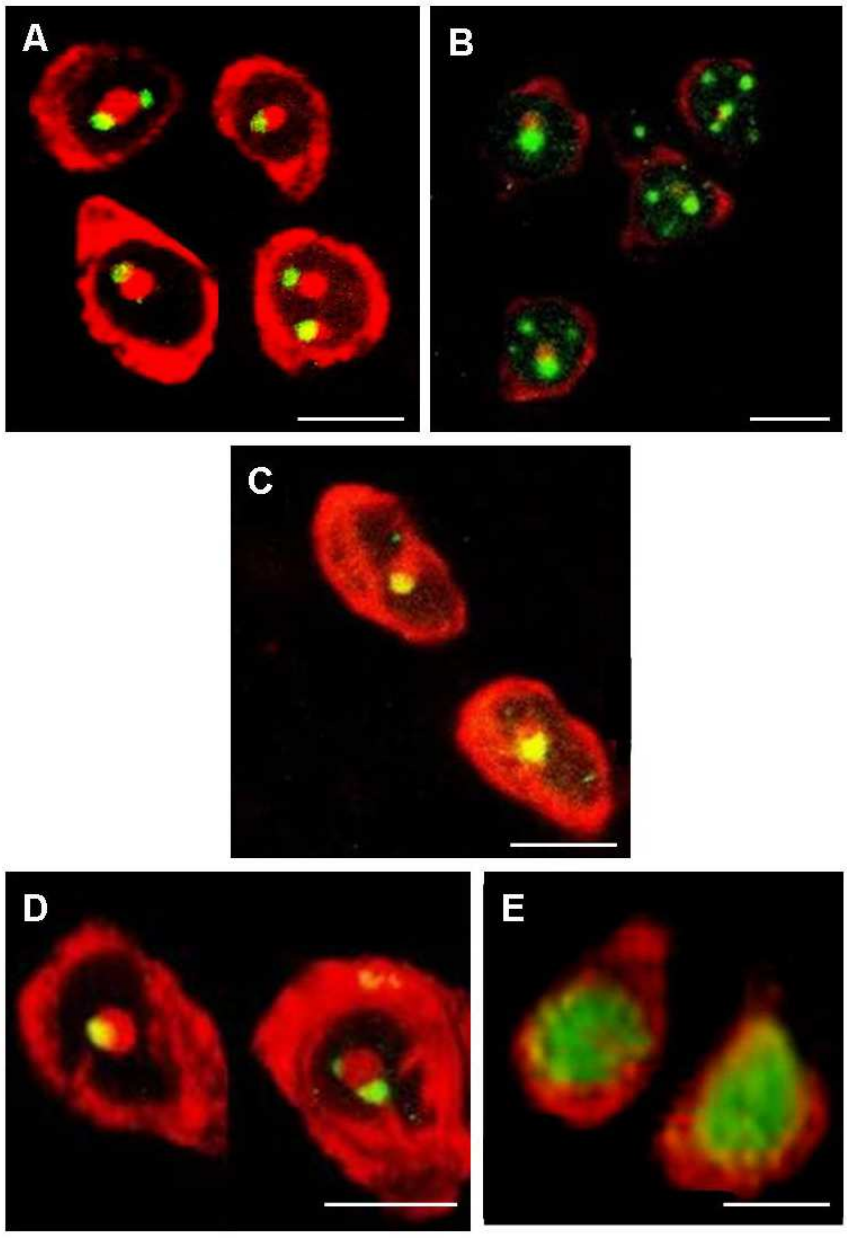

Figure 3.2

Immunolocalization of Methyl-CpG binding domain proteins and heterochromatin associated proteins in striatal neuronal nucleus

Perinucleolar immunofluorescence (green) of MeCP2 (A), Phospho-MeCP2-pS421 (C), and ATRX (D) adjacent to the nucleoli (red dots) stained with pyronin Y. Immunofluorescence (green) of Phospho-MeCP2-pS80 (B) demonstrated perinucleolar and nuclear foci. Homogeneous nucleoplasmic staining (green) was found with antibody against HP1α (E) counterstained with pyronin Y (red) showing the cytoplasm. Scale bars = 10μm

3.1.3 Perinucleolar Heterochromatin

Neuronal nuclei can stained for their content of DNA and RNA with the fluorescent dyes 4',6-diamidino-2-phenylindole (DAPI) and pyronin Y (PYY). Within the nucleoplasm are further defined areas of DAPI-positive heterochromatin. Despite the absence of heterochromatin around the nuclear membrane, there is a distinct perinucleolar ring of heterochromatin in addition to 1-2 large masses of perinucleolar heterochromatin and nucleoplasmic masses of heterochromatin (Fig 3.3). Epigenetic analysis of the molecular composition of the perinucleolar heterochromatin (PNH) suggested that it contains methylated DNA, bound by high levels of MeCP2, ATRX and the epigenetic marks of histone variants H3K9M3 and H3K27M3. Genomic regions present within the PNH were identified using a combination of 3D-fluorescence in situ hybridization (FISH) and 3D-immunocytochemistry (ICC) analyses. Antibodies against the kinetochore protein CENP-A or ACA (autoimmune antisera from patients with CREST-type scleroderma) revealed multiple foci, centromeres, within the neuronal nuclei. Interestingly, triple labeling for DNA, RNA and centromeres illustrated that the majority of centromeres were found on the borders of the PNH. Using either 3D-FISH with pan-centromeric probes or ACA antibodies, it was confirmed that the majority of centromeres (86%) were found in clusters associated with PNH (Fig 3.4). Moreover, 3D-FISH with the pan-telomeric probes also demonstrated that telomeres clustered around the nucleolus and 80% were found on the borders of PNH (Fig 3.4). These results suggested that most of the chromosomes loop into the nuclear interior while having both ends associated with the PNH, which therefore implied that these neurons do not follow the classical Rabl

model for radiating chromosomal arrangement. Further investigations of the PNH using electron microscopy in both male and female mice illustrated that these areas of PNH were 30% larger in female compared to male mice. In addition, ICC analysis with antibody against the histone variant macro-H2A.1, which is specifically associated with the inactive X chromosome, identified the PNH in female but not male mice (data not shown). These together indicated that the large caps of PNH which characterize the striatal neuronal nucleus are an amalgamation of constitutive and facultative heterochromatin.

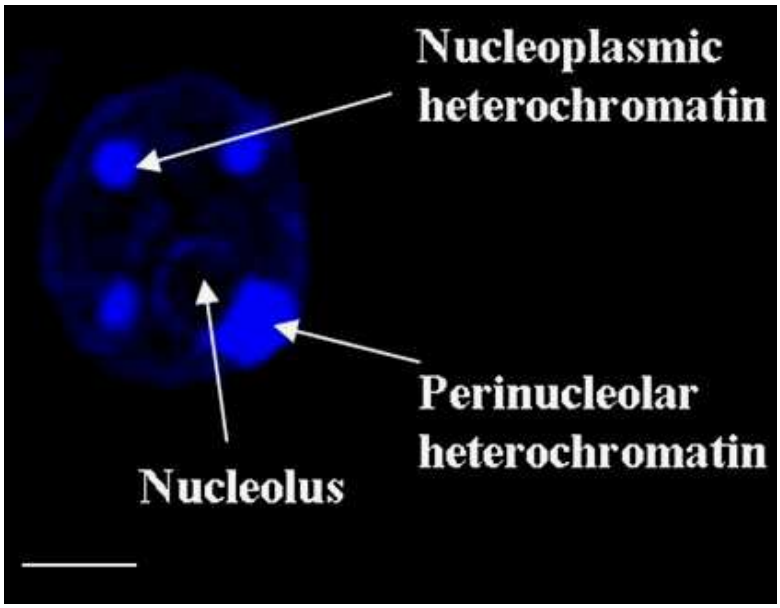

Figure 3.3

DAPI staining of the striatal neuronal nucleus

The nucleolus, the perinucleolar and nucleoplasmic heterochromatin are revealed by DAPI staining.

Scale bar = 5μm

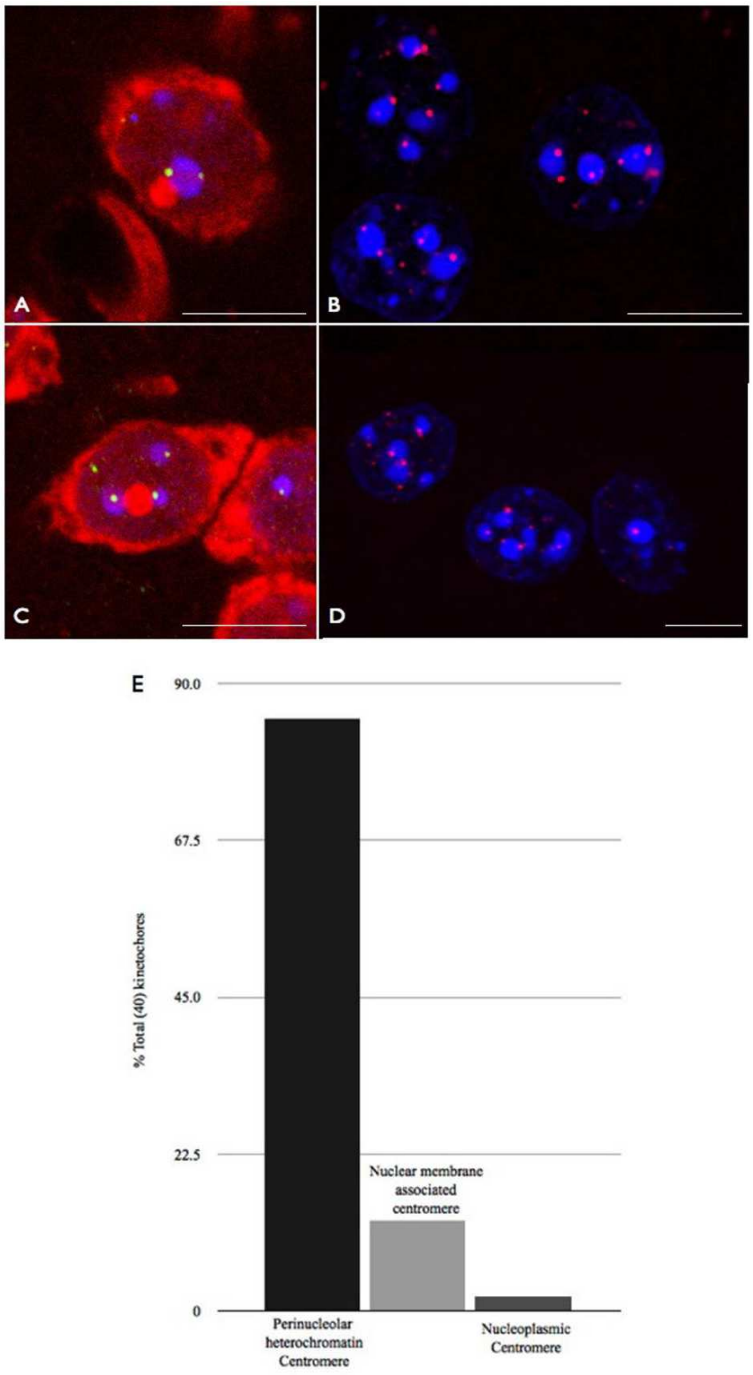

Figure 3.4

Association of centromeres and telomeres with perinucleolar heterochromatin

(A) and (C) Triple labeled sections of striatum revealing heterochromatin (condensed DNA stained blue with DAPI), nucleolus and cytoplasm (RNA stained red with pyronin Y) and centromeres (green ACA antibody, FITC).

(B) and (D) Striatal neuronal nuclei double labeled for DNA (DAPI) and 3D FISH for telomeres (red).

(E) 3D FISH with pan-centromeric probes revealed that the majority of centromeres (86%) were found in clusters associated with PNH, much greater than that associated with the nuclear membrane or within nucleoplasm. Scale bars = 10μm

3.1.4 Rosettes of Perinucleolar Cajal Bodies

Interspersed between these large masses of PNH were found the Cajal body marker proteins Nopp140 and p80 coilin, which localized to several spherical and crescent shaped structures distributed around the periphery of the nucleolus (Fig 3.5 and Fig 3.6). However under electron microscopy, only the largest p80 coilin/Nopp140/SMN positive structures were seen as coiled bodies (Fig 3.8C). Thus, the nucleolus appeared to be completely encircled in a rim of heterochromatin to which large caps of heterochromatic masses (PNH) and intercalated rosettes of perinucleolar Cajal bodies were attached (Fig 3.6).

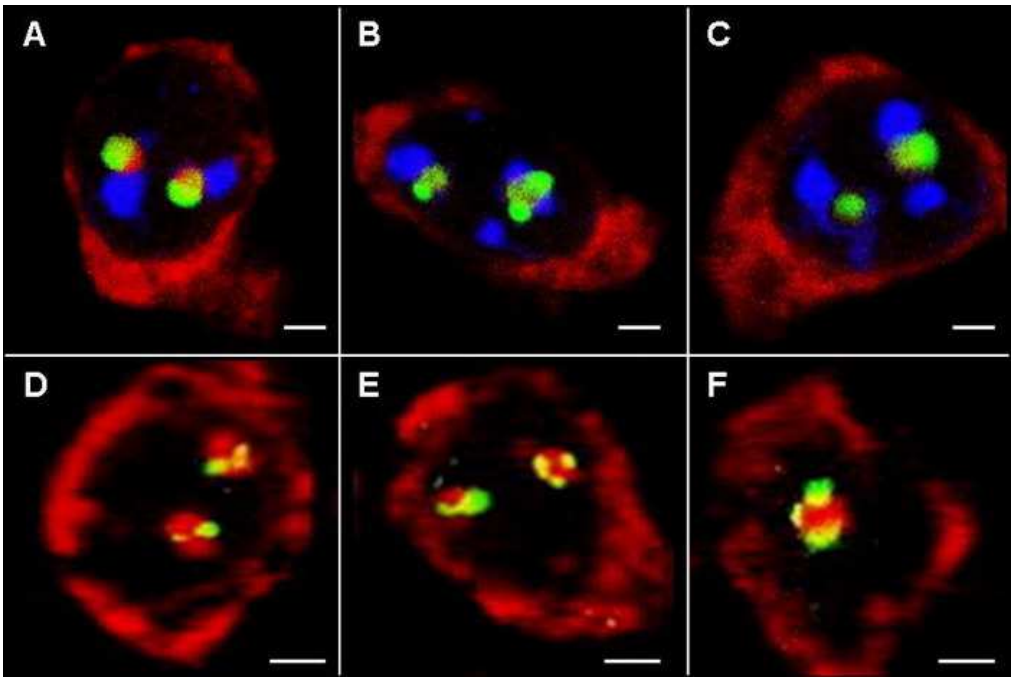

Figure 3.5

Immunolocalization of the Cajal body markers Nopp140 and p80 coilin in the striatal neuronal nucleus

(A-C) Triple labeling with FITC (green), DAPI (blue) and pyronin Y (red) demonstrated immunolocalization of Nopp140 (green) adjacent to DAPI stained heterochromatin foci (blue) and overlapped with pyronin Y stained nucleoli.

(D-F) Immunofluorescence of p80 coilin (green) localized as perinucleolar caps surrounding pyronin Y stained nucleoli (red dots). Scale bars = 2μm

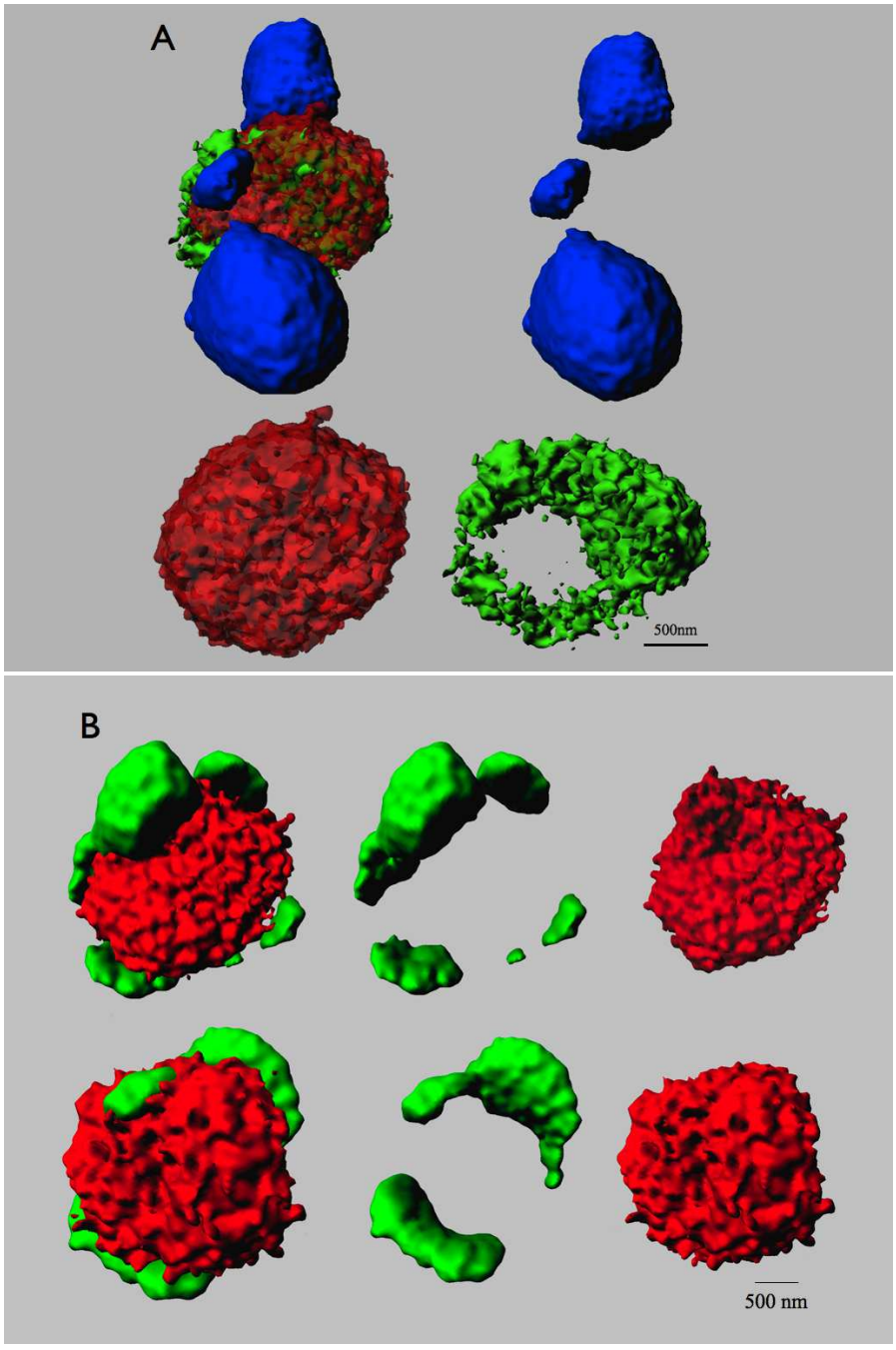

Figure 3.6

Isosurface rendered images of striatal neuronal nuclei immunostained for markers of CBs

(A) Isosurface rendered image of triple labeled z-series of sections (N=52) of nucleolus (stained red for RNA with pyronin Y), PNH (stained blue for condensed DNA with DAPI) and perinucleolar rosette of Cajal bodies (FITC green immunofluorescence for Nopp140).

(B) Isosurface rendered images from two nuclei of striatal neurons (confocal z-series of 30 sections) immunostained for p80 coilin (green) and counterstained for pyronin Y (red nucleolus) clearly showing the perinucleolar rosette of Cajal body marker p80 coilin.

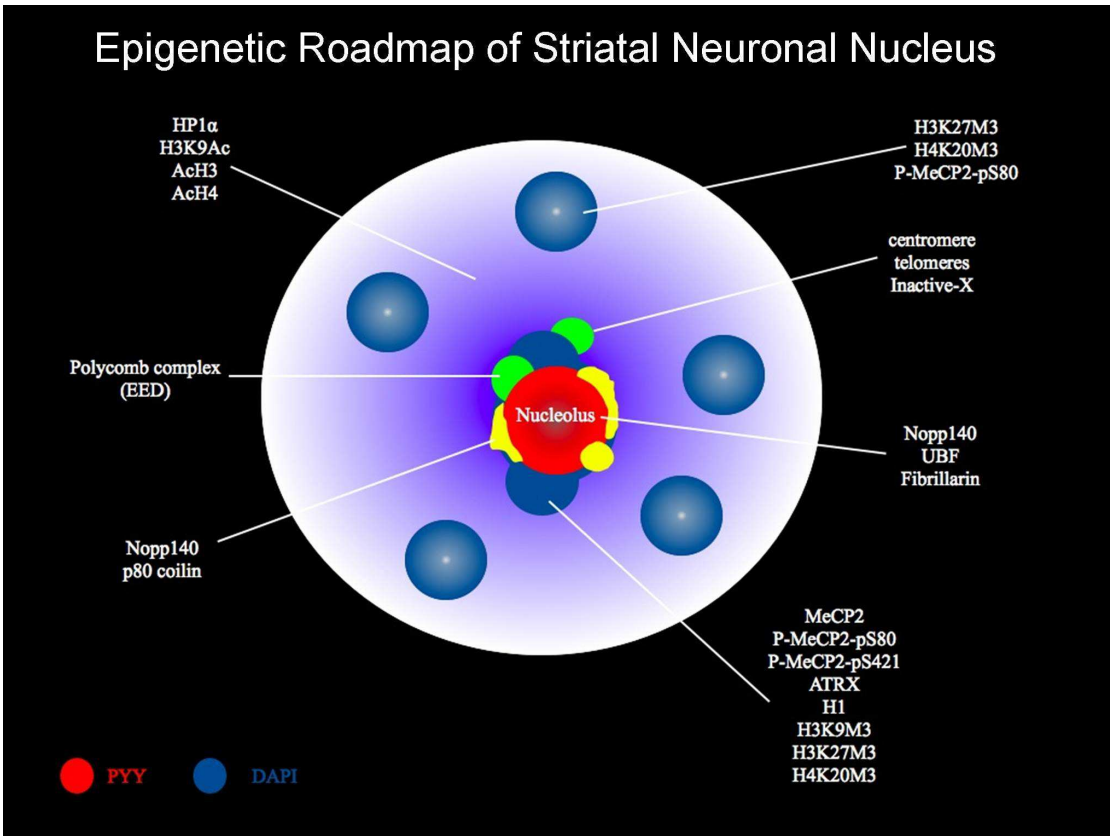

Figure 3.7

Schematic diagram summarizing the immunofluorescence staining results with different antibodies in the striatal neuronal nucleus

Immunofluorescence of antibodies under confocal microscopy demonstrated the distribution and localization of various proteins associated with epigenetic modifications. Blue dots represent DAPI stained heterochromatin foci and red dot represents pyronin Y stained nucleolus. MeCP2, phosphor-MeCP2-pS80, phosphor-MeCP2-pS421, ATRX, H1, H3K9M3, H3K27M3 and H4K20M3 were associated with perinucleolar heterochromatin. H3K27M3, H4K20M3 and phosph-MeCP2-pS80 were also localized in nucleoplasmic heterochromatin. HP1α, H3K9Ac, AcH3 and AcH4 were distributed throughout the nucleoplasm representing the euchromatin. The Cajal body markers Nopp140 and p80 coilin were found adjacent to the perinucleolar heterochromatin around the nucleolus. (Results not shown for EED, H4K20M3, UBF, fibrillarin and inactive X)

3.2 Functional Transcriptional Characterization of Neuronal Nucleus

3.2.1 *In vivo* Transcription

To investigate the functional significance of this epigenetic and ultrastructural organization of the neuronal nucleus, a novel *in vivo* nuclear transcription run-on assay was used to detect nascent RNA synthesized within specific time frames in the mouse bran. Nascent RNA produced 15 minutes after an intraperitoneal *in vivo* injection of 5'fluorouridine localized to the striatal neuronal nucleus was shown in Fig 3.8A, in which RNA was distributed throughout the nucleoplasm as discrete puncta, or transcription factories. Analysis of serial sections through several neuronal nuclei revealed that in a nucleus there are on average 8580 +/- 1296 (mean +/- sd) such sites, which occupy approximately 12% of the nucleoplasm. Together with a recent report of 8800 expressed genes within the mouse striatum, approximately 1 gene per transcription factory is suggested. Although the authors suggest that this estimate is highly conservative, the true value is likely to be between 1 and 2.5 taken account of the 21,622 expressed genes in the mouse genome (Zhang et al., 2004). It is therefore unlikely that neurons have any super-transcription-factories, transcribing up to 20 genes, as described in other cell types (Eskiw and Fraser, 2011). Surprisingly, the PNH appeared to be heavily labeled for nascent RNA whereas very low levels of RNA synthesis were found within the nucleolus. In addition, high levels of transcription were also observed at nuclear periphery adjacent to the nuclear membranes (Fig

3.8A). This punctuate pattern of labeling became less distinct with increasing time after fluorouridine injection, in which the nuclear pores and cytoplasm were additionally labeled. At later time points the axons and dendrites were also labeled.

Post-embedding immunogold ICC was used to further detect and quantify nascent RNA in the nucleolus, PNH and Cajal body (Fig 3.8B-D). A Z-stack of approximately 50 sections was taken for serial section analysis and this was repeated three times. No RNA synthesis was detected within the Cajal body and very low levels of transcription were found in the nucleolus. However within the PNH, significantly higher levels of transcription, a rate of synthesis 1500% greater than that in the nucleoplasm was found which nevertheless accounted for only 27% of the total transcription in the nucleus. This suggested that in the striatal neuronal nucleus, RNA synthesis is continuously taking place at different rates within various nuclear sub-compartments, with the highest rates within the PNH. The patterns of nascent RNA distribution detected in both immunofluorescence and immunoelectron microscopy analyses demonstrated consistent results which presented striking differences to the accepted patterns of transcription in the eukaryotic cell nucleus (Chakalova and Fraser, 2010, Papantonis and Cook, 2010, Fraser and Bickmore, 2007, Akhtar and Gasser, 2007). (See chapter 2.2.3 Control experiments for *in vivo* transcription run-on assay)

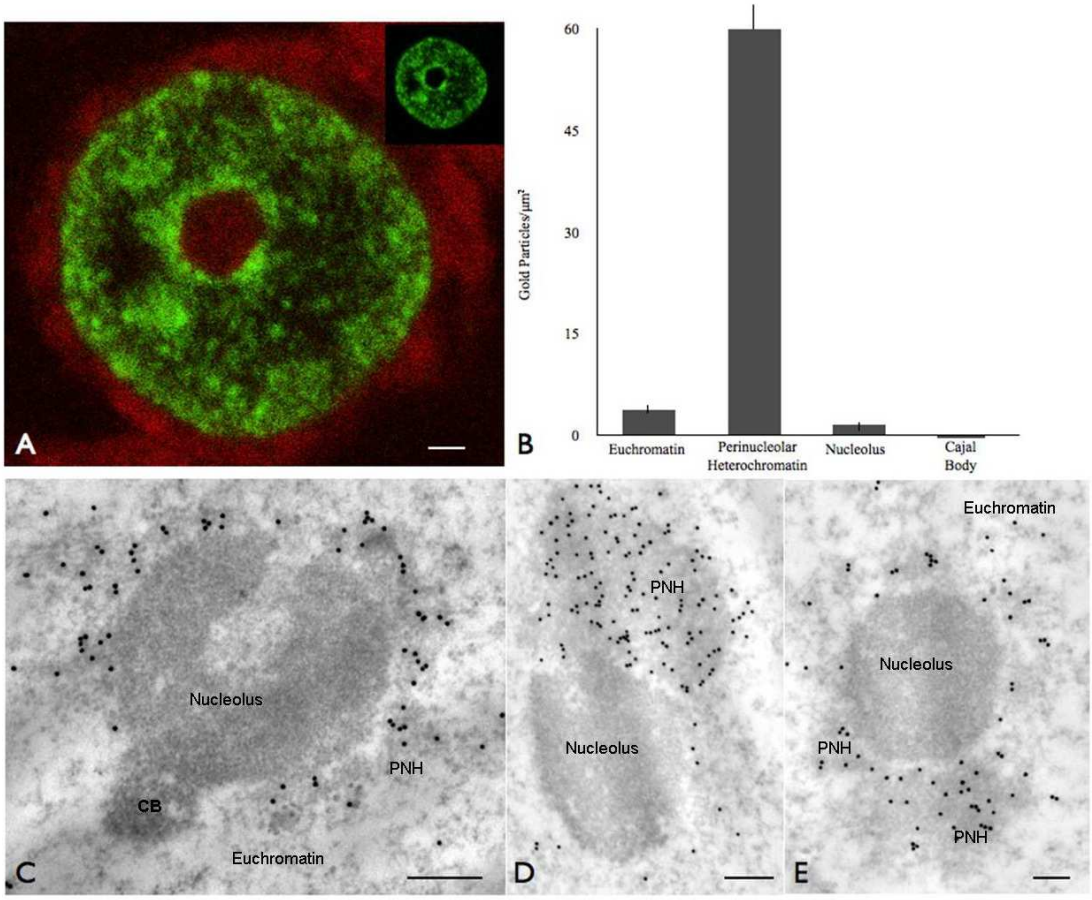

Figure 3.8

Sections of striatal neurons stained for the transcription run-on assay localizing nascent RNA

(A) Striatal neuronal nucleus stained with Fluoro-UTP (green FITC) for nascent RNA and for total RNA (red pyronin Y). Scale bar = 1µm.

(B) Analysis of 50 thin sections (70nm) through striatal neuronal nuclei 15 minutes after administration of fluorouridine *in vivo*. Detection and quantification of nascent RNA using post-embedding immunogold immunocytochemistry indicated the significant highest rate of RNA synthesis within the perinucleolar heterochromatin.

(C), (D), (E) EM immuno-localization of nascent RNA with post-embedding nano-gold detection. Scale bars = 500nm.

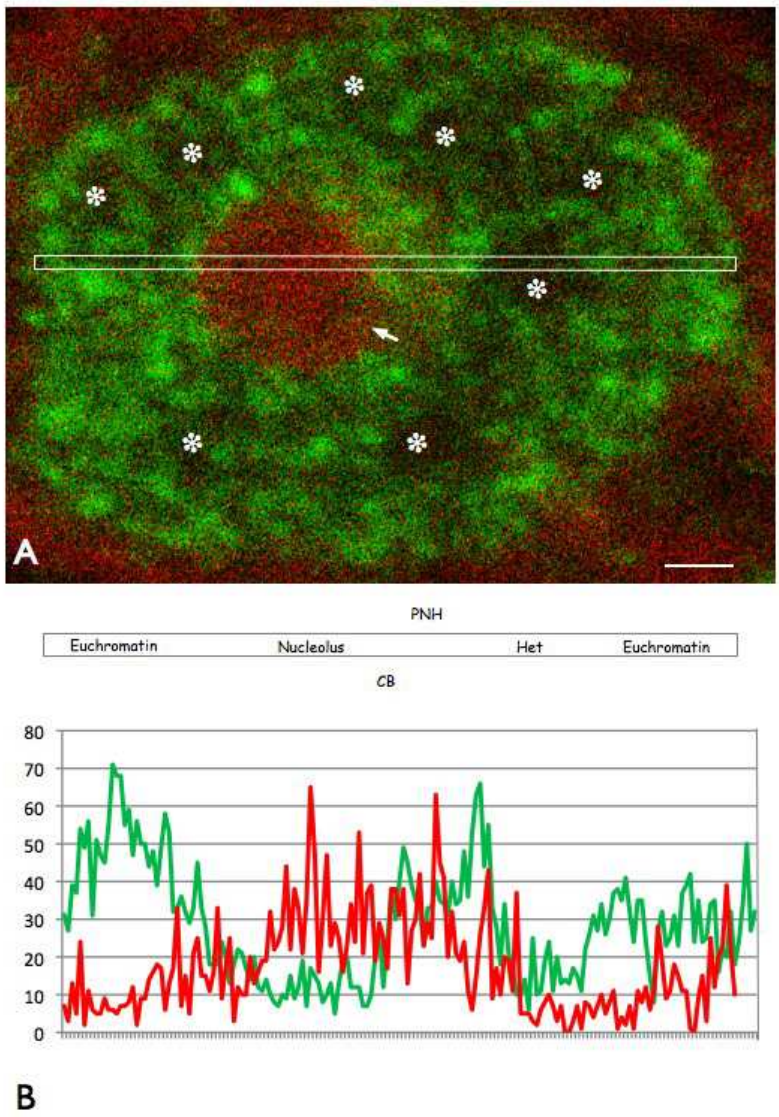

Figure 3.9

Nucleus of striatal neuron stained for nascent RNA (green FITC) and total RNA (red pyronin Y) in (A), and densitometric scan across transect of nucleus encompassing euchromatin, heterochromatin (asterisks), nucleolus and Cajal body (CB, arrowed) and perinucleolar heterochromatin (PNH) in (B). Scale bar in (A) = 1µm.

3.2.2 Ultrastructural Localization of the RNA Polymerase Enzymes

Apart from nascent RNA production, the demonstration of active subunits of RNA polymerase enzymes provided further support and evidence as to the nature of the transcripts. ICC with various antibodies to both dephosphorylated

and phosphorylated forms of the C-terminal domain of RNA polymerase II, which recognized RNA pol II in the poised, initiation and elongation phases of mRNA transcription, demonstrated extensive labeling throughout the nucleoplasm and yet failed to detect any sites within the PNH (Fig 3.10). Surprisingly, PNH was clearly labeled with antibodies to RNA polymerase III albeit with fairly low density (Fig 3.10G). Post-embedding ICC further labeled RNA polymerase I within the nucleolus, in addition to UBF, an essential component of RNA pol I mediated transcription. These antibodies clearly labeled the nucleolus but not the PNH (data not shown). It is therefore postulated that the nascent RNA detected at early time points within the PNH was the product of RNA polymerase III mediated transcription. No labeling was found in the perinucleolar Cajal bodies with antibodies to 5'fluorouridine or any of the RNA polymerase enzymes, suggesting that the Cajal bodies were not involved in transcription or transcriptosome assembly.

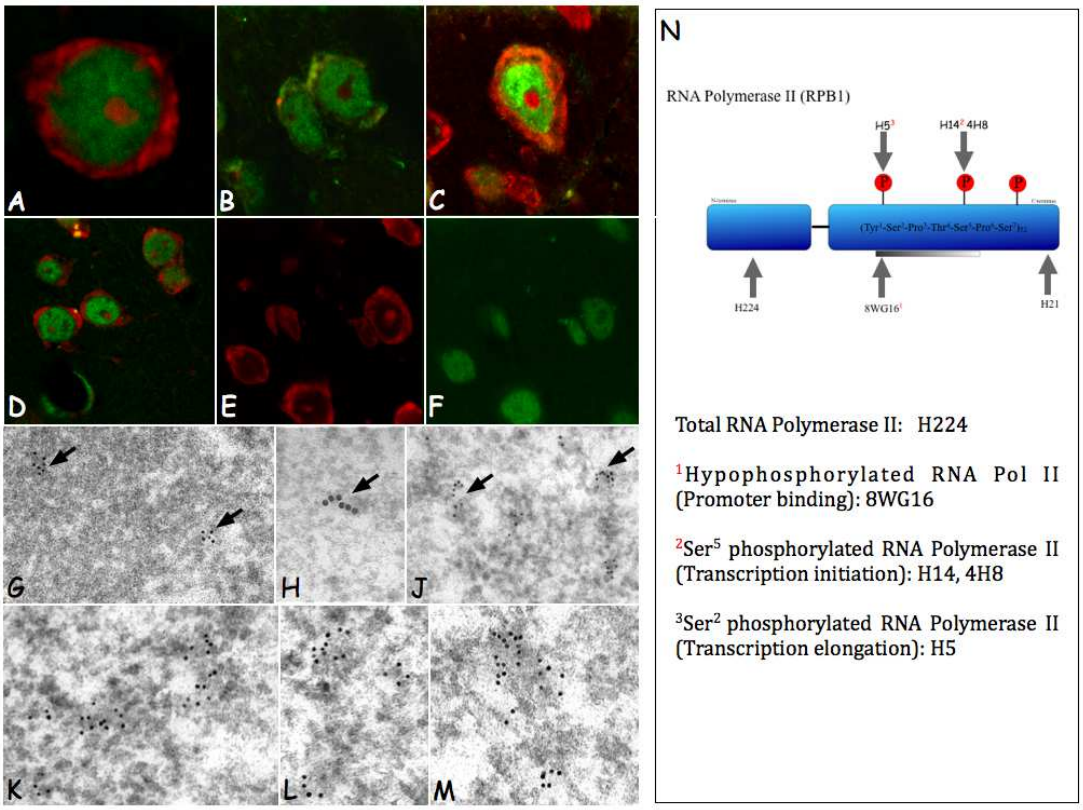

Figure 3.10

Immunocytochemical localization of RNA polymerases in the striatal neuronal nucleus

RNA polymerase II detected in euchromatin by antibodies 8WG16 (A, K), H5 (B, H), H14 (C, M), H224 (D, L) and 4H8 (F, J). RNA polymerase III detected in the perinucleolar heterochromatin with antibody RPC32 (H-136) (G). Section in (E) was stained with pyronin Y showing nucleolus and perinucleolar heterochromatin, and was shown stained for RNA polymerase II in (F). Schematic diagram in (N) illustrates the C-terminal domain of RNA polymerase II, this heptad repeat is present in 52 copies in the murine protein. The antigenic specificity of the antibodies used is illustrated.

3.2.3 Post-transcriptional Processing

Despite the high levels of RNA seen within the nucleolus, a very low level of transcription was detected. This was in accord with a detailed and thorough ultrastructural and ICC analysis of the striatal neuronal nucleolus, which failed to demonstrate the classic tripartite structure; fibrillar centre (FC), granular component (GC) and dense fibrillar component (DFC) for a large percentage

of striatal neurons. Rather there seemed to be FC surrounding by an entanglement of the GC and DFC (Elizabeth Slavik-Smith PhD thesis, personal communications).

Surprisingly, localization of several RNA modifying enzymes with ICC ascribed additional functions to the nucleolus. Antibodies to the RNA-editing enzymes ADAR2 (RED1), Dicer, Drosha and DGCR8 were all localized in the neuronal nucleoli (Fig 3.11). This might suggest that the neuronal nucleolus is additionally specialized for non-coding RNA (ncRNA) editing and processing. Indeed, additional roles of the nucleolus other than rRNA transcription have currently become a topic of considerable interest (Boulon et al., 2010). This would appear to be in accord with the previous demonstration of RNA pol III mediated transcription within the PNH around the nucleolus. Taken together the perinucleolar rosette of Cajal bodies, these results suggest that the PNH, nucleolus and Cajal bodies form an integrated complex which is highly developed in neurons. It might be suggested that transcription of ncRNA takes place in the PNH, editing and processing in the nucleolus, and then maturation in the Cajal bodies. However, this hypothesis remains to be proven.

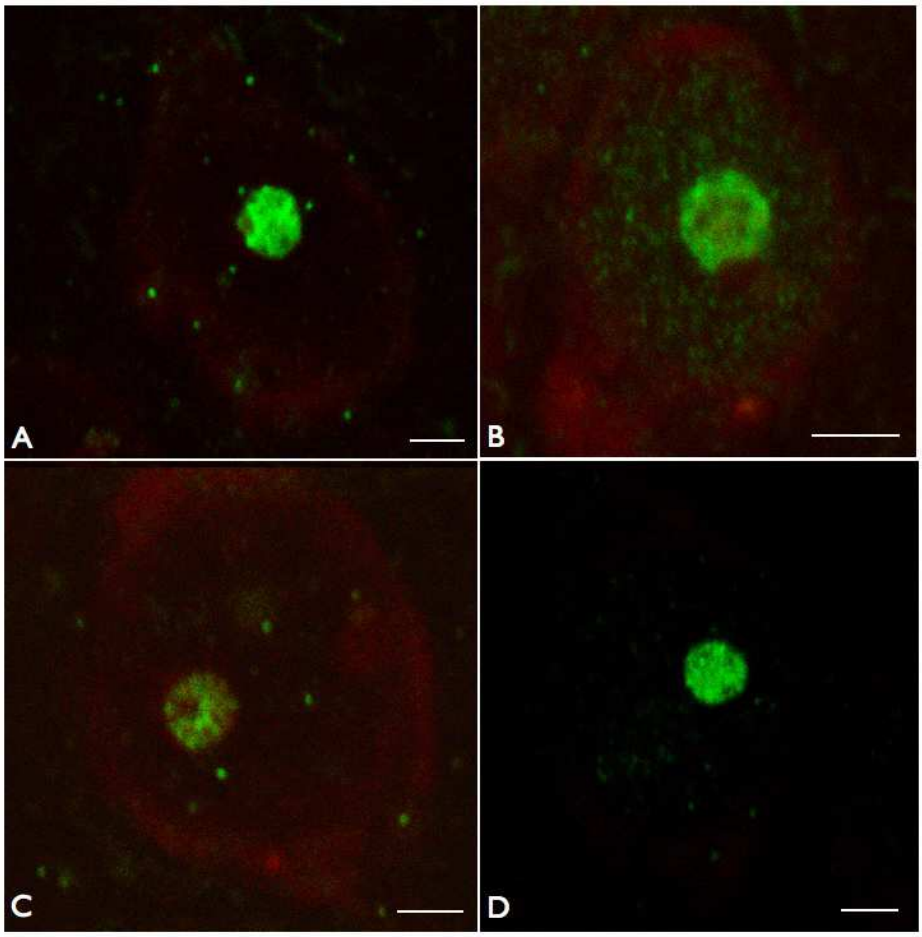

Figure 3.11

Immunofluorescence of RNA processing enzymes in the striatal neuronal nucleoli

Nucleoli of striatal neurons stained with antibodies to the RNA processing enzymes ADAR2 (RED1) in (A), DICER1 (B), Drosha (C), and DGCR8 (Pasha) in (D). Sections were lightly counterstained with pyronin Y. Scale bars = 2μm.

3.3 Neuronal Nuclear Rearrangement Induced by HDAC Inhibition

In order to investigate any change in the patterns of epigenetic modifications in the striatal neurons following histone deacetylase (HDAC) inhibition which activates transcription, ICC was carried out with antibodies used previously to localize their nuclear distribution in the nuclei of drug

treated mice. Two clinically used histone deacetylase inhibitors (HDACi) were used for the studies: selective HDACi sodium valporate (VPA); and non-selective HDACi suberoylanilide hydroxamic acid (SAHA, Vorinostat), which are both potent and CNS active. Mice without drug treatment were injected with saline as controls for comparison. All brain sections of control and drug treated mice were processed equally in paired processing. For each study, around 10 non-adjacent sections were examined per mouse and 5-10 mice were studied in each saline, VPA and SAHA treatment.

3.3.1 Histone H1 and Histone Acetylation

Immunofluorescence of the linker histone H1 demonstrated perinucleolar foci in striatal neuronal nuclei of saline treated mice. The same staining pattern was also observed following both VPA and SAHA treatment (Fig 3.12).

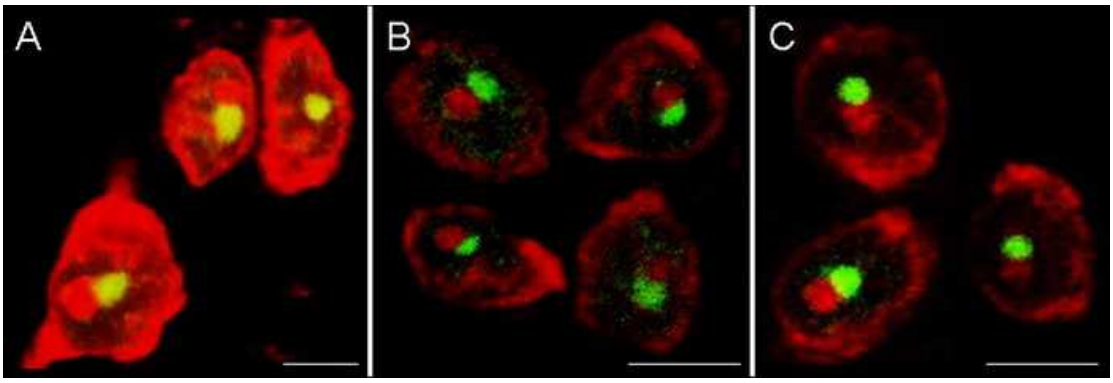

Figure 3.12

Histone H1 immunolocalization in the striatal neuronal nuclei of saline, VPA and SAHA treated mice

Immunofluorescence (green) revealed perinucleolar foci adjacent to the nucleoli (red dots) in saline treated mice (A). Similar staining was found in both VPA treated (B) and SAHA treated (C) mice. Pyronin Y counterstaining (red) illustrated the nucleoli and cytoplasm. Scale bars = 10μm

In addition to ICC, transect analysis was carried out using ImageJ software

in order to access and quantify the intensity of staining within the nuclei. Transects were taken through the nuclei, each of which represented the diameter (around 10μm/40 pixels) and the intensity of staining was analyzed within each transect using line profiles. 40 transects from 40 nuclei were taken each from saline, VPA and SAHA treated mice. An average staining intensity was then plotted as a line graph as shown in Fig 3.14A and Fig 3.16A. AcH3 immunofluorescence revealed homogeneous nucleoplasmic staining in both saline and VPA treated mice (Fig 3.13A and B). However a much brighter staining was found in VPA treated mice, with a significantly higher average intensity of nucleoplasmic staining (21.4% increase compared with saline controls) as shown in Fig 3.14. This indicated that following HDAC inhibition with VPA treatment, there was indeed an increased acetylation of histone (on lysine residues 9 and 14 on H3 tail). The nuclear distribution of AcH4 in both saline and VPA treated mice was comparatively heterogeneous (Fig 3.13C and D). However unlike AcH3, there was a significant decrease (10.9% compared with controls) in the average nucleoplasmic staining intensity following VPA treatment (Fig 3.14).

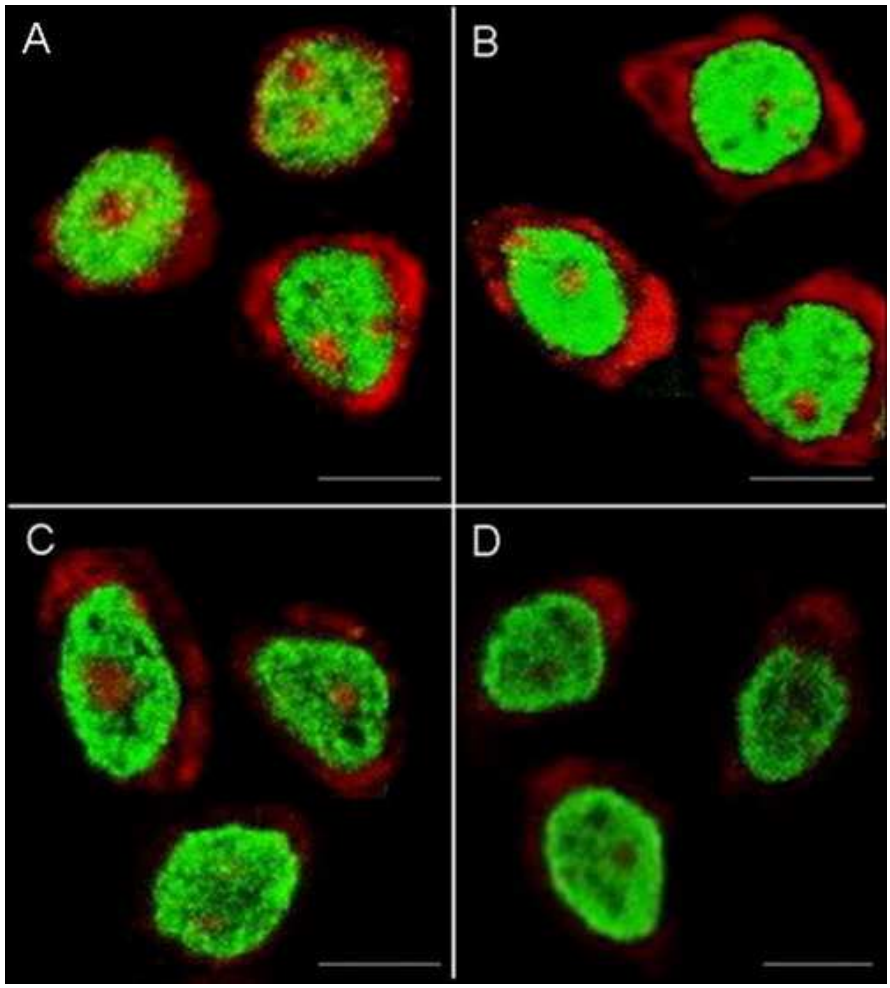

Figure 3.13

AcH3 and AcH4 immunolocalization in striatal neuronal nuclei of saline and VPA treated mice

Brighter AcH3 nucleoplasmic staining (green) was observed in the nuclei of VPA treated mice (B) compared to that in saline treated mice (A). Immunofluorescence (green) of AcH4 revealed heterogeneous nucleoplasmic staining in both saline (C) and VPA treated (D) mice. However, staining intensity was relatively weaker with VPA treatment. Pyronin Y counterstaining (red) revealed the nucleolus and cytoplasm. Scale bars = 10μm.

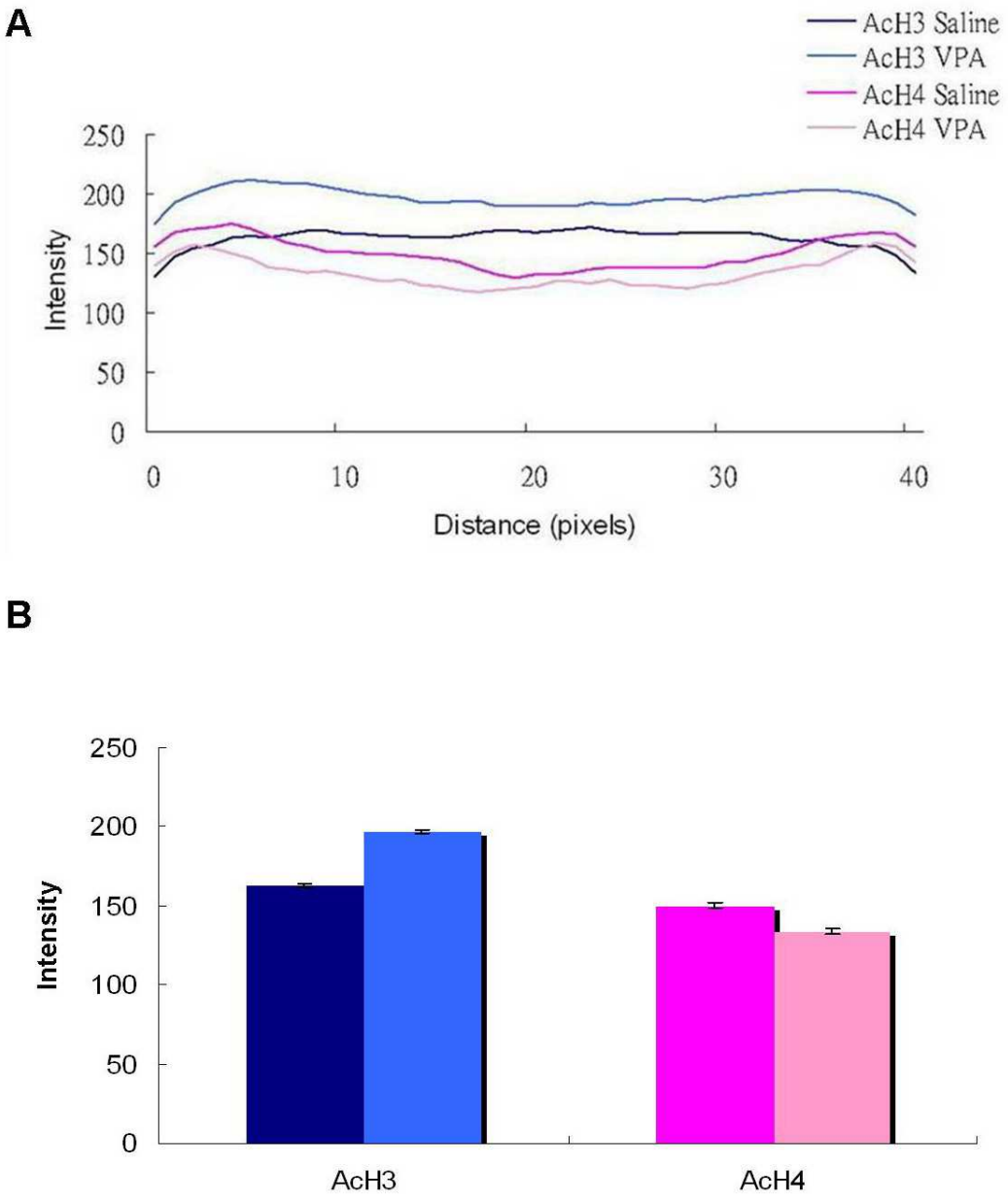

Figure 3.14

Average intensities of AcH3 and AcH4 nucleoplasmic staining in saline and VPA treated mice

(A) Transect analysis through the cells stained for AcH3 and AcH4 in saline and VPA treated mice. The average intensities of FITC (green) nucleoplasmic staining were plotted as a line graph (n=40). Each transect represented the cell diameter with a length of 10μm/40 pixels.

(B) The average intensity of AcH3 nucleoplasmic staining was significantly increased in the nuclei of VPA treated mice compared with that in saline treated mice. However, a significant decrease in the average intensity of AcH4 nucleoplasmic staining was found following VPA treatment compared with saline treated controls.

A more prominent increase in both histones H3 and H4 acetylation was observed with the non-selective HDACi SAHA. Immunofluorescence of AcH3 revealed similar homogeneous nucleoplasmic staining in the striatal neuronal nuclei of both saline and SAHA treated mice. Again a much brighter staining was found following SAHA treatment (Fig 3.15A and B), with an 18.8% increase in the average nucleoplasmic staining intensity compared with the saline controls (Fig 3.16). Similar heterogeneous nucleoplasmic distribution of AcH4 was observed in saline and SAHA treated mice (Fig 3.15C and D). Interestingly, a more significant increase in the average intensity of AcH4 staining (26.8% compared with saline controls) was found in the nuclei of SAHA treated mice (Fig 3.16).

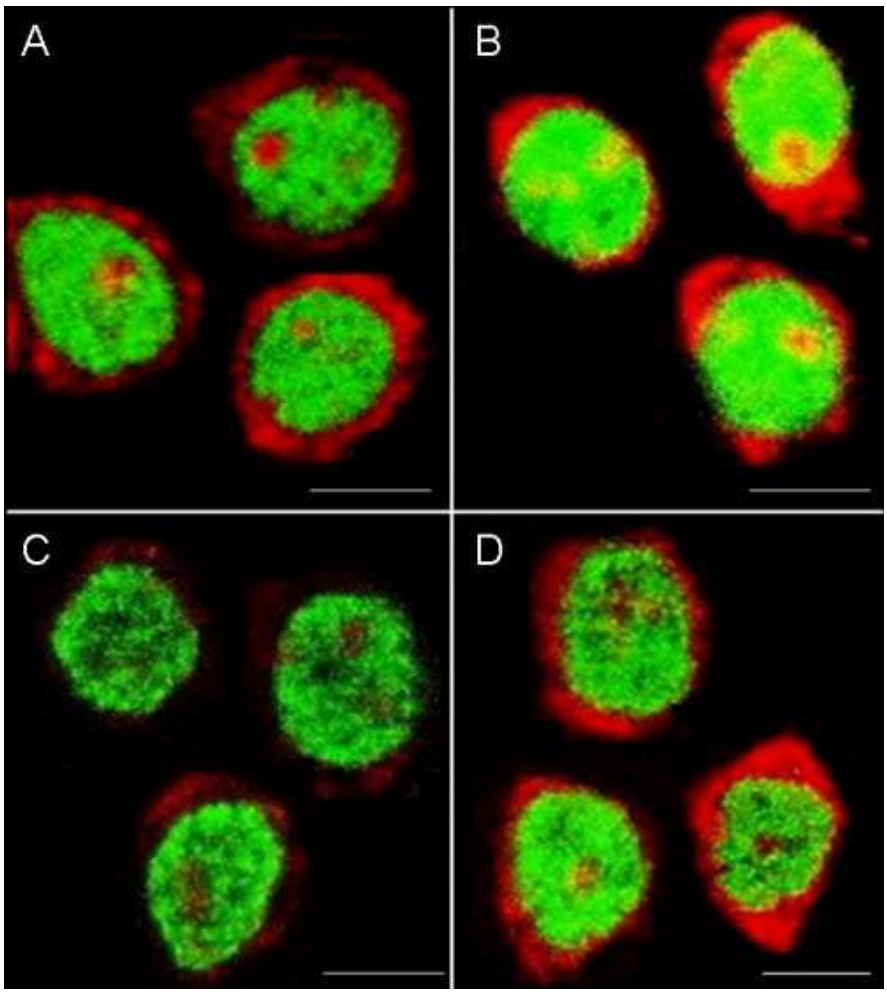

Figure 3.15

AcH3 and AcH4 immunolocalization in striatal neuronal nuclei of saline and SAHA treated mice

Brighter homogeneous nucleoplasmic staining (green) with antibody against AcH3 was observed in the nuclei of SAHA treated mice (B) compared to that in saline treated mice (A). Immunofluorescence (green) of AcH4 revealed heterogeneous nucleoplasmic staining in both saline (C) and SAHA treated (D) mice. It was found that staining intensity was also increased following SAHA treatment, compared with saline treated controls. Pyronin Y counterstaining (red) revealed the nucleolus and cytoplasm. Scale bars = 10μm.

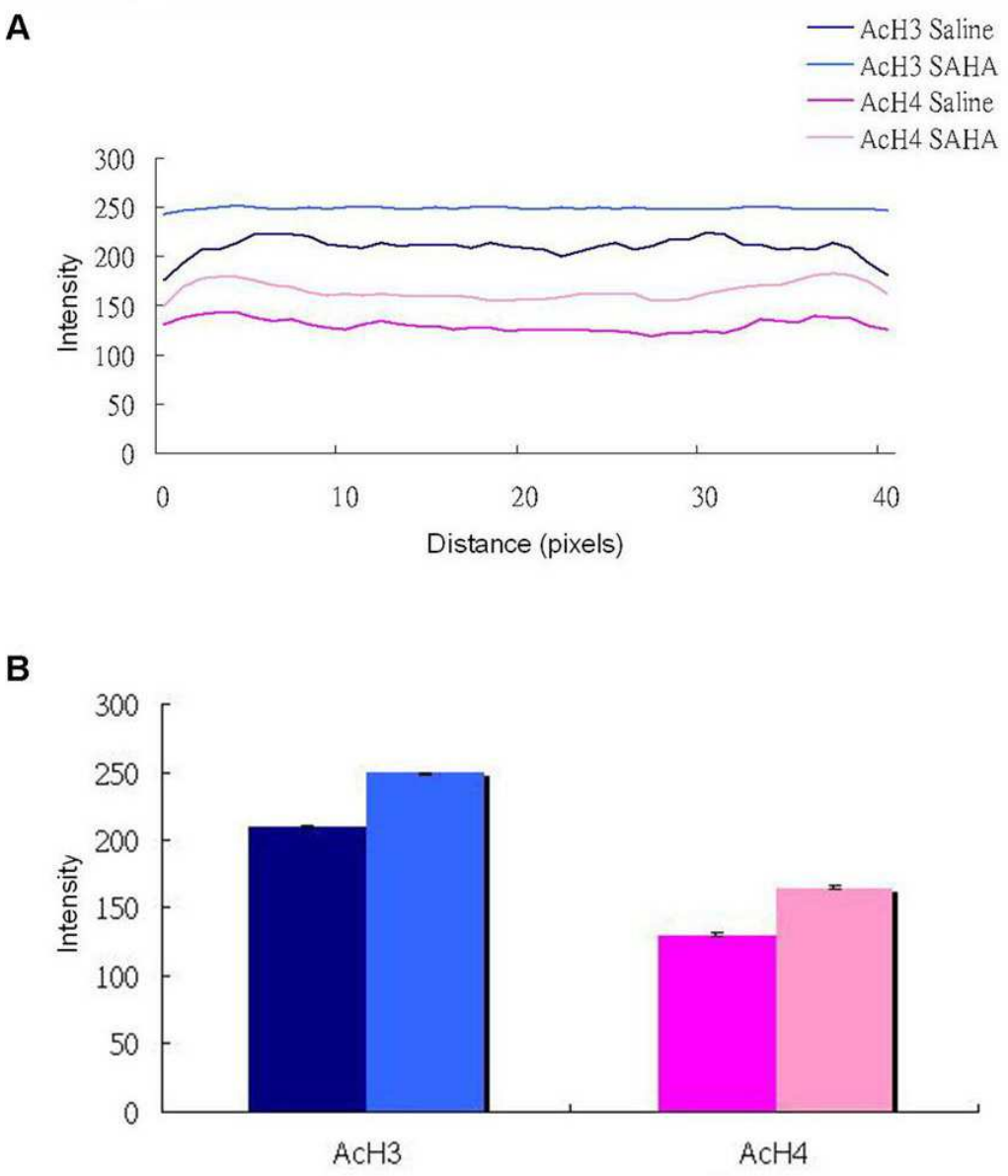

Figure 3.16

Average intensities of AcH3 and AcH4 nucleoplasmic staining in saline and SAHA treated mice

(A) Transect analysis through the cells stained for AcH3 and AcH4 in saline and SAHA treated mice. The average intensities of FITC (green) nucleoplasmic staining were plotted as a line graph (n=40). Each transect represented the cell diameter with a length of 10μm/40 pixels.

(B) The average intensity of AcH3 nucleoplasmic staining was significantly greater in the nuclei of SAHA treated mice compared with that in saline treated mice. A significant increase in the average intensity of AcH4 nucleoplasmic staining was also found in SAHA treated mice compared with saline treated controls.

3.3.2 Perinucleolar Heterochromatin

Immunofluorescence of the PNH associated protein H3K9M3 revealed a dramatic change in its nuclear distribution following VPA treatment, suggesting a reorganization of the PNH domains upon transcriptional activation. Clear perinucleolar foci were identified adjacent to the nucleoli in the striatal neuronal nuclei of saline treated mice (Fig 3.17A), whereas in VPA treated mice, H3K9M3 stained foci were bigger in size with an average of 1.78 +/- 0.03μm^2 compared with saline controls (1.18 +/- 0.02μm^2). These bigger foci were localized towards the nuclear periphery and bits of scattered nucleoplasmic staining were observed (Fig 3.17B and C). Shell analysis was also carried out using the Concentric Circles plugin in ImageJ 1.43s (2010) to assess the relative radial distribution of these immunostained foci. Concentric rings were displayed in a non-destructive overlay such that the nucleoplasm was divided into 5 shells of equal thickness (1-5 from the centre towards the nuclear periphery). Area of foci was measured in each ring and plotted against the respective ring number. Fig 3.17D illustrated clearly the peripheralized localization of H3K9M3 immunofluorescence.

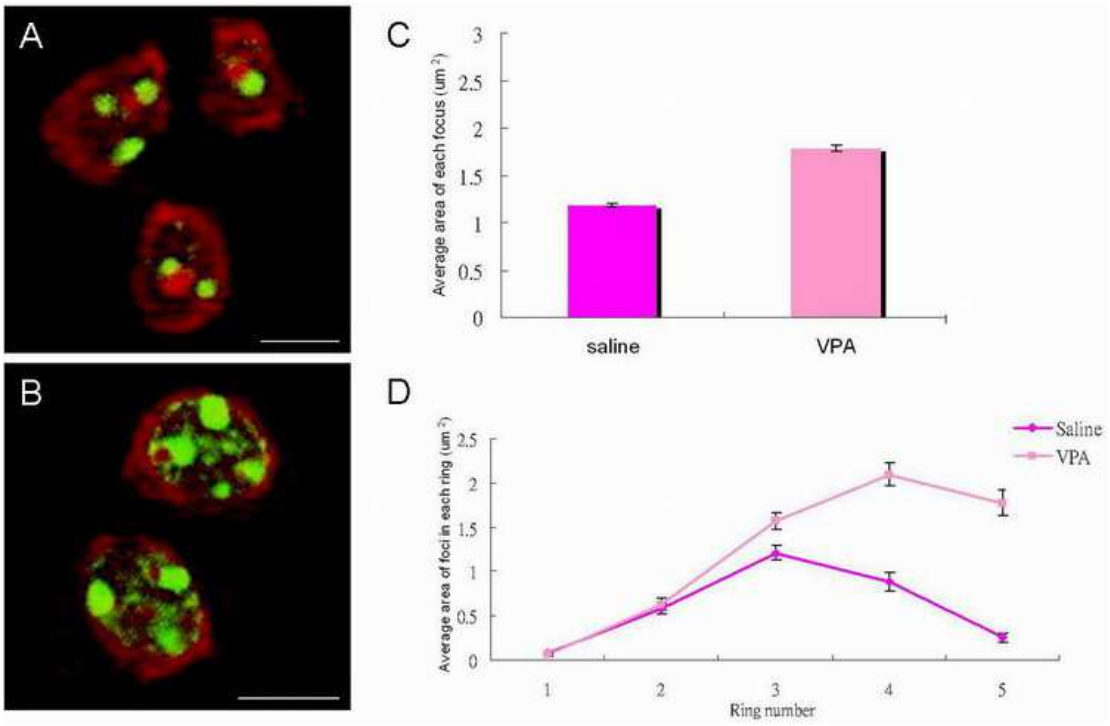

Figure 3.17

Immunolocalization of H3K9M3 in striatal neuronal nuclei of saline treated mice and its change in nuclear distribution in VPA treated mice

(A) Immunofluorescence (green) revealed perinucleolar foci adjacent to the nucleoli (red dots) in saline treated controls. (B) H3K9M3 stained foci (green) in the nuclei of VPA treated mice were bigger in size and localized towards nuclear periphery.

(C) Average area of each H3K9M3 stained perinucleolar focus was significantly increased in VPA treated mice compared with saline treated controls (n=200). (D) Shell analysis of H3K9M3 distribution illustrating a peripheralized radial distribution of the protein in VPA treated mice compared with controls. The nucleoli and cytoplasm were identified with pyronin Y (red). Scale bars = 10µm

ICC studies with antibody against the same PNH marker H3K9M3 demonstrated similar changes following treatment with the other HDACi SAHA (Fig 3.18C). Nevertheless, there was a more dramatic increase in the average area of immunostained perinucleolar foci from 1.72 +/- 0.04µm^2 in the saline treated mice to 3.84 +/- 0.11µm^2 following SAHA treatment (Fig 3.18A). These foci were also redistributed towards the nuclear periphery with bits of scattered nucleoplasmic staining observed (Fig 3.18C).

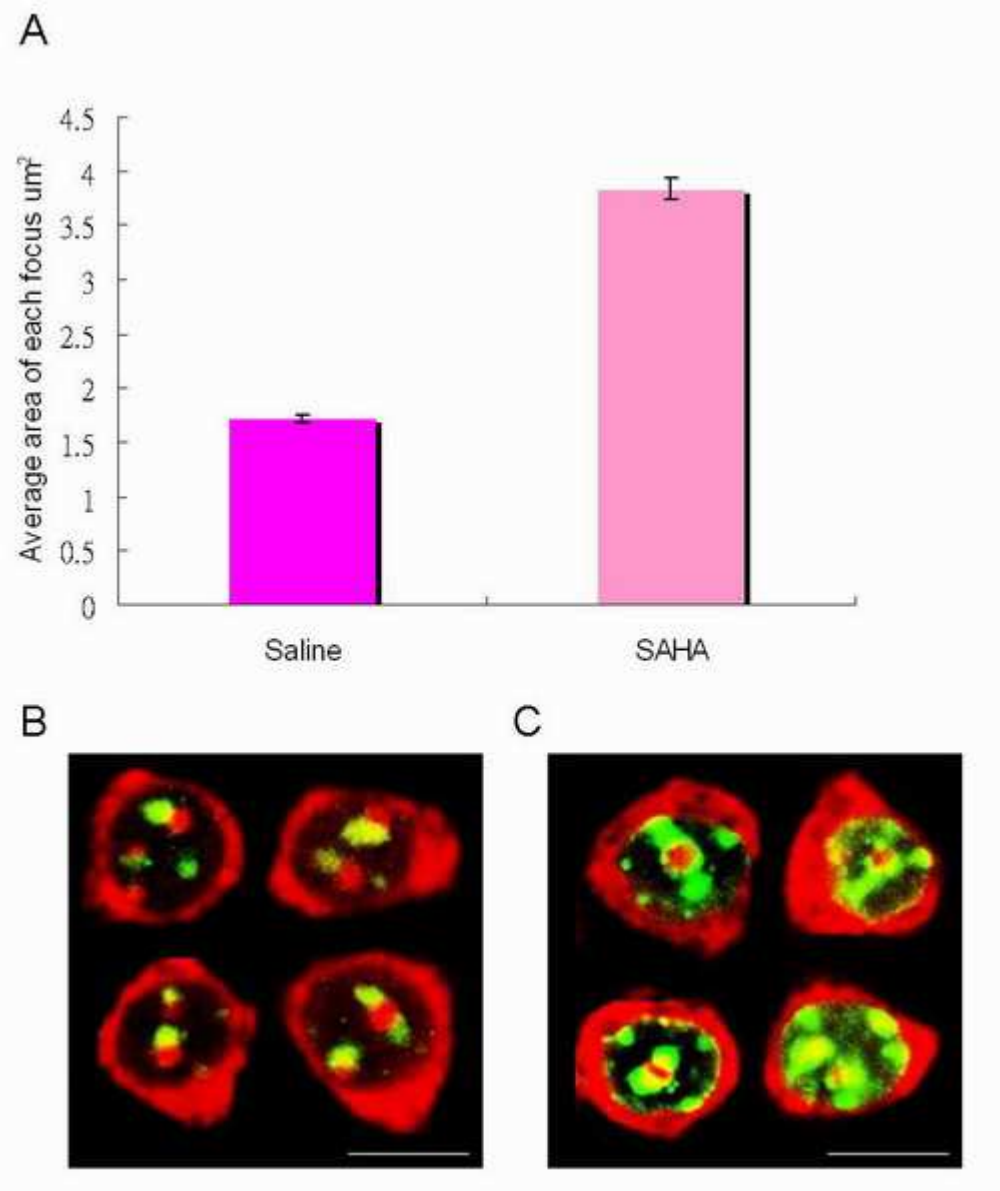

Figure 3.18

Immunolocalization of H3K9M3 in striatal neuronal nuclei of saline treated mice and its change in nuclear distribution in SAHA treated mice

(A) Average area of each H3K9M3 stained perinucleolar focus was significantly increased (more than doubled) in SAHA treated mice compared with saline treated controls (n=200).

(B) Immunofluorescence (green) revealed perinucleolar foci adjacent to the nucleoli (red dots) in saline treated controls.

(C) H3K9M3 stained foci (green) in the nuclei of SAHA treated mice were much bigger in size and redistributed towards the nuclear periphery.

Pyronin Y staining (red) revealed the nucleoli and cytoplasm. Scale bars = 10μm

Immunofluorescence of another established marker of PNH, MeCP2, in the nuclei of saline and HDACi treated mice provided further evidence for the reorganization of the PNH domains following transcriptional activation. Perinucleolar foci were identified in saline treated controls, similar to H3K9M3 immunofluorescence (Fig 3.19B). A dramatic relocalization of MeCP2, with a strong nucleoplasmic distribution throughout the whole nucleus in addition to perinucleolar foci, was observed following VPA treatment (Fig 3.19C). The average area of each MeCP2 stained perinucleolar focus was significantly increased from 0.87 +/- 0.04μm^2 in saline treated controls to 1.57 +/- 0.05μm^2 in VPA treated mice (Fig 3.19A).

Similar relocalization of MeCP2 was also revealed in the nuclei of SAHA treated mice. Apart from increased size of perinucleolar foci, prominent nucleoplasmic staining was observed although it was relatively heterogeneous (Fig 3.20C). Again there was a more significant increase in the average area of each MeCP2 stained perinucleolar focus in SAHA treated mice compared with VPA treatment. The average area of perinucleolar foci increased from 1.35 +/- 0.06μm^2 in controls to 2.85 +/- 0.11μm^2 following SAHA treatment (Fig 3.20A).

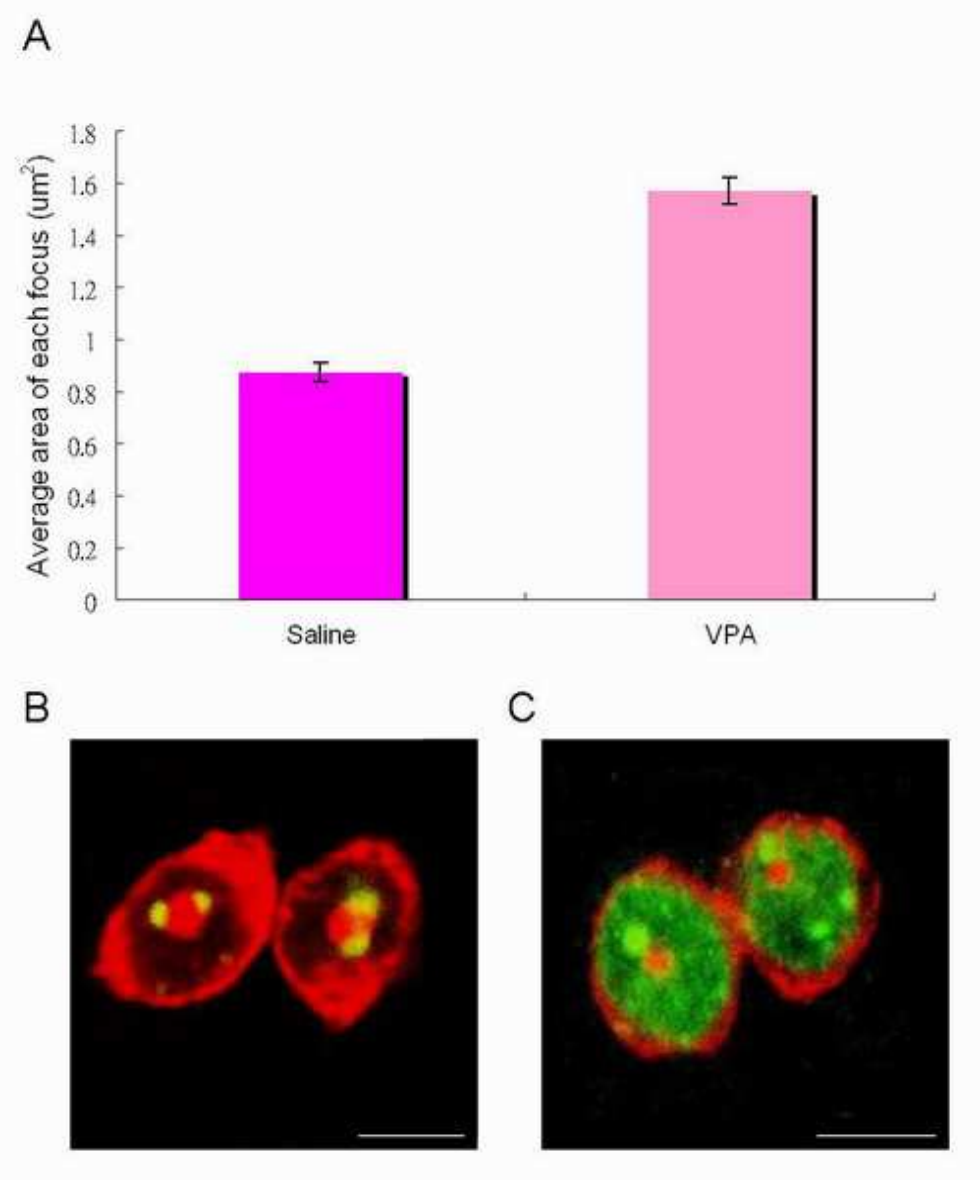

Figure 3.19

Immunolocalization of MeCP2 in striatal neuronal nuclei of saline treated mice and its redistribution in VPA treated mice

(A) The average area of each perinucleolar focus was significantly greater in VPA treated mice compared with saline treated controls (n=200). (B) MeCP2 stained perinucleolar foci (green) around the nucleoli (red dots) in saline treated mice. (C) Immunofluorescence (green) revealed perinucleolar foci as well as nucleoplasmic staining following VPA treatment.

Pyronin Y (red) localized the nucleoli and cytoplasm. Scale bars = 10μm

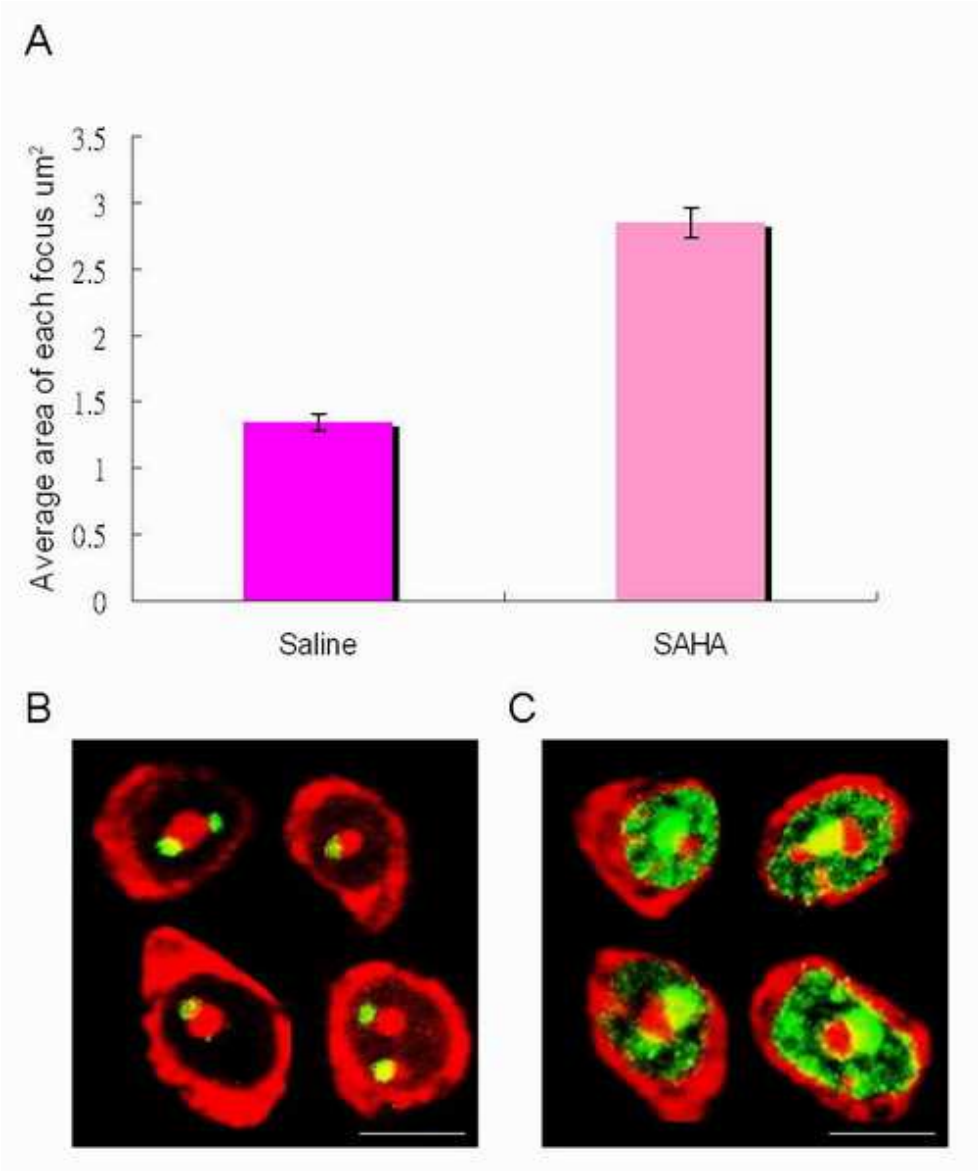

Figure 3.20

Immunolocalization of MeCP2 in striatal neuronal nuclei of saline treated mice and its redistribution in SAHA treated mice

(A) The average area of each perinucleolar focus was significantly increased in SAHA treated mice compared with saline treated controls (n=200). (B) MeCP2 stained perinucleolar foci (green) around the nucleoli (red dots) in saline treated mice. (C) Heterogeneous nucleoplasmic staining in addition to perinucleolar foci were observed in the nuclei of SAHA treated mice.

Pyronin Y (red) localized the nucleoli and cytoplasm. Scale bars = 10μm

3.3.3 MBDs and Other Heterochromatin Associated Proteins

Transcriptional activation by VPA treatment resulted in nuclear redistribution of both phosph-MeCP2-pS80 and pS421 similar to that observed with MeCP2 antibody, with nucleoplasmic staining in addition to perinucleolar foci (Fig 3.21B and E). HDAC inhibition by SAHA demonstrated perinucleolar and nuclear foci apart from a lightly stained nucleoplasm with antibody against phosph-MeCP2-pS80 (Fig 3.21C).

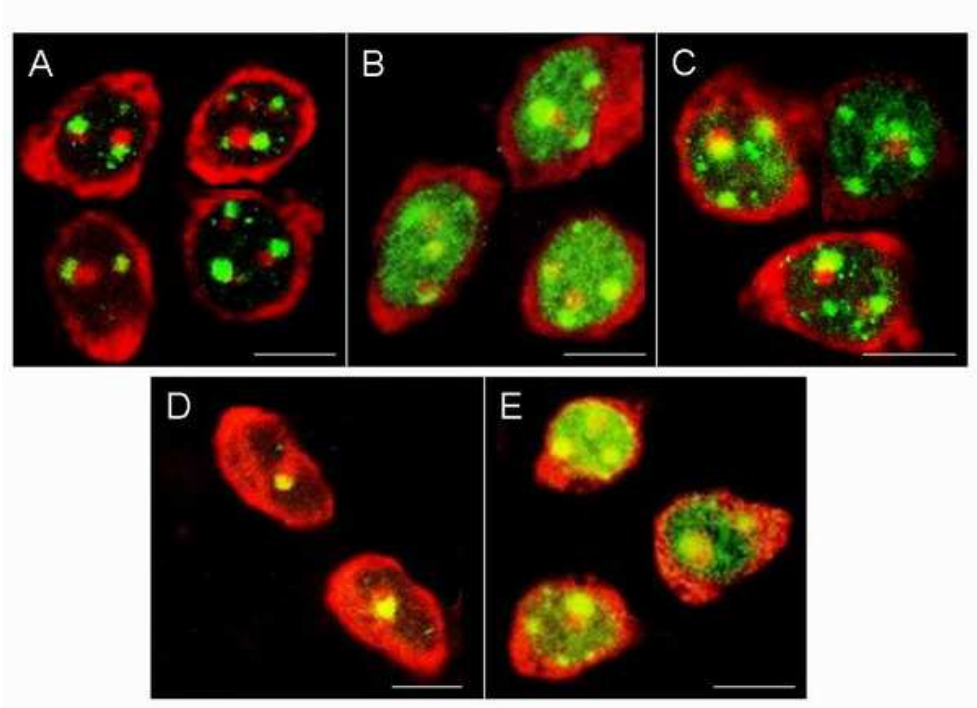

Figure 3.21

Phospho-MeCP2-pS80 and phosphor-MeCP2-pS421 immunolocalization in the striatal neuronal nuclei of saline, VPA and SAHA treated mice

(A-C) Phospho-MeCP2-pS80 Immunofluorescence (green) revealed perinucleolar foci adjacent to the nucleoli (red dots) as well as nuclear foci in saline treated mice (A). However, nucleoplasmic staining in addition to perinucleolar foci (green) was found in VPA treated mice (B). In the nuclei of SAHA treated mice, nucleoplasm was lightly stained apart from nuclear and perinucleolar foci (green) (C).

(D-E) Phospho-MeCP2-pS421 immunofluorescence (green) revealed perinucleolar foci (green) adjacent to the nucleoli (red dots) in saline treated mice (D). However, in the nuclei of VPA treated mice, both nucleoplasmic staining and perinucleolar foci (green) were observed (E). The nucleoli and cytoplasm were illustrated with pyronin Y counterstaining (red). Scale bars = 10μm

Although a similar redistribution of MeCP2 was observed in the striatal neuronal nuclei following either VPA or SAHA treatment, ATRX immunofluorescence revealed typical perinucleolar foci in both saline and VPA treated mice (Fig 3.22A and B), while nuclear microfoci away from the nucleoli were found in SAHA treated mice (Fig 3.22C). ATRX is a chromatin remodeling protein that typically recognizes and binds to MeCP2. The differences in MeCP2 and ATRX redistribution after VPA and SAHA treatment implied dissociation between MeCP2 and ATRX upon transcriptional activation by HDACi.

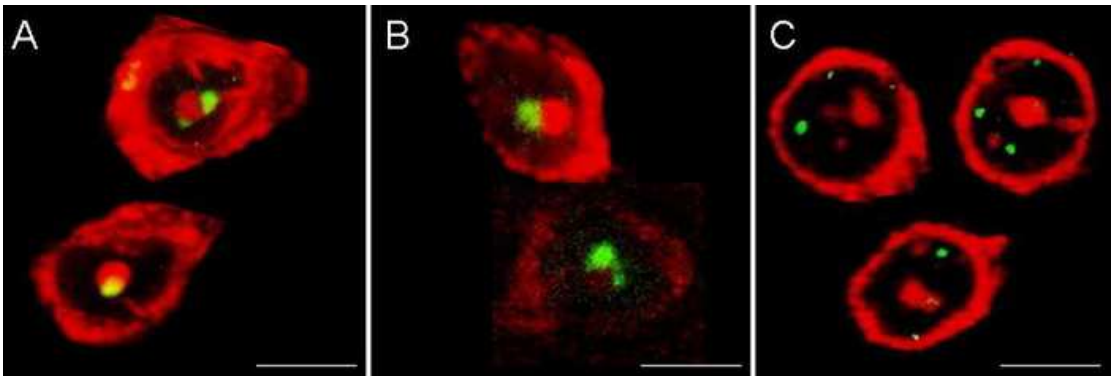

Figure 3.22

ATRX immunolocalization in the striatal neuronal nuclei of saline, VPA and SAHA treated mice

Immunofluorescence (green) revealed perinucleolar foci adjacent to the nucleoli (red dots) in saline treated mice (A). Similar staining was found in VPA treated mice (B). However, nuclear microfoci away from the nucleoli were found following SAHA treatment (C). Pyronin Y counterstaining (red) illustrated the nucleoli and cytoplasm. Scale bars = 10μm

Despite the dramatic reorganization of the PNH marker proteins observed following HDACi treatment, no significant change was found with antibodies against other heterochromatin associated proteins such as the heterochromatin protein HP1α and H3K27M3 (marker of facultative heterochromatin). HP1α immunofluorescence revealed similar staining pattern

in the nuclei of saline, VPA and SAHA treated mice (Fig 3.23). Similarly, no significant change in H3K27M3 immunolocalization was found in either VPA or SAHA treated mice, although staining was relatively weaker following SAHA treatment (Fig 3.24).

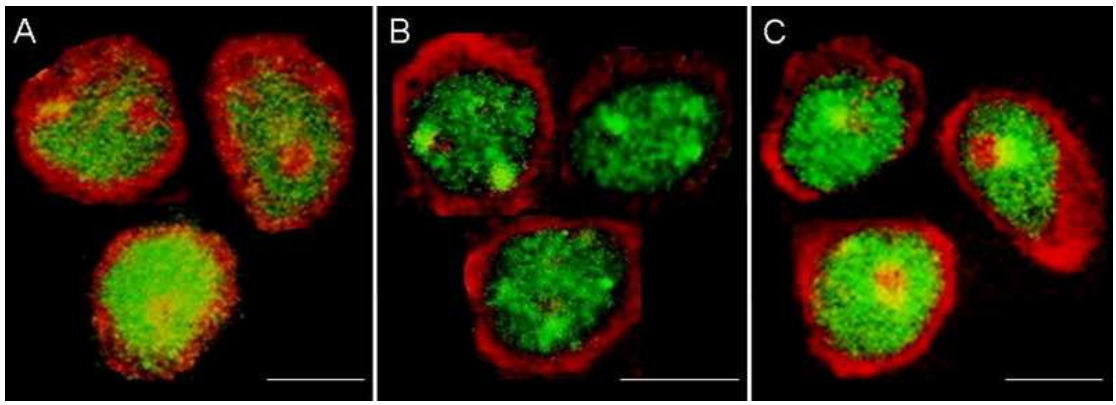

Figure 3.23

HP1α immunolocalization in the striatal neuronal nuclei of saline, VPA and SAHA treated mice

Immunofluorescence (green) revealed nucleoplasmic staining and perinucleolar foci adjacent to the nucleoli (red dots) in saline treated mice (A). Similar staining was found in both VPA treated (B) and SAHA treated (C) mice. Pyronin Y counterstaining (red) illustrated the nucleoli and cytoplasm. Scale bars = 10μm

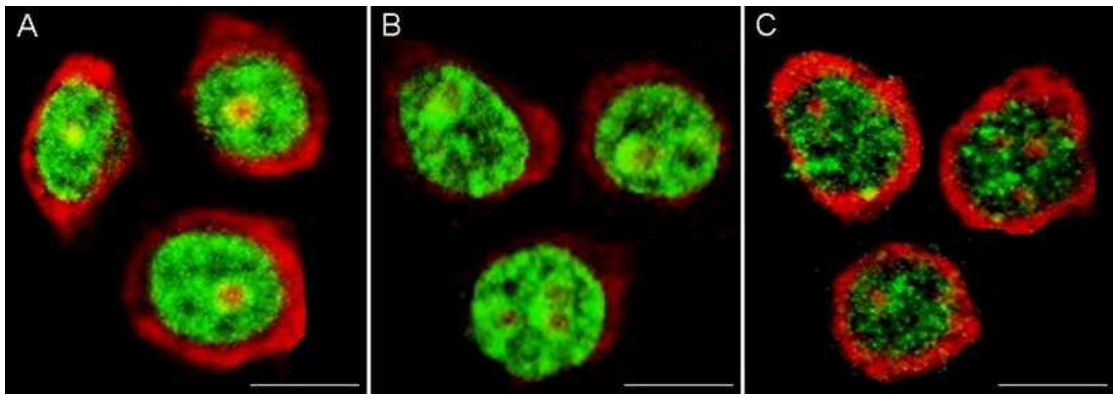

Figure 3.24

H3K27M3 immunolocalization in the striatal neuronal nuclei of saline, VPA and SAHA treated mice

Immunofluorescence (green) revealed perinucleolar and nucleoplasmic foci in saline treated mice (A). Similar staining was found following VPA treatment (B). In the nuclei of SAHA treated mice, the amount of perinucleolar and nucleoplasmic staining was decreased (C). The nucleoli and cytoplasm were identified with pyronin Y (red). Scale bars = 10μm

3.3.4 Cajal Bodies

Apart from PNH, another perinucleolar body, the Cajal bodies, appeared to be dramatically reorganized by HDAC inhibition. ICC studies with the marker proteins p80 coilin and Nopp140 revealed an overall increase in size and number of immunostained foci in the nuclei of both VPA and SAHA treated mice. Following both treatment, Nopp140 immunofluorescence demonstrated a massive increase in the size of foci which covered the nucleoli and occupied a larger volume of the nucleoplasm, in addition to an increased number of foci (Fig 3.25A-C). There was also a significant increase in the size of the perinucleolar caps stained with p80 coilin in VPA treated mice (Fig 3.25E). In the nuclei of SAHA treated mice, p80 coilin stained nuclear foci and microfoci were present throughout the nucleoplasm away from the nucleoli (Fig 3.25F).

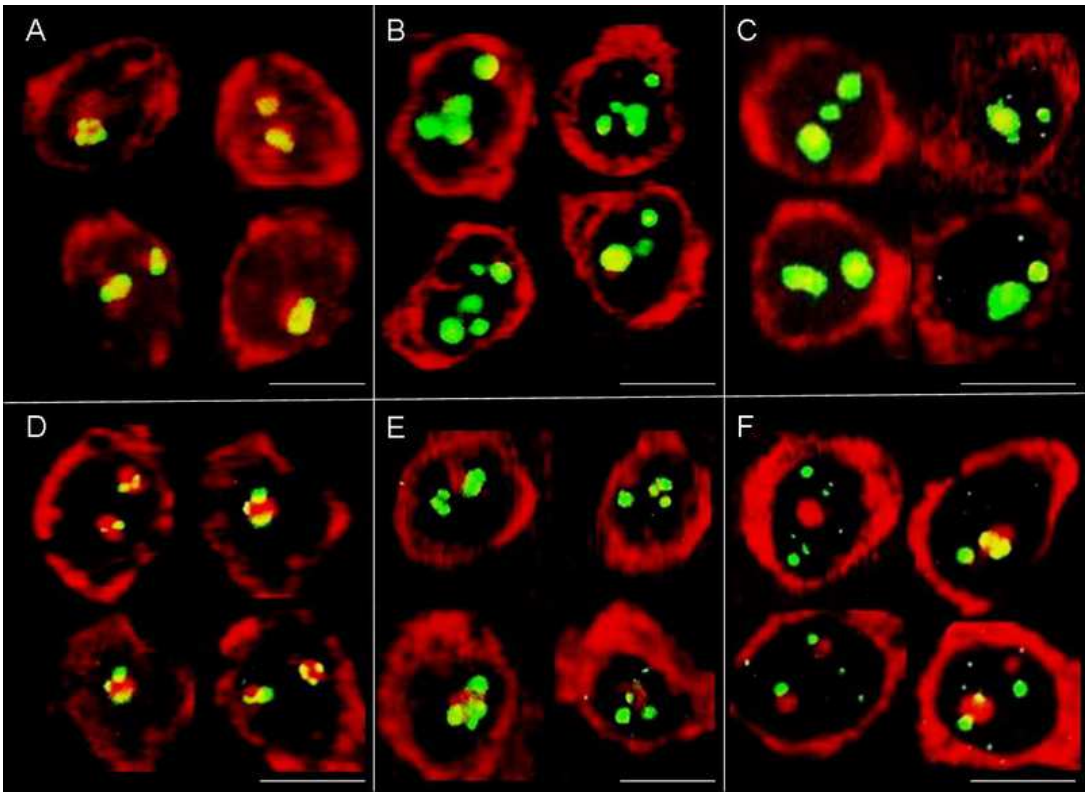

Figure 3.25

Immunolocalization of the Cajal body marker proteins Nopp140 and p80 coilin in the striatal neuronal nuclei of saline, VPA and SAHA treated mice

(A-C) Immunofluorescence of Nopp140 (green) as nucleolar foci in saline treated mice (A), and the increased size and number of foci in the nuclei of VPA treated (B) and SAHA treated (C) mice.

(D-F) Immunofluorescence of p80 coilin (green) localized as perinucleolar caps surrounding pyronin Y stained nucleoli (red dots) in saline treated mice (D). An increased size and number of perinucleolar and nucleoplasmic foci (green) were observed in VPA treated (E) and SAHA treated (F) mice. Pyronin Y (red) stained the nucleoli and cytoplasm. Scale bars = 10μm

Linker Histone and Histone Acetylation	VPA	SAHA
H1	No change	No change
AcH3	↑ ↑ intensity	↑ ↑ intensity
AcH4	↓ intensity	↑ ↑ intensity
Heterochromatin		
H3K9M3	↑ ↑ area of foci Nuclear peripheralization	↑ ↑ ↑ area of foci Nuclear peripheralization
MeCP2	↑ ↑ area of foci Nucleoplasmic staining	↑ ↑ ↑ area of foci Nucleoplasmic staining
Phospho-MeCP2-pS80	↑ ↑ number of foci Nucleoplasmic staining	↑ ↑ number of foci
ATRX	No change	↑ ↑ number of microfoci
HP1α	No change	No change
H3K27M3	No change	↓ ↓ intensity
Cajal Bodies		
Nopp140	↑ ↑ area and number of foci	↑ ↑ area and number of foci
p80 coilin	↑ ↑ area and number of foci	↑ ↑ area of foci and number of microfoci

Table 3.1

A table summarizing the principal findings in the HDACi treated mice. Striatal neuronal nuclear reorganization induced by VPA and SAHA is illustrated. ↑ denotes the extent of increase, ↓ denotes the extent of decrease.

3.4 Neuronal Nuclear Rearrangement in Neurodegenerative Disease Models

In all transgenic mouse models of Huntington's disease, ALS/FTLD, FTDP-17 and their respective litter mate controls, striatal neurons were analysed for any pathological changes. In all three human neurodegenerative diseases prominent changes within the striatum have been documented (DiFiglia et al., 1997, Halabi et al., 2012). It should be noted however that the HD transgene was expressed downstream of human HD gene promoter sequences and expressed at approximately control levels, the Tau^{P301S} and $TDP\text{-}43^{M337V}$ transgenes were expressed downstream of Thy1 promoter sequences and exceeded the level of expression of the wild type gene. For each study, approximately 10 non-adjacent sections were examined per mouse and 5-10 transgenic mice (R6/2, TDP-43 and Tau respectively) together with their litter mate controls were studied.

3.4.1 Heterochromatin and Cajal Bodies in R6/2 Transgenic Mice

The heterochromatic organization in the striatal neuronal nuclei of the Huntington's disease models R6/2 transgenic mice was studied and compared with that in the wild type mice with DAPI staining. Condensed DNA was readily stained with DAPI and therefore heterochromatic foci (comprised of condensed DNA) were revealed in the striatal neuronal nuclei (Fig 3.26B and C). In the R6/2 mice, the average area of nucleoplasm was significantly reduced compared with that in the wild type mice, suggesting shrinkage of

neurons (Fig 3.26B and C). Despite the reduced size of nuclei, the number of heterochromatic foci and the proportion of heterochromatin over nucleoplasm were significantly increased. Heterochromatin around the nucleolus (perinucleolar heterochromatin) and heterochromatin in the nucleoplasm (nucleoplasmic heterochromatin) were distinguished, and the area and proportion of perinucleolar and nucleoplasmic heterochromatin were analyzed in the nuclei of both R6/2 and wild type mice. In the R6/2 mice, there was a significant increase in both types of heterochromatin and the proportion of perinucleolar heterochromatin was found to be doubled (7% to 14%) compared with that in the wild type mice ($p<0.001$) (Fig 3.26A). Moreover, the proportion of perinucleolar heterochromatin (14%) was significantly higher than the proportion of nucleoplasmic heterochromatin (9%) in the R6/2 mice ($p<0.001$), whereas there was no significant difference between the proportion of perinucleolar (7%) and nucleoplasmic (7%) heterochromatin in the wild type mice (Fig 3.26A).

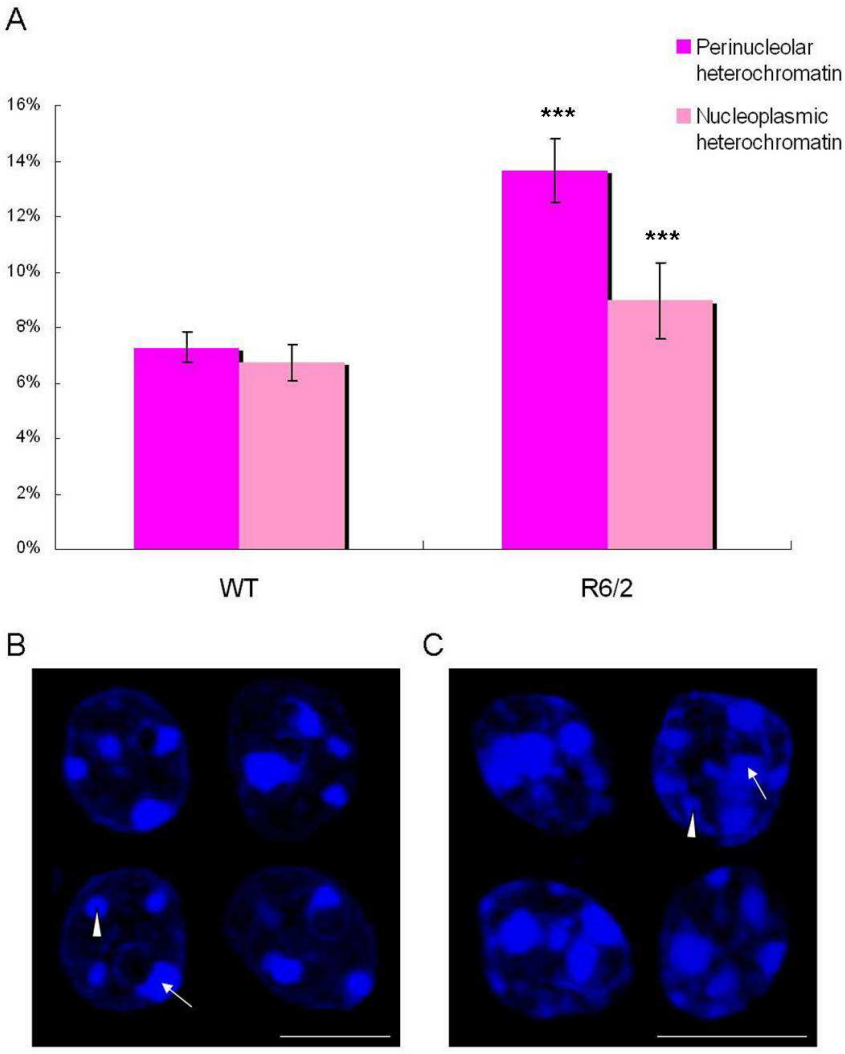

Figure 3.26

Perinucleolar and nucleoplasmic heterochromatin in the striatal neuronal nuclei of wild type and R6/2 transgenic mice

(A) The proportion of perinucleolar and nucleoplasmic heterochromatin was significantly increased in the R6/2 transgenic mice. The proportion of perinucleolar heterochromatin in the R6/2 mice was found to be doubled comparing with that in the wild type mice (p<0.001). No significant difference was found between the proportion of perinucleolar and nucleoplasmic heterochromatin within the wild type mice. However in the R6/2 mice, the proportion of perinucleolar heterochromatin was significantly higher than the proportion of nucleoplasmic heterochromatin (p<0.001).

(B) DAPI staining of the striatal neuronal nuclei in wild type controls. No significant difference between the amount of perinucleolar heterochromatin (white arrow) and nucleoplasmic heterochromatin (white arrow head). Scale bar = 10μm

(C) An increased amount of perinucleolar (white arrow) and nucleoplasmic heterochromatin (white arrow head) was observed in the R6/2 mice under DAPI staining, despite the reduced size of nuclei compared with the wild type. Scale bar = 10μm

ICC studies of the PNH marker proteins MeCP2 and H3K9M3 as well as the Cajal body marker p80 coilin further illustrated disorganization of these perinucleolar structures in the disease state in R6/2 mice. In the striatal neuronal nuclei of these transgenic mice, an increased number and size of MeCP2 stained nuclear foci was observed, some of which relocalized towards the nuclear periphery (Fig 3.27D). H3K9M3 immunofluorescence demonstrated pronounced increase in the size of nucleolar foci covering the nucleoli. There were also additional nucleoplasmic microfoci (Fig 3.27E) which were never present in the wild type mice (Fig 3.27B). Moreover, an increased area of p80 coilin stained perinucleolar caps were observed together with numerous free nucleoplasmic foci in the nuclei of R6/2 mice (Fig 3.27F).

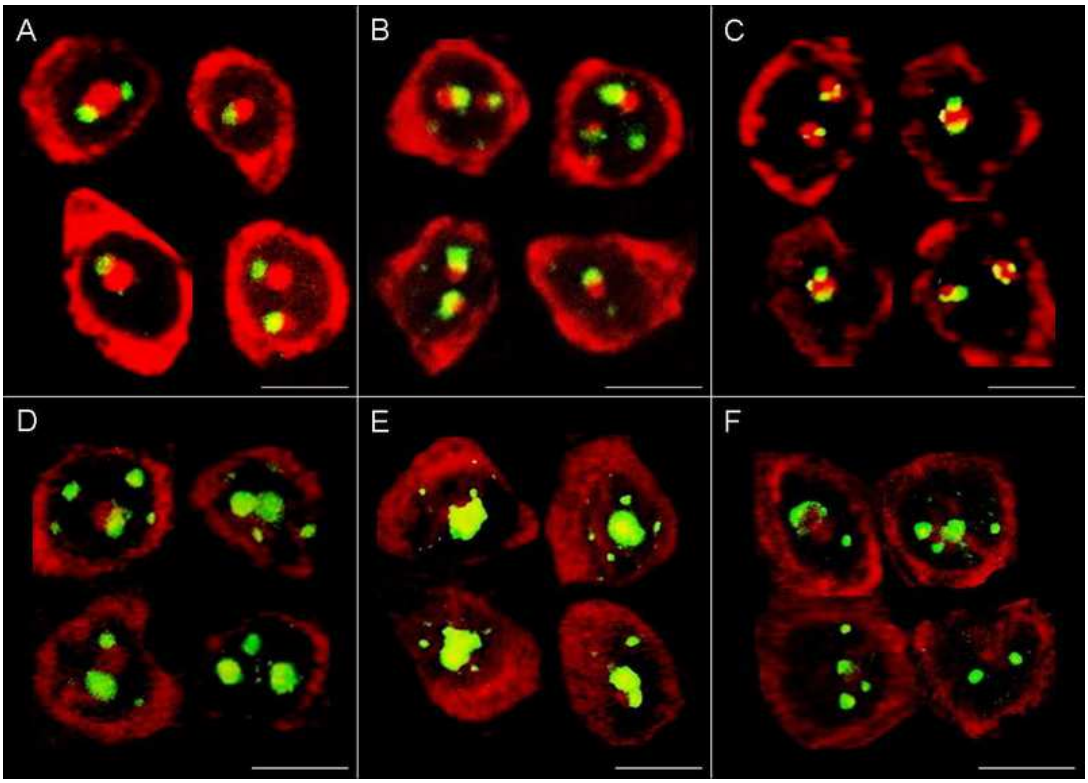

Figure 3.27

Immunofluorescence of MeCP2, H3K9M3 and p80 coilin in the striatal neuronal nuclei of wild type and R6/2 transgenic mice

(A, D) MeCP2 stained perinucleolar foci (green) around the nucleoli (red dots) in the wild type mice (A) and the increased number and size of MeCP2 stained nuclear foci (green) in the R6/2 mice (D).

(B, E) H3K9M3 immunofluorescence (green) revealed perinucleolar foci adjacent to the nucleoli (red dots) in the wild type mice (B), whereas a significantly increased size of nucleolar foci (green) in addition to free nucleoplasmic foci were found in the R6/2 mice (E).

(C, F) p80 coilin immunofluorescence (green) localized as perinucleolar caps around the nucleoli (red dots) in the wild type (C). In the nuclei of R6/2 mice, an increased size of p80 coilin stained perinucleolar foci and free nucleoplasmic foci (green) were observed (F).

The nucleoli and cytoplasm were stained with pyronin Y (red) and scale bars = 10μm.

3.4.2 Perinucleolar Heterochromatin in TDP-43 and Tau Transgenic Mice

Apart from the R6/2 Huntington's disease models, two other transgenic mice, TDP-43^{M337V} and Tau^{P301S}, neurodegenerative disease models of amyotrophic lateral sclerosis/frontotemporal lobar degeneration and Frontotemporal Dementia with Parkinsonism-17 respectively, were used to study any changes in the perinucleolar structures with ICC. Detailed studies on the neuropathological mechanism specifically in the TDP-43^{M337V} mice are described in the following section.

Immunolocalization of the PNH marker proteins H3K9M3 and MeCP2, which were typically found as perinucleolar foci in the wild type, revealed interesting reorganization in the disease models and these changes varied between TDP-43 and Tau transgenic mice. In the nuclei of TDP-43 transgenic mice, H3K9M3 stained foci increased significantly in size and clustered around the nucleoli (Fig 3.28C), whereas MeCP2 immunofluorescence demonstrated a dramatic increase in the number of small nuclear microfoci distributed throughout the nucleoplasm (Fig 3.29C). In the nuclei of Tau transgenic mice, H3K9M3 immunofluorescence revealed a massive increase in the size of both perinucleolar and nucleoplasmic foci away from the nucleoli (Fig 3.28D). However, there was no increase in the size of MeCP2 stained perinucleolar foci in the Tau transgenic mice, despite the appearance of additional nuclear foci towards the periphery (Fig 3.29D).

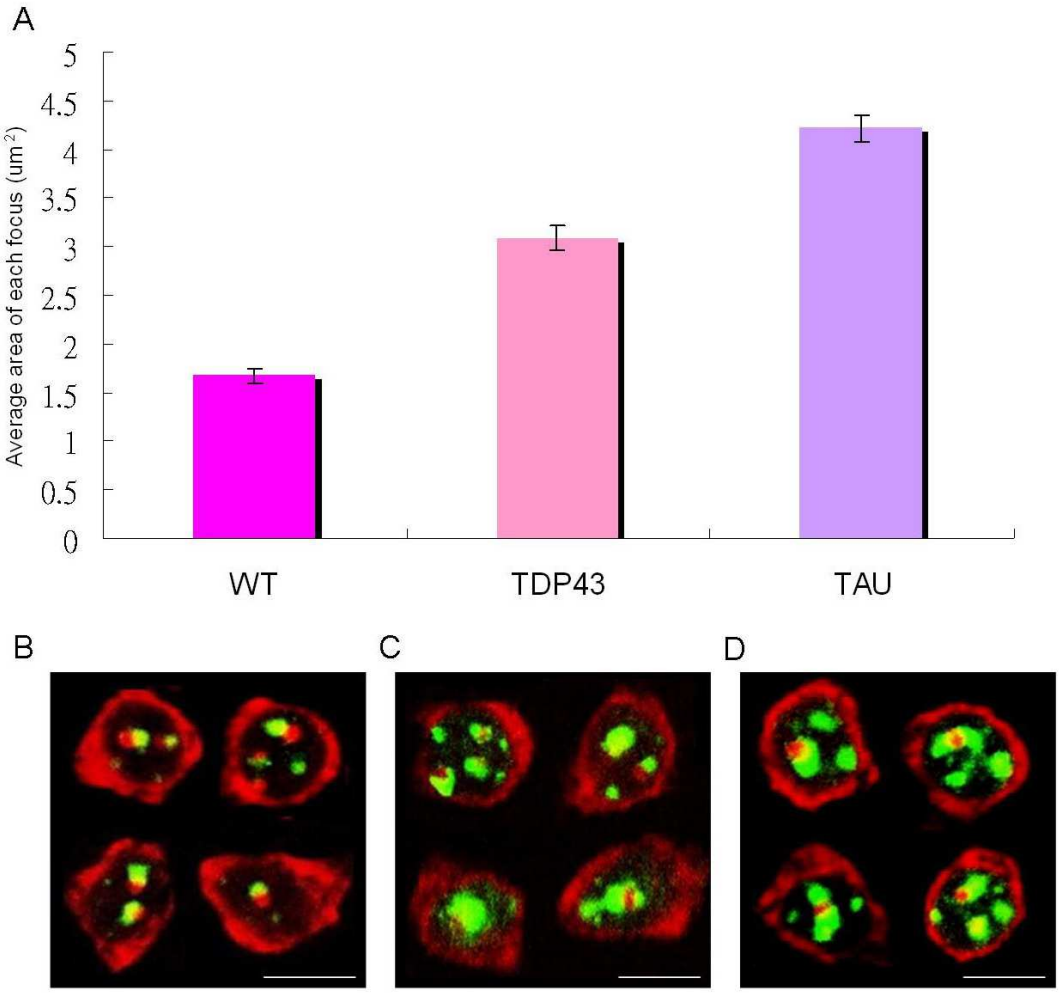

Figure 3.28

Immunolocalization of H3K9M3 in striatal neuronal nuclei of wild type, TDP-43 and Tau transgenic mice (A) Average area of each perinucleolar focus was significantly increased in TDP-43 (3.09 +/- 0.13μm^2) and Tau (4.22 +/- 0.14μm^2) transgenic mice compared with that in the wild type (1.67 +/- 0.06μm^2) n=200, *p*<0.001. (B) H3K9M3 immunofluorescence (green) as perinucleolar foci adjacent to the nucleoli (red) in wild type mice. (C) H3K9M3 stained foci (green) were much bigger in size and clustered around the nucleoli (red) in TDP-43 transgenic mice. (D) Significantly increased size of perinucleolar foci together with nucleoplasmic foci (green) were observed in Tau transgenic mice.

The nucleoli and cytoplasm were identified with pyronin Y (red) and scale bars = 10μm

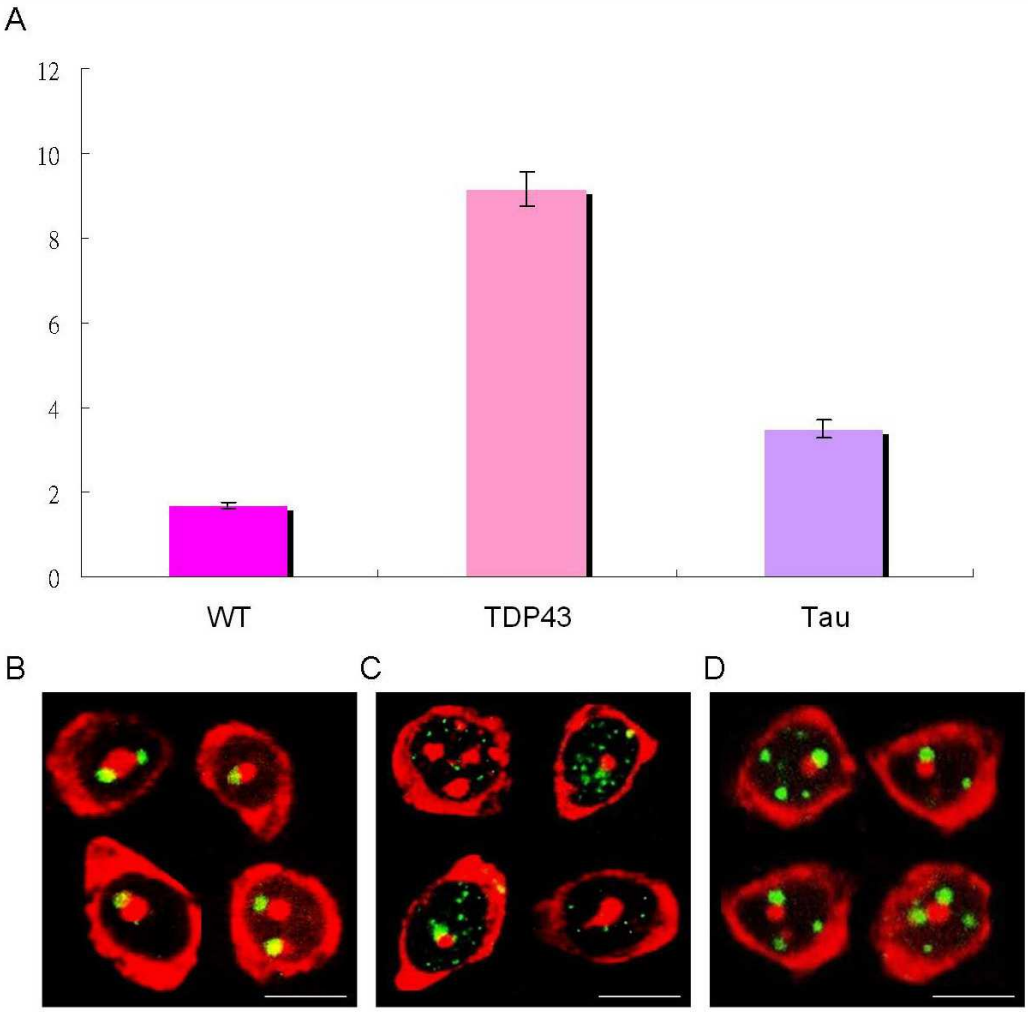

Figure 3.29

MeCP2 stained nuclear foci in striatal neuronal nuclei of wild type, TDP-43 and Tau transgenic mice (A) Average number of nuclear foci immunostained with antibodies to MeCP2 was significantly increased in TDP-43 (9.15 +/- 0.40) and Tau (3.5 +/- 0.20) transgenic mice compared with the wild type (1.69 +/- 0.07) n=200, p<0.001. (B) Immunofluorescence (green) revealed perinucleolar foci adjacent to the nucleoli (red dots) in wild type mice. (C) Perinucleolar foci as well as smaller nuclear foci (green) were observed in TDP-43 transgenic mice. (D) Perinucleolar and nucleoplasmic foci (green) in Tau transgenic mice.

Pyronin Y (red) localized the nucleoli and the cytoplasm. Scale bars = 10μm

3.4.3 Cajal Bodies in TDP-43 and Tau Transgenic Mice

ICC studies with the Cajal body marker protein p80 coilin illustrated reorganization of the perinucleolar rosettes of Cajal bodies in the striatal neuronal nuclei of both TDP-43 and Tau transgenic mice. These was a significant increase in the number of p80 coilin stained foci from 2.00 +/- 0.11 in the wild type to 2.54 +/- 0.12 in the TDP-43 and 2.96 +/- 0.15 in the Tau transgenic mice (p<0.01) (Fig 3.30A). In addition, the size of these p80 coilin stained foci was also increased and apart from perinucleolar foci, free nucleoplasmic foci away from the nucleoli were observed in these transgenic mice (Fig 3.30D and E). Therefore, these foci occupied a much larger volume of the nucleoplasm and the average area of p80 coilin stained Cajal bodies per neuron increased significantly from 1.28 +/- 0.09μm^2 in the wild type to 2.97 +/- 0.14μm^2 and 2.93 +/- 0.19μm^2 in the TDP-43 and Tau transgenic mice respectively (p<0.001) (Fig 3.30B).

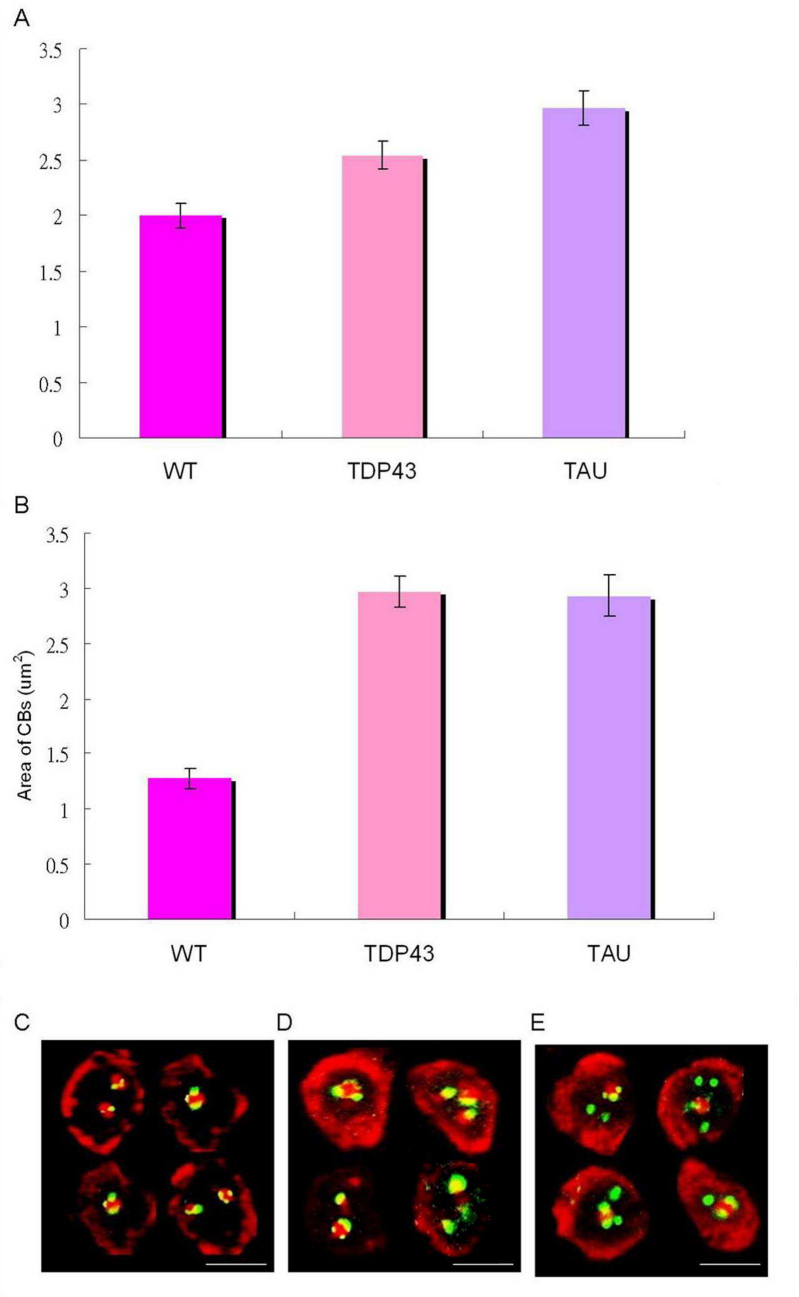

Figure 3.30

Immunolocalization of Cajal body marker p80 coilin in striatal neuronal nuclei of wild type, TDP-43 and Tau transgenic mice

(A) Average number of p80 coilin stained Cajal bodies per neuron was significantly increased in both TDP-43 transgenic mice and Tau transgenic mice (p<0.01). (B) Average area of p80 coilin stained Cajal bodies per neuron was significantly increased in both TDP-43 and Tau transgenic mice compared with the wild type (p<0.001) n=200. (C) Immunofluorescence (green) revealed perinucleolar foci surrounding the nucleoli (red dots) in wild type mice. (D) p80 coilin stained foci (green) around the nucleoli (red dots) occupied a larger volume of the nucleoplasm in the TDP-43 transgenic mice. (E) Both perinucleolar and free nucleoplasmic foci (green) were observed in Tau transgenic mice.

Pyronin Y (red) recognized the nucleoli and cytoplasm. Scale bars = 10μm

3.5 Bipartite Pathological Mechanism in TDP-43^{M337V} Transgenic Mice

The neuron-specific elements of the mouse thy1 promoter were used to produce the TDP-43^{M337V} transgenic mice expressing human TDP-43. Homozygous mice were not viable and died at 15 days postnatal with signs of delayed development (smaller size and lower weight compared to age matched controls) as well as motor impairments. Therefore heterozygous mice (TDP-43$^{M337V+/-}$) were used in the studies which developed an unsteady gait and tremors at around 1 month of age. This phenotype persisted throughout the lifespan of these mice, which expressed 2.2× the level of TDP-43 found in the wild type mice, albeit with a different sub-cellular localization. Two prominent pathological features were identified in these novel transgenic mice.

Transmission electron microscopy (TEM) was used to evaluate the ultrastructural changes occurring in the TDP-43 transgenic mice compared to littermate controls at 3 and 6 months of age. Confocal microscopy and post-embedding immunogold electron microscopy were used to identify the sub-cellular location of a variety of proteins. TEM analyses demonstrated striking ultrastructural changes in both the nucleus and the cytoplasm of striatal and cortical neurons. These include the appearance of punctuate, dark nuclear foci as well as multiple large vacuoles within the cytoplasm, suggesting a bipartite pathological mechanism in the TDP-43^{M337V} transgenic mice.

3.5.1 Nuclear Pathology

Neuronal nuclei within the striatum and cortex of TDP-43^{M337V} transgenic mice contain multiple dark foci that resemble nuclear stress bodies or paraspeckles in TEM studies (Fig 3.31A and 3.32A). However immunocytochemical studies with antibodies that recognize such structures (9G8, HAP, PSP1, P54^{nrb} and PSF) failed to colocalize with these novel nuclear bodies. Surprising, the methyl-cytosine binding protein MeCP2 (Fig 3.31B) and the RNA binding protein muscleblind MBNL-1 (Fig 3.32B) appeared to colocalise with these nuclear foci. Since MeCP2 is normally localized within perinucleolar heterochromatin, I additionally studied the distribution of the marker protein H3K9M3. The perinucleolar heterochromatic regions recognized by this protein encircled the nucleoli and were much larger (Fig 3.31D) compared with those from control mice (Fig 3.31E). In the TDP-43^{M337V} mice, nuclear Cajal bodies indicated by the marker p80 coilin occupied a larger volume of nucleoplasm and were more numerous (Fig 3.31F) compared with those found in the wild type (Fig 3.31G).

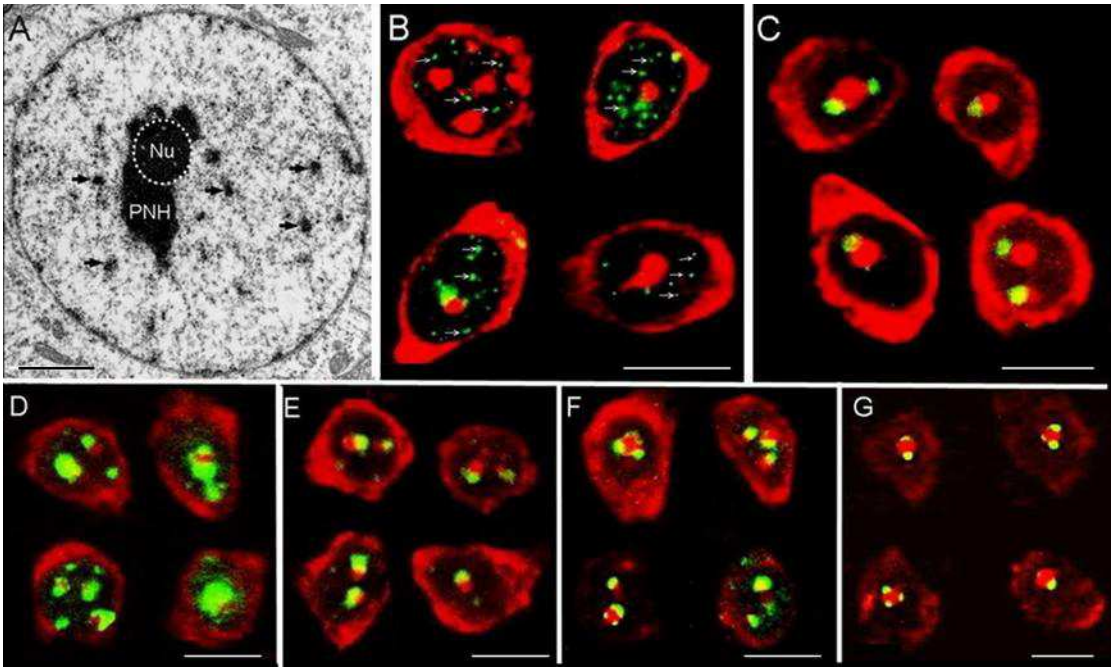

Figure 3.31

Nuclear pathology of TDP-43^{M337V} transgenic mice

(A) Transmission electron micrograph of a striatal neuron in the TDP-43^{M337V} transgenic mouse. Numerous dark foci were found throughout the spherical nucleus (Black arrows) surrounding the central nucleolus (Nu) and perinucleolar heterochromatin (PNH). Many such small foci were immunostained with antibodies to MeCP2, which were more numerous in the TDP-43 transgenic mice (while arrows in B) than in the control (C). PNH stained with the marker H3K9M3 was more abundant in nuclei from the TDP-43 transgenic mice (D) than in the control (E). In the TDP-43 transgenic mice, the Cajal body marker protein p80 coilin was found within both perinucleolar and free nucleoplasmic Cajal bodies, which were more numerous and occupied a larger volume of the nucleoplasm (F) compared with that in the control (G). In (B)-(G) immunostaining is green, RNA stained with pyronin Y is stained red.

Scale bars = 2μm in (A) and 10μm in (B)-(G).

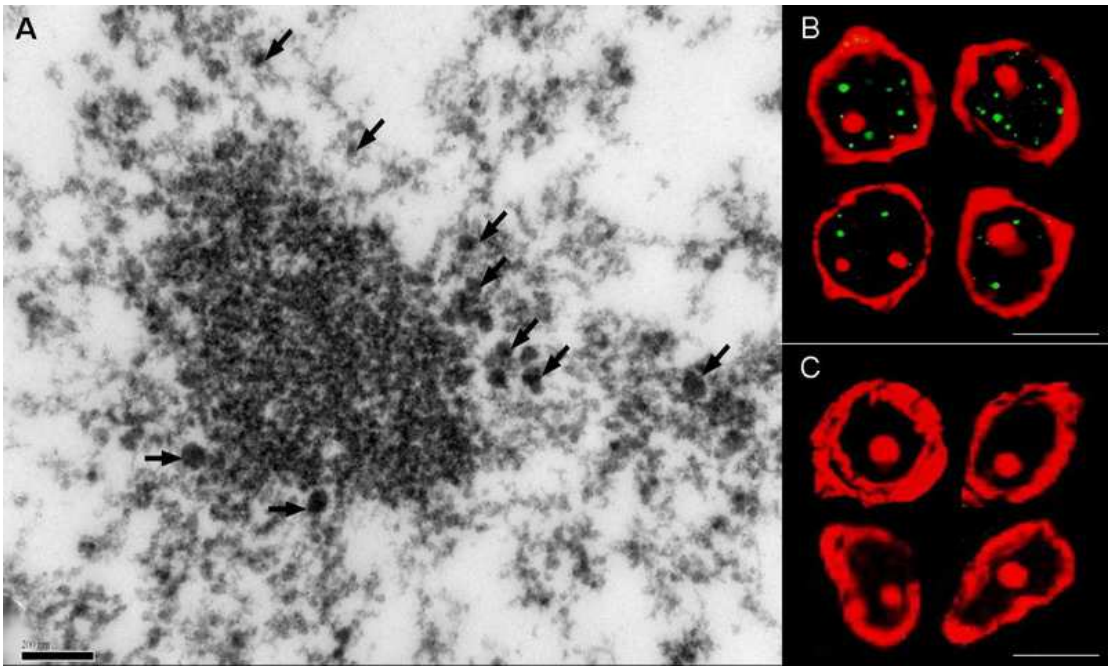

Figure 3.32

Dark nuclear microfoci and muscleblind immunofluorescence in TDP-43 transgenic mice

(A) Transmission electron micrograph of a striatal neuronal nucleus under high power revealed multiple dark grape-like foci (black arrows) in the TDP-43 transgenic mice. Scale bar = 600nm

(B) Muscleblind MBNL-1 immunofluorescence (green) identified multiple nuclear microfoci (4.75 +/- 0.70 foci per neuron which were only present in TDP-43 transgenic mice.

(C) No muscleblind MBNL-1 immunofluorescence was detected in wild type mice.

Nucleoli and cytoplasm were stained with pyronin Y (red), n=50, scale bars = 10μm

3.5.2 Cytoplasmic Vacuolation

Within the cytoplasm of striatal and cortical neurons of TDP-43^{M337V} transgenic mice, numerous double membrane enclosed vacuoles of varying sizes could be seen with TEM (Fig 3.33). These vacuoles (autophagosomes) appeared to colocalize with TDP-43 immunostained cytoplasmic foci (Fig 3.34) in which theTDP-43 was phosphorylated at serine 403/404 and 409/410, as well as being ubiquitinated (Fig 3.38). LC3 staining further colocalized with phosphorylated TDP-43, and Western blots showing an increase in the ratio of LC3-I to LC3-II confirmed the activation of autophagy (data not shown).

Moreover, a clear redistribution of TDP-43 from the nucleus in the wild type, to the cytoplasm in the transgenic mice was observed (Fig 3.35) and western blotting revealed these were sarkosyl-insoluble (data not shown). Interestingly, 35 kDa fragments of cytoplasmic TDP-43 were also detected (Fig 3.36), suggesting that insoluble TDP-43 was C-terminally cleaved into a shorter 35kDa fragment which therefore no longer contained the nuclear localization signal (NLS) (Fig 3.37).

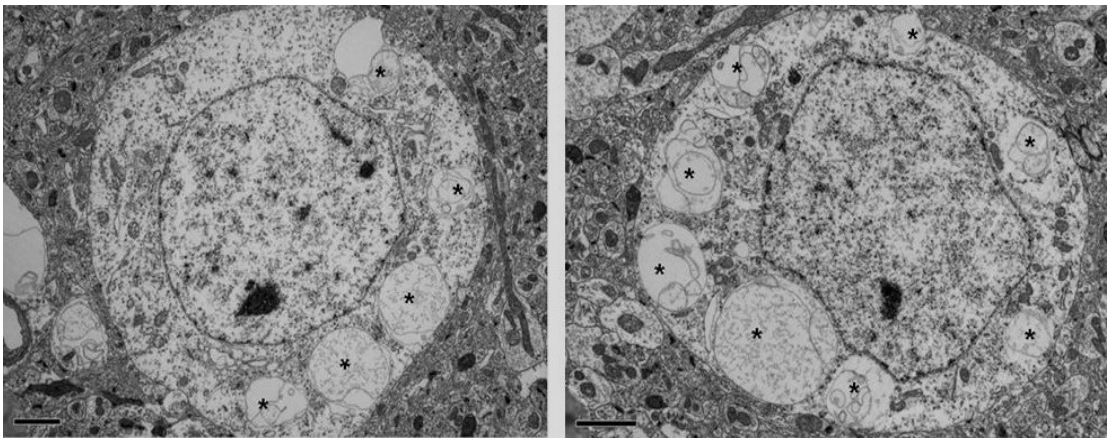

Figure 3.33

Electron micrographs of striatal neurons exhibiting prominent vacuolation

Multiple vacuoles bordered by a double membrane (asterisks) were found throughout the neuronal cytoplasm between the nuclear membrane and cell membrane.

Scale bars = 2µm

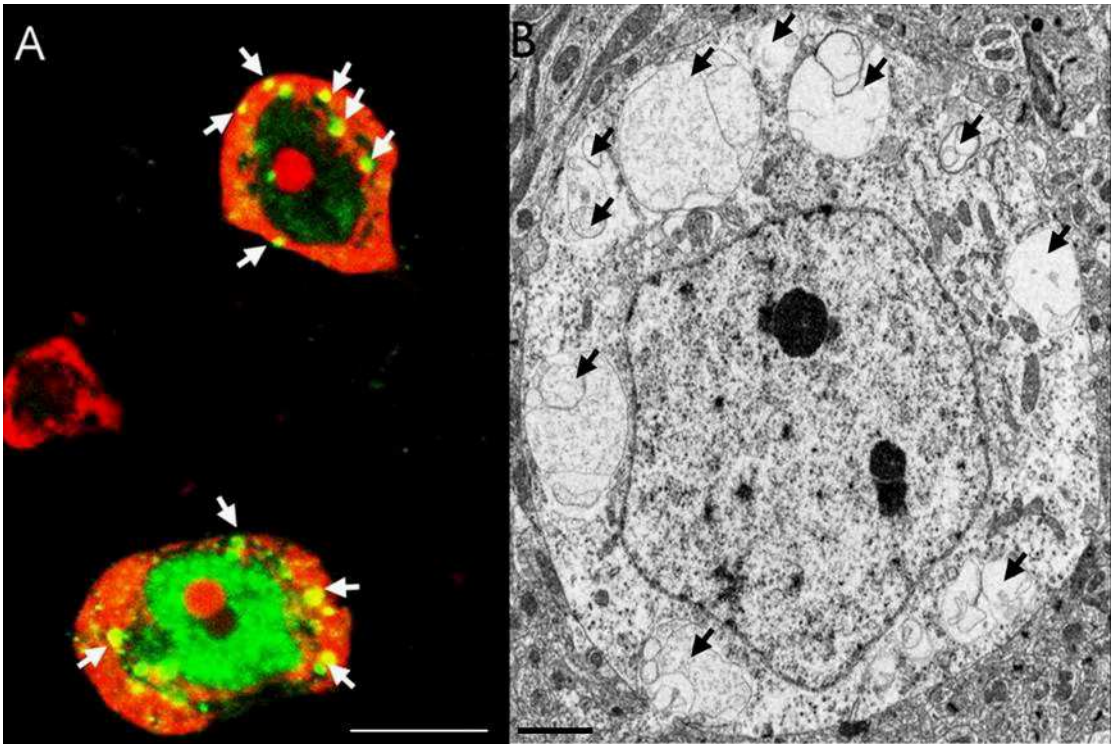

Figure 3.34

Cytoplasmic vacuolation in the striatal neuron of TDP-43 transgenic mice

(A) Immunofluorescence (green) identified TDP-43 as multiple cytoplasmic foci (white arrows) which appeared to colocalize with the vacuoles observed with TEM. Nucleoli and cytoplasm were stained with pyronin Y (red), scale bar = 10μm

(B) Numerous double membrane enclosed vacuoles (black arrows) of varying sizes (diameter 1.54+/-0.22μm range from 0.4μm to 3.5μm) were found within the cytoplasm with TEM.

Scale bar = 2μm

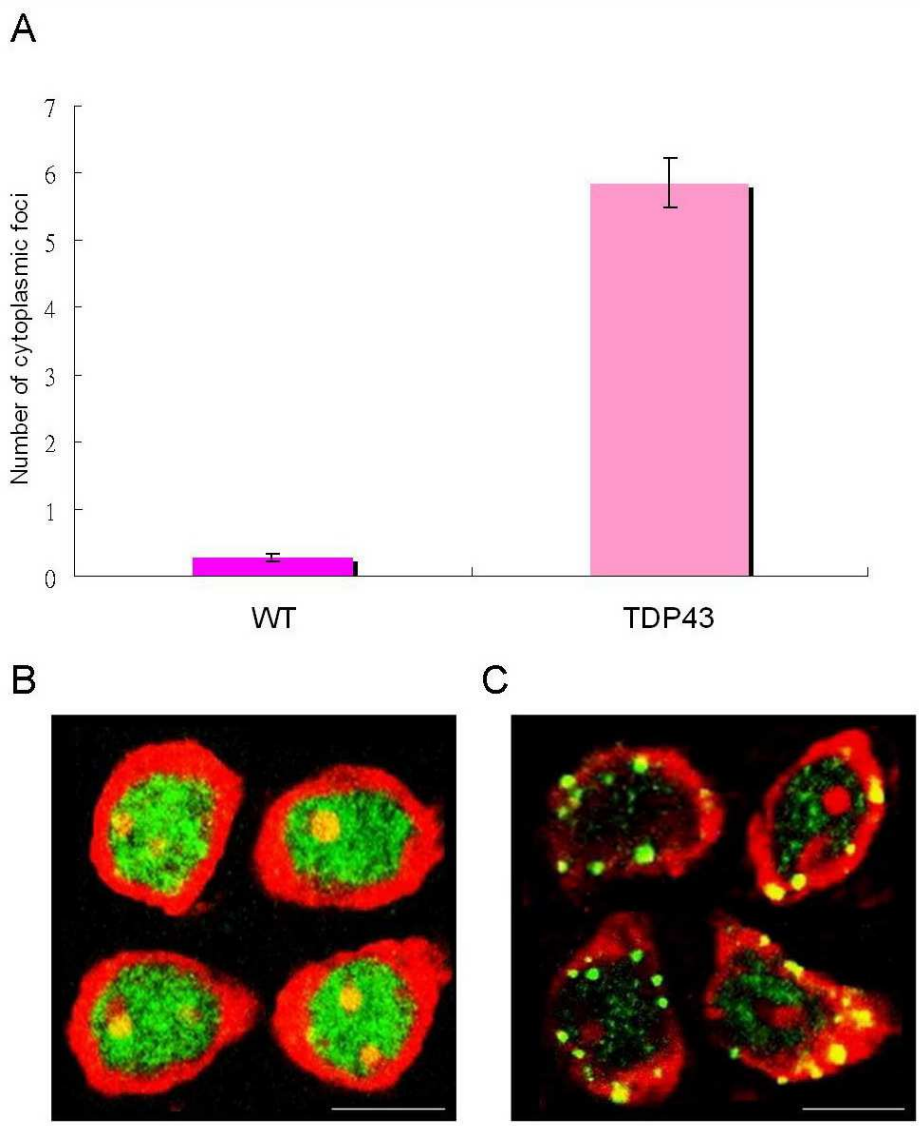

Figure 3.35

Redistribution of TDP-43 from the nucleus to the cytoplasm

(A) Average number of TDP-43 stained cytoplasmic foci was 5.86 +/- 0.38 per neuron in TDP-43 transgenic mice, compared with virtually none 0.27 +/- 0.06 in wild type mice. (n=150)

(B) TDP-43 immunofluorescence (green) was localized throughout the nucleoplasm but not in the cytoplasm in the wild type.

(C) A clear redistribution of TDP-43 immunofluorescence (green) to the cytoplasm as multiple foci in TDP-43 transgenic mice.

Pyronin Y (red) identified the nucleoli and cytoplasm, scale bars = 10μm

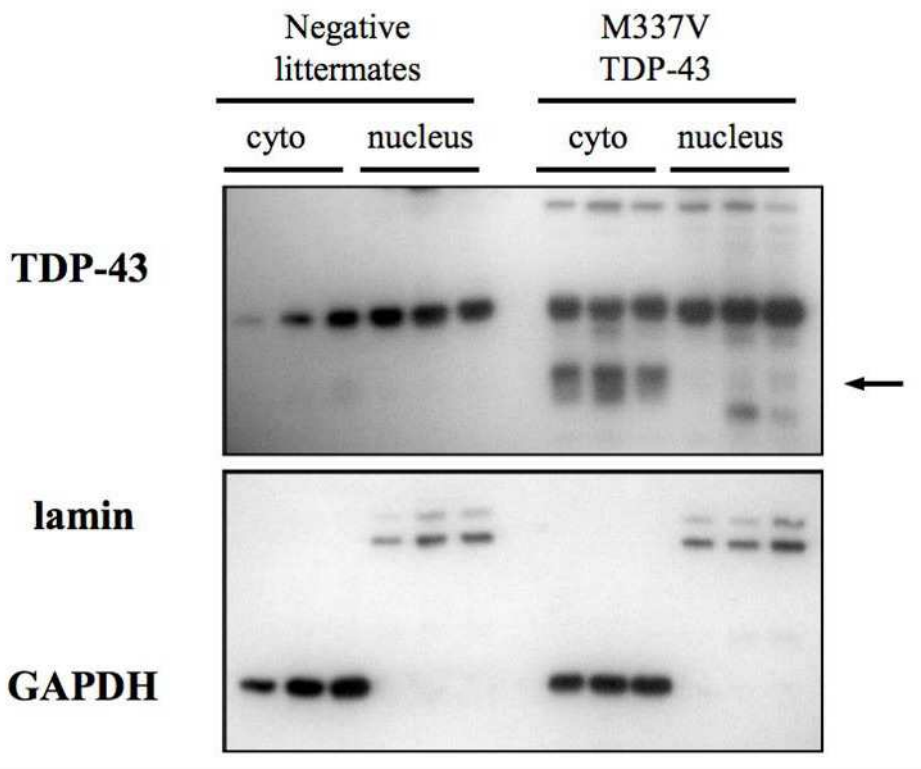

Figure 3.36

Immunoblot analysis depicting the cytoplasmic localization of TDP-43 and the detection of a 35kDa TDP-43 fragment in TDP-43 transgenic mice

Western blotting of cytoplasmic and nuclear fractions revealed an increased expression of total TDP-43 and relatively increased amounts of cytoplasmic TDP-43 in the transgenic mice compared to wild type mice. Interestingly, cleavage of TDP-43 was suggested by the detection of a 35kDa TDP-43 fragment in the TDP-43 transgenic mice (black arrow). Lamin and GAPDH are the specific markers of nucleus and cytoplasm respectively. The equivalent sized bands of these markers in the columns of both wild type and TDP-43 transgenic mice indicated the equal amounts of nuclear and cytoplasmic protein loaded onto the gel.

(Immunoblot courtesy of Veronique Schaeffer, unpublished)

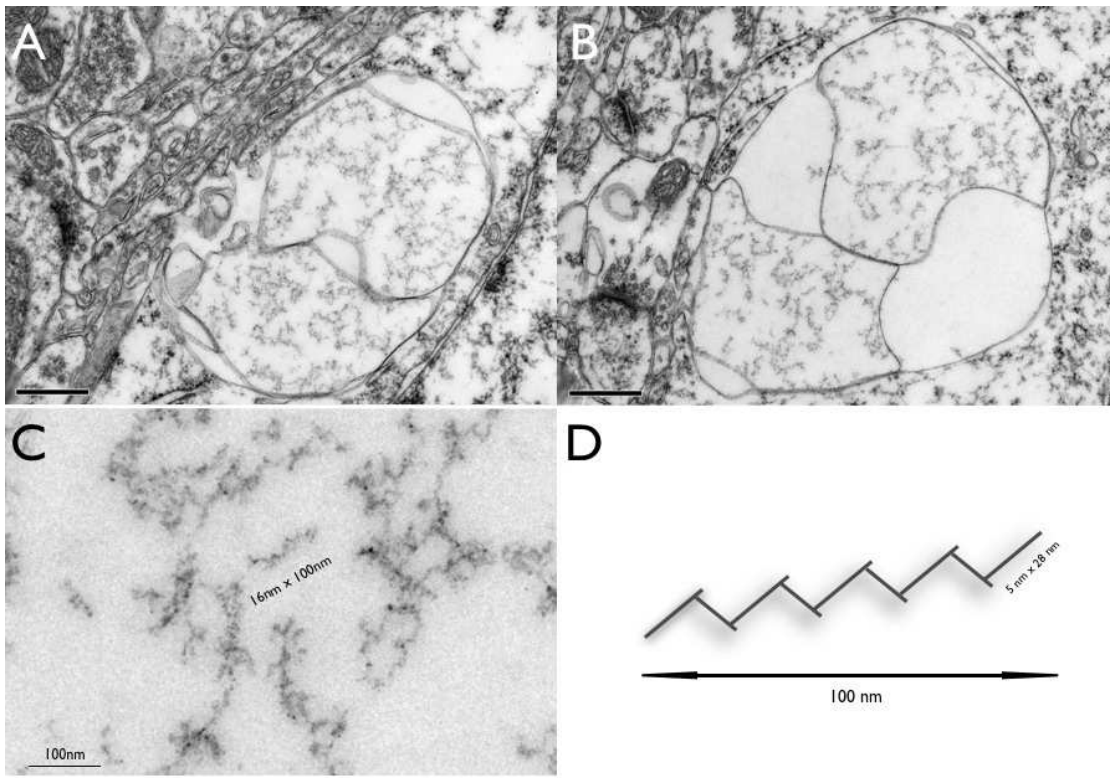

Figure 3.37

Transmission electron micrograph of cytoplasmic vacuoles containing filamentous structures

(A) and (B) High power TEM reveled filamentous contents within the cytoplasmic vacuoles.

Scale bars = 0.5μm

(C) and (D) TDP-43 stained cytoplasmic foci colocalization with autophagic vacuoles suggested these fiber-like structures were possibly C-terminally cleaved (35kDa) fragments of TDP-43.

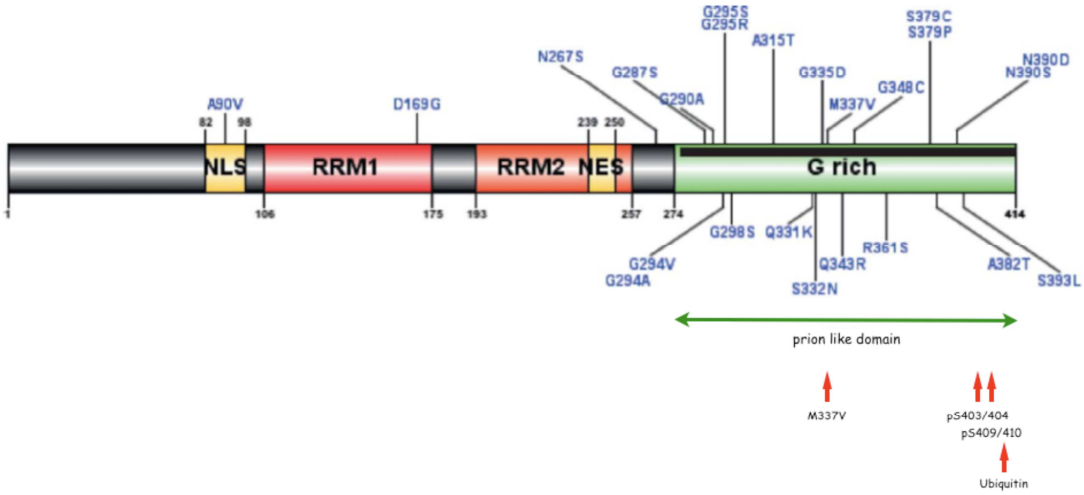

Figure 3.38

Pathology associated TDP-43 fragments potentially found in the cytoplasmic vacuoles

Filamentous structures within the vacuoles might comprise the glycine (G) rich region (green) of the TDP-43 protein, with the M337V mutation sites, S403/404, S409/410 phosphorylation and ubiquitination, which is also a prion-like domain located further away from the nuclear localization signal (NLS).

3.5.3 Nuclear Origin and Nuclear Contents of Vacuoles

TEM studies revealed that these double membrane enclosed vacuoles were derived by a process of budding-off from the outer nuclear membrane (Fig 3.39) which then migrated towards the plasma membrane. Remarkably, apart from TDP-43, immunofluorescence with antibodies against the RNA-binding proteins (RBPs) SF2/ASF, 9G8, FUS/TLS (fused in sarcoma/translated in liposarcoma) and p54^{nrb} demonstrated cytoplasmic foci, suggesting that these nuclear proteins were redistributed to the cytoplasmic vacuoles in the TDP-43 transgenic mice (Fig 3.40). Nevertheless, these were highly selective as many other nuclear proteins such as MeCP2, H3K9M3, p80 coilin, AcH3 and AcH4 were never similarly redistributed.

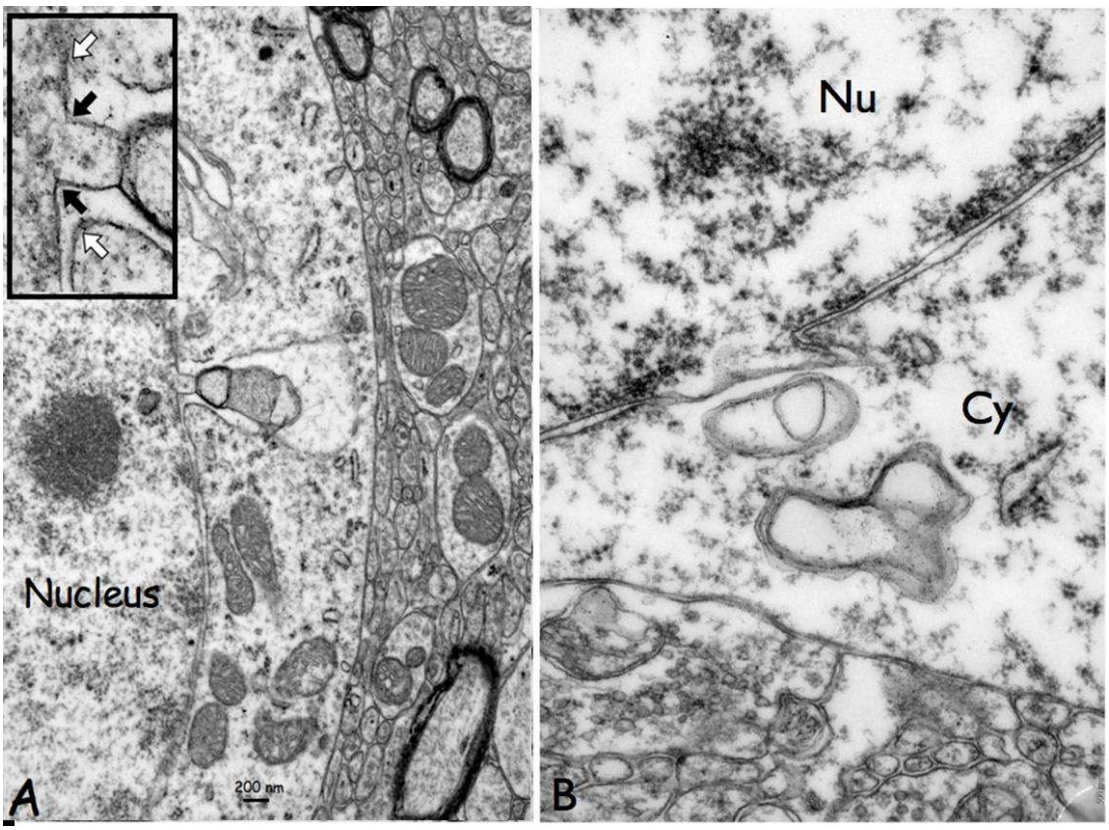

Figure 3.39

Nuclear origin of cytoplasmic vacuoles

Double membrane enclosed vacuoles in the cytoplasm (Cy) appeared to be derived by a process of budding-off from the nuclear (Nu) membrane (B). High power TEM further identified the outer nuclear membrane (white arrows) to be the origin of these cytoplasmic vacuoles (A). Scale bar = 200nm

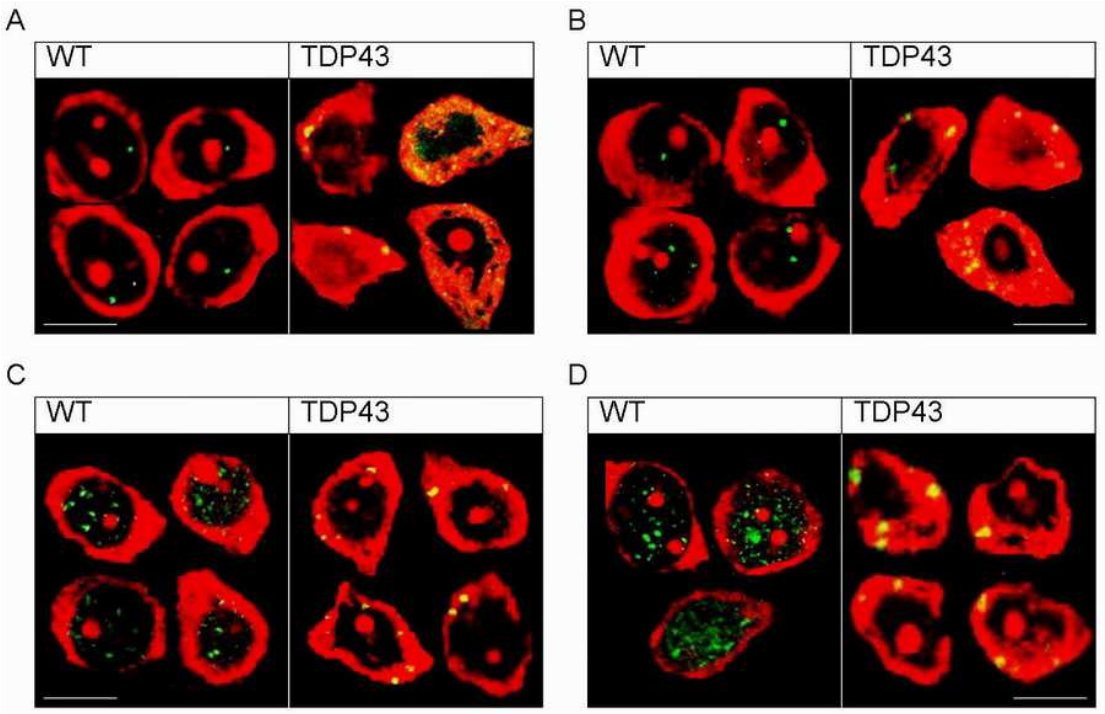

Figure 3.40

Redistribution of a highly select group of nuclear proteins (RBPs) to the cytoplasmic vacuoles

Immunofluorescence (green) identified the RBPs as nuclear foci in the wild type, and relocalized as cytoplasmic foci in the TDP-43 transgenic mice. These included the SR proteins and splicing factors SF2/ASF (A) and 9G8 (B), as well as FUS/TLS (C) and $p54^{nrb}$ (D). Both RNA and RBPs were sequestered within the cytoplasmic vacuoles, indicated by the colocalization of RNA staining (red) and immunofluorescence (green) which therefore appeared yellow. Pyronin Y (red) revealed the nucleoli and the cytoplasm, scale bars = 10μm

3.5.4 Fusion of Vacuoles with Plasma Membrane and Recruitment of Phagocytotic Glial Cells

These nuclear membrane derived vacuoles, or autophagosomes, traversed the somal cytoplasm and eventually fused with the cell membrane and extruded their contents into the extracellular space (Fig 3.41). In no instances have I seen the fusion of these autophagosomes with either dense core lysosomes or multivesicular bodies. Apart from LC3, no other autophagic markers were localized to these structures (data not shown). Moreover,

neurons within the brains of the TDP-43 transgenic mice contained very little lipofuscin, in contrast to similar neurons in Tau^{P301S} transgenic mice of the same age and background strain. At some sites where the autophagosomes fused with the plasma membrane, microglial cells were found attached to the outside of the neuron (Fig 3.42), suggesting that the fusion of the autophagosomes recruited both microglial cells and astrocytes and stimulated engulfment of cellular debris by these cells (Fig 3.43). Occasionally, the autophagosome might fuse with an adjacent neuron via the plasma membrane (Fig 3.44) and possibly releasing the contents into the neighboring cell. These together suggested a novel type of autophagic processing (exophagy or nucleophagy) by nuclear membrane derived autophagosomes (exosomes) containing truncated, phosphorylated and ubiquitinated TDP-43 in addition to selected nuclear proteins, which resulted in the extrusion of intracellular material and activation of a glial response. The novel cellular process identified in these TDP-43 transgenic mice might well contribute to the spread of transmissible filamentous proteinaceous agents within the central nervous system.

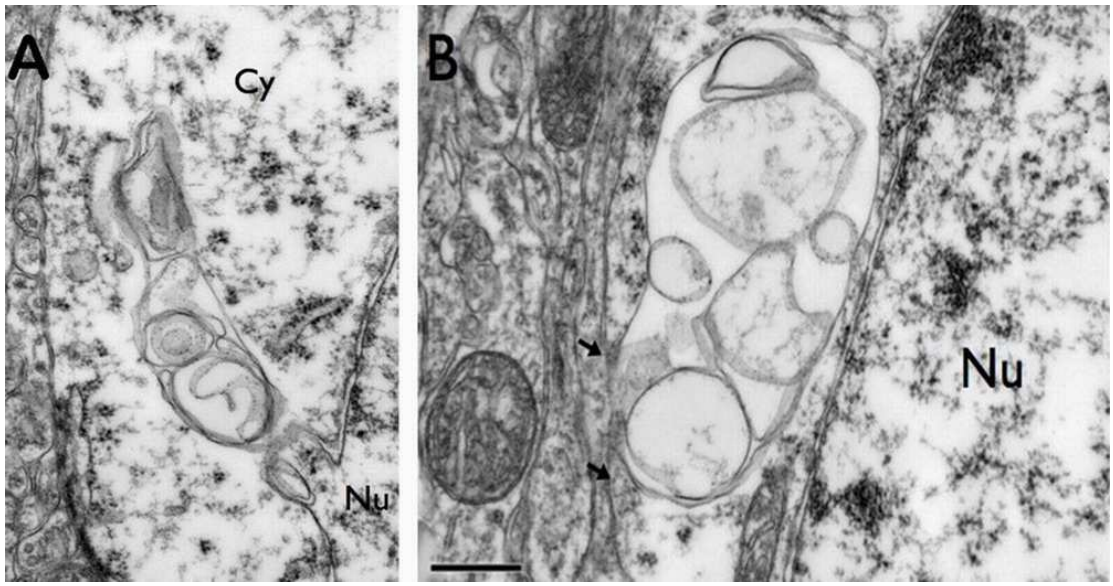

Figure 3.41

Autophagosomes originated from the nuclear membrane fused with plasma membrane

(A) Electron micrograph of a cytoplasmic (Cy) vacuole, or autophagosome, derived from the nuclear (Nu) membrane. (B) The autophagosome then fused with the cell membrane (black arrows) and extruded the contents into the surrounding neuropil. Scale bar = 500nm

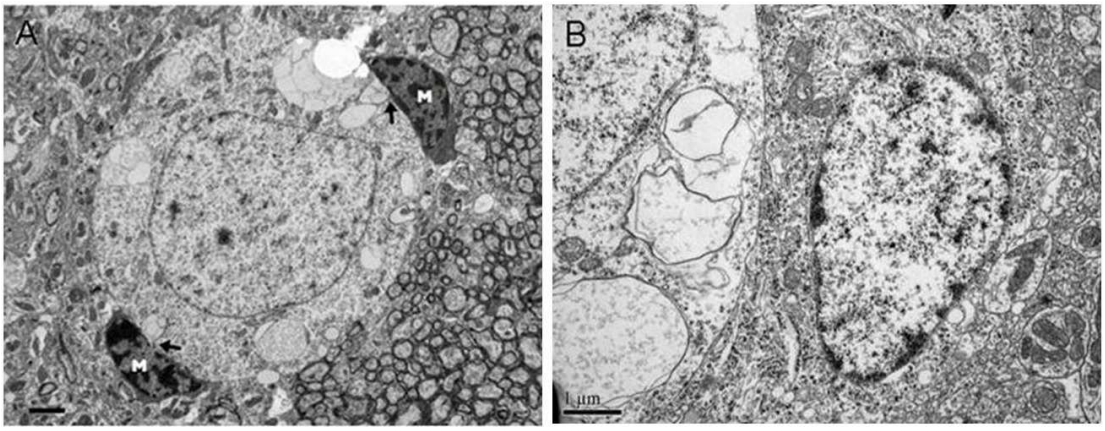

Figure 3.42

Recruitment of phagocytotic glial cells

(A) and (B) Cytoplasmic vacuolation and the recruitment of microglial cells. The fusion of autophagosomes with the cell membrane (black arrows) was associated with the presence of microglia (M) attached to the outside of the neuron. Scale bar = 2µm in (A).

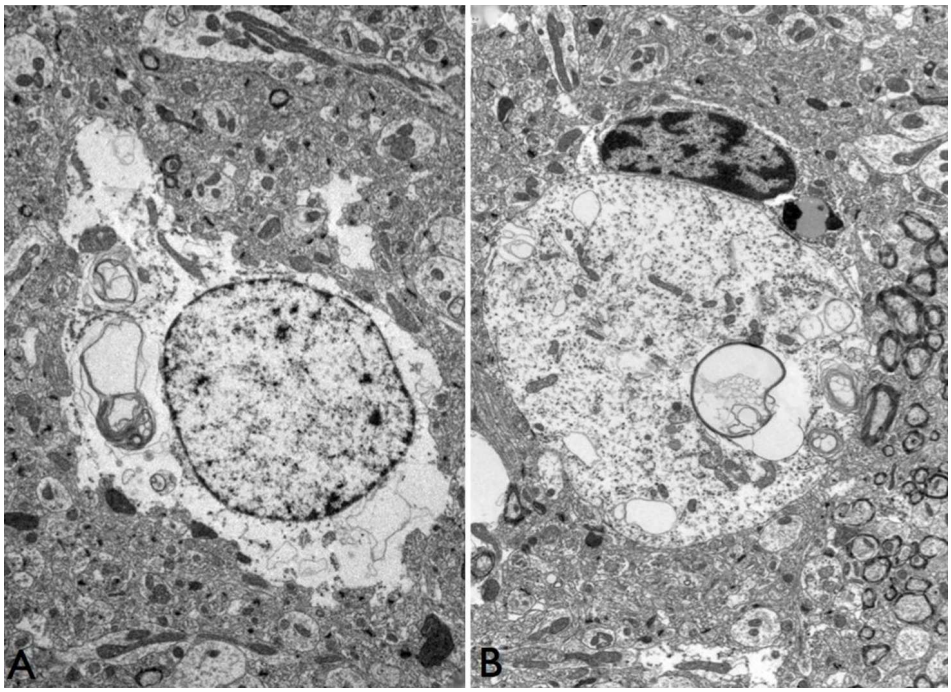

Figure 3.43

Recruitment of both astrocytes (A) and microglial cells (B) and engulfment of cellular debris by these cells. (A) An astrocyte with a cytoplasmic vacuole which appeared to contain cellular debris. This vacuole might have been taken up by the astrocyte from a vacuolated neuron.

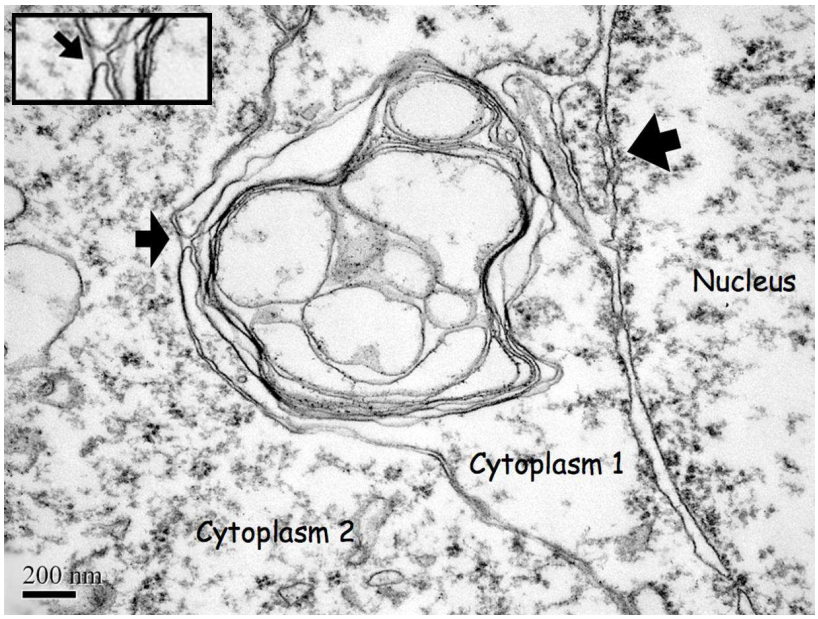

Figure 3.44

Fusion of the autophagosome with an adjacent neuron

TEM revealed the fusion of a nuclear membrane derived autophagosome with the neighboring neuron (big arrows). Under high power membrane of the autophagosome in cytoplasm 1 was found to be in contact with the plasma membrane in cytoplasm 2 (top left corner box).

3.5.5 Degenerating Neurons

Interspersed between these highly vacuolated cells, there were numerous degenerating neurons undergoing dark cell degeneration, with typical condensed features of nucleus and cytoplasm under TEM (Fig 3.45). Whether these neurons were dying because of losing much of their cytoplasmic volume via extrusion of vacuoles, or failure to dispose of toxic aggregates, remained to be explored.

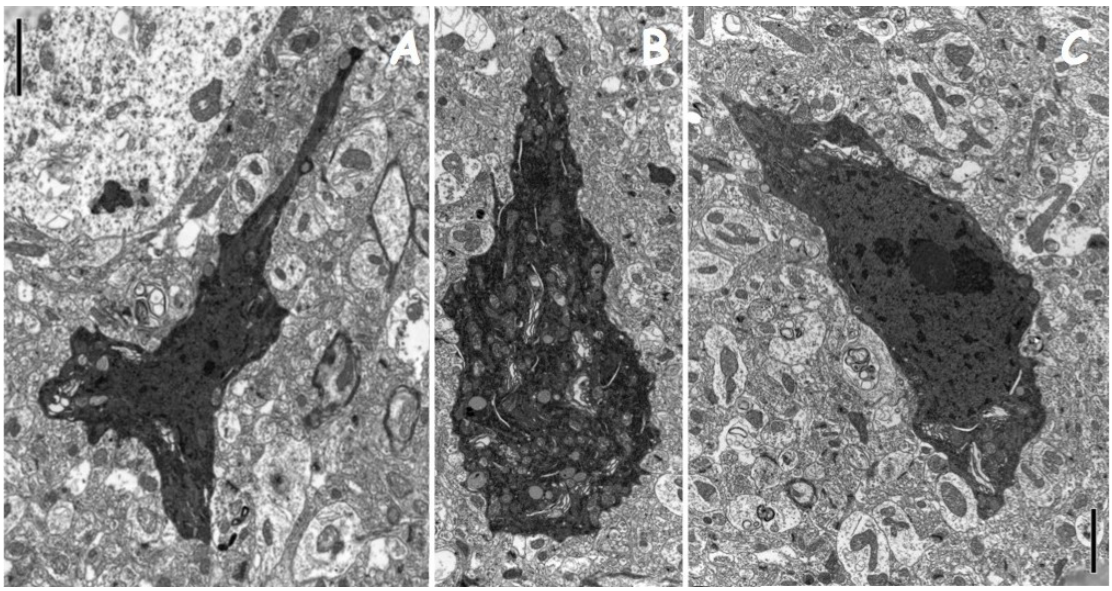

Figure 3.45

TEM revealed neurons undergoing dark cell degeneration

(A), (B) and (C) Examples of degenerating neurons undergoing dark cell degeneration were found throughout the tissue in the TDP-43 transgenic mice. Shrinkage and condensed appearance of neurons were observed interspersed between highly vacuolated cells. Scale bar = 2μm

In conclusion, dynamic changes in the striatal neuronal nuclear organization of the perinucleolar structures, including the PNH and CBs, are identified in transgenic mouse models of three human neurodegenerative

diseases (HD, ALS/FTLD and FTDP-17). The dramatic rearrangement of the neuronal nucleolar complex might implicate dysregulation of both transcription and splicing in these mice. Remarkably, the novel TDP-43^{M337V} transgenic mice further exhibited a bipartite pathological mechanism in both the nucleus and the cytoplasm. These include the striking appearance of dark nuclear microfoci as well as double membrane enclosed vacuoles within the cytoplasm, accompanied by the sub-cellular redistribution of TDP-43 from the nucleus to the cytoplasm. In addition, the cellular process observed for the extrusion of TDP-43 aggregates from the nucleus through the cytoplasm and eventually out of the neuron might suggest a novel mechanism leading to the extracellular spread of transmissible protein aggregates within the CNS. These unique pathological features have never been demonstrated in other neurodegenerative disease models including the R6/2 and Tau transgenic mice.

Discussion
&
Conclusions

CHAPTER 4

Discussion

4.1 Overview of the Neuronal Nucleus

4.1.1 Milestones in the Understanding of the Neuronal Nucleus

More than a century ago, the neuronal nucleolus and the associated “cap” structure were first described by Giuseppe Levi. In 1896, he discovered an unusual feature of the neuronal nucleus, namely the Levi “basophil grume”, which corresponds to the large nucleolus-associated mass of heterochromatin (Levi, 1896). Another significant discovery in the mammalian neurons was made by Santiago Ramón y Cajal in 1903, in which the accessory body (Cajal body) was visualized with the reduced silver nitrate method. Seven years later, a thorough description and analysis of the organization of some major nuclear components at the light microscopic level was also published (Cajal, 1910, Lafarga et al., 2009). Towards the 1990s, accumulating data demonstrated a distinct pattern of chromatin organization in interphase nuclei, particularly in neurons. This resulted in an emerging interest in the spatial organization of the nucleus during interphase. Studies followed to reveal the dynamic reposition of specific chromatin domains such as the centromeres under physiological stimuli. In addition, the association between nuclear compartmentalization and regulation of transcription was further implicated by the non-random organization of specific genomic sequences in neurons (Manuelidis, 1984, Manuelidis, 1985, Borden and Manuelidis, 1988, Billia and de Boni, 1991,

Holowacz and De Boni, 1991). Subsequently, molecular analysis of various nuclear components, for instance the coiled (Cajal) body, led to a more comprehensive picture of their non-random interphasic position and functions (Lamond and Carmo-Fonseca, 1993, Bohmann et al., 1995).

Transcriptionally active and inactive chromatin domains in neurons were characterized in a relatively recent study, which emphasized the presence of a distinctive shell of heterochromatin separating the single nucleolus from the rest of the nucleus in large neurons, to which inactive ribosomal DNA repeats are attached to (Akhmanova et al., 2000). Contemporary research has focused on the localization of specific chromosomal loci within the nucleus (Cremer et al., 2001, Cremer and Cremer, 2010) and additionally the role of ncRNAs in determining the location and formation of nuclear bodies (Dundr and Misteli, 2010). However, these studies have not been performed in neurons.

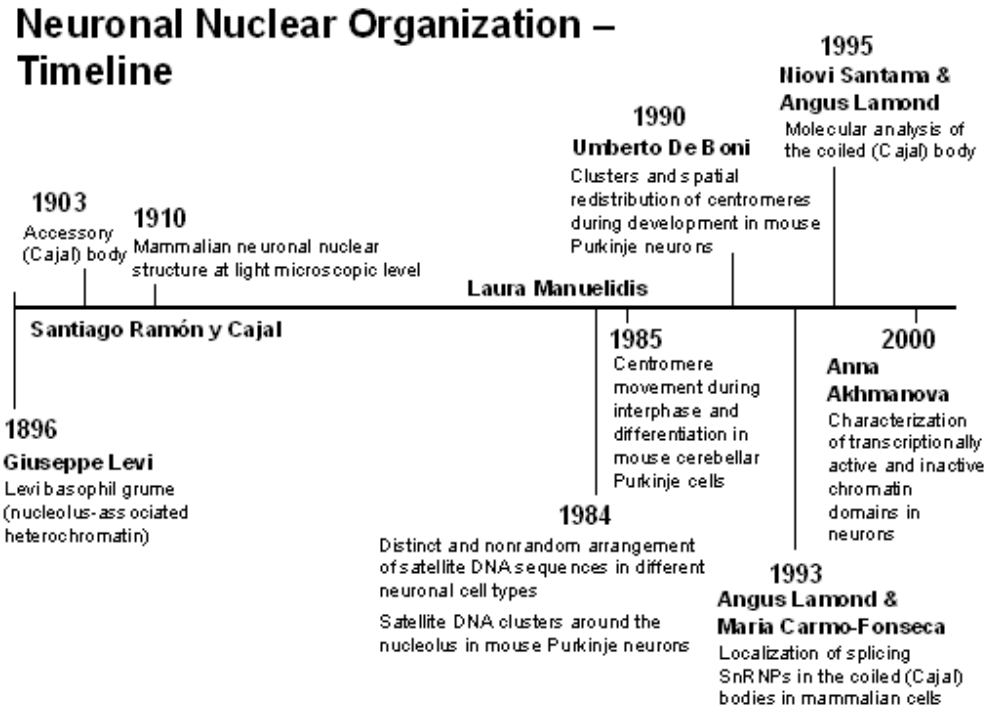

Figure 4.1

Milestones in the understanding of the neuronal nuclear organization. Timeline illustrating the important discoveries and contributions to the knowledge of the neuronal nuclear organization and the understanding of nuclear structure and function.

4.1.2 Unique Nuclear Organization of the Post-mitotic Neuron

The mammalian neuron is highly specialized with a unique biology, independent from its nerve impulse generating and conducting properties. Most neurons of the adult CNS are fully differentiated which neither divide nor regenerate, and do not grow substantially. With the absence of DNA replication and chromosome segregation, the post-mitotic nature of neurons suggests a unique neuronal nuclear organization most efficient for RNA transcription and processing (Akhmanova et al., 2000).

It is important to realize that the majority of studies of the nuclear

architecture and function have been undertaken in cells in culture, most frequently in rapidly growing, dividing and highly transformed cells such as HeLa cells. Therefore, little is known regarding the unique neuronal nuclear organization and up to now, the spatial organization as well as the heterochromatic arrangement within the neuronal nucleus is still poorly understood. One of the very few studies attempting to investigate the neuronal chromatin organization was carried out by Akhmanova and co-workers, in which the neuronal nuclear and nucleolar chromatin domains in the Purkinje and granule cells of the cerebellum in adult FVB mice were characterized (Akhmanova et al., 2000). The presence of the perinucleolar heterochromatin (PNH) in large neurons was suggested to serve as an attachment site for inactive DNA such that RNA pol II (and III) transcriptional domains in the nucleus are separated from RNA pol I domain in the nucleolus (Akhmanova et al., 2000). In addition, two perinucleolar heterochromatin domains, each with different protein and DNA constituents, were reported in the study and the results obtained are summarized in Fig 4.2.

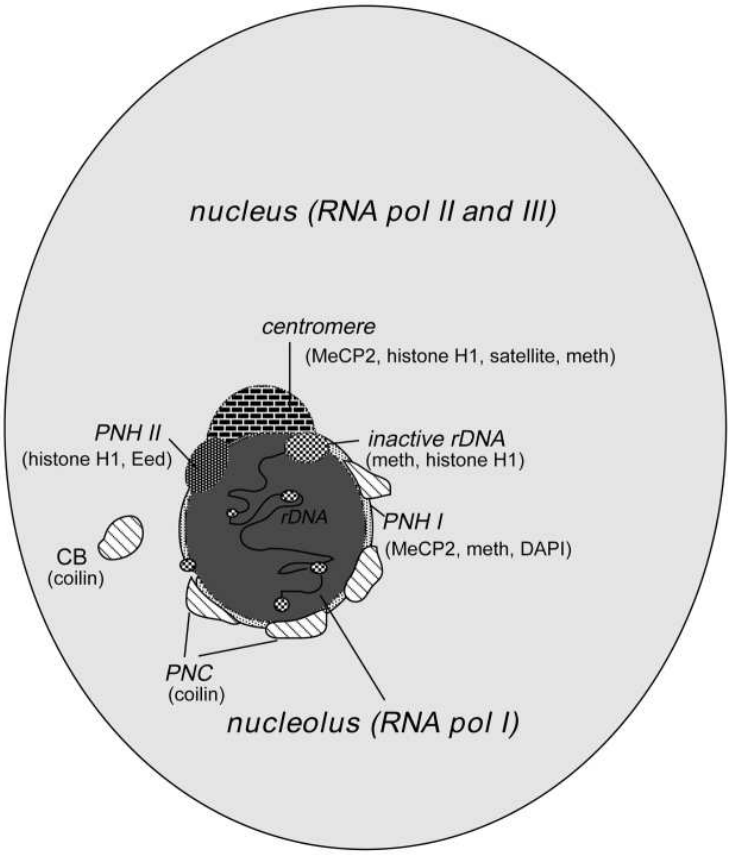

Figure 4.2

Neuronal nuclear and nucleolar chromatin domains. A schematic overview illustrating the transcriptionally active and inactive chromatin domains in the FVB neuron. A large single nucleolus is surrounded by a shell of heterochromatin, to which inactive DNA domains are attached. The protein and DNA composition of PNH I and II are indicated. A perinucleolar cap (PNC) of Cajal body (coilin) is localized surrounding the nucleolus. (Adapted from Akhmanova et al., 2000)

Recently, the perinucleolar complex, especially the heterochromatic domains, has become one of the hottest areas of research in the field. A growing body of evidence has illustrated the intimate association between the highly organized PNH and the maintenance of nucleolar structure. Remarkably, the present study revealed the highest level of transcription within the specialized PNH, together with the localization of the key heterochromatic structures including centromeres, telomeres and the inactivated X chromosome. As the pattern of the unique genomic organization in neurons needs to be maintained throughout the whole lifespan, there has to

be a dedicated mechanism, potentially operating for a lifetime (approximately 80 years in humans), and it appears that epigenetic regulation holds the key for the maintenance of this specialized neuronal nuclear organization.

4.2 Organization of the Neuronal Nucleus

This thesis has determined the ultrastructural and molecular composition of the neuronal nucleus in the mouse striatum, including the characterization of the unique organization of the chromosomal domains, subnuclear bodies and epigenetic marking. In addition, using a novel *in vivo* transcription run on assay to detect nascent RNA (Casafont et al., 2006, Cmarko et al., 2000, Casafont et al., 2009), the patterns of RNA transcription within these subnuclear structures are demonstrated and further combined with the ultrastructural localization of RNA polymerases I, II and III.

These novel findings provide important insights into the organization of the mammalian neuronal nucleus, which indicate that the nucleus of the CNS neuron exhibits a distinct structural and functional organization that has never been recognized previously. The exciting and unexpected results also implicate a novel mechanism for the establishment and maintenance of the post-mitotic nature of neurons. These findings provide fundamental basis for our understanding of the complex 3D spatial arrangement of transcription and post-transcriptional processing in the neuronal nucleus. There is no doubt that elucidation of the impact of dysregulation of these processes, which are observed in a number of neurodegenerative diseases, would lead to a better understanding of the pathogenic mechanisms of these devastating diseases.

4.2.1 Epigenetic Characterization of the Neuronal Nucleus

The chromosomal architecture and epigenetic status of various nuclear domains in the mouse striatum are characterized in this study, with a definitive epigenetic roadmap established by immunofluorescence with antibodies against specific epigenetic modifications (Fig 3.7). Characteristic markers of euchromatin and heterochromatin domains are localized including those typically associated with the PNH. Heterochromatin markers are generally localized as perinucleolar foci, in contrast with markers of euchromatin (histone acetylation) which reveal homogeneous nucleoplasmic staining. The complex structural and molecular arrangement of the neuronal nucleolus and the perinucleolar region, a unique feature of neurons, is demonstrated in this study, which has never been reported previously.

The DNA and RNA content of the neuronal nucleus can be visualized with the fluorescent dyes DAPI and PYY respectively. It is demonstrated that a typical striatal neuronal nucleus contains a large nucleolus (stained with PYY due to the presence of rRNA) surrounded by a rim of heterochromatin (condensed DNA) and attached to large caps of PNH, which is intercalated with a nucleolar rosette of CBs (Fig 3.5 and 3.6). In addition to the PNH domain I and II described previously by Akhmanova (Akhmanova et al., 2000), a novel perinucleolar heterochromatic mass (PNH III) has been characterized which contains methylated DNA and a range of epigenetic markers such as MeCP2, ATRX, H1 and H3K9M3 (Fig 4.3). Using a combination of 3D-FISH and 3D-ICC analyses, the genomic regions present within this newly defined enigmatic mass are further identified. Results illustrate that the majority of

centromeres (86%) and telomeres (80%) are found on the borders of PNH (Fig 3.4). Further EM and ICC analyses have also implicated the localization of the inactive X chromosome within the PNH (data not shown). This suggests that the majority of chromosomes loop into the nuclear interior with both ends associated with the PNH, which indicates that the radiating chromosomal arrangement of the classical Rabl model may not be found in CNS neurons. Indeed, the nuclear peripheral ring of heterochromatin, typically found in many cells, is often absent in neurons. These findings confirm the early observations that the PNH contains DNA repeat sequences found in centromeres and telomeres, as well as the inactive X chromosome in female mice (Manuelidis, 1984, Borden and Manuelidis, 1988, Vadakkan et al., 2006, Moore and Barr, 1953). Therefore, this intriguing perinucleolar heterochromatic mass appears to be an amalgamation of both constitutive and facultative heterochromatin.

Surprisingly, a number of RNA modifying enzymes are found to be localized within the striatal neuronal nucleolus, including the RNA-editing enzymes ADAR2 as well as the RNA-processing enzymes DICER, Drosha and DGCR8 (Pasha) (Fig 3.11). This indicates that the neuronal nucleolus might also be specialized for ncRNA editing and processing. Although DICER was previously found to be localized in the cytoplasm, accumulating evidence has recently identified this miRNA-processing enzyme in the nucleus, and specifically within the nucleolus (Shiohama et al., 2007). Other studies have also reported the association of RNA-editing enzymes such as ADAR2 with the nucleolus (Desterro et al., 2003). At present, additional nucleolar functions unrelated to rRNA transcription have become the topic of considerable interest (Boulon et al., 2010). Figure 4.3 summarizes and describes the epigenetic

characterization of the neuronal nucleolar complex in the mouse striatum.

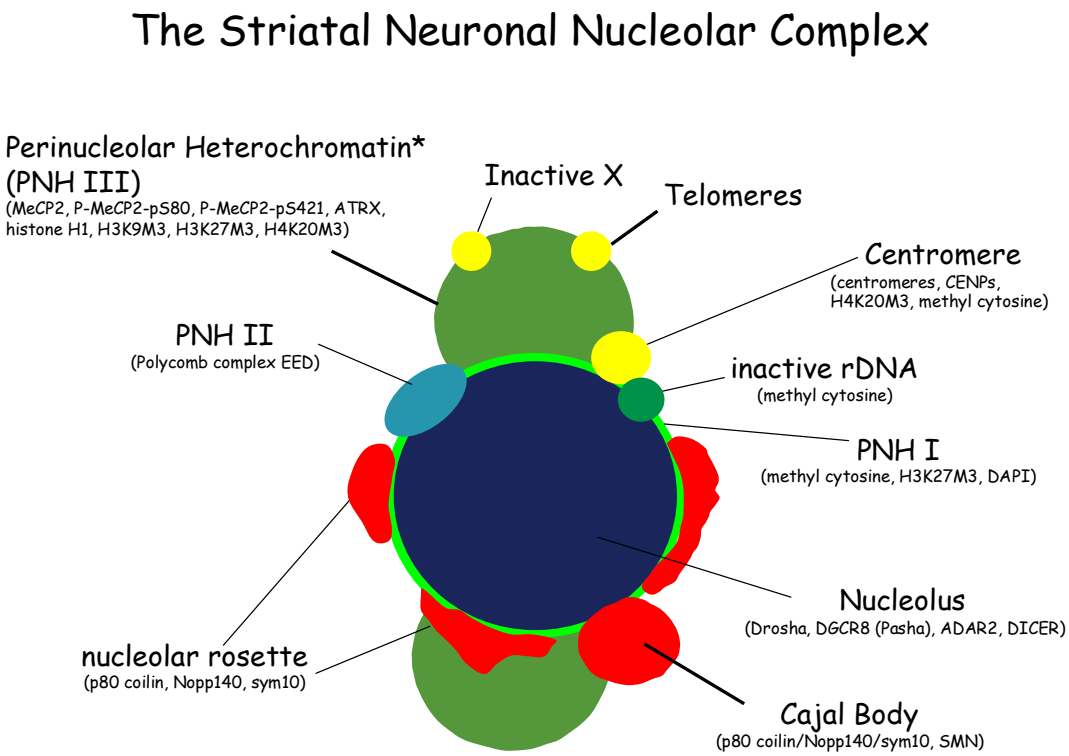

*Pericentromeric Heterochromatin

Figure 4.3

The striatal neuronal nucleolar complex. A schematic diagram illustrating the nucleolar chromatin domains and the associated proteins in the mouse striatal neuronal nucleus. The nucleolus (dark blue) is surrounded by a characteristic ring of heterochromatin (light green) which is intercalated between a nucleolar rosette of Cajal bodies (red). A number of RNA modifying enzymes are localized within the nucleolus. Perinucleolar heterochromatin (PNH) I and II have been reported previously by Akhmanova. A novel PNH, PNH III (green) is characterized in the present study which is associated with a range of epigenetic markers as well as the centromeres, telomeres and inactive X chromosome. *PNH III is also regarded as pericentromeric heterochromatin as results revealed its association with the majority of centromeres.

4.2.2 Ultrastructural and Functional Significance

In order to understand the functional significance of this unique neuronal nuclear organization, an *in vivo* nuclear transcription run-on assay is used to

detect nascent RNA synthesized within various subnuclear domains. Remarkably, the newly defined PNH is heavily labeled for nascent RNA, whereas no RNA synthesis is detected within the CBs, and very low levels are found in the nucleolus. Further analyses using post-embedding immunogold ICC indicate the significantly higher rate of transcription within the PNH, which appears to be 15 times greater than that in the nucleoplasm, although accounts for only 27% of the total transcription in the nucleus (Fig 3.8). It is therefore suggested that in conscious freely moving mice, RNA is synthesized at different rates within various sub-compartments of the neuronal nucleus. These findings are strikingly different to the accepted patterns of transcription in the eukaryotic nucleus (Chakalova and Fraser, 2010, Papantonis and Cook, 2010, Fraser and Bickmore, 2007, Akhtar and Gasser, 2007).

In contrast with Akhmanova's finding that the perinucleolar heterochromatic domain is transcriptionally silent as dogma suggests, this study has challenged the classical view that heterochromatin is transcriptionally inactive due to the high level of chromatin condensation. Remarkably, recent studies in a variety of organisms have shed new light on this paradoxical argument and provide evidence demonstrating the association between heterochromatin and gene expression. Sequencing projects have revealed the influences of heterochromatin on gene expression, in which they found several hundred of heterochromatic genes in drosophila, plants and mammals (Yasuhara and Wakimoto, 2006). It is also realized that the boundaries between heterochromatin and euchromatin are not always precise, as studies suggest that euchromatin-heterochromatin transition zones may exist (Yasuhara and Wakimoto, 2006, Yasuhara and Wakimoto, 2008).

Indeed, transcription in heterochromatin has been well documented in the fission yeast *Schizosaccharomyces pombe*, which implicates RNA interference mechanisms in targeting and maintaining heterochromatin. These mechanisms are suggested to be crucially dependent on small ncRNA transcription (Grewal and Jia, 2007, Eymery et al., 2009, Grewal and Elgin, 2007, Cam et al., 2009). Therefore it might be speculated that transcriptional activities detected within the PNH are associated with ncRNA and hence RNA interference, whereas transcription of coding RNA are shut. Furthermore, mounting evidence has recently illustrated a multifunctional and perhaps gene activating role of MeCP2 (Chahrour et al., 2008, Yasui et al., 2007). The specific localization of MeCP2 within the PNH found in this study suggests that the PNH and its associated MeCP2 may not be dedicated to transcriptional inactivation but expression of particular genes.

In addition to the detection of nascent RNA synthesis within the neuronal nucleus, ultrastructural localization of the three RNA polymerase enzymes further provides evidence as to the nature of the transcripts. RNA pol I is associated with the production of rRNA, RNA pol II with mRNA synthesis, and RNA pol III with tRNA, ncRNA and short interspersed nuclear elements (SINEs) transcription. Antibodies to RNA pol I label the nucleolus, whereas the CBs do not label with any of the RNA polymerase enzymes. Surprisingly, the highly active level of transcription detected within the PNH is not associated with RNA pol I or II, but instead specifically labeled with RNA pol III. In contrast to the PNH, other non-nucleolar associated heterochromatic regions do not exhibit active transcription and fail to label with RNA pol III. Thus, these results have additionally determined a unique feature of the newly defined PNH,

namely a high density of RNA pol III mediated transcription *in vivo*. What is then the significance of a prominent perinucleolar heterochromatic domain with high levels of transcription specifically by RNA III?

In many organisms particularly vertebrates, SINEs are the most abundant DNA elements containing tRNA-class pol III promoters. These ncRNAs are actively and specifically transcribed within the centromeric heterochromatic regions by RNA pol III and are highly expressed in the mouse brain (Prades et al., 1996, Ponicsan et al., 2010, Allen et al., 2004). Studies have demonstrated that there are approximately 550,000 B1 and 350,000 B2 SINEs which together comprise 6% of the mouse genome (Boyle et al., 1990). Interestingly, recent studies reveal that there may be multiple regulatory interactions between SINEs and the miRNA-processing enzyme DICER, which has been found to localize within the neuronal nucleolus in this study. Apart from miRNA processing, DICER1 is implicated in heterochromatin assembly, and chromatin remodeling at human Alu SINE repeats is suggested to play important roles in the regulation of miRNA expression (Saito et al., 2009, Murchison et al., 2005, Kanellopoulou et al., 2005). Moreover, accumulation of human Alu RNA or Alu-like B1 and B2 RNAs in the mouse is found to be highly toxic which is associated with a decreased activity of DICER (Kaneko et al., 2011). Together with other reports, it is suggested that SINE RNA accumulation associated with DICER depletion may result in degeneration observed in various pathological degenerative conditions (Kaneko et al., 2011, Schaefer et al., 2007, Cuellar et al., 2008). Furthermore, increased B2 SINE expression may repress mRNA transcription by binding directly to RNA pol II in response to stress (Ponicsan et al., 2010, Allen et al., 2004, Yakovchuk et

al., 2011).

4.2.3 The Integrated Neuronal Nucleolar Complex

Recently, a growing body of evidence has demonstrated that ongoing transcription of ncRNA is a prerequisite for the formation and maintenance of different nuclear subdomains, including the CBs, speckles, paraspeckles and nuclear stress bodies (Shevtsov and Dundr, 2011, Mao et al., 2011, Souquere et al., 2010). In the neuronal nucleus, transcription of specific SINEs within the PNH may be crucial for forming and maintaining this complex heterochromatic domain. New functions of CBs in the maturation and processing of a variety of ncRNA species have also been reported (Stanek and Neugebauer, 2006, Pontes and Pikaard, 2008). It may be postulated that the perinucleolar rosette of CBs in the neuronal nucleus function as sites for the maturation of ncRNA formed in the PNH. Additional support is provided by the localization of a number of RNA processing and editing enzymes within the neuronal nucleolus. Together, these suggest that the PNH, nucleolus and the intercalated CBs function as an integrated complex for the transcription, processing, editing and maturation of ncRNAs such as SINEs. RNA pol III mediated transcription taking place in the PNH, post-transcriptional RNA processing and editing in the nucleolus, and finally maturation in the CBs. This specific complex is believed to be highly developed and specialized in neurons.

Why is this unique nuclear organization specific to neurons and when does it first become apparent in neuronal development? The formation of a single centrally located nucleolus surrounded by perinucleolar shell of CBs and PNH

occurs around 2-3 weeks postnatally in the mouse striatal neuronal nucleus (unpublished observations). This is some time after the neurons have gone through their last round of cell division (E12-E21) and exited the cell cycle. Remarkably, it coincides with the period when the activity of RNA pol I is down regulated and neuronal cell growth is reduced, It would be tempting to speculate that the cessation of cell division together with decreasing cell growth, reflected in reduced ribosome biogenesis, bring together centromeres, telomeres and rDNA in a single stable complex. The prevention of chromosome segregation and mitosis initiation would need to be maintained for the lifespan of the neuron (Verdaasdonk and Bloom, 2011). Moreover, the low rates of RNA pol I transcription observed in these neurons, which appear to trigger nuclear reorganization, are consistent with the exceptionally long half life of rRNA reported in the mammalian brain (Mallwain and Bachelard, 1985). These may implicate an intimate relationship among the perinucleolar structures which may be crucial in the maintenance of the unique neuronal nucleolar complex.

4.3 Neuronal Nuclear Rearrangement Induced by HDAC Inhibition

Having established the ultrastructural and functional organization of the unique nuclear and nucleolar structures in the striatal neuron, it is surprising to find that this highly specialized arrangement of the neuronal nucleus is not static but dynamic. Changes in the patterns of epigenetic modifications are induced by HDAC inhibitors VPA and SAHA which activate transcription. The

unique neuronal nucleolar complex also appears to be a focus for disorganization.

4.3.1 Histone Modifications

Although immunofluorescence of the linker histone H1 remains the same following both VPA and SAHA treatment, staining intensity of AcH3 protein is significantly increased. A prominent increase in AcH3 level after VPA treatment has also been reported in a clinical study, which further demonstrated that the percent increase in AcH3 was positively correlated with the levels of VPA, suggesting a dose-response characteristic of the chromatin remodeling response (Sharma et al., 2006). A relatively heterogeneous nuclear distribution of AcH4 is found in both saline and HDACi treated mice. However, an increase in nucleoplasmic staining intensity is observed only in SAHA treated mice, which is absent following VPA treatment (Fig 3.14 and 3.16). This is consistent with Sharma's study that there may be no clear cut correlation between the dose of VPA and the levels of histone H4 acetylation (Sharma et al., 2006). This may also indicate the different selectivities between the two HDACi, in which the fatty acid VPA is a class I-selective HDACi, whereas the hydroxamic acid SAHA is a potent but non-selective inhibitor of class I/II HDACs. Moreover, there appears to be an enhanced staining of AcH4 at the nuclear periphery following SAHA treatment, in agreement with other studies illustrating a strong and rapid enhancement of histone H4 acetylation at the nuclear periphery following a wide range of doses of HDACi treatment in different cell types (Taddei et al., 1999). The acetylation levels of histones H3 and H4 are strongly predictive of a chromatin

structure which is favorable for gene expression. The significant increase in histone acetylation, especially of lysine residues 9 and 14 on H3 tail, induced by VPA and SAHA treatment illustrates that inhibition of histone deacetylases indeed plays a causative role in histone hyperacetylation which is conducive to transcriptional activation.

4.3.2 Perinucleolar Heterochromatin

A dramatic change in the nuclear distribution of the PNH marker protein H3K9M3 is induced by both VPA and SAHA, indicating a rearrangement of the PNH domains in the neuronal nucleus following transcriptional activation. Following HDACi treatment, H3K9M3 stained foci appear much bigger in size and demonstrate a nuclear peripheralized distribution in addition to scattered nucleoplasmic staining (Fig 3.17and 3.18). A greater increase in the size of immunostained perinucleolar foci is also found in the neuronal nuclei of SAHA treated mice. Nuclear peripheralization of the heterochromatic domains has previously been reported in a number of studies following HDACi treatment. Relocation of pericentric heterochromatin at the nuclear periphery as well as an increase in size of the regions were observed in mammalian cells after TSA treatment (Taddei et al., 2001). Peripheralization of centromeric heterochromatin induced by TSA and sodium butyrate has also been demonstrated, in which a global histone hyperacetylation leading to chromatin decondensation was further characterized (Bartova et al., 2005). Remarkably, apart from reduced levels of HP1 proteins following HDAC inhibition, these studies illustrated an internal reposition of HP1 together with peripheral redistribution of centromeric clusters in the nucleus. These findings appear to

suggest an important role of histone under-acetylation within pericentromeric heterochromatin for their association with HP1 and their specialized nuclear compartmentalization. Specifically, this under-acetylated state may be crucial in centromere function and chromosomal segregation (Taddei et al., 2001, Bartova et al., 2005, Bartova et al., 2008). Although in the present study, no significant changes are observed regarding the levels of HP1 proteins and their nuclear distribution following VPA or SAHA treatment, which may be due to the differences in cell types, there is no doubt that HDAC inhibition may cause dynamic rearrangement of chromatin in parallel with changes in the patterns of epigenetic modifications. It may therefore be postulated that the ultrastructural organization of the nucleus is driven by the cellular state of gene expression.

Further evidence for the reorganization of PNH following transcriptional activation by HDACi is revealed by immunolocalization of MeCP2, another characteristic epigenetic marker of PNH. A dramatic redistribution of MeCP2 is induced by VPA and SAHA. Instead of clear perinucleolar foci as observed in saline treated mice, prominent nucleoplasmic staining in addition to larger perinucleolar foci are found (Fig 3.19 and 3.20). This may implicate a reorganization of the chromatin domains resulting in a switch in the transcriptional state of MeCP2 from inactive to active. Interestingly, despite the significant nucleoplasmic redistribution of MeCP2, ATRX immunofluorescence reveals no such changes in nuclear distribution after HDACi treatment. VPA has no effect on ATRX immunolocalization whereas SAHA induces nucleoplasmic microfoci away from the nucleoli (Fig 3.22). ATRX is a chromatin remodeling protein which characteristically binds to MeCP2. The

differences in MeCP2 and ATRX redistribution following both VPA and SAHA treatment indicate that there may be dissociation between MeCP2 and ATRX upon transcriptional activation by HDACi. The absence of ATRX redistribution in VPA treated mice and its nuclear rearrangement in SAHA treated mice may again demonstrate their differences in HDAC selectivities.

The intriguing findings in MeCP2 are very important since mutations in the gene encoding MeCP2 cause the progressive neurodevelopmental disorder Rett syndrome (RTT), an autism-spectrum disorder characterized by a range of neurobehavioral abnormalities and neurological dysfunction (Chahrour et al., 2008). A growing body of evidence has recently challenged the predominant 'enzymatic' model of MeCP2 function and hypothesizes a multifunctional nature of MeCP2. Studies with MeCP2 mouse models reported that MeCP2 is involved in the regulation of many different genes in the hypothalamus, and surprisingly up to 85% of genes are activated by MeCP2. Together with its association with the major transcriptional activator CREB1, MeCP2 is postulated as both an activator and a repressor of transcription (Chahrour et al., 2008). Further evidence is revealed by integrated epigenomic analyses of neuronal MeCP2, in which 63% of MeCP2-bound promoters are actively expressed whereas only 6% are highly methylated (Yasui et al., 2007). Taken together these suggest that the primary function of MeCP2 extends beyond transcriptional repression, with a more predominant role in the modulation of active genes (Lasalle and Yasui, 2009). The understanding of MeCP2 function and how it regulates target genes would be crucial towards the elucidation of the molecular basis of RTT and the development of therapeutic treatments. In the future, it would be fascinating to study the organization of chromatin

domains in the neuronal nuclei of MeCP2 knock-out mice, such that the effect of the absence of MeCP2 on nuclear organization and the distribution of various epigenetic modifications could be explored.

The differential phosphorylation of MeCP2 in response to changes in the state of neuronal activity is a mechanism employed by MeCP2 in the modulation of gene expression (Chao and Zoghbi, 2009). In resting neurons, MeCP2 is predominately phosphorylated at serine 80 and dephosphorylated at serine 421, in which S80 phosphorylation promotes binding of MeCP2 to promoters and thus reduces gene transcription. On the contrary in active neurons, MeCP2 is dephosphorylated at S80 but phosphorylated at S421 which results in the release of MeCP2 from promoters and thus gene transcription (Zhou et al., 2006) (Fig 1.10). Taken into account of the antagonistic roles played by S80 and S421, it would be expected to see S80 dephosphorylation and S421 phosphorylation following transcriptional activation induced by HDACi. In the present study however, phospho-MeCP2-pS80 immunofluorescence staining is increased after HDAC inhibition by both VPA and SAHA. Moreover, similar reorganization and increased staining of phospho-MeCP2-pS80 and pS421 are observed following VPA treatment (Fig 3.21).

In this study, both MeCP2 and H3K9M3 are established markers of the PNH, in which reorganization following HDACi-induced transcriptional activation is clearly demonstrated. This has further implied the association between the ultrastructural organization of the neuronal nucleus, specifically the PNH, and the cellular state of functional transcriptional activity.

4.3.3 Cajal Bodies

In addition to nuclear redistribution of the PNH, the CBs also appear to be dramatically reorganized following both VPA and SAHA treatment, with an overall increase in size and number of p80 coilin and Nopp140 immunostained foci in the nuclei. Moreover, SAHA treatment induces p80 coilin stained nuclear foci and microfoci away from the nucleoli within the nucleoplasm (Fig 3.25). Very little is known about the organization and distribution of CBs following HDACi treatment except a few studies on the SMN protein, which mediates the assembly of snRNPs, the crucial components for pre-mRNA splicing. Mutations in SMN, leading to insufficient levels of the protein, cause the autosomal-recessive motor neuron disease spinal muscular atrophy (SMA) (Avila et al., 2007). HDACi such as VPA, SAHA and sodium butyrate have been illustrated to stimulate an increase in SMN protein, in which VPA also demonstrated a dose-responsive elevation in the number of gems, indicating the increased SMN protein levels (Mattis et al., 2006). Another study in a mouse model of SMA reported that single intraperitoneal doses of TSA resulted in modest increases in SMN expression, in addition to increased levels of H3 and H4 acetylation (Avila et al., 2007). Repeated daily doses of TSA further demonstrated attenuated weight loss, improved survival and motor behavior. These show that the hydroxamic acid TSA increases SMN expression *in vivo* and may ameliorate the disease phenotype when delivered after disease onset (Avila et al., 2007).

4.3.4 Association between Ultrastructural Nuclear Organization and Transcriptional Activity

The effects of HDACi treatments on both the PNH and CBs appear to implicate transcriptional interference in the reorganization of the nuclear structure. Such changes in the balance of cellular transcriptional activity have been studied further with Actinomycin D (Act D) treatment which inhibits transcription. Changes in the patterns of nuclear distribution of both markers of PNH and CBs are detected in the neuronal nuclei of mice following Act D treatment. In contrast with nuclear peripheralization induced by HDACi which activate transcription, transcriptional inhibition by Act D results in centralized redistribution of the PNH marker protein H3K9M3 as well as the formation of distinct nucleolar caps with the CBs marker Nopp140 (data not shown, see chapter 2.2.3 *Actinomycin D). These intriguing findings are consistent with previous studies in HeLa cells which demonstrated the segregation of nucleolar components during Act D-induced transcriptional inhibition, with the formation of nucleolar caps accompanied by heterochromatic domain surrounding the segregated nucleolus (Shav-Tal et al., 2005). It has been further illustrated that nucleolar segregation and capping are energy-dependent and concerted process, which involve dynamic nuclear spatial reshuffling and formation of specific domains in response to stress conditions such as transcriptional arrest (Shav-Tal et al., 2005). The formation of Nopp140-stained perinucleolar caps following Act D treatment is also reported in Shav-Tal's study and such nucleolar capping has been observed in a variety of studies following drug administration that leads to transcriptional shut down (Dousset et al., 2000, Andersen et al., 2002). Reduction in RNA

transcription may result in an excess pool of free posttranscriptional factors which accumulate and cause the observed clustering of perinucleolar proteins (Shav-Tal et al., 2005). These provide additional support for the theory that nuclear organization is driven by the cellular state of gene expression.

4.4 Neuronal Nuclear Rearrangement in Neurodegenerative Disease Models

Dynamic changes in the nuclear distribution of epigenetic modifications as well as the organization of the perinucleolar structures, including the PNH and CBs, are demonstrated in the striatal neurons upon HDACi treatment which are the potential therapeutics of neurodegenerative diseases. Remarkably, dramatic rearrangement of the neuronal nucleus is also found in neurodegenerative disease models of Huntington's disease (HD), ALS/FTLD and FTDP-17. Disorganization of the perinucleolar complex is further illustrated in these transgenic mice.

4.4.1 Reorganization of the Perinucleolar Heterochromatin

A growing body of evidence has illustrated a linkage between changes in DNA methylation as well as histone modifications and progression of HD (Urdinguio et al., 2009). Heterochromatic foci comprised of condensed DNA are readily stained with DAPI and therefore staining with DAPI may indirectly reflect the pattern of DNA methylation. In the striatal neuronal nuclei of R6/2 transgenic mice, a significantly increased proportion of heterochromatin (6%

increase in area) compared with that in the wild type mice (Fig 3.26) might indicate an increased level of DNA methylation and hence gene silencing, a potential pathogenic mechanism suggested in HD. Various studies in HD patients and disease models have provided further support by demonstrating altered patterns of histone modifications associated with increased silencing of chromatin. These include a decreased level of histones H3 and H4 acetylation and increased H3K9 methylation (Steffan et al., 2000, Ryu et al., 2006, Stack et al., 2007). In addition to the overall increase in heterochromatin, a significantly higher proportion of PNH (7% increase in area) is found in the R6/2 mice compared with that in the wild type mice. This is in agreement with previous HD studies reporting an increase in the specific PNH marker H3K9M3 (Stack et al., 2007). In order to verify the association between the increase in DNA compaction and increase in the level of DNA methylation, immunocytochemical analysis with the antibody against methyl cytosine may be carried out in the future to directly visualize the distribution of methylated DNA in the neuronal nucleus.

Recently, studies in the fission yeast *S. Pombe* have proposed that transient transcriptional derepression may lead to functional reorganization of the nucleus involving post-transcriptional regulation by RNA interference, such that heterochromatin may remain in silence (Grewal and Jia, 2007, Eymery et al., 2009, Grewal and Elgin, 2007, Cam et al., 2009). This together with the high level of transcription found specifically within the PNH in the neuronal nuclei of wild type mice may suggest that in these R6/2 mice, an increased transcriptional activity in the PNH results in the maintenance of silencing of some particular genes. It would be fascinating to study and compare the

transcriptional activity in this specific perinucleolar heterochromatic domain with other regions of the chromatin in the R6/2 mice using the *in vivo* transcription run-on assay developed in the present study. Interestingly, a recent study of gene expression profiles in the R6/2 mice revealed differential upregulation of genes which might be associated with the onset and progression of HD (Tang et al., 2011).

Apart from the R6/2 mice, TDP-43^{M337V} and Tau^{P301S} transgenic mice, mouse models of ALS/FTLD and FTDP-17 respectively, have further implicated the reorganization of the PNH in neurodegeneration. Consistent with the increased proportion of PNH found in the R6/2 mice, immunofluorescence of the PNH marker H3K9M3 reveals pronounced increase in the size of perinucleolar foci together with extra nucleoplasmic foci in R6/2, TDP-43 and Tau transgenic mice. Interestingly, ICC studies with another marker of PNH, MeCP2, reveal differential reorganization which varies among the three neurodegenerative disease models. In the neuronal nuclei of R6/2 mice, MeCP2 immunofluorescence demonstrates a dramatic increase in both the size and number of foci (Fig 3.27D), whereas in the Tau transgenic mice, no increase in the size of MeCP2-stained foci is found despite the presence of additional nuclear foci towards the periphery (Fig 3.29D). MeCP2 in the nuclei of TDP-43 transgenic mice is reorganized into numerous microfoci distributed throughout the nucleoplasm (Fig 3.29C). These novel nuclear structures in the TDP-43 transgenic mice would be further discussed in the following section. The observed differences in the nuclear rearrangement of MeCP2 in these disease models may be due to the intriguing multifunctional nature of MeCP2 and its specific involvement in the

different disease mechanisms.

4.4.2 Reorganization of the Cajal Bodies

Nuclear rearrangement of the PNH is accompanied by reorganization of the perinucleolar rosettes of CBs in the striatal neuronal nuclei of both TDP-43 and Tau transgenic mice. The size and number of CB marker p80 coilin stained foci are significantly increased which occupy a much larger volume of the nucleoplasm. In addition to the typical perinucleolar foci, p80 coilin immunofluorescence reveals prominent nucleoplasmic foci away from the nucleoli (Fig 3.30). The increase in the proportion of free nucleoplasmic CBs together with a decrease in the proportion of nucleolus-associated CBs have been observed previously in the striatal neuronal nuclei of R6/2 mice (E. Slavik-Smith, unpublished data). Surprisingly, many of the CBs containing the proteins such as p80 coilin, SMN and Nopp140 which have lost their association with the nucleolus are found to be associated with the neuronal intranuclear inclusions (NIIs) (data not shown). The presence of NIIs in HD transgenic mice and human post-mortem brains, as well as in other CAG repeat diseases has been well documented (Davies et al., 1997, Yamada et al., 2001). The observation of CBs in close contact with NIIs was also reported in human brains of dentatorubral-pallidoluysian atrophy and Machado-Joseph disease. There is a possibility that these NII-CBs could be associated with specific genes and the interaction between NIIs and CBs may also play a role in the pathogenesis of these diseases (Platani et al., 2000, Yamada et al., 2001).

The rearrangement of the CBs and the dissociation from the nucleolus may indicate a reduced transport of the basic constituents of the pre-rRNA processing machinery into the nucleolus. This may reflect an overall decrease in the cytoplasmic needs for ribosome biogenesis and hence protein synthesis, or transcriptional dysregulation under disease conditions. This could be further coupled with the dramatic increase in the perinucleolar heterochromatic domain demonstrated in various disease models in order to maintain silencing of some particular genes.

Very little has been explored on the behavior of CBs in neurodegenerative diseases at present, apart from SMA in which reduced SMN protein levels result in changes in the organization of CBs and the associated gems containing SMN. Recently, a study in the Purkinje cell (PC) degeneration (*pcd*) mice, mouse models of the human inherited spinocerebellar ataxias (SCA), has shed new light on the organization of the nucleolus and CBs in neurodegeneration (Baltanas et al., 2011). DNA damage-induced PC degeneration was found to disrupt the structure and function of the nucleolus, with inhibition of rRNA synthesis and the biogenesis of ribosomes. This was accompanied by reorganization and reduction in the number of CBs, and the overall disassembly of the protein synthesis machinery might eventually result in neuronal cell death (Baltanas et al., 2011). Apart from nuclear redistribution of the CB marker coilin, irregularly shaped CBs were found in the PCs in these *pcd* mice. These suggest that disruption of both the nucleolus and CBs are nuclear hallmarks of neurodegeneration in PCs.

Another study in transgenic mice expressing human TDP-43 in neurons

has recently reported an altered distribution of the CBs in which the increased level of TDP-43 caused a disruption in the normal nuclear distribution of SMN-associated Gemini of coiled bodies (GEMs) in motor neurons (Shan et al., 2010). ICC analysis using SMN antibody revealed a significant increase in the number of GEMs in the transgene-expressing motor neurons. However, instead of losing association with the nucleolus, these SMN stained foci were present diffusely within the nucleolus (Shan et al., 2010). In addition, it was also demonstrated that SMN-containing GEMs failed to form in the neuronal nuclei of TDP-43 knockout mice. These appear to implicate the critical role of TDP-43 in RNA processing and the pathways that control RNA splicing (Shan et al., 2010). Nevertheless, these studies have never included p80 coilin or Nopp140 and hence unable to give a comprehensive overview of the distribution of all CBs within the nucleus. The dramatic redistribution of both p80 coilin and Nopp140 demonstrated in the present study is therefore very interesting and provocative, which needs to be further explored.

4.4.3 Disorganization of the Neuronal Nucleolar Complex

In this study, an ultrastructural nuclear reorganization of the chromatin, particularly the PNH and CBs, has been illustrated in the neurodegenerative disease models of HD, ALS/FTLD and FTDP-17. Interestingly, an emerging literature has suggested that an elevated expression of certain transposable elements, such as SINEs, may be correlated with a number of neurodegenerative diseases (Li et al., 2012). These elements, which are normally active in the brain, have been demonstrated to associate with TDP-43. However in FTLD patients and TDP-43 disease models, such

association was reduced and a large fraction of these elements became de-repressed (Li et al., 2012). This might indicate mis-regulation of SINEs and a potential increase in expression, which could be reflected by the increased PNH observed in the disease models in the present study. Regarding the postulated functional significance of the unique neuronal nucleolar complex (chapter 4.2.3), disorganization of the integrated perinucleolar structures found in these transgenic mice may imply dysregulation of transcription, post-transcriptional RNA processing and splicing, which leads to imbalances in gene expression. Indeed, transcriptional dysregulation and perturbation in RNA metabolism are increasingly being recognized as the key players in the pathogenic mechanisms of a variety of neurodegenerative diseases.

4.5 Bipartite Pathological Mechanism in TDP-43^{M337V} Transgenic Mice

The new transgenic mouse line expressing human mutant TDP-43M337V develops a marked neurological phenotype by 3 months of age (V. Schaeffer, unpublished data). This phenotype persisted throughout the lifespan of these transgenic mice, which express 2.2× the level of TDP-43 found in the wild type, albeit with a sub-cellular redistribution from the nucleus to the cytoplasm. Prominent pathological features in both the nucleus and the cytoplasm are identified in these novel mouse models of ALS/FTLD, suggesting a bipartite pathological mechanism. The cellular process observed for the extrusion of aberrantly truncated, phosphorylated and aggregated TDP-43 from the nucleus through the cytoplasm and eventually out of the neuron might further

implicate a novel mechanism for the extracellular spread of transmissible proteinopathies.

4.5.1 Nuclear Pathology

Within the CNS, one of the most striking ultrastructural pathological changes is the appearance of multiple small punctate foci in the neuronal nucleus. These novel nuclear bodies appear to be colocalized with the RNA-binding proteins muscleblind-like 1 (MBNL-1) and MeCP2 (Fig 3.31A-B and 3.32). Muscleblind proteins are important in the regulation of alternative splicing of pre-mRNAs Recently, the multifunctional nature of MeCP2 has also implicated its role in mRNA splicing (Long et al., 2011). In humans, MBNL1 proteins are crucial in diseases caused by microsatellite expansions, especially in myotonic dystrophy (DM). A key pathogenic mechanism of DM is associated with splicing misregulation due to depletion of MBNL1 activity through sequestration (Fernandez-Costa et al., 2011). DM is originated by the expansion of RNA repeats in which the expanded CUG or CCUG repeats form nuclear RNA foci and sequester MBNL1. As a result, depletion of the splicing factor MBNL1 may lead to disruption of the normal splicing pattern and contribute to DM pathogenesis (Ho et al., 2004). Various studies have further reported MBNL1 relevance in other neurological disorders caused by trinucleotide expansion. For instance, RNA foci which colocalize with MBNL1 were identified in neurons in Huntington's disease-like 2 (HDL2) cortex and in brains from spinocerebellar ataxia type 8 (SCA8) patients (Fernandez-Costa et al., 2011). Intranuclear RNA inclusions found in fragile X-associated tremor ataxia syndrome (FXTAS) caused by an expansion of CGG repeats were also

demonstrated to recruit MBNL1. These may suggest a mutant repeat RNA toxic gain-of-function mechanism of pathogenesis (Wojciechowska and Krzyzosiak, 2011).

The appearance of nuclear micro-foci associated with MBNL1 observed in the TDP-43 transgenic mice might similarly indicate splicing dysregulation. This would be consistent with the significant changes in nuclear distribution of CBs, which are associated with the cellular splicing activities. Moreover, rearrangement of both the PNH and CBs may suggest dysregulation of transcription and splicing, which are both regulated by TDP-43. Thus, loss of TDP-43 nuclear function could also be the underlying disease mechanism in these transgenic mice.

4.5.2 Cytoplasmic Vacuolation

In addition to the profound ultrastructural changes in the nucleus, striking pathological features within the cytoplasm are also observed in the TDP-43 transgenic mice. TEM analyses reveal numerous double membrane enclosed vacuoles throughout the cytoplasm containing pale, flocculent material. Remarkably, these vacuoles appear to colocalize with TDP-43 immunostained cytoplasmic foci (Fig 3.34). ICC studies further illustrate the colocalization of these cytoplasmic vacuoles with phosphorylated, ubiquitinated and C-terminal truncated TDP-43, accompanied by a dramatic TDP-43 redistribution from the nucleus to the cytoplasm (Fig 3.35). The accumulation of TDP-43 into cytoplasmic aggregates has been identified not only in ALS and FTLD, but also in many other neurodegenerative diseases such as Parkinson’s disease,

Alzheimer's disease and Huntington's diseases (Sreedharan et al., 2008, Neumann, 2009, Sephton et al., 2010). In many of these diseases, TDP-43 cytoplasmic redistribution and aggregation are accompanied by phosphorylation, ubiquitination and the C-terminal truncation of TDP-43 (Igaz et al., 2009, Neumann, 2009). A recent study in cultured cell models demonstrated *in vitro* aggregation and fibrillization of human mutant TDP-43, in which intracellular seeding appeared to reproduce some prominent features of TDP-43 inclusions observed in patients (Furukawa et al., 2011). Although cytoplasmic aggregation of mutant TDP-43 has been reported in yeast, C. elegans, drosophila, mice and HeLa cells (Johnson et al., 2008a, Liachko et al., 2010, Xu et al., 2011, Che et al., 2011), cytoplasmic TDP-43 sequestered in double membrane enclosed vacuoles illustrated in the present study has never been found previously.

4.5.3 Nuclear Origin and Nuclear Contents of Vacuoles

Surprisingly, TEM analyses reveal that the double membrane enclosed vacuoles are derived by a process of budding-off from the outer nuclear membrane (Fig 3.39), which then migrate towards the plasma membrane before fusing and releasing their contents into the extracellular space (Fig 3.41). Although the autophagic nature is supported by the colocalization of LC3 immunostaining as well as the upregulation of LC3-II (data not shown), these autophagosomes do not appear to fuse with either lysosomes or multivesicular bodies. No interaction is found between the autophagosomes and the autophagic markers including lysosome-associated membrane protein 2 (LAMP2), sequestesome 1 (SQSTM1), valosin containing protein (VCP) and

charged multivesicular body protein 2B (CHMP2B), indicating the lack of association with autophagic processing apart from LC3 (data not shown). Further ICC analysis with the specific outer nuclear membrane protein nesprin may be carried out in the future to verify the nuclear origin of the autophagosomes.

The process of formation of an autophagosome from the nuclear membrane has previously been described in skeletal and cardiac muscles from mutant mouse models of Emery-Dreifuss muscular dystrophy (EDMD) and termed nucleophagy, an autophagic process in which parts of the nucleus are specifically degraded (Ozawa et al., 2006, Mijaljica et al., 2010). Nucleophagy has been described in yeast and recent studies provide further evidence for autophagic degradation of nuclear components in mammalian cells in nuclear envelopathies caused by mutations in the genes encoding A-type lamins (LMNA) and emerin (EMD) (Mijaljica et al., 2010, Park et al., 2009). However in EDMD, autophagosomes containing emerin fuse with lysosomes and multivesicular bodies followed by autophagic processing of their contents, with no evidence for the extracellular release of their contents as described in the TDP-43 transgenic mice in the present study.

A more recent study in drosophila larval muscle cells demonstrated that nuclear envelope budding may act as an endogenous nuclear export pathway for large ribonucleoprotein particles (RNPs), and these RNP granules exit the nucleus by budding through the inner and outer nuclear membranes in a mechanism similar to that of herpes viruses following neuronal infection (Speese et al., 2012). Remarkably, in the TDP-43 transgenic mice, both RNA

and a highly select group of nuclear proteins are found within the cytoplasmic vacuoles including SF2/ASF, 9G8, FUS/TLS and $p54^{nrb}$ in addition to TDP-43 (Fig 3.40). These nuclear proteins are all specific RNA-binding proteins (RBPs) in which SF2/ASF and 9G8 are splicing factors, $p54^{nrb}$ is a marker of paraspeckle, FUS/TLS is another ALS disease protein and a homolog to TDP-43. Mutations in FUS/TLS have been discovered in ALS and together with TDP-43, both RBPs are recognized as the major components of cytoplasmic inclusions in ALS as well as FTLD-U (Kwiatkowski et al., 2009). Studies have further identified prion-like domains in these proteins (Gitler and Shorter, 2011) which appear to be at the opposite end of the protein molecule to the nuclear localization signal. Proteolytic cleavage of these proteins may therefore result in cytoplasmic localization and aggregation of the truncated fragments containing the prion-like domains (Fig 4.4). Moreover, TDP-43 has recently been illustrated to bind to FUS/TLS and such binding was enhanced by TDP-43 mutations due to the increased stability of mutant TDP-43 (Ling et al., 2010). Interestingly, the study has also identified TDP-43 complexes with Drosha and ADARs, suggesting that TDP-43 may be involved in both mRNA and microRNA processing (Ling et al., 2010). This might further implicate microRNA dysregulation as another pathogenic mechanism for TDP-43.

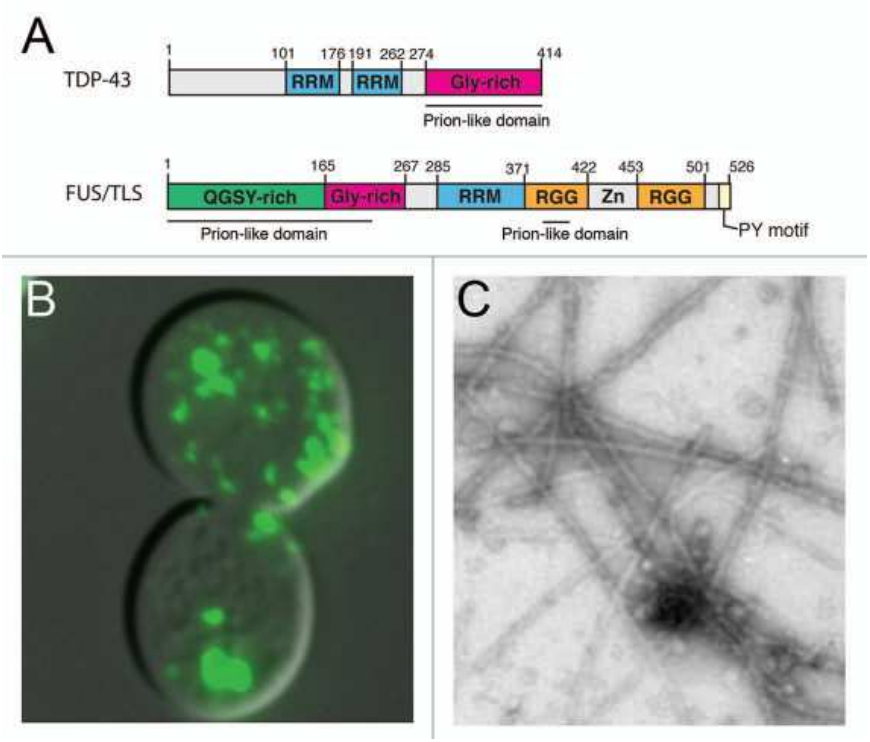

Figure 4.4

Cytoplasmic aggregation of TDP-43 and FUS/TLS which contain prion-like domains

A) Domain architecture of TDP-43 and FUS/TLS. Both ALS disease proteins contain prion-like domains in addition to RNA-recognition motifs (RRMs) and glycine-rich regions (Gly-rich). B) Cytoplasmic aggregation of TDP-43 and FUS/TLS. A yeast cell expressing a FUS-YFP fusion protein is shown. C) *in vitro* filamentous aggregation of FUS (1-422). (Adapted from Gitler and Shorter, 2011)

A central role for RBPs and RNA metabolism has become increasingly recognized in ALS and FTLD-U. In addition to FUS/TLS, two other proteins Ewing sarcoma break point region 1 (EWSR1) and TATA-binding protein-associated factor 15 (TAF15), which constitute the FET protein family, have recently been identified to cause ALS (Couthouis et al., 2011, Couthouis et al., 2012). Studies in yeast demonstrate that TDP-43 together with the FET protein family are prominent members of a select group of RBPs with prion-like properties, which harbor a RNA recognition motif (RRM) and a putative prion domain (Alberti et al., 2009, Toombs et al., 2010, King et al.,

2012) (Fig 4.5). An algorithm has been designed to detect prion domains and by using this algorithm, 29 RRM-bearing proteins with a prion domain are identified in the human genome (King et al., 2012). Startlingly, an increasing number of these RRM-bearing prion candidates have been associated with the pathology of various neurodegenerative diseases including ALS, FTLD-U, Alzheimer's disease and Huntington's disease. It is postulated that the unique pairing of RRM binding domains and prion-like domains is the important element for the high propensity of aggregation formation, and such prion-like mechanism of disease propagation has been theorized in many neurodegenerative diseases (Prusiner, 2012).

The FET family of proteins are ranked as the top 3 RNA-binding prion candidates, and TDP-43 is ranked 10th (King et al., 2012). Remarkably, ICC studies reveal both EWSR1 and TAF15 as cytoplasmic aggregates in the TDP-43 transgenic mice (Fig 4.6), which further illustrate colocalization of TDP-43 and EWSR1 cytoplasmic aggregates in the striatal neurons of these mice (Fig 4.7). This strongly implicates the four RBPs with prion-like domains (TDP-43, FUS/TLS, EWSR1 and TAF15) in the pathogenesis of ALS and FTLD-U.

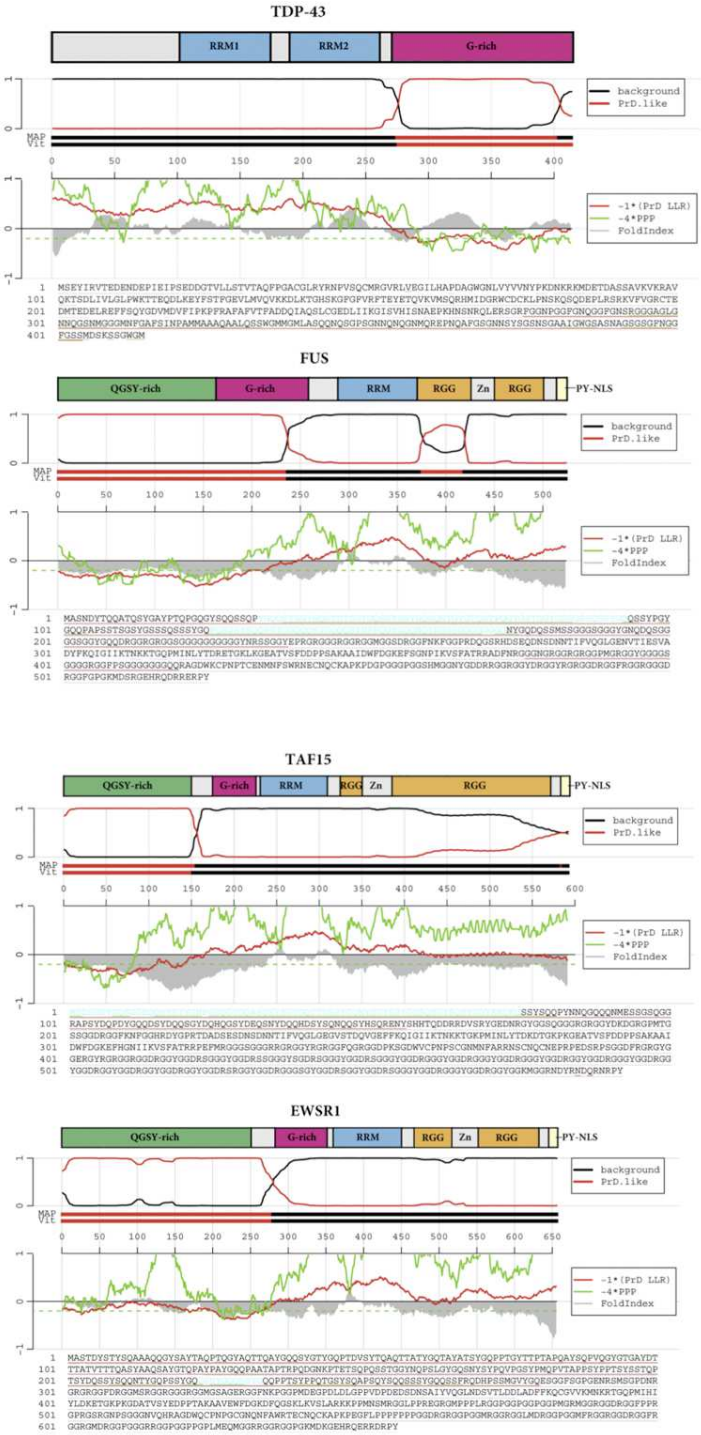

Figure 4.5

Schematic view of the domain architecture, prion propensities and sequences of TDP-43, FUS/TLS, EWSR1 and TAF15 proteins

The domain construct of each protein is illustrated in which all four proteins contain at least 1 RRM domain and a G-rich (prion-like) domain. The prion propensities predicted by different algorithms are depicted in the plots below the domain architecture. The sequence of each protein is demonstrated at the bottom. (Adapted from King et al., 2012)

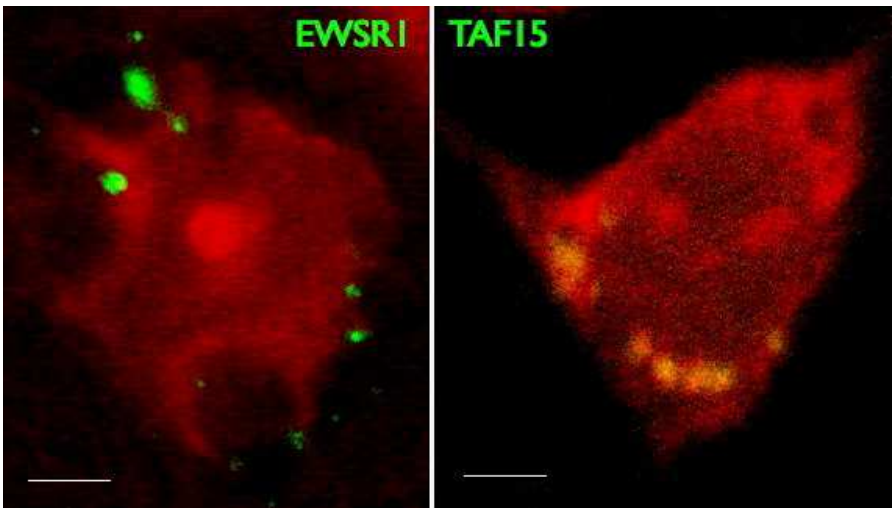

Figure 4.6

Immunofluorescence of EWSR1 and TAF15 (green) identify cytoplasmic aggregates in the striatal neurons of a 6-month-old TDP-43 transgenic mouse. Pyronin Y (red) recognizes the nucleoli and the cytoplasm. Scale bars = 5μm

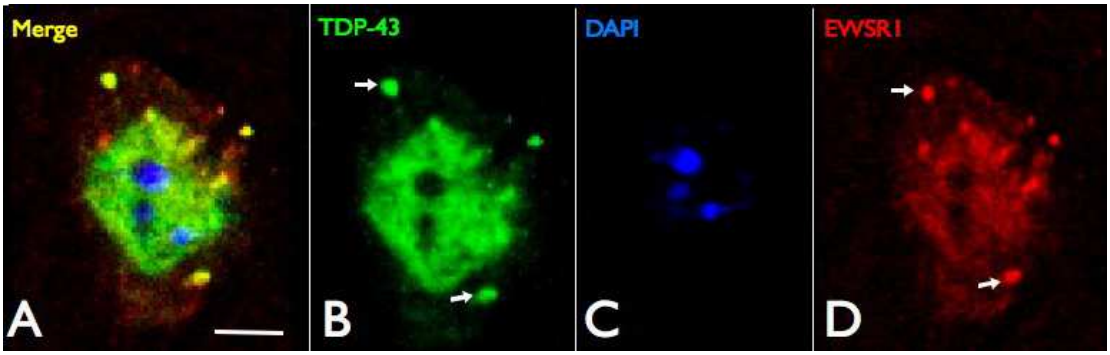

Figure 4.7

Colocalization of TDP-43 with EWSR1 in the striatal neuronal cytoplasm

Triple labeling with TDP-43 (green, B), EWSR1 (red, D) and DAPI (blue, C) reveals colocalization of TDP-43 and EWSR1 in cytoplasmic aggregates as shown by the yellow aggregates in A).

Scale bars = 5μm

Taken together these results may suggest a potential mechanism for the formation of cytoplasmic aggregates in the TDP-43 transgenic mice. Mutant TDP-43 is redistributed from the nucleus to the cytoplasm in which the prion-like domain contained in the C-terminus induces aggregation of TDP-43,

and possibly also the FET protein family. RNA then recognizes and binds to the RRM domains of these proteins. Subsequently, RBPs such as SF2/ASF, 9G8 and p54^{nrb} bind to the RNA and together these form the ribonuclear protein complex (RNP) in the cytoplasm (Fig 4.8). It is important to realize that these RBPs are associated with nuclear speckles, paraspeckles and have predominant nuclear functions in RNA splicing. Therefore, the sequestration of these proteins in the cytoplasm may result in splicing dysregulation and perturbation in RNA metabolism. Interestingly, the newly discovered repeat expansion in the C9orf72 gene, which is currently the most common genetic cause of both ALS and FTLD, also similarly indicates sequestration of RBPs in pathological RNA foci leading to disruption of RNA processing (DeJesus-Hernandez et al., 2011, Renton et al., 2011).

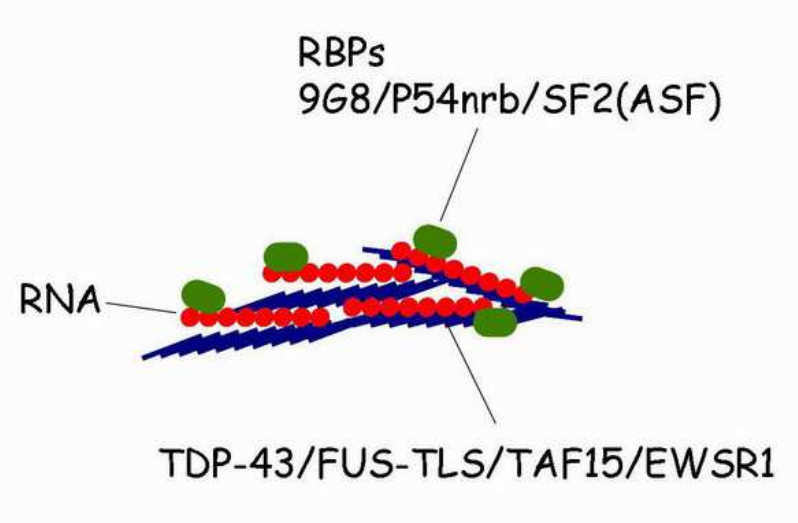

Figure 4.8

Schematic diagram depicting the proposed mechanism of the formation of cytoplasmic aggregates

Proteins comprising both RRM binding domains and prion-like domains aggregate in the cytoplasm via their prion-like domain (blue). RNA (red) binds to the RRM domains of these proteins. Subsequently, RNA-binding proteins (green) recognize and bind to the RNA. These together form the ribonuclear protein complex (RNP) in the cytoplasm.

4.5.4 Novel Mechanism for the Extracellular Spread of Transmissible Proteinopathies

The fusion of cytoplasmic vacuoles with the plasma membrane appears to recruit both microglial cells and astrocytes and stimulate engulfment of cellular debris by these cells (Fig 3.41, 3.42, 3.43). Throughout the tissue there are also degenerating neurons undergoing dark cell degeneration (Fig 3.45). Whether these are neurons which have lost much of their cytoplasmic volume via extrusion of vacuoles, or are degenerating because they fail to dispose the toxic aggregates, remains elusive. Nevertheless, the extracellular release of vacuolar contents into the extracellular space suggests an unconventional egress mechanism by exophagy, which has recently been illustrated in yeast. A number of studies reported a previously unknown secretion route taken by the yeast acyl-coenzymes A-binding protein. This protein is sequestered into autophagic vesicles which are re-routed to the plasma membrane where these vesicles fuse with the plasma membrane and release their contents (Abrahamsen and Stenmark, 2010, Duran et al., 2010).

The fusion of the vacuoles with the adjacent neurons observed in the TDP-43 transgenic mice has provided robust evidence for the extracellular spreading of protein aggregates (Fig 3.44). Remarkably, TDP-43 immunofluorescence reveals further support in which extracellular aggregates of TDP-43 in addition to cytoplasmic aggregates are found in both the striatum and the dentate granule cell layer of the dentate gyrus (Fig 4.9). Preliminary studies also identify these aggregates in the hippocampal CA1 and CA3 areas as well as the frontal cortex. This indicates the extracellular spreading of

TDP-43 aggregates within the brain of the transgenic mice.

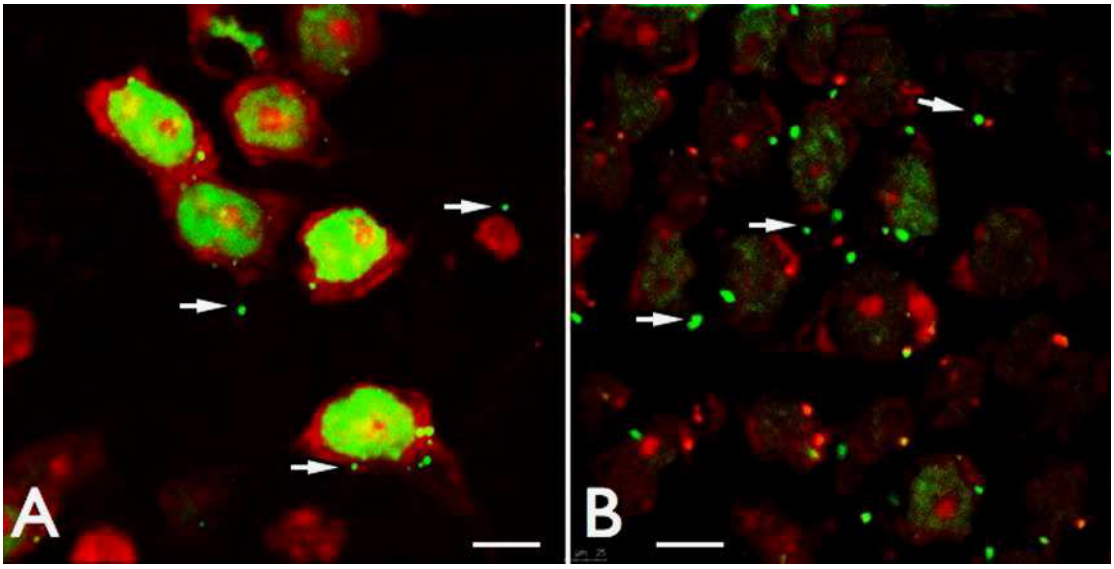

Figure 4.9

Extracellular spreading of TDP-43 aggregates

TDP-43 immunofluorescence (green) reveals extracellular aggregates (white arrows) in addition to cytoplasmic aggregates in both the striatum (A) and the dentate granule cell layer of the dentate gyrus (B). Pyronin Y (red) recognizes the nucleoli and the cytoplasm. Scale bars = 10μm

These results therefore suggest that selected features of both nucleophagy and exophagy are exhibited in the TDP-43 transgenic mice and this might provide a novel mechanism for the extracellular spread of protein aggregates in transmissible proteinopathies (Fig 4.10). The twin nuclear and cytoplasmic pathologies also appear to link both RBPs/RNA splicing together with autophagic processes. Furthermore, a prion-like transfer mechanism involving RBPs with putative prion domains might underlie the emanation of neurodegenerative pathology from one cell to another throughout the CNS (King et al., 2012). Such hypothesis of common prion-like mechanism of seeding, aggregation and potential transmissibility involving aggregates such

as tau, amyloid-β, huntingtin and α-synuclein has emerged from recent studies in various neurodegenerative diseases, including Alzheimer's disease, Huntington's disease, Parkinson's disease and FTLD (Frost and Diamond, 2010) (chapter 1.5.4.2).

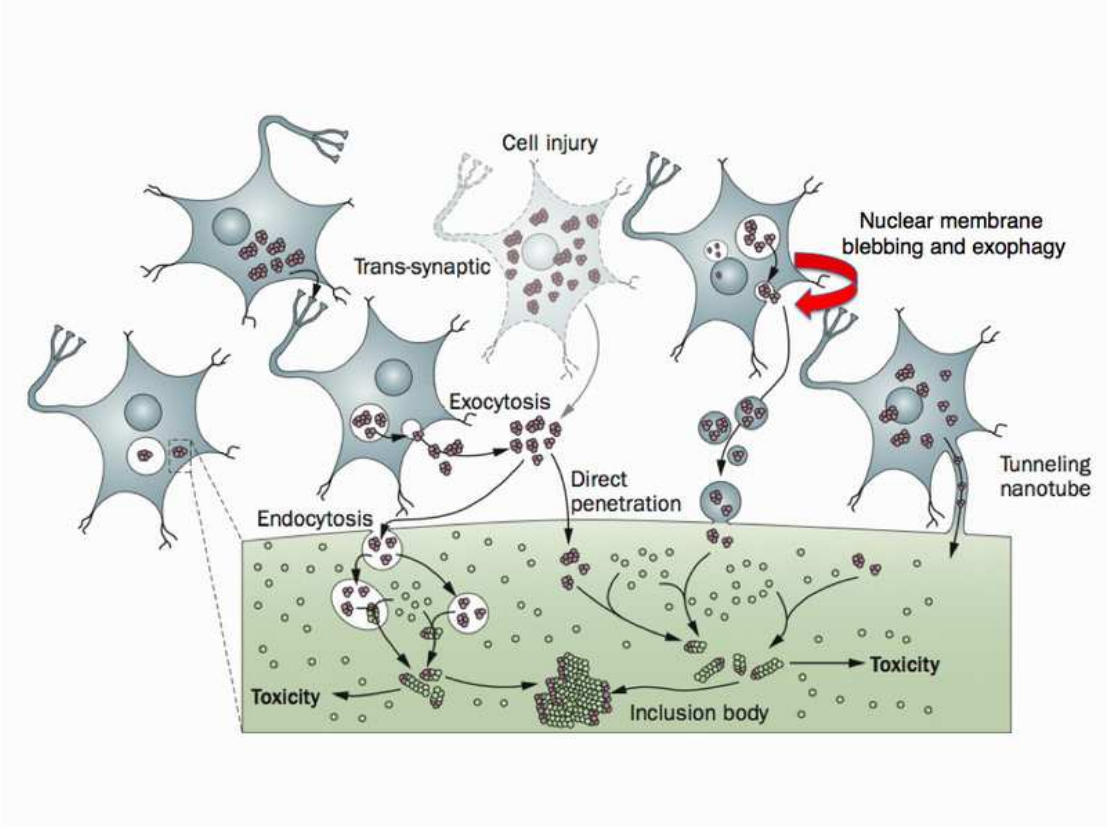

Figure 4.10

Mechanisms of cell-to-cell transmission of protein aggregates

Protein aggregates might be released from neurons and internalized into neighboring neurons via different mechanisms. Internalized aggregates could act as seeds and induce further aggregation leading to the formation of pathological inclusions. In the present study, a novel mechanism involving nuclear membrane blebbing and exophagy (red bended arrow) is implicated for the extracellular spread of protein aggregates in the TDP-43^{M337V} transgenic mice. (Adapted from Lee et al., 2010)

4.6 Conclusions

The neuronal nucleus is highly specialized with a unique and characteristic organization of the genome, transcription and epigenetic regulation. Little information is available on its chromatin organization as most studies have focused on cells which are rapidly growing and dividing. This study has investigated the ultrastructural and molecular organization of the mouse striatal neuronal nucleus and to correlate this with the distribution of a range of epigenetic modifications. The relationship of the structural organization to a functional assay of *in vivo* transcription detecting nascent RNA together with the localization of RNA pol I, II and III have been explored. These studies provide strikingly different results to the literature, including a unique pattern of RNA transcription within the neuronal nucleus, and the oxymoron of transcriptionally active heterochromatin. Moreover, a novel mechanistic theory of the unique neuronal nucleolar complex has been postulated based on the transcription, processing and maturation of RNA pol III transcribed ncRNAs.

Surprisingly, this highly specialized neuronal nuclear arrangement appears to be dynamic, as changes in the patterns of epigenetic modifications as well as reorganization of the perinucleolar structures including the PNH and CBs are induced by two clinically used HDACi (VPA and SAHA) which activate transcription. Dramatic rearrangement of the neuronal nucleus is also found in several neurodegenerative disease models, which further illustrate disruption of the perinucleolar complex. Remarkably, these results implicate the unique neuronal nucleolar complex as the focus for disorganization upon HDACi treatment and in neurodegenerative diseases. In addition, the bipartite

pathological mechanism in both the nucleus and cytoplasm of the novel TDP-43^{M337V} transgenic mouse models of ALS/FTLD appears to link both RBPs/RNA splicing with autophagic processes. The cellular process observed for the extrusion of TDP-43 aggregates out of the neuron might also implicate a novel mechanism for the extracellular spread of transmissible proteinopathies. Findings of this study together with recent literature further postulate that prion-like propagation involving RBPs with putative prion domains might underlie the emanation of neurodegenerative pathology from one cell to another throughout the CNS.

4.6.1 The Unique Neuronal Nuclear Organization

This thesis has determined the ultrastructural and molecular composition of the mouse striatal neuronal nucleus, including the characterization of the unique organization of the chromosomal domains, subnuclear bodies and epigenetic modifications (Fig 4.3). In addition, the patterns of RNA transcription detected by a novel *in vivo* transcription run on assay have been demonstrated in combination with the ultrastructural localization of RNA polymerases I, II and III. The relative rates of transcription within different subnuclear structures reveal surprising results as the highest rate of transcription is detected within the PNH, which is mediated by RNA pol III. This provides further evidence against the dogma that heterochromatin is transcriptionally silent (Yasuhara and Wakimoto, 2006). Taken together, it is postulated that the PNH, nucleolus and the intercalated CBs function as an integrated complex for the transcription, processing, editing and maturation of ncRNAs such as SINEs. RNA pol III mediated transcription taking place in the

PNH, post-transcriptional RNA processing and editing in the nucleolus, and finally maturation in the CBs. This neuronal nucleolar complex is believed to be highly developed and specialized in neurons.

These novel findings provide important insights into the organization of the mammalian neuronal nucleus, which exhibits a distinct structural and functional organization that has never been reported previously. The exciting findings may further implicate a novel mechanism for the establishment and maintenance of the post-mitotic nature of neurons. There is no doubt that these also provide fundamental basis for our understanding of the complex 3D spatial arrangement of transcription and post-transcriptional processing in the neuronal nucleus.

4.6.2 Epigenetic Regulation and Its Dynamics in the Neuronal Nucleus

Having established the ultrastructural and functional organization of the neuronal nucleus in terms of chromatin, transcription and epigenetic regulation, it is astonishing to realize that such unique and specialized organization is not static but dynamic. Changes in the patterns of epigenetic modifications as well as reorganization of the prominent perinucleolar structures, PNH and CBs, are induced upon treatments with the HDACi VPA and SAHA, which are the potential therapeutics of neurodegenerative diseases. The effects of HDACi treatments on these nuclear subdomains appear to implicate transcriptional interference in the reorganization of the neuronal nucleus, supporting the theory that nuclear organization is driven by the cellular state of gene expression. Remarkably, dramatic rearrangement of the neuronal nucleus is

also found in the R6/2, TDP-43^{M337V} and Tau^{P301S} transgenic mouse models of HD, ALS/FTLD and FTDP-17 respectively. ICC and TEM studies in these transgenic mice further demonstrate disruption of the perinucleolar bodies.

Recently, the critical role of HDACs in the epigenetic regulation of neuronal function has come into focus. Deciphering the molecular nature of the epigenetic mechanisms in the CNS may provide important insight into the development of novel therapeutics (Haggarty and Tsai, 2011). Taken together, these results implicate the unique neuronal nucleolar complex as the focus for disorganization following HDACi treatments as well as in neurodegenerative diseases. Regarding the postulated functional significance of the unique neuronal nucleolar complex (chapter 4.2.3), disorganization of these integrated perinucleolar structures may indicate dysregulation of transcription, post-transcriptional RNA processing and splicing, leading to imbalances in gene expression. It is noteworthy that transcriptional dysregulation and perturbation in the RNA metabolism are increasingly being recognized as the key players in the common pathogenic mechanisms of a variety of neurodegenerative diseases (Hanson et al., 2012).

4.6.3 Common Mechanisms of Pathogenesis in Neurodegenerative Diseases

The bipartite pathological mechanism in both the nucleus and cytoplasm of the novel TDP-43^{M337V} transgenic mice appears to link both RBPs/RNA splicing with autophagic processes. The cellular process observed for the extrusion of TDP-43 aggregates from the nucleus through the cytoplasm and

eventually out of the neuron might also implicate a novel mechanism, involving nuclear membrane blebbing and exophagy, for the extracellular spread of transmissible proteinopathies (Fig 4.10).

A growing body of evidence has suggested a role for perturbed RNA metabolism in neurodegenerative diseases. The importance of RBPs in RNA processing and their dysfunction in these diseases indicate that there may be common themes in RNA dysregulation such as deficits in pre-mRNA splicing (Hanson et al., 2012). Recently, an increasing number of RBPs with prion-like domains have been associated with the pathology of various neurodegenerative diseases which exhibit prion-like mechanism of disease propagation (Prusiner, 2012). Remarkably, ICC and TEM studies in the TDP-43^{M337V} transgenic mice reveal cytoplasmic aggregation of TDP-43 and the FET family of proteins (FUS/TLS, EWSR1, TAF15) in the striatal neurons, which are all RNA-binding prion candidates implicated in ALS (Couthouis et al., 2011, Couthouis et al., 2012). These findings may suggest a potential disease mechanism for the formation of cytoplasmic inclusions, in which pathogenic proteins containing both RRM binding domains and prion-like domains aggregate in the cytoplasm, with subsequent binding of RNA and RBPs (Fig 4.8). Sequestration of these RBPs, which are important splicing regulators, may eventually result in perturbation in RNA splicing and processing.

Furthermore, it is also postulated that a prion-like mechanism involving RBPs with putative prion domains might underlie the cell-to-cell transmission of neurodegenerative pathology throughout the nervous system (King et al., 2012). The theory of common prion-like mechanism of seeding, aggregation

and transmission involving protein aggregates such as tau, amyloid-β, huntingtin and α-synuclein has recently emerged from studies in a range of neurodegenerative diseases, including Alzheimer's disease, Huntington's disease, Parkinson's disease and FTLD (Frost and Diamond, 2010). The unifying pathogenic mechanisms underlying these neuropathologically and anatomically distinct diseases have profound therapeutic implications which may give rise to the development of novel diagnostic techniques and treatments.

4.7 Future Studies

Having determined the ultrastructural and molecular composition of the mouse striatal neuronal nucleus, including its chromosomal and subnuclear domains, it would be fascinating to investigate the presence of the splicing factor speckles (SFS) and paraspeckles (PS) in the neuronal nucleus. Recently a number of specific subnuclear domains such as the SFS and PS have been found in the mammalian cell types which are nucleated by a variety of ncRNAs. Although the ultrastructural appearance of the PS has recently been characterized (Souquere et al., 2010), it has never been demonstrated in neurons. The nuclear distribution of the SFS and their spatial relationship to the PS, as well as the relationship between SFS/PS and other subnuclear domains may be addressed. In addition, RNA in situ hybridization techniques could be used to determine the distribution of the ncRNAs NEAT1 and MALAT1 within the SFS/PS if found in the neuronal nucleus. The SFS/PS complex may further be studied in HDACi treated mice and transgenic disease models. This thesis has already demonstrated prominent nuclear changes

occurring in these mice, and preliminary data also reveal an increase in the SFS marker SF2/ASF following HDACi treatment. It would be interesting to see if the SFS/PS complex is another focus for disorganization leading to splicing dysregulation.

The unique neuronal nucleolar complex has been determined as a focus for disorganization in both HDACi treated mice and neurodegenerative disease models. In addition to the rearrangement of the PNH and CBs, it would be crucial to investigate the organization and distribution of the nucleolus in these mice. ICC and TEM analyses using the specific marker fibrillarin might reveal any changes in this central subnuclear structure. Regarding its enrichment in RNA processing and editing enzymes found in the neuronal nucleus, disorganization may also reflect RNA dysregulation. Moreover, the dramatic disruption of the unique perinucleolar structures demonstrated in both neurodegenerative disease models and mice treated with HDACi, the potential therapeutics for these diseases, may indicate some promising areas for future research. These might include investigating the potential restorative effects of HDACi in these disease models.

5’-fluorouridine labeling of nascent RNA as well as immunogold localization of RNA polymerases may further address the pattern of transcriptional activity within various nuclear subdomains in HDACi treated mice and disease models. These patterns may then be compared and related to that identified in the neuronal nucleus in this study. Functional implications of the disorganized neuronal nucleolar complex could be revealed in changes in these patterns which might indicate transcriptional dysregulation.

The intriguing identification of RBPs with prion-like domains in neurodegenerative diseases has provided enormous insight into the pathogenic mechanism of these diseases. Out of the 210 RBPs in the human genome, 29 have a putative prion domain (King et al., 2012). It is believed that additional RNA-binding prion candidates will soon be identified which might be important disease-causing proteins. Investigation of their presence as pathological protein aggregates in neurodegenerative disease models, for instance the TDP-43^{M337V} transgenic mice, would add to the list of ALS/FTLD associated RBPs in addition to TDP-43 and the FET protein family identified.

The concept of the unifying mechanism of prion-like spreading in neurodegenerative diseases represents an exciting direction for future studies. Seeding, aggregation and self-propagation of proteins such as amyloid-β, tau, huntingtin and α-synuclein have been reported recently in different studies (Lee et al., 2010, Prusiner, 2012). Remarkably, the present study in the TDP-43^{M337V} transgenic mice reveals extracellular spreading of TDP-43 aggregates in the dentate gyrus, hippocampal CA1 and CA3 regions and the frontal cortex, in addition to the striatum. This might indicate the potential transmissibility of TDP-43 pathology. These studies could also be carried out in the Tau^{P301S} and R6/2 transgenic mice, as studies have demonstrated the self-propagating properties and *in vivo* spreading of tau and huntingtin (Soto, 2011). Deciphering the underlying mechanisms of how these aggregates gain access to the extracellular space and get internalized into the neighboring neurons would have important therapeutic implications for these devastating diseases.

In the present study, transgenic mice expressing TDP43^{M337V} and tau^{P301S} under the control of murine Thy1.2 promoter were used as the disease models to study ALS/FTLD and FTDP-17 respectively. Although Thy1.2 promoter is generally “neuron-specific” and drives expression of the mutated protein predominately in the neurons, transgene expression may be exhibited in other non-neural tissues outside the CNS. Expression patterns may also demonstrate background strain and line-to-line variation correlated to the severity of phenotype, such that the expression of transgene may be varied in different founder lines generated even from the same transgene construct. A number of broad promoters may induce especially high levels of transgene expression in neurons that are typically not affected in particular diseases, which therefore unable to reflect the phenotypes observed in patients. Different regional expression under Thy1.2 promoter has been observed in some studies which reported higher transgene expression in particular brain regions and less in other regions and the spinal cord. ALS is a motor neuron disease affecting both upper and lower motor neurons, and FTLD affects neurons in the frontal and temporal lobes of the brain. However, this study focused primarily on neurons in the striatum, which is predominately affected in HD, but not in ALS or FTLD. It could be more important to study the effects of transgene expression in motor neurons in ALS, and other promoters such as the CNS-specific prion promoter might be used to drive high level of transgene expression in the motor neurons. In addition, it would be crucial to study these transgenic mice in the pre-symptomatic stage apart from the end stage in order to dissect any earlier changes involved in disease pathogenesis.

References

CHAPTER 5

References

ABHYANKAR, M. M., UREKAR, C. & REDDI, P. P. (2007) A novel CpG-free vertebrate insulator silences the testis-specific SP-10 gene in somatic tissues: role for TDP-43 in insulator function. *J Biol Chem,* 282**,** 36143-54.

ABRAHAMSEN, H. & STENMARK, H. (2010) Protein secretion: unconventional exit by exophagy. *Curr Biol,* 20**,** R415-8.

AGRANAT, L., RAITSKIN, O., SPERLING, J. & SPERLING, R. (2008) The editing enzyme ADAR1 and the mRNA surveillance protein hUpf1 interact in the cell nucleus. *Proc Natl Acad Sci U S A,* 105**,** 5028-33.

AGUZZI, A. & RAJENDRAN, L. (2009) The transcellular spread of cytosolic amyloids, prions, and prionoids. *Neuron,* 64**,** 783-90.

AKHMANOVA, A., VERKERK, T., LANGEVELD, A., GROSVELD, F. & GALJART, N. (2000) Characterisation of transcriptionally active and inactive chromatin domains in neurons. *J Cell Sci,* 113 Pt 24**,** 4463-74.

AKHTAR, A. & GASSER, S. M. (2007) The nuclear envelope and transcriptional control. *Nat Rev Genet,* 8**,** 507-17.

ALBERTI, S., HALFMANN, R., KING, O., KAPILA, A. & LINDQUIST, S. (2009) A systematic survey identifies prions and illuminates sequence features of prionogenic proteins. *Cell,* 137**,** 146-58.

ALBRIGHT, T. D., JESSELL, T. M., KANDEL, E. R. & POSNER, M. I. (2000) Neural science: a century of progress and the mysteries that remain. *Cell,* 100 Suppl**,** S1-55.

ALLEN, B., INGRAM, E., TAKAO, M., SMITH, M. J., JAKES, R., VIRDEE, K., YOSHIDA, H., HOLZER, M., CRAXTON, M., EMSON, P. C., ATZORI, C., MIGHELI, A., CROWTHER, R. A., GHETTI, B., SPILLANTINI, M. G. & GOEDERT, M. (2002) Abundant tau filaments and nonapoptotic neurodegeneration in transgenic mice expressing human P301S tau protein. *J Neurosci,* 22**,** 9340-51.

ALLEN, T. A., VON KAENEL, S., GOODRICH, J. A. & KUGEL, J. F. (2004) The SINE-encoded mouse B2 RNA represses mRNA transcription in response to heat shock. *Nat Struct Mol Biol,* 11**,** 816-21.

ANDERSEN, J. S., LYON, C. E., FOX, A. H., LEUNG, A. K., LAM, Y. W., STEEN, H., MANN, M. & LAMOND, A. I. (2002) Directed proteomic analysis of the human nucleolus. *Curr Biol,* 12**,** 1-11.

ANDRADE, L. E., CHAN, E. K., RASKA, I., PEEBLES, C. L., ROOS, G. & TAN, E. M. (1991) Human autoantibody to a novel protein of the nuclear coiled body: immunological characterization and cDNA cloning of p80-coilin. *J Exp Med,* 173**,** 1407-19.

ARAI, T., HASEGAWA, M., AKIYAMA, H., IKEDA, K., NONAKA, T., MORI, H., MANN, D., TSUCHIYA, K., YOSHIDA, M., HASHIZUME, Y. & ODA, T. (2006) TDP-43 is a component of ubiquitin-positive tau-negative inclusions in frontotemporal lobar degeneration and amyotrophic lateral sclerosis. *Biochem Biophys Res Commun,* 351**,** 602-11.

AVILA, A. M., BURNETT, B. G., TAYE, A. A., GABANELLA, F., KNIGHT, M. A., HARTENSTEIN, P., CIZMAN, Z., DI PROSPERO, N. A., PELLIZZONI, L., FISCHBECK, K. H. & SUMNER, C. J. (2007) Trichostatin A increases SMN expression and survival in a mouse model of spinal muscular atrophy. *J Clin Invest,* 117**,** 659-71.

AYALA, Y. M., MISTELI, T. & BARALLE, F. E. (2008a) TDP-43 regulates retinoblastoma protein phosphorylation through the repression of cyclin-dependent kinase 6 expression. *Proc Natl Acad Sci U S A,* 105**,** 3785-9.

AYALA, Y. M., ZAGO, P., D'AMBROGIO, A., XU, Y. F., PETRUCELLI, L., BURATTI, E. & BARALLE, F. E. (2008b) Structural determinants of the cellular localization and shuttling of TDP-43. *J Cell Sci,* 121**,** 3778-85.

BABU, M. M., JANGA, S. C., DE SANTIAGO, I. & POMBO, A. (2008) Eukaryotic gene regulation in three dimensions and its impact on genome evolution. *Curr Opin Genet Dev,* 18**,** 571-82.

BAKER, M., MACKENZIE, I. R., PICKERING-BROWN, S. M., GASS, J., RADEMAKERS, R., LINDHOLM, C., SNOWDEN, J., ADAMSON, J., SADOVNICK, A. D., ROLLINSON, S., CANNON, A., DWOSH, E., NEARY, D., MELQUIST, S., RICHARDSON, A., DICKSON, D., BERGER, Z., ERIKSEN, J., ROBINSON, T., ZEHR, C., DICKEY, C. A., CROOK, R., MCGOWAN, E., MANN, D., BOEVE, B., FELDMAN, H. & HUTTON, M. (2006) Mutations in progranulin cause tau-negative frontotemporal dementia linked to chromosome 17. *Nature,* 442**,** 916-9.

BALTANAS, F. C., CASAFONT, I., WERUAGA, E., ALONSO, J. R., BERCIANO, M. T. & LAFARGA, M. (2011) Nucleolar disruption and cajal body disassembly are nuclear hallmarks of DNA damage-induced neurodegeneration in purkinje cells. *Brain Pathol,* 21**,** 374-88.

BANERJEE, R., BEAL, M. F. & THOMAS, B. (2010) Autophagy in neurodegenerative disorders: pathogenic roles and therapeutic implications. *Trends Neurosci,* 33**,** 541-9.

BANKS, G. T., KUTA, A., ISAACS, A. M. & FISHER, E. M. (2008) TDP-43 is a culprit in human neurodegeneration, and not just an innocent bystander. *Mamm Genome,* 19**,** 299-305.

BARTOVA, E., KREJCI, J., HARNICAROVA, A., GALIOVA, G. & KOZUBEK, S. (2008) Histone modifications and nuclear architecture: a review. *J Histochem Cytochem,* 56**,** 711-21.

BARTOVA, E., PACHERNIK, J., HARNICAROVA, A., KOVARIK, A., KOVARIKOVA, M., HOFMANOVA, J., SKALNIKOVA, M., KOZUBEK, M. & KOZUBEK, S. (2005) Nuclear levels and patterns of histone H3 modification and HP1 proteins after inhibition of histone deacetylases. *J Cell Sci,* 118**,** 5035-46.

BENAJIBA, L., LE BER, I., CAMUZAT, A., LACOSTE, M., THOMAS-ANTERION, C., COURATIER, P., LEGALLIC, S., SALACHAS, F., HANNEQUIN, D., DECOUSUS, M., LACOMBLEZ, L., GUEDJ, E., GOLFIER, V., CAMU, W., DUBOIS, B., CAMPION, D., MEININGER, V., BRICE, A., FRENCH, C. & GENETIC RESEARCH NETWORK ON FRONTOTEMPORAL LOBAR DEGENERATION/FRONTOTEMPORAL LOBAR DEGENERATION WITH MOTONEURON, D. (2009) TARDBP mutations in motoneuron disease with frontotemporal lobar degeneration. *Ann Neurol,* 65**,** 470-3.

BENTLEY, D. (2002) The mRNA assembly line: transcription and processing machines in the same factory. *Curr Opin Cell Biol,* 14**,** 336-42.

BERNARD, D., PRASANTH, K. V., TRIPATHI, V., COLASSE, S., NAKAMURA, T., XUAN, Z., ZHANG, M. Q., SEDEL, F., JOURDREN, L., COULPIER, F., TRILLER, A., SPECTOR, D. L. & BESSIS, A. (2010) A long nuclear-retained non-coding RNA regulates synaptogenesis by modulating gene expression. *EMBO J,* 29**,** 3082-93.

BILLIA, F. & DE BONI, U. (1991) Localization of centromeric satellite and telomeric DNA sequences in dorsal root ganglion neurons, in vitro. *J Cell Sci,* 100 (Pt 1)**,** 219-26.

BIRD, A. (2002) DNA methylation patterns and epigenetic memory. *Genes Dev,* 16**,** 6-21.

BJERLING, P., SILVERSTEIN, R. A., THON, G., CAUDY, A., GREWAL, S. & EKWALL, K. (2002) Functional divergence between histone deacetylases in fission yeast by distinct cellular localization and in vivo specificity. *Mol Cell Biol,* 22**,** 2170-81.

BOGDANOVIC, O. & VEENSTRA, G. J. (2009) DNA methylation and methyl-CpG binding proteins: developmental requirements and function. *Chromosoma,* 118**,** 549-65.

BOHMANN, K., FERREIRA, J., SANTAMA, N., WEIS, K. & LAMOND, A. I. (1995) Molecular analysis of the coiled body. *J Cell Sci Suppl,* 19**,** 107-13.

BOISVERT, F. M., VAN KONINGSBRUGGEN, S., NAVASCUES, J. & LAMOND, A. I. (2007) The multifunctional nucleolus. *Nat Rev Mol Cell Biol,* 8**,** 574-85.

BORDEN, J. & MANUELIDIS, L. (1988) Movement of the X chromosome in epilepsy. *Science,* 242**,** 1687-91.

BOULON, S., WESTMAN, B. J., HUTTEN, S., BOISVERT, F. M. & LAMOND, A. I. (2010) The nucleolus under stress. *Mol Cell,* 40**,** 216-27.

BOVERI, T. (1909) Die Blastomerenkerne von Ascaris megalocephala und die Theorie der Chromosomenindividualität. *Arch Zellforsch,* 3**,** 181-268.

BOYLE, A. L., BALLARD, S. G. & WARD, D. C. (1990) Differential distribution of long and short interspersed element sequences in the mouse genome: chromosome karyotyping by fluorescence in situ hybridization. *Proc Natl Acad Sci U S A,* 87**,** 7757-61.

BOYLE, S., GILCHRIST, S., BRIDGER, J. M., MAHY, N. L., ELLIS, J. A. & BICKMORE, W. A. (2001) The spatial organization of human chromosomes within the nuclei of normal and emerin-mutant cells. *Hum Mol Genet,* 10**,** 211-9.

BRAAK, H. & BRAAK, E. (1991) Neuropathological stageing of Alzheimer-related changes. *Acta Neuropathol,* 82**,** 239-59.

BRANCO, M. R., BRANCO, T., RAMIREZ, F. & POMBO, A. (2008) Changes in chromosome organization during PHA-activation of resting human lymphocytes measured by cryo-FISH. *Chromosome Res,* 16**,** 413-26.

BRANDT, R., HUNDELT, M. & SHAHANI, N. (2005) Tau alteration and neuronal degeneration in tauopathies: mechanisms and models. *Biochim Biophys Acta,* 1739**,** 331-54.

BRIDGE, E., XIA, D. X., CARMO-FONSECA, M., CARDINALI, B., LAMOND, A. I. & PETTERSSON, U. (1995) Dynamic organization of splicing factors in adenovirus-infected cells. *J Virol,* 69**,** 281-90.

BUCKLEY, N. J., JOHNSON, R., ZUCCATO, C., BITHELL, A. & CATTANEO, E. (2010) The role of REST in transcriptional and epigenetic dysregulation in Huntington's disease. *Neurobiol Dis,* 39**,** 28-39.

BUGIANI, O., MURRELL, J. R., GIACCONE, G., HASEGAWA, M., GHIGO, G., TABATON, M., MORBIN, M., PRIMAVERA, A., CARELLA, F., SOLARO, C., GRISOLI, M., SAVOIARDO, M., SPILLANTINI, M. G., TAGLIAVINI, F.,

GOEDERT, M. & GHETTI, B. (1999) Frontotemporal dementia and corticobasal degeneration in a family with a P301S mutation in tau. *J Neuropathol Exp Neurol,* 58**,** 667-77.

CAJAL, S. R. (1910) El núcleo de las células piramidales del cerebro humano y de algunos mamíferos. *Trab Lab Invest Biol,* 8**,** 27-62.

CAM, H. P., CHEN, E. S. & GREWAL, S. I. (2009) Transcriptional scaffolds for heterochromatin assembly. *Cell,* 136**,** 610-4.

CARMO-FONSECA, M., FERREIRA, J. & LAMOND, A. I. (1993) Assembly of snRNP-containing coiled bodies is regulated in interphase and mitosis--evidence that the coiled body is a kinetic nuclear structure. *J Cell Biol,* 120**,** 841-52.

CARMO-FONSECA, M. & RINO, J. (2011) RNA seeds nuclear bodies. *Nat Cell Biol,* 13**,** 110-2.

CARTER, D. R., ESKIW, C. & COOK, P. R. (2008) Transcription factories. *Biochem Soc Trans,* 36**,** 585-9.

CASAFONT, I., BENGOECHEA, R., TAPIA, O., BERCIANO, M. T. & LAFARGA, M. (2009) TDP-43 localizes in mRNA transcription and processing sites in mammalian neurons. *J Struct Biol,* 167**,** 235-41.

CASAFONT, I., NAVASCUES, J., PENA, E., LAFARGA, M. & BERCIANO, M. T. (2006) Nuclear organization and dynamics of transcription sites in rat sensory ganglia neurons detected by incorporation of 5'-fluorouridine into nascent RNA. *Neuroscience,* 140**,** 453-62.

CHA, J. H. (2007) Transcriptional signatures in Huntington's disease. *Prog Neurobiol,* 83**,** 228-48.

CHA, J. H., FREY, A. S., ALSDORF, S. A., KERNER, J. A., KOSINSKI, C. M., MANGIARINI, L., PENNEY, J. B., JR., DAVIES, S. W., BATES, G. P. & YOUNG, A. B. (1999) Altered neurotransmitter receptor expression in transgenic mouse models of Huntington's disease. *Philos Trans R Soc Lond B Biol Sci,* 354**,** 981-9.

CHAHROUR, M., JUNG, S. Y., SHAW, C., ZHOU, X., WONG, S. T., QIN, J. & ZOGHBI, H. Y. (2008) MeCP2, a key contributor to neurological disease, activates and represses transcription. *Science,* 320**,** 1224-9.

CHAHROUR, M. & ZOGHBI, H. Y. (2007) The story of Rett syndrome: from clinic to neurobiology. *Neuron,* 56**,** 422-37.

CHAKALOVA, L. & FRASER, P. (2010) Organization of transcription. *Cold Spring Harb Perspect Biol,* 2**,** a000729.

CHAO, H. T. & ZOGHBI, H. Y. (2009) The yin and yang of MeCP2 phosphorylation. *Proc Natl Acad Sci U S A,* 106**,** 4577-8.

CHE, M. X., JIANG, Y. J., XIE, Y. Y., JIANG, L. L. & HU, H. Y. (2011) Aggregation of the 35-kDa fragment of TDP-43 causes formation of cytoplasmic inclusions and alteration of RNA processing. *FASEB J,* 25**,** 2344-53.

CHEN-PLOTKIN, A. S., LEE, V. M. & TROJANOWSKI, J. Q. (2010) TAR DNA-binding protein 43 in neurodegenerative disease. *Nat Rev Neurol,* 6**,** 211-20.

CHEN, S., ZHANG, X., SONG, L. & LE, W. (2012) Autophagy dysregulation in amyotrophic lateral sclerosis. *Brain Pathol,* 22**,** 110-6.

CIOCE, M. & LAMOND, A. I. (2005) Cajal bodies: a long history of discovery. *Annu Rev Cell Dev Biol,* 21**,** 105-31.

CLAVAGUERA, F., BOLMONT, T., CROWTHER, R. A., ABRAMOWSKI, D., FRANK, S., PROBST, A., FRASER, G., STALDER, A. K., BEIBEL, M., STAUFENBIEL, M., JUCKER, M., GOEDERT, M. & TOLNAY, M. (2009) Transmission and spreading of tauopathy in transgenic mouse brain. *Nat Cell Biol,* 11**,** 909-13.

CLOUAIRE, T. & STANCHEVA, I. (2008) Methyl-CpG binding proteins: specialized transcriptional repressors or structural components of chromatin? *Cell Mol Life Sci,* 65**,** 1509-22.

CMARKO, D., VERSCHURE, P. J., ROTHBLUM, L. I., HERNANDEZ-VERDUN, D., AMALRIC, F., VAN DRIEL, R. & FAKAN, S. (2000) Ultrastructural analysis of nucleolar transcription in cells microinjected with 5-bromo-UTP. *Histochem Cell Biol,* 113**,** 181-7.

COHEN, S. & GREENBERG, M. E. (2010) A bird's-eye view of MeCP2 binding. *Mol Cell,* 37**,** 451-2.

COOK, P. R. (1999) The organization of replication and transcription. *Science,* 284**,** 1790-5.

COUTHOUIS, J., HART, M. P., ERION, R., KING, O. D., DIAZ, Z., NAKAYA, T., IBRAHIM, F., KIM, H. J., MOJSILOVIC-PETROVIC, J., PANOSSIAN, S., KIM, C. E., FRACKELTON, E. C., SOLSKI, J. A., WILLIAMS, K. L., CLAY-FALCONE, D., ELMAN, L., MCCLUSKEY, L., GREENE, R., HAKONARSON, H., KALB, R. G., LEE, V. M., TROJANOWSKI, J. Q., NICHOLSON, G. A., BLAIR, I. P., BONINI, N. M., VAN DEERLIN, V. M., MOURELATOS, Z., SHORTER, J. & GITLER, A. D. (2012) Evaluating the role of the FUS/TLS-related gene EWSR1 in amyotrophic lateral sclerosis. *Hum Mol Genet,* 21**,** 2899-911.

COUTHOUIS, J., HART, M. P., SHORTER, J., DEJESUS-HERNANDEZ, M., ERION, R., ORISTANO, R., LIU, A. X., RAMOS, D., JETHAVA, N., HOSANGADI, D., EPSTEIN, J., CHIANG, A., DIAZ, Z., NAKAYA, T., IBRAHIM, F., KIM, H. J., SOLSKI, J. A., WILLIAMS, K. L., MOJSILOVIC-PETROVIC, J., INGRE, C.,

BOYLAN, K., GRAFF-RADFORD, N. R., DICKSON, D. W., CLAY-FALCONE, D., ELMAN, L., MCCLUSKEY, L., GREENE, R., KALB, R. G., LEE, V. M., TROJANOWSKI, J. Q., LUDOLPH, A., ROBBERECHT, W., ANDERSEN, P. M., NICHOLSON, G. A., BLAIR, I. P., KING, O. D., BONINI, N. M., VAN DEERLIN, V., RADEMAKERS, R., MOURELATOS, Z. & GITLER, A. D. (2011) A yeast functional screen predicts new candidate ALS disease genes. *Proc Natl Acad Sci U S A,* 108**,** 20881-90.

CREMER, M., VON HASE, J., VOLM, T., BRERO, A., KRETH, G., WALTER, J., FISCHER, C., SOLOVEI, I., CREMER, C. & CREMER, T. (2001) Non-random radial higher-order chromatin arrangements in nuclei of diploid human cells. *Chromosome Res,* 9**,** 541-67.

CREMER, T. & CREMER, M. (2010) Chromosome territories. *Cold Spring Harb Perspect Biol,* 2**,** a003889.

CROFT, J. A., BRIDGER, J. M., BOYLE, S., PERRY, P., TEAGUE, P. & BICKMORE, W. A. (1999) Differences in the localization and morphology of chromosomes in the human nucleus. *J Cell Biol,* 145**,** 1119-31.

CROSS, D. C., MUNOZ, J. P., HERNANDEZ, P. & MACCIONI, R. B. (2000) Nuclear and cytoplasmic tau proteins from human nonneuronal cells share common structural and functional features with brain tau. *J Cell Biochem,* 78**,** 305-17.

CUELLAR, T. L., DAVIS, T. H., NELSON, P. T., LOEB, G. B., HARFE, B. D., ULLIAN, E. & MCMANUS, M. T. (2008) Dicer loss in striatal neurons produces behavioral and neuroanatomical phenotypes in the absence of neurodegeneration. *Proc Natl Acad Sci U S A,* 105**,** 5614-9.

DARZACQ, X., JADY, B. E., VERHEGGEN, C., KISS, A. M., BERTRAND, E. & KISS, T. (2002) Cajal body-specific small nuclear RNAs: a novel class of 2'-O-methylation and pseudouridylation guide RNAs. *EMBO J,* 21**,** 2746-56.

DAVIES, S. W., SATHASIVAM, K., HOBBS, C., DOHERTY, P., MANGIARINI, L., SCHERZINGER, E., WANKER, E. E. & BATES, G. P. (1999) Detection of polyglutamine aggregation in mouse models. *Methods Enzymol,* 309**,** 687-701.

DAVIES, S. W., TURMAINE, M., COZENS, B. A., DIFIGLIA, M., SHARP, A. H., ROSS, C. A., SCHERZINGER, E., WANKER, E. E., MANGIARINI, L. & BATES, G. P. (1997) Formation of neuronal intranuclear inclusions underlies the neurological dysfunction in mice transgenic for the HD mutation. *Cell,* 90**,** 537-48.

DE CALIGNON, A., POLYDORO, M., SUAREZ-CALVET, M., WILLIAM, C., ADAMOWICZ, D. H., KOPEIKINA, K. J., PITSTICK, R., SAHARA, N., ASHE, K. H., CARLSON, G. A., SPIRES-JONES, T. L. & HYMAN, B. T. (2012)

Propagation of tau pathology in a model of early Alzheimer's disease. *Neuron,* 73**,** 685-97.

DE DUVE, C. (1963) The lysosome. *Sci Am,* 208**,** 64-72.

DE MEZER, M., WOJCIECHOWSKA, M., NAPIERALA, M., SOBCZAK, K. & KRZYZOSIAK, W. J. (2011) Mutant CAG repeats of Huntingtin transcript fold into hairpins, form nuclear foci and are targets for RNA interference. *Nucleic Acids Res,* 39**,** 3852-63.

DEJESUS-HERNANDEZ, M., MACKENZIE, I. R., BOEVE, B. F., BOXER, A. L., BAKER, M., RUTHERFORD, N. J., NICHOLSON, A. M., FINCH, N. A., FLYNN, H., ADAMSON, J., KOURI, N., WOJTAS, A., SENGDY, P., HSIUNG, G. Y., KARYDAS, A., SEELEY, W. W., JOSEPHS, K. A., COPPOLA, G., GESCHWIND, D. H., WSZOLEK, Z. K., FELDMAN, H., KNOPMAN, D. S., PETERSEN, R. C., MILLER, B. L., DICKSON, D. W., BOYLAN, K. B., GRAFF-RADFORD, N. R. & RADEMAKERS, R. (2011) Expanded GGGGCC hexanucleotide repeat in noncoding region of C9ORF72 causes chromosome 9p-linked FTD and ALS. *Neuron,* 72**,** 245-56.

DELCUVE, G. P., RASTEGAR, M. & DAVIE, J. R. (2009) Epigenetic control. *J Cell Physiol,* 219**,** 243-50.

DESTERRO, J. M., KEEGAN, L. P., LAFARGA, M., BERCIANO, M. T., O'CONNELL, M. & CARMO-FONSECA, M. (2003) Dynamic association of RNA-editing enzymes with the nucleolus. *J Cell Sci,* 116**,** 1805-18.

DIFIGLIA, M., SAPP, E., CHASE, K. O., DAVIES, S. W., BATES, G. P., VONSATTEL, J. P. & ARONIN, N. (1997) Aggregation of huntingtin in neuronal intranuclear inclusions and dystrophic neurites in brain. *Science,* 277**,** 1990-3.

DORIGO, B., SCHALCH, T., KULANGARA, A., DUDA, S., SCHROEDER, R. R. & RICHMOND, T. J. (2004) Nucleosome arrays reveal the two-start organization of the chromatin fiber. *Science,* 306**,** 1571-3.

DOUSSET, T., WANG, C., VERHEGGEN, C., CHEN, D., HERNANDEZ-VERDUN, D. & HUANG, S. (2000) Initiation of nucleolar assembly is independent of RNA polymerase I transcription. *Mol Biol Cell,* 11**,** 2705-17.

DUNDR, M. & MISTELI, T. (2001) Functional architecture in the cell nucleus. *Biochem J,* 356**,** 297-310.

DUNDR, M. & MISTELI, T. (2010) Biogenesis of nuclear bodies. *Cold Spring Harb Perspect Biol,* 2**,** a000711.

DURAN, J. M., ANJARD, C., STEFAN, C., LOOMIS, W. F. & MALHOTRA, V. (2010) Unconventional secretion of Acb1 is mediated by autophagosomes. *J Cell Biol,* 188**,** 527-36.

ECKER, J. R., BICKMORE, W. A., BARROSO, I., PRITCHARD, J. K., GILAD, Y. & SEGAL, E. (2012) Genomics: ENCODE explained. *Nature,* 489**,** 52-5.

EL-AGNAF, O. M., SALEM, S. A., PALEOLOGOU, K. E., CURRAN, M. D., GIBSON, M. J., COURT, J. A., SCHLOSSMACHER, M. G. & ALLSOP, D. (2006) Detection of oligomeric forms of alpha-synuclein protein in human plasma as a potential biomarker for Parkinson's disease. *FASEB J,* 20**,** 419-25.

ESKIW, C. H. & FRASER, P. (2011) Ultrastructural study of transcription factories in mouse erythroblasts. *J Cell Sci,* 124**,** 3676-83.

ESPADA, J. & ESTELLER, M. (2007) Epigenetic control of nuclear architecture. *Cell Mol Life Sci,* 64**,** 449-57.

EYMERY, A., CALLANAN, M. & VOURC'H, C. (2009) The secret message of heterochromatin: new insights into the mechanisms and function of centromeric and pericentric repeat sequence transcription. *Int J Dev Biol,* 53**,** 259-68.

FEDOROVA, E. & ZINK, D. (2008) Nuclear architecture and gene regulation. *Biochim Biophys Acta,* 1783**,** 2174-84.

FERNANDEZ-COSTA, J. M., LLAMUSI, M. B., GARCIA-LOPEZ, A. & ARTERO, R. (2011) Alternative splicing regulation by Muscleblind proteins: from development to disease. *Biol Rev Camb Philos Soc,* 86**,** 947-58.

FERRANTE, R. J., KUBILUS, J. K., LEE, J., RYU, H., BEESEN, A., ZUCKER, B., SMITH, K., KOWALL, N. W., RATAN, R. R., LUTHI-CARTER, R. & HERSCH, S. M. (2003) Histone deacetylase inhibition by sodium butyrate chemotherapy ameliorates the neurodegenerative phenotype in Huntington's disease mice. *J Neurosci,* 23**,** 9418-27.

FILIMONENKO, M., STUFFERS, S., RAIBORG, C., YAMAMOTO, A., MALEROD, L., FISHER, E. M., ISAACS, A., BRECH, A., STENMARK, H. & SIMONSEN, A. (2007) Functional multivesicular bodies are required for autophagic clearance of protein aggregates associated with neurodegenerative disease. *J Cell Biol,* 179**,** 485-500.

FONG, N. & BENTLEY, D. L. (2001) Capping, splicing, and 3' processing are independently stimulated by RNA polymerase II: different functions for different segments of the CTD. *Genes Dev,* 15**,** 1783-95.

FOX, A. H., LAM, Y. W., LEUNG, A. K., LYON, C. E., ANDERSEN, J., MANN, M. & LAMOND, A. I. (2002) Paraspeckles: a novel nuclear domain. *Curr Biol,* 12**,** 13-25.

FOX, A. H. & LAMOND, A. I. (2010) Paraspeckles. *Cold Spring Harb Perspect Biol,* 2**,** a000687.

FRASER, P. & BICKMORE, W. (2007) Nuclear organization of the genome and the potential for gene regulation. *Nature,* 447**,** 413-7.

FROST, B. & DIAMOND, M. I. (2010) Prion-like mechanisms in neurodegenerative diseases. *Nat Rev Neurosci,* 11**,** 155-9.

FROST, B., OLLESCH, J., WILLE, H. & DIAMOND, M. I. (2009) Conformational diversity of wild-type Tau fibrils specified by templated conformation change. *J Biol Chem,* 284**,** 3546-51.

FURUKAWA, Y., KANEKO, K., WATANABE, S., YAMANAKA, K. & NUKINA, N. (2011) A seeding reaction recapitulates intracellular formation of Sarkosyl-insoluble transactivation response element (TAR) DNA-binding protein-43 inclusions. *J Biol Chem,* 286**,** 18664-72.

GALL, J. G. (2000) Cajal bodies: the first 100 years. *Annu Rev Cell Dev Biol,* 16**,** 273-300.

GENDRON, T. F., JOSEPHS, K. A. & PETRUCELLI, L. (2010) Review: transactive response DNA-binding protein 43 (TDP-43): mechanisms of neurodegeneration. *Neuropathol Appl Neurobiol,* 36**,** 97-112.

GENDRON, T. F. & PETRUCELLI, L. (2009) The role of tau in neurodegeneration. *Mol Neurodegener,* 4**,** 13.

GEORGEL, P. T., HOROWITZ-SCHERER, R. A., ADKINS, N., WOODCOCK, C. L., WADE, P. A. & HANSEN, J. C. (2003) Chromatin compaction by human MeCP2. Assembly of novel secondary chromatin structures in the absence of DNA methylation. *J Biol Chem,* 278**,** 32181-8.

GESER, F., LEE, V. M. & TROJANOWSKI, J. Q. (2010) Amyotrophic lateral sclerosis and frontotemporal lobar degeneration: a spectrum of TDP-43 proteinopathies. *Neuropathology,* 30**,** 103-12.

GITLER, A. D. & SHORTER, J. (2011) RNA-binding proteins with prion-like domains in ALS and FTLD-U. *Prion,* 5**,** 179-87.

GOEDERT, M. (2004) Tau protein and neurodegeneration. *Semin Cell Dev Biol,* 15**,** 45-9.

GOEDERT, M., GHETTI, B. & SPILLANTINI, M. G. (2012) Frontotemporal dementia: implications for understanding Alzheimer disease. *Cold Spring Harb Perspect Med,* 2**,** a006254.

GOEDERT, M., JAKES, R. & CROWTHER, R. A. (1999) Effects of frontotemporal dementia FTDP-17 mutations on heparin-induced assembly of tau filaments. *FEBS Lett,* 450**,** 306-11.

GOEDERT, M. & SPILLANTINI, M. G. (2011) Pathogenesis of the tauopathies. *J Mol Neurosci,* 45**,** 425-31.

GOEDERT, M., SPILLANTINI, M. G., JAKES, R., RUTHERFORD, D. & CROWTHER, R. A. (1989) Multiple isoforms of human microtubule-associated protein tau: sequences and localization in neurofibrillary tangles of Alzheimer's disease. *Neuron,* 3**,** 519-26.

GREWAL, S. I. & ELGIN, S. C. (2007) Transcription and RNA interference in the formation of heterochromatin. *Nature,* 447**,** 399-406.

GREWAL, S. I. & JIA, S. (2007) Heterochromatin revisited. *Nat Rev Genet,* 8**,** 35-46.

GUO, J. L. & LEE, V. M. (2011) Seeding of normal Tau by pathological Tau conformers drives pathogenesis of Alzheimer-like tangles. *J Biol Chem,* 286**,** 15317-31.

HAGGARTY, S. J. & TSAI, L. H. (2011) Probing the role of HDACs and mechanisms of chromatin-mediated neuroplasticity. *Neurobiol Learn Mem,* 96**,** 41-52.

HAHNEN, E., HAUKE, J., TRANKLE, C., EYUPOGLU, I. Y., WIRTH, B. & BLUMCKE, I. (2008) Histone deacetylase inhibitors: possible implications for neurodegenerative disorders. *Expert Opin Investig Drugs,* 17**,** 169-84.

HALABI, C., HALABI, A., DEAN, D. L., WANG, P. N., BOXER, A. L., TROJANOWSKI, J. Q., DEARMOND, S. J., MILLER, B. L., KRAMER, J. H. & SEELEY, W. W. (2012) Patterns of Striatal Degeneration in Frontotemporal Dementia. *Alzheimer Dis Assoc Disord*.

HANSON, K. A., KIM, S. H. & TIBBETTS, R. S. (2012) RNA-binding proteins in neurodegenerative disease: TDP-43 and beyond. *Wiley Interdiscip Rev RNA,* 3**,** 265-85.

HDCR (1993) A novel gene containing a trinucleotide repeat that is expanded and unstable on Huntington's disease chromosomes. The Huntington's Disease Collaborative Research Group. *Cell,* 72**,** 971-983.

HEITZ, E. (1928) Das Heterochromatin der Moose, 1. *Jahrb Wiss Bot,* 69**,** 762-818.

HINES, K. A., CRYDERMAN, D. E., FLANNERY, K. M., YANG, H., VITALINI, M. W., HAZELRIGG, T., MIZZEN, C. A. & WALLRATH, L. L. (2009) Domains of heterochromatin protein 1 required for Drosophila melanogaster heterochromatin spreading. *Genetics,* 182**,** 967-77.

HO, T. H., CHARLET, B. N., POULOS, M. G., SINGH, G., SWANSON, M. S. & COOPER, T. A. (2004) Muscleblind proteins regulate alternative splicing. *EMBO J,* 23**,** 3103-12.

HOCINE, S., SINGER, R. H. & GRUNWALD, D. (2010) RNA processing and export. *Cold Spring Harb Perspect Biol,* 2**,** a000752.

HOCKLY, E., RICHON, V. M., WOODMAN, B., SMITH, D. L., ZHOU, X., ROSA, E., SATHASIVAM, K., GHAZI-NOORI, S., MAHAL, A., LOWDEN, P. A., STEFFAN, J. S., MARSH, J. L., THOMPSON, L. M., LEWIS, C. M., MARKS,

P. A. & BATES, G. P. (2003) Suberoylanilide hydroxamic acid, a histone deacetylase inhibitor, ameliorates motor deficits in a mouse model of Huntington's disease. *Proc Natl Acad Sci U S A,* 100**,** 2041-6.

HOLOWACZ, T. & DE BONI, U. (1991) Arrangement of kinetochore proteins and satellite DNA in neuronal interphase nuclei: changes induced by gamma-aminobutyric acid (GABA). *Exp Cell Res,* 197**,** 36-42.

HORIKE, S., CAI, S., MIYANO, M., CHENG, J. F. & KOHWI-SHIGEMATSU, T. (2005) Loss of silent-chromatin looping and impaired imprinting of DLX5 in Rett syndrome. *Nat Genet,* 37**,** 31-40.

HUA, Q. & HE, R. Q. (2002) Effect of phosphorylation and aggregation on tau binding to DNA. *Protein Pept Lett,* 9**,** 349-57.

HUTCHINSON, J. N., ENSMINGER, A. W., CLEMSON, C. M., LYNCH, C. R., LAWRENCE, J. B. & CHESS, A. (2007) A screen for nuclear transcripts identifies two linked noncoding RNAs associated with SC35 splicing domains. *BMC Genomics,* 8**,** 39.

HUTTON, M., LENDON, C. L., RIZZU, P., BAKER, M., FROELICH, S., HOULDEN, H., PICKERING-BROWN, S., CHAKRAVERTY, S., ISAACS, A., GROVER, A., HACKETT, J., ADAMSON, J., LINCOLN, S., DICKSON, D., DAVIES, P., PETERSEN, R. C., STEVENS, M., DE GRAAFF, E., WAUTERS, E., VAN BAREN, J., HILLEBRAND, M., JOOSSE, M., KWON, J. M., NOWOTNY, P., CHE, L. K., NORTON, J., MORRIS, J. C., REED, L. A., TROJANOWSKI, J., BASUN, H., LANNFELT, L., NEYSTAT, M., FAHN, S., DARK, F., TANNENBERG, T., DODD, P. R., HAYWARD, N., KWOK, J. B., SCHOFIELD, P. R., ANDREADIS, A., SNOWDEN, J., CRAUFURD, D., NEARY, D., OWEN, F., OOSTRA, B. A., HARDY, J., GOATE, A., VAN SWIETEN, J., MANN, D., LYNCH, T. & HEUTINK, P. (1998) Association of missense and 5'-splice-site mutations in tau with the inherited dementia FTDP-17. *Nature,* 393**,** 702-5.

IBORRA, F. J., POMBO, A., JACKSON, D. A. & COOK, P. R. (1996a) Active RNA polymerases are localized within discrete transcription "factories' in human nuclei. *J Cell Sci,* 109 (Pt 6)**,** 1427-36.

IBORRA, F. J., POMBO, A., MCMANUS, J., JACKSON, D. A. & COOK, P. R. (1996b) The topology of transcription by immobilized polymerases. *Exp Cell Res,* 229**,** 167-73.

IGAZ, L. M., KWONG, L. K., CHEN-PLOTKIN, A., WINTON, M. J., UNGER, T. L., XU, Y., NEUMANN, M., TROJANOWSKI, J. Q. & LEE, V. M. (2009) Expression of TDP-43 C-terminal Fragments in Vitro Recapitulates Pathological Features of TDP-43 Proteinopathies. *J Biol Chem,* 284**,** 8516-24.

ITO, D. & SUZUKI, N. (2011) Conjoint pathologic cascades mediated by ALS/FTLD-U linked RNA-binding proteins TDP-43 and FUS. *Neurology,* 77**,** 1636-43.

JACKSON, D. A., HASSAN, A. B., ERRINGTON, R. J. & COOK, P. R. (1993) Visualization of focal sites of transcription within human nuclei. *EMBO J,* 12**,** 1059-65.

JAENISCH, R. & BIRD, A. (2003) Epigenetic regulation of gene expression: how the genome integrates intrinsic and environmental signals. *Nat Genet,* 33 Suppl**,** 245-54.

JEPSON, J. E. & REENAN, R. A. (2008) RNA editing in regulating gene expression in the brain. *Biochim Biophys Acta,* 1779**,** 459-70.

JOHANNESSEN, C. U. (2000) Mechanisms of action of valproate: a commentatory. *Neurochem Int,* 37**,** 103-10.

JOHNSON, B. S., MCCAFFERY, J. M., LINDQUIST, S. & GITLER, A. D. (2008a) A yeast TDP-43 proteinopathy model: Exploring the molecular determinants of TDP-43 aggregation and cellular toxicity. *Proc Natl Acad Sci U S A,* 105**,** 6439-44.

JOHNSON, R., ZUCCATO, C., BELYAEV, N. D., GUEST, D. J., CATTANEO, E. & BUCKLEY, N. J. (2008b) A microRNA-based gene dysregulation pathway in Huntington's disease. *Neurobiol Dis,* 29**,** 438-45.

KABASHI, E., VALDMANIS, P. N., DION, P., SPIEGELMAN, D., MCCONKEY, B. J., VANDE VELDE, C., BOUCHARD, J. P., LACOMBLEZ, L., POCHIGAEVA, K., SALACHAS, F., PRADAT, P. F., CAMU, W., MEININGER, V., DUPRE, N. & ROULEAU, G. A. (2008) TARDBP mutations in individuals with sporadic and familial amyotrophic lateral sclerosis. *Nat Genet,* 40**,** 572-4.

KANEKO, H., DRIDI, S., TARALLO, V., GELFAND, B. D., FOWLER, B. J., CHO, W. G., KLEINMAN, M. E., PONICSAN, S. L., HAUSWIRTH, W. W., CHIODO, V. A., KARIKO, K., YOO, J. W., LEE, D. K., HADZIAHMETOVIC, M., SONG, Y., MISRA, S., CHAUDHURI, G., BUAAS, F. W., BRAUN, R. E., HINTON, D. R., ZHANG, Q., GROSSNIKLAUS, H. E., PROVIS, J. M., MADIGAN, M. C., MILAM, A. H., JUSTICE, N. L., ALBUQUERQUE, R. J., BLANDFORD, A. D., BOGDANOVICH, S., HIRANO, Y., WITTA, J., FUCHS, E., LITTMAN, D. R., AMBATI, B. K., RUDIN, C. M., CHONG, M. M., PROVOST, P., KUGEL, J. F., GOODRICH, J. A., DUNAIEF, J. L., BAFFI, J. Z. & AMBATI, J. (2011) DICER1 deficit induces Alu RNA toxicity in age-related macular degeneration. *Nature,* 471**,** 325-30.

KANELLOPOULOU, C., MULJO, S. A., KUNG, A. L., GANESAN, S., DRAPKIN, R., JENUWEIN, T., LIVINGSTON, D. M. & RAJEWSKY, K. (2005) Dicer-deficient

mouse embryonic stem cells are defective in differentiation and centromeric silencing. *Genes Dev,* 19**,** 489-501.

KIEFER, J. C. (2007) Epigenetics in development. *Dev Dyn,* 236**,** 1144-56.

KIM, S. H., MCQUEEN, P. G., LICHTMAN, M. K., SHEVACH, E. M., PARADA, L. A. & MISTELI, T. (2004) Spatial genome organization during T-cell differentiation. *Cytogenet Genome Res,* 105**,** 292-301.

KING, O. D., GITLER, A. D. & SHORTER, J. (2012) The tip of the iceberg: RNA-binding proteins with prion-like domains in neurodegenerative disease. *Brain Res,* 1462**,** 61-80.

KLEIN, A. F., GASNIER, E. & FURLING, D. (2011) Gain of RNA function in pathological cases: Focus on myotonic dystrophy. *Biochimie,* 93**,** 2006-12.

KRAEMER, B. C., SCHUCK, T., WHEELER, J. M., ROBINSON, L. C., TROJANOWSKI, J. Q., LEE, V. M. & SCHELLENBERG, G. D. (2010) Loss of murine TDP-43 disrupts motor function and plays an essential role in embryogenesis. *Acta Neuropathol,* 119**,** 409-19.

KURODA, M., TANABE, H., YOSHIDA, K., OIKAWA, K., SAITO, A., KIYUNA, T., MIZUSAWA, H. & MUKAI, K. (2004) Alteration of chromosome positioning during adipocyte differentiation. *J Cell Sci,* 117**,** 5897-903.

KWIATKOWSKI, T. J., JR., BOSCO, D. A., LECLERC, A. L., TAMRAZIAN, E., VANDERBURG, C. R., RUSS, C., DAVIS, A., GILCHRIST, J., KASARSKIS, E. J., MUNSAT, T., VALDMANIS, P., ROULEAU, G. A., HOSLER, B. A., CORTELLI, P., DE JONG, P. J., YOSHINAGA, Y., HAINES, J. L., PERICAK-VANCE, M. A., YAN, J., TICOZZI, N., SIDDIQUE, T., MCKENNA-YASEK, D., SAPP, P. C., HORVITZ, H. R., LANDERS, J. E. & BROWN, R. H., JR. (2009) Mutations in the FUS/TLS gene on chromosome 16 cause familial amyotrophic lateral sclerosis. *Science,* 323**,** 1205-8.

KWONG, L. K., URYU, K., TROJANOWSKI, J. Q. & LEE, V. M. (2008) TDP-43 proteinopathies: neurodegenerative protein misfolding diseases without amyloidosis. *Neurosignals,* 16**,** 41-51.

LAFARGA, M., CASAFONT, I., BENGOECHEA, R., TAPIA, O. & BERCIANO, M. T. (2009) Cajal's contribution to the knowledge of the neuronal cell nucleus. *Chromosoma,* 118**,** 437-43.

LAGIER-TOURENNE, C., POLYMENIDOU, M. & CLEVELAND, D. W. (2010) TDP-43 and FUS/TLS: emerging roles in RNA processing and neurodegeneration. *Hum Mol Genet,* 19**,** R46-64.

LAMOND, A. I. & CARMO-FONSECA, M. (1993) The coiled body. *Trends Cell Biol,* 3**,** 198-204.

LASALLE, J. M. (2004) Paradoxical role of methyl-CpG-binding protein 2 in Rett syndrome. *Curr Top Dev Biol,* 59**,** 61-86.

LASALLE, J. M. & YASUI, D. H. (2009) Evolving role of MeCP2 in Rett syndrome and autism. *Epigenomics,* 1**,** 119-130.

LEE, C. J. & IRIZARRY, K. (2003) Alternative splicing in the nervous system: an emerging source of diversity and regulation. *Biol Psychiatry,* 54**,** 771-6.

LEE, S. J., DESPLATS, P., SIGURDSON, C., TSIGELNY, I. & MASLIAH, E. (2010) Cell-to-cell transmission of non-prion protein aggregates. *Nat Rev Neurol,* 6**,** 702-6.

LEE, V. M., GOEDERT, M. & TROJANOWSKI, J. Q. (2001) Neurodegenerative tauopathies. *Annu Rev Neurosci,* 24**,** 1121-59.

LEVI, G. (1896) Su alcune particolarità di struttura del nucleo delle cellule nervose. *Riv Patol Nerv Ment,* 1**,** 141-149.

LEWIS, J. D., MEEHAN, R. R., HENZEL, W. J., MAURER-FOGY, I., JEPPESEN, P., KLEIN, F. & BIRD, A. (1992) Purification, sequence, and cellular localization of a novel chromosomal protein that binds to methylated DNA. *Cell,* 69**,** 905-14.

LI, G. & REINBERG, D. (2011) Chromatin higher-order structures and gene regulation. *Curr Opin Genet Dev,* 21**,** 175-86.

LI, L., ZHANG, X. & LE, W. (2008) Altered macroautophagy in the spinal cord of SOD1 mutant mice. *Autophagy,* 4**,** 290-3.

LI, W., JIN, Y., PRAZAK, L., HAMMELL, M. & DUBNAU, J. (2012) Transposable Elements in TDP-43-Mediated Neurodegenerative Disorders. *PLoS One,* 7**,** e44099.

LIACHKO, N. F., GUTHRIE, C. R. & KRAEMER, B. C. (2010) Phosphorylation promotes neurotoxicity in a Caenorhabditis elegans model of TDP-43 proteinopathy. *J Neurosci,* 30**,** 16208-19.

LING, S. C., ALBUQUERQUE, C. P., HAN, J. S., LAGIER-TOURENNE, C., TOKUNAGA, S., ZHOU, H. & CLEVELAND, D. W. (2010) ALS-associated mutations in TDP-43 increase its stability and promote TDP-43 complexes with FUS/TLS. *Proc Natl Acad Sci U S A,* 107**,** 13318-23.

LONG, S. W., OOI, J. Y., YAU, P. M. & JONES, P. L. (2011) A brain-derived MeCP2 complex supports a role for MeCP2 in RNA processing. *Biosci Rep,* 31**,** 333-43.

LOPEZ-MUNOZ, F., BOYA, J. & ALAMO, C. (2006) Neuron theory, the cornerstone of neuroscience, on the centenary of the Nobel Prize award to Santiago Ramon y Cajal. *Brain Res Bull,* 70**,** 391-405.

MACDONALD, J. L. & ROSKAMS, A. J. (2009) Epigenetic regulation of nervous system development by DNA methylation and histone deacetylation. *Prog Neurobiol,* 88**,** 170-83.

MALLWAIN, H. & BACHELARD, H. S. (1985) *Biochemistry and the Central Nervous System*, Churchill Livingstone, Edinburgh.

MANGIARINI, L., SATHASIVAM, K., SELLER, M., COZENS, B., HARPER, A., HETHERINGTON, C., LAWTON, M., TROTTIER, Y., LEHRACH, H., DAVIES, S. W. & BATES, G. P. (1996) Exon 1 of the HD gene with an expanded CAG repeat is sufficient to cause a progressive neurological phenotype in transgenic mice. *Cell,* 87**,** 493-506.

MANUELIDIS, L. (1984) Different central nervous system cell types display distinct and nonrandom arrangements of satellite DNA sequences. *Proc Natl Acad Sci U S A,* 81**,** 3123-7.

MANUELIDIS, L. (1985) Indications of centromere movement during interphase and differentiation. *Ann N Y Acad Sci,* 450**,** 205-21.

MAO, Y. S., ZHANG, B. & SPECTOR, D. L. (2011) Biogenesis and function of nuclear bodies. *Trends Genet,* 27**,** 295-306.

MARSHALL, L., KENNETH, N. S. & WHITE, R. J. (2008) Elevated tRNA(iMet) synthesis can drive cell proliferation and oncogenic transformation. *Cell,* 133**,** 78-89.

MATLIN, A. J. & MOORE, M. J. (2007) Spliceosome assembly and composition. *Adv Exp Med Biol,* 623**,** 14-35.

MATTICK, J. S. & MEHLER, M. F. (2008) RNA editing, DNA recoding and the evolution of human cognition. *Trends Neurosci,* 31**,** 227-33.

MATTIS, V. B., RAI, R., WANG, J., CHANG, C. W., COADY, T. & LORSON, C. L. (2006) Novel aminoglycosides increase SMN levels in spinal muscular atrophy fibroblasts. *Hum Genet,* 120**,** 589-601.

MEANEY, M. J. & FERGUSON-SMITH, A. C. (2010) Epigenetic regulation of the neural transcriptome: the meaning of the marks. *Nat Neurosci,* 13**,** 1313-8.

MIJALJICA, D., PRESCOTT, M. & DEVENISH, R. J. (2010) The intricacy of nuclear membrane dynamics during nucleophagy. *Nucleus,* 1**,** 213-23.

MIZUSHIMA, N. (2007) Autophagy: process and function. *Genes Dev,* 21**,** 2861-73.

MOHAMMAD, F., PANDEY, R. R., NAGANO, T., CHAKALOVA, L., MONDAL, T., FRASER, P. & KANDURI, C. (2008) Kcnq1ot1/Lit1 noncoding RNA mediates transcriptional silencing by targeting to the perinucleolar region. *Mol Cell Biol,* 28**,** 3713-28.

MONNERON, A. & BERNHARD, W. (1969) Fine structural organization of the interphase nucleus in some mammalian cells. *J Ultrastruct Res,* 27**,** 266-88.

MOORE, K. L. & BARR, M. L. (1953) Morphology of the nerve cell nucleus in mammals, with special reference to the sex chromatin. *J Comp Neurol,* 98**,** 213-31.

MOORE, M. J. & PROUDFOOT, N. J. (2009) Pre-mRNA processing reaches back to transcription and ahead to translation. *Cell,* 136**,** 688-700.

MORRIS, G. E. (2008) The Cajal body. *Biochim Biophys Acta,* 1783**,** 2108-15.

MORRIS, H. R., KHAN, M. N., JANSSEN, J. C., BROWN, J. M., PEREZ-TUR, J., BAKER, M., OZANSOY, M., HARDY, J., HUTTON, M., WOOD, N. W., LEES, A. J., REVESZ, T., LANTOS, P. & ROSSOR, M. N. (2001) The genetic and pathological classification of familial frontotemporal dementia. *Arch Neurol,* 58**,** 1813-6.

MORRIS, M., MAEDA, S., VOSSEL, K. & MUCKE, L. (2011) The many faces of tau. *Neuron,* 70**,** 410-26.

MURCHISON, E. P., PARTRIDGE, J. F., TAM, O. H., CHELOUFI, S. & HANNON, G. J. (2005) Characterization of Dicer-deficient murine embryonic stem cells. *Proc Natl Acad Sci U S A,* 102**,** 12135-40.

MYKOWSKA, A., SOBCZAK, K., WOJCIECHOWSKA, M., KOZLOWSKI, P. & KRZYZOSIAK, W. J. (2011) CAG repeats mimic CUG repeats in the misregulation of alternative splicing. *Nucleic Acids Res,* 39**,** 8938-51.

NAN, X., NG, H. H., JOHNSON, C. A., LAHERTY, C. D., TURNER, B. M., EISENMAN, R. N. & BIRD, A. (1998) Transcriptional repression by the methyl-CpG-binding protein MeCP2 involves a histone deacetylase complex. *Nature,* 393**,** 386-9.

NAYYAR, R. P. & BARR, M. L. (1968) Histochemical studies on the accessory body of cajal in neurones of the cat. *J Comp Neurol,* 132**,** 125-34.

NEUMANN, M. (2009) Molecular neuropathology of TDP-43 proteinopathies. *Int J Mol Sci,* 10**,** 232-46.

NEUMANN, M., BENTMANN, E., DORMANN, D., JAWAID, A., DEJESUS-HERNANDEZ, M., ANSORGE, O., ROEBER, S., KRETZSCHMAR, H. A., MUNOZ, D. G., KUSAKA, H., YOKOTA, O., ANG, L. C., BILBAO, J., RADEMAKERS, R., HAASS, C. & MACKENZIE, I. R. (2011) FET proteins TAF15 and EWS are selective markers that distinguish FTLD with FUS pathology from amyotrophic lateral sclerosis with FUS mutations. *Brain,* 134**,** 2595-609.

NEUMANN, M., KWONG, L. K., SAMPATHU, D. M., TROJANOWSKI, J. Q. & LEE, V. M. (2007) TDP-43 proteinopathy in frontotemporal lobar degeneration and amyotrophic lateral sclerosis: protein misfolding diseases without amyloidosis. *Arch Neurol,* 64**,** 1388-94.

NEUMANN, M., RADEMAKERS, R., ROEBER, S., BAKER, M., KRETZSCHMAR, H. A. & MACKENZIE, I. R. (2009) A new subtype of frontotemporal lobar degeneration with FUS pathology. *Brain,* 132**,** 2922-31.

NEUMANN, M., SAMPATHU, D. M., KWONG, L. K., TRUAX, A. C., MICSENYI, M. C., CHOU, T. T., BRUCE, J., SCHUCK, T., GROSSMAN, M., CLARK, C. M., MCCLUSKEY, L. F., MILLER, B. L., MASLIAH, E., MACKENZIE, I. R., FELDMAN, H., FEIDEN, W., KRETZSCHMAR, H. A., TROJANOWSKI, J. Q. & LEE, V. M. (2006) Ubiquitinated TDP-43 in frontotemporal lobar degeneration and amyotrophic lateral sclerosis. *Science,* 314**,** 130-3.

NIZAMI, Z., DERYUSHEVA, S. & GALL, J. G. (2010) The Cajal body and histone locus body. *Cold Spring Harb Perspect Biol,* 2**,** a000653.

OSBORNE, R. J. & THORNTON, C. A. (2006) RNA-dominant diseases. *Hum Mol Genet,* 15 Spec No 2**,** R162-9.

OVALLE, W. K. & NAHIRNEY, P. C. (2007) Netter's Essential Histology.

OZAWA, R., HAYASHI, Y. K., OGAWA, M., KUROKAWA, R., MATSUMOTO, H., NOGUCHI, S., NONAKA, I. & NISHINO, I. (2006) Emerin-lacking mice show minimal motor and cardiac dysfunctions with nuclear-associated vacuoles. *Am J Pathol,* 168**,** 907-17.

PAPANTONIS, A. & COOK, P. R. (2010) Genome architecture and the role of transcription. *Curr Opin Cell Biol,* 22**,** 271-6.

PAPANTONIS, A. & COOK, P. R. (2011) Fixing the model for transcription: the DNA moves, not the polymerase. *Transcription,* 2**,** 41-4.

PARK, Y. E., HAYASHI, Y. K., BONNE, G., ARIMURA, T., NOGUCHI, S., NONAKA, I. & NISHINO, I. (2009) Autophagic degradation of nuclear components in mammalian cells. *Autophagy,* 5**,** 795-804.

PAULE, M. R. & WHITE, R. J. (2000) Survey and summary: transcription by RNA polymerases I and III. *Nucleic Acids Res,* 28**,** 1283-98.

PAULSON, H. L., PEREZ, M. K., TROTTIER, Y., TROJANOWSKI, J. Q., SUBRAMONY, S. H., DAS, S. S., VIG, P., MANDEL, J. L., FISCHBECK, K. H. & PITTMAN, R. N. (1997) Intranuclear inclusions of expanded polyglutamine protein in spinocerebellar ataxia type 3. *Neuron,* 19**,** 333-44.

PEDERSON, T. (2011) The nucleolus. *Cold Spring Harb Perspect Biol,* 3.

PETKOVA, A. T., LEAPMAN, R. D., GUO, Z., YAU, W. M., MATTSON, M. P. & TYCKO, R. (2005) Self-propagating, molecular-level polymorphism in Alzheimer's beta-amyloid fibrils. *Science,* 307**,** 262-5.

PICKFORD, F., MASLIAH, E., BRITSCHGI, M., LUCIN, K., NARASIMHAN, R., JAEGER, P. A., SMALL, S., SPENCER, B., ROCKENSTEIN, E., LEVINE, B. & WYSS-CORAY, T. (2008) The autophagy-related protein beclin 1 shows

reduced expression in early Alzheimer disease and regulates amyloid beta accumulation in mice. *J Clin Invest,* 118**,** 2190-9.

PLATANI, M., GOLDBERG, I., SWEDLOW, J. R. & LAMOND, A. I. (2000) In vivo analysis of Cajal body movement, separation, and joining in live human cells. *J Cell Biol,* 151**,** 1561-74.

POLLOCK, C. & HUANG, S. (2009) The perinucleolar compartment. *J Cell Biochem,* 107**,** 189-93.

POMBO, A., JACKSON, D. A., HOLLINSHEAD, M., WANG, Z., ROEDER, R. G. & COOK, P. R. (1999) Regional specialization in human nuclei: visualization of discrete sites of transcription by RNA polymerase III. *EMBO J,* 18**,** 2241-53.

PONICSAN, S. L., KUGEL, J. F. & GOODRICH, J. A. (2010) Genomic gems: SINE RNAs regulate mRNA production. *Curr Opin Genet Dev,* 20**,** 149-55.

PONTES, O. & PIKAARD, C. S. (2008) siRNA and miRNA processing: new functions for Cajal bodies. *Curr Opin Genet Dev,* 18**,** 197-203.

POORKAJ, P., BIRD, T. D., WIJSMAN, E., NEMENS, E., GARRUTO, R. M., ANDERSON, L., ANDREADIS, A., WIEDERHOLT, W. C., RASKIND, M. & SCHELLENBERG, G. D. (1998) Tau is a candidate gene for chromosome 17 frontotemporal dementia. *Ann Neurol,* 43**,** 815-25.

PRADES, C., LAURENT, A. M., PUECHBERTY, J., YUROV, Y. & ROIZES, G. (1996) SINE and LINE within human centromeres. *J Mol Evol,* 42**,** 37-43.

PRASANTH, K. V., PRASANTH, S. G., XUAN, Z., HEARN, S., FREIER, S. M., BENNETT, C. F., ZHANG, M. Q. & SPECTOR, D. L. (2005) Regulating gene expression through RNA nuclear retention. *Cell,* 123**,** 249-63.

PROUDFOOT, N. (2004) New perspectives on connecting messenger RNA 3' end formation to transcription. *Curr Opin Cell Biol,* 16**,** 272-8.

PRUSINER, S. B. (2012) Cell biology. A unifying role for prions in neurodegenerative diseases. *Science,* 336**,** 1511-3.

RABL, C. (1885) Über Zellteilung. *Morph Jb,* 10**,** 214-330.

RADEMAKERS, R., NEUMANN, M. & MACKENZIE, I. R. (2012) Advances in understanding the molecular basis of frontotemporal dementia. *Nat Rev Neurol*.

RAJAPAKSE, I. & GROUDINE, M. (2011) On emerging nuclear order. *J Cell Biol,* 192**,** 711-21.

RASKA, I. (2003) Oldies but goldies: searching for Christmas trees within the nucleolar architecture. *Trends Cell Biol,* 13**,** 517-25.

RAVIKUMAR, B., VACHER, C., BERGER, Z., DAVIES, J. E., LUO, S., OROZ, L. G., SCARAVILLI, F., EASTON, D. F., DUDEN, R., O'KANE, C. J. & RUBINSZTEIN, D. C. (2004) Inhibition of mTOR induces autophagy and

reduces toxicity of polyglutamine expansions in fly and mouse models of Huntington disease. *Nat Genet,* 36**,** 585-95.

REINER, A., ALBIN, R. L., ANDERSON, K. D., D'AMATO, C. J., PENNEY, J. B. & YOUNG, A. B. (1988) Differential loss of striatal projection neurons in Huntington disease. *Proc Natl Acad Sci U S A,* 85**,** 5733-7.

REN, P. H., LAUCKNER, J. E., KACHIRSKAIA, I., HEUSER, J. E., MELKI, R. & KOPITO, R. R. (2009) Cytoplasmic penetration and persistent infection of mammalian cells by polyglutamine aggregates. *Nat Cell Biol,* 11**,** 219-25.

RENTON, A. E., MAJOUNIE, E., WAITE, A., SIMON-SANCHEZ, J., ROLLINSON, S., GIBBS, J. R., SCHYMICK, J. C., LAAKSOVIRTA, H., VAN SWIETEN, J. C., MYLLYKANGAS, L., KALIMO, H., PAETAU, A., ABRAMZON, Y., REMES, A. M., KAGANOVICH, A., SCHOLZ, S. W., DUCKWORTH, J., DING, J., HARMER, D. W., HERNANDEZ, D. G., JOHNSON, J. O., MOK, K., RYTEN, M., TRABZUNI, D., GUERREIRO, R. J., ORRELL, R. W., NEAL, J., MURRAY, A., PEARSON, J., JANSEN, I. E., SONDERVAN, D., SEELAAR, H., BLAKE, D., YOUNG, K., HALLIWELL, N., CALLISTER, J. B., TOULSON, G., RICHARDSON, A., GERHARD, A., SNOWDEN, J., MANN, D., NEARY, D., NALLS, M. A., PEURALINNA, T., JANSSON, L., ISOVIITA, V. M., KAIVORINNE, A. L., HOLTTA-VUORI, M., IKONEN, E., SULKAVA, R., BENATAR, M., WUU, J., CHIO, A., RESTAGNO, G., BORGHERO, G., SABATELLI, M., CONSORTIUM, I., HECKERMAN, D., ROGAEVA, E., ZINMAN, L., ROTHSTEIN, J. D., SENDTNER, M., DREPPER, C., EICHLER, E. E., ALKAN, C., ABDULLAEV, Z., PACK, S. D., DUTRA, A., PAK, E., HARDY, J., SINGLETON, A., WILLIAMS, N. M., HEUTINK, P., PICKERING-BROWN, S., MORRIS, H. R., TIENARI, P. J. & TRAYNOR, B. J. (2011) A hexanucleotide repeat expansion in C9ORF72 is the cause of chromosome 9p21-linked ALS-FTD. *Neuron,* 72**,** 257-68.

RYU, H., LEE, J., HAGERTY, S. W., SOH, B. Y., MCALPIN, S. E., CORMIER, K. A., SMITH, K. M. & FERRANTE, R. J. (2006) ESET/SETDB1 gene expression and histone H3 (K9) trimethylation in Huntington's disease. *Proc Natl Acad Sci U S A,* 103**,** 19176-81.

SAITO, Y., SUZUKI, H., TSUGAWA, H., NAKAGAWA, I., MATSUZAKI, J., KANAI, Y. & HIBI, T. (2009) Chromatin remodeling at Alu repeats by epigenetic treatment activates silenced microRNA-512-5p with downregulation of Mcl-1 in human gastric cancer cells. *Oncogene,* 28**,** 2738-44.

SAVAS, J. N., MAKUSKY, A., OTTOSEN, S., BAILLAT, D., THEN, F., KRAINC, D., SHIEKHATTAR, R., MARKEY, S. P. & TANESE, N. (2008) Huntington's disease protein contributes to RNA-mediated gene silencing through

association with Argonaute and P bodies. *Proc Natl Acad Sci U S A,* 105**,** 10820-5.

SCHAEFER, A., O'CARROLL, D., TAN, C. L., HILLMAN, D., SUGIMORI, M., LLINAS, R. & GREENGARD, P. (2007) Cerebellar neurodegeneration in the absence of microRNAs. *J Exp Med,* 204**,** 1553-8.

SEPHTON, C. F., GOOD, S. K., ATKIN, S., DEWEY, C. M., MAYER, P., 3RD, HERZ, J. & YU, G. (2010) TDP-43 is a developmentally regulated protein essential for early embryonic development. *J Biol Chem,* 285**,** 6826-34.

SHAN, X., CHIANG, P. M., PRICE, D. L. & WONG, P. C. (2010) Altered distributions of Gemini of coiled bodies and mitochondria in motor neurons of TDP-43 transgenic mice. *Proc Natl Acad Sci U S A,* 107**,** 16325-30.

SHARMA, R. P., ROSEN, C., KARTAN, S., GUIDOTTI, A., COSTA, E., GRAYSON, D. R. & CHASE, K. (2006) Valproic acid and chromatin remodeling in schizophrenia and bipolar disorder: preliminary results from a clinical population. *Schizophr Res,* 88**,** 227-31.

SHATKIN, A. J. & MANLEY, J. L. (2000) The ends of the affair: capping and polyadenylation. *Nat Struct Biol,* 7**,** 838-42.

SHAV-TAL, Y., BLECHMAN, J., DARZACQ, X., MONTAGNA, C., DYE, B. T., PATTON, J. G., SINGER, R. H. & ZIPORI, D. (2005) Dynamic sorting of nuclear components into distinct nucleolar caps during transcriptional inhibition. *Mol Biol Cell,* 16**,** 2395-413.

SHELBY, R. D., VAFA, O. & SULLIVAN, K. F. (1997) Assembly of CENP-A into centromeric chromatin requires a cooperative array of nucleosomal DNA contact sites. *J Cell Biol,* 136**,** 501-13.

SHEVTSOV, S. P. & DUNDR, M. (2011) Nucleation of nuclear bodies by RNA. *Nat Cell Biol,* 13**,** 167-73.

SHIOHAMA, A., SASAKI, T., NODA, S., MINOSHIMA, S. & SHIMIZU, N. (2007) Nucleolar localization of DGCR8 and identification of eleven DGCR8-associated proteins. *Exp Cell Res,* 313**,** 4196-207.

SHOPLAND, L. S., JOHNSON, C. V., BYRON, M., MCNEIL, J. & LAWRENCE, J. B. (2003) Clustering of multiple specific genes and gene-rich R-bands around SC-35 domains: evidence for local euchromatic neighborhoods. *J Cell Biol,* 162**,** 981-90.

SHUMAN, S. (2001) Structure, mechanism, and evolution of the mRNA capping apparatus. *Prog Nucleic Acid Res Mol Biol,* 66**,** 1-40.

SIRRI, V., URCUQUI-INCHIMA, S., ROUSSEL, P. & HERNANDEZ-VERDUN, D. (2008) Nucleolus: the fascinating nuclear body. *Histochem Cell Biol,* 129**,** 13-31.

SJOBERG, M. K., SHESTAKOVA, E., MANSUROGLU, Z., MACCIONI, R. B. & BONNEFOY, E. (2006) Tau protein binds to pericentromeric DNA: a putative role for nuclear tau in nucleolar organization. *J Cell Sci,* 119**,** 2025-34.

SLEEMAN, J. E., TRINKLE-MULCAHY, L., PRESCOTT, A. R., OGG, S. C. & LAMOND, A. I. (2003) Cajal body proteins SMN and Coilin show differential dynamic behaviour in vivo. *J Cell Sci,* 116**,** 2039-50.

SOTO, C. (2011) Prion hypothesis: the end of the controversy? *Trends Biochem Sci,* 36**,** 151-8.

SOTO, C. (2012) In vivo spreading of tau pathology. *Neuron,* 73**,** 621-3.

SOUQUERE, S., BEAUCLAIR, G., HARPER, F., FOX, A. & PIERRON, G. (2010) Highly ordered spatial organization of the structural long noncoding NEAT1 RNAs within paraspeckle nuclear bodies. *Mol Biol Cell,* 21**,** 4020-7.

SPECTOR, D. L. (2003) The dynamics of chromosome organization and gene regulation. *Annu Rev Biochem,* 72**,** 573-608.

SPECTOR, D. L. & LAMOND, A. I. (2011) Nuclear speckles. *Cold Spring Harb Perspect Biol,* 3.

SPEESE, S. D., ASHLEY, J., JOKHI, V., NUNNARI, J., BARRIA, R., LI, Y., ATAMAN, B., KOON, A., CHANG, Y. T., LI, Q., MOORE, M. J. & BUDNIK, V. (2012) Nuclear envelope budding enables large ribonucleoprotein particle export during synaptic Wnt signaling. *Cell,* 149**,** 832-46.

SPILLANTINI, M. G., MURRELL, J. R., GOEDERT, M., FARLOW, M. R., KLUG, A. & GHETTI, B. (1998) Mutation in the tau gene in familial multiple system tauopathy with presenile dementia. *Proc Natl Acad Sci U S A,* 95**,** 7737-41.

SREEDHARAN, J., BLAIR, I. P., TRIPATHI, V. B., HU, X., VANCE, C., ROGELJ, B., ACKERLEY, S., DURNALL, J. C., WILLIAMS, K. L., BURATTI, E., BARALLE, F., DE BELLEROCHE, J., MITCHELL, J. D., LEIGH, P. N., AL-CHALABI, A., MILLER, C. C., NICHOLSON, G. & SHAW, C. E. (2008) TDP-43 mutations in familial and sporadic amyotrophic lateral sclerosis. *Science,* 319**,** 1668-72.

STACK, E. C., DEL SIGNORE, S. J., LUTHI-CARTER, R., SOH, B. Y., GOLDSTEIN, D. R., MATSON, S., GOODRICH, S., MARKEY, A. L., CORMIER, K., HAGERTY, S. W., SMITH, K., RYU, H. & FERRANTE, R. J. (2007) Modulation of nucleosome dynamics in Huntington's disease. *Hum Mol Genet,* 16**,** 1164-75.

STANEK, D. & NEUGEBAUER, K. M. (2006) The Cajal body: a meeting place for spliceosomal snRNPs in the nuclear maze. *Chromosoma,* 115**,** 343-54.

STARK, H. & LUHRMANN, R. (2006) Cryo-electron microscopy of spliceosomal components. *Annu Rev Biophys Biomol Struct,* 35**,** 435-57.

STEFFAN, J. S., KAZANTSEV, A., SPASIC-BOSKOVIC, O., GREENWALD, M., ZHU, Y. Z., GOHLER, H., WANKER, E. E., BATES, G. P., HOUSMAN, D. E. & THOMPSON, L. M. (2000) The Huntington's disease protein interacts with p53 and CREB-binding protein and represses transcription. *Proc Natl Acad Sci U S A,* 97**,** 6763-8.

STRONG, M. J., VOLKENING, K., HAMMOND, R., YANG, W., STRONG, W., LEYSTRA-LANTZ, C. & SHOESMITH, C. (2007) TDP43 is a human low molecular weight neurofilament (hNFL) mRNA-binding protein. *Mol Cell Neurosci,* 35**,** 320-7.

SULTAN, A., NESSLANY, F., VIOLET, M., BEGARD, S., LOYENS, A., TALAHARI, S., MANSUROGLU, Z., MARZIN, D., SERGEANT, N., HUMEZ, S., COLIN, M., BONNEFOY, E., BUEE, L. & GALAS, M. C. (2011) Nuclear tau, a key player in neuronal DNA protection. *J Biol Chem,* 286**,** 4566-75.

TADDEI, A., MAISON, C., ROCHE, D. & ALMOUZNI, G. (2001) Reversible disruption of pericentric heterochromatin and centromere function by inhibiting deacetylases. *Nat Cell Biol,* 3**,** 114-20.

TADDEI, A., ROCHE, D., SIBARITA, J. B., TURNER, B. M. & ALMOUZNI, G. (1999) Duplication and maintenance of heterochromatin domains. *J Cell Biol,* 147**,** 1153-66.

TAKIZAWA, T. & MESHORER, E. (2008) Chromatin and nuclear architecture in the nervous system. *Trends Neurosci,* 31**,** 343-52.

TANG, B., SEREDENINA, T., COPPOLA, G., KUHN, A., GESCHWIND, D. H., LUTHI-CARTER, R. & THOMAS, E. A. (2011) Gene expression profiling of R6/2 transgenic mice with different CAG repeat lengths reveals genes associated with disease onset and progression in Huntington's disease. *Neurobiol Dis,* 42**,** 459-67.

TAO, J., HU, K., CHANG, Q., WU, H., SHERMAN, N. E., MARTINOWICH, K., KLOSE, R. J., SCHANEN, C., JAENISCH, R., WANG, W. & SUN, Y. E. (2009) Phosphorylation of MeCP2 at Serine 80 regulates its chromatin association and neurological function. *Proc Natl Acad Sci U S A,* 106**,** 4882-7.

TOOMBS, J. A., MCCARTY, B. R. & ROSS, E. D. (2010) Compositional determinants of prion formation in yeast. *Mol Cell Biol,* 30**,** 319-32.

ULE, J., ULE, A., SPENCER, J., WILLIAMS, A., HU, J. S., CLINE, M., WANG, H., CLARK, T., FRASER, C., RUGGIU, M., ZEEBERG, B. R., KANE, D., WEINSTEIN, J. N., BLUME, J. & DARNELL, R. B. (2005) Nova regulates brain-specific splicing to shape the synapse. *Nat Genet,* 37**,** 844-52.

URDINGUIO, R. G., SANCHEZ-MUT, J. V. & ESTELLER, M. (2009) Epigenetic mechanisms in neurological diseases: genes, syndromes, and therapies. *Lancet Neurol,* 8**,** 1056-72.

VADAKKAN, K. I., LI, B. & DE BONI, U. (2006) Trend towards varying combinatorial centromere association in morphologically identical clusters in Purkinje neurons. *Cell Chromosome,* 5**,** 1.

VANCE, C., ROGELJ, B., HORTOBAGYI, T., DE VOS, K. J., NISHIMURA, A. L., SREEDHARAN, J., HU, X., SMITH, B., RUDDY, D., WRIGHT, P., GANESALINGAM, J., WILLIAMS, K. L., TRIPATHI, V., AL-SARAJ, S., AL-CHALABI, A., LEIGH, P. N., BLAIR, I. P., NICHOLSON, G., DE BELLEROCHE, J., GALLO, J. M., MILLER, C. C. & SHAW, C. E. (2009) Mutations in FUS, an RNA processing protein, cause familial amyotrophic lateral sclerosis type 6. *Science,* 323**,** 1208-11.

VANDERMEEREN, M., MERCKEN, M., VANMECHELEN, E., SIX, J., VAN DE VOORDE, A., MARTIN, J. J. & CRAS, P. (1993) Detection of tau proteins in normal and Alzheimer's disease cerebrospinal fluid with a sensitive sandwich enzyme-linked immunosorbent assay. *J Neurochem,* 61**,** 1828-34.

VERDAASDONK, J. S. & BLOOM, K. (2011) Centromeres: unique chromatin structures that drive chromosome segregation. *Nat Rev Mol Cell Biol,* 12**,** 320-32.

WADDINGTON, C. (1942) The epigenotype. *Endeavour,* 1**,** 18-20.

WALDEYER, W. (1891) Ueber einige neuere Forschungen im Gebiete der Anatomie des Centralnervensystems. . *Dtsch. Med. Wochenschr.,* 50**,** 1352-1356.

WANG, H. Y., WANG, I. F., BOSE, J. & SHEN, C. K. (2004) Structural diversity and functional implications of the eukaryotic TDP gene family. *Genomics,* 83**,** 130-9.

WANG, I. F., WU, L. S., CHANG, H. Y. & SHEN, C. K. (2008) TDP-43, the signature protein of FTLD-U, is a neuronal activity-responsive factor. *J Neurochem,* 105**,** 797-806.

WANG, L., HAEUSLER, R. A., GOOD, P. D., THOMPSON, M., NAGAR, S. & ENGELKE, D. R. (2005) Silencing near tRNA genes requires nucleolar localization. *J Biol Chem,* 280**,** 8637-9.

WANG, Y., LOOMIS, P. A., ZINKOWSKI, R. P. & BINDER, L. I. (1993) A novel tau transcript in cultured human neuroblastoma cells expressing nuclear tau. *J Cell Biol,* 121**,** 257-67.

WANSINK, D. G., SCHUL, W., VAN DER KRAAN, I., VAN STEENSEL, B., VAN DRIEL, R. & DE JONG, L. (1993) Fluorescent labeling of nascent RNA

reveals transcription by RNA polymerase II in domains scattered throughout the nucleus. *J Cell Biol,* 122**,** 283-93.

WARRAICH, S. T., YANG, S., NICHOLSON, G. A. & BLAIR, I. P. (2010) TDP-43: a DNA and RNA binding protein with roles in neurodegenerative diseases. *Int J Biochem Cell Biol,* 42**,** 1606-9.

WEINGARTEN, M. D., LOCKWOOD, A. H., HWO, S. Y. & KIRSCHNER, M. W. (1975) A protein factor essential for microtubule assembly. *Proc Natl Acad Sci U S A,* 72**,** 1858-62.

WILHELMSEN, K. C., LYNCH, T., PAVLOU, E., HIGGINS, M. & NYGAARD, T. G. (1994) Localization of disinhibition-dementia-parkinsonism-amyotrophy complex to 17q21-22. *Am J Hum Genet,* 55**,** 1159-65.

WOJCIECHOWSKA, M. & KRZYZOSIAK, W. J. (2011) Cellular toxicity of expanded RNA repeats: focus on RNA foci. *Hum Mol Genet,* 20**,** 3811-21.

WONG, E. & CUERVO, A. M. (2010) Autophagy gone awry in neurodegenerative diseases. *Nat Neurosci,* 13**,** 805-11.

WOODCOCK, C. L. & GHOSH, R. P. (2010) Chromatin higher-order structure and dynamics. *Cold Spring Harb Perspect Biol,* 2**,** a000596.

XU, Y. F., ZHANG, Y. J., LIN, W. L., CAO, X., STETLER, C., DICKSON, D. W., LEWIS, J. & PETRUCELLI, L. (2011) Expression of mutant TDP-43 induces neuronal dysfunction in transgenic mice. *Mol Neurodegener,* 6**,** 73.

YAKOVCHUK, P., GOODRICH, J. A. & KUGEL, J. F. (2011) B2 RNA represses TFIIH phosphorylation of RNA polymerase II. *Transcription,* 2**,** 45-49.

YAMADA, M., SATO, T., SHIMOHATA, T., HAYASHI, S., IGARASHI, S., TSUJI, S. & TAKAHASHI, H. (2001) Interaction between neuronal intranuclear inclusions and promyelocytic leukemia protein nuclear and coiled bodies in CAG repeat diseases. *Am J Pathol,* 159**,** 1785-95.

YANG, X. J. & SETO, E. (2008) The Rpd3/Hda1 family of lysine deacetylases: from bacteria and yeast to mice and men. *Nat Rev Mol Cell Biol,* 9**,** 206-18.

YASUHARA, J. C. & WAKIMOTO, B. T. (2006) Oxymoron no more: the expanding world of heterochromatic genes. *Trends Genet,* 22**,** 330-8.

YASUHARA, J. C. & WAKIMOTO, B. T. (2008) Molecular landscape of modified histones in Drosophila heterochromatic genes and euchromatin-heterochromatin transition zones. *PLoS Genet,* 4**,** e16.

YASUI, D. H., PEDDADA, S., BIEDA, M. C., VALLERO, R. O., HOGART, A., NAGARAJAN, R. P., THATCHER, K. N., FARNHAM, P. J. & LASALLE, J. M. (2007) Integrated epigenomic analyses of neuronal MeCP2 reveal a role for long-range interaction with active genes. *Proc Natl Acad Sci U S A,* 104**,** 19416-21.

YONETANI, M., NONAKA, T., MASUDA, M., INUKAI, Y., OIKAWA, T., HISANAGA, S. & HASEGAWA, M. (2009) Conversion of wild-type alpha-synuclein into mutant-type fibrils and its propagation in the presence of A30P mutant. *J Biol Chem,* 284**,** 7940-50.

ZHANG, L. F., HUYNH, K. D. & LEE, J. T. (2007) Perinucleolar targeting of the inactive X during S phase: evidence for a role in the maintenance of silencing. *Cell,* 129**,** 693-706.

ZHANG, W., MORRIS, Q. D., CHANG, R., SHAI, O., BAKOWSKI, M. A., MITSAKAKIS, N., MOHAMMAD, N., ROBINSON, M. D., ZIRNGIBL, R., SOMOGYI, E., LAURIN, N., EFTEKHARPOUR, E., SAT, E., GRIGULL, J., PAN, Q., PENG, W. T., KROGAN, N., GREENBLATT, J., FEHLINGS, M., VAN DER KOOY, D., AUBIN, J., BRUNEAU, B. G., ROSSANT, J., BLENCOWE, B. J., FREY, B. J. & HUGHES, T. R. (2004) The functional landscape of mouse gene expression. *J Biol,* 3**,** 21.

ZHANG, Y. J., XU, Y. F., COOK, C., GENDRON, T. F., ROETTGES, P., LINK, C. D., LIN, W. L., TONG, J., CASTANEDES-CASEY, M., ASH, P., GASS, J., RANGACHARI, V., BURATTI, E., BARALLE, F., GOLDE, T. E., DICKSON, D. W. & PETRUCELLI, L. (2009) Aberrant cleavage of TDP-43 enhances aggregation and cellular toxicity. *Proc Natl Acad Sci U S A,* 106**,** 7607-12.

ZHAO, R., BODNAR, M. S. & SPECTOR, D. L. (2009) Nuclear neighborhoods and gene expression. *Curr Opin Genet Dev,* 19**,** 172-9.

ZHOU, Z., HONG, E. J., COHEN, S., ZHAO, W. N., HO, H. Y., SCHMIDT, L., CHEN, W. G., LIN, Y., SAVNER, E., GRIFFITH, E. C., HU, L., STEEN, J. A., WEITZ, C. J. & GREENBERG, M. E. (2006) Brain-specific phosphorylation of MeCP2 regulates activity-dependent Bdnf transcription, dendritic growth, and spine maturation. *Neuron,* 52**,** 255-69.

ZIMBER, A., NGUYEN, Q. D. & GESPACH, C. (2004) Nuclear bodies and compartments: functional roles and cellular signalling in health and disease. *Cell Signal,* 16**,** 1085-104.

ZINSHTEYN, B. & NISHIKURA, K. (2009) Adenosine-to-inosine RNA editing. *Wiley Interdiscip Rev Syst Biol Med,* 1**,** 202-9.

ZOGHBI, H. Y. & ORR, H. T. (2000) Glutamine repeats and neurodegeneration. *Annu Rev Neurosci,* 23**,** 217-47.